Stochastic Geometric Modeling and Analysis of Wireless Communications Systems

by

Prasanna Madhusudhanan

B.E, Telecommunication Engineering, Visvesvaraya Technological University,

Bangalore, India, 2006

M. S., Electrical, Computer and Energy Engineering, University of Colorado,

Boulder, USA, 2010

A thesis submitted to the

Faculty of the Graduate School of the

University of Colorado in partial fulfillment

of the requirements for the degree of

Doctor of Philosophy

Department of Electrical, Computer, and Energy Engineering

2013

This thesis entitled:
Stochastic Geometric Modeling and Analysis of Wireless Communications Systems
written by Prasanna Madhusudhanan
has been approved for the Department of Electrical, Computer, and Energy Engineering

_____
Prof. Timothy X Brown

_____
Prof. Youjian (Eugene) Liu

_____
Prof. Francois G. Meyer

_____
Prof. Juan G. Restrepo

Date _____

The final copy of this thesis has been examined by the signatories, and we find that both the content and the form meet acceptable presentation standards of scholarly work in the above mentioned discipline.

Madhusudhanan, Prasanna (Ph.D., Electrical, Computer, and Energy Engineering)

Stochastic Geometric Modeling and Analysis of Wireless Communications Systems

Thesis work directed by Prof. Timothy X Brown and Prof. Youjian (Eugene) Liu

Abstract

This thesis studies the interference performance of large-scale wireless communications systems. Mathematical models are developed for ad-hoc networks, cellular networks, multi-tier (heterogeneous cellular) networks, cognitive radio networks and the massive-MIMO networks based on stochastic geometry where the nodes of the network are distributed in a space according to a spatial stochastic (random) process. Analytical characterizations for important performance metrics such as the distribution of the signal to interference plus noise ratio, outage probability, average rate, etc. are obtained for the most general channel conditions and system scenarios.

In the past the above mentioned wireless systems have been studied through large system simulations which suffer from computational infeasibilities and provide limited insights about the system. The mathematical models are shown to closely approximate the practical systems in scattering and fading rich environments. Using the tools in stochastic geometry and stochastic ordering, we demonstrate analytical tractability of these models and closed-form characterizations of important performance metrics of the systems. The tools developed in this work can be used to characterize the achievable performance gains with interference mitigation techniques employed in 4G LTE such as fractional frequency reuse, relays, multi-cell coordination and in the study of MIMO and secrecy networks.

Dedication

I dedicate this thesis in memory of Satyabhama Ajji. I also dedicate it to Amma, Anna, Ajji and Thatha.

Acknowledgements

I would like to thank my advisors, Prof. Timothy Brown and Prof. Youjian Liu for their unrelenting help and cooperation since my Day 1 at the University of Colorado, Boulder. It would not have been possible for me to have come this far without their support. I am indebted to them for their role as a teacher and mentor, for providing direction to my research, and for having confidence in me through my tough times. I have thoroughly enjoyed my research under their supervision and have learnt a lot of important lessons in research and life during this period.

I am very grateful to Prof. Larry Esposito for his timely support and advice, and for having introduced to me the wonderful world of Astrophysics. I would like to thank Prof. Juan Restrepo and Prof. Kenneth Baker for their insights and inputs in tackling the research problems. I would like to thank Prof. Francois Meyer and Dr. Sayandev Mukherjee for serving in my PhD thesis defense committee. I am also thankful to Prof. Clifford Mullis, Prof. Sergei Kuznetsov, Prof. Peter D. Elliott, Prof. Sam Siewert, Prof. Jem Corcoran and Prof. Mahesh Varanasi for the courses I have taken with them.

I would like to thank my friends Suresh, Jyothi, Chinmay, Manav, Ekta, Rajesh, Srividya, Kaniska, Nava, Anil, Raveesh, Vivek, Anurag, Ankit, Sriram, Henry, Sanjay and all my labmates for having made my graduate life wonderful and memorable.

Last but not the least, I would like to thank my parents, grandparents and Sreenivas for their support all throughout my life.

Contents

Chapter

Tables

Table

Figures

Figure

Chapter 1

Introduction

1.1 Background

Wireless communication involves the transfer of information between a set of sources (or transmitters) and destinations (or receivers) over a common noisy medium (channel) as shown in Figure 1.1. Over the last three decades, wireless communication networks have evolved in such a manner that it has been one of the most striking successes in information technology. In this time, the wireless networks have proliferated to ubiquity, and have totally changed our day-to-day living. This period has also seen a rapid increase in the number of consumers and an even more dramatic increase in their demands.

To cope with such an ever increasing demand, we need to better understand the two fundamental aspects that make wireless communications both challenging and interesting, namely, fading and interference. The signal from the transmitter undergoes variation in the received power at the receiver with distance and this phenomena is referred to as fading. It can be divided into three types, namely, path-loss, shadowing and multi-path fading. A pictorial representation for the effect of fading is shown in Figure 1.2. Path-loss is the attenuation of the received signal caused by the dissipation of signal power radiated by the transmitter as well as the propagation channel, and causes received power variations over long distances, typically 100-1000 meters. Shadowing is caused by obstacles between the transmitter and receiver that attenuate signal power through absorption, reflection, scattering, and diffraction; leading to received power variations over distances of 10-100 meters. Lastly, multi-path fading is the received power variations caused by the constructive and destructive combination of several signal components at the receiver. Such power variations occur over

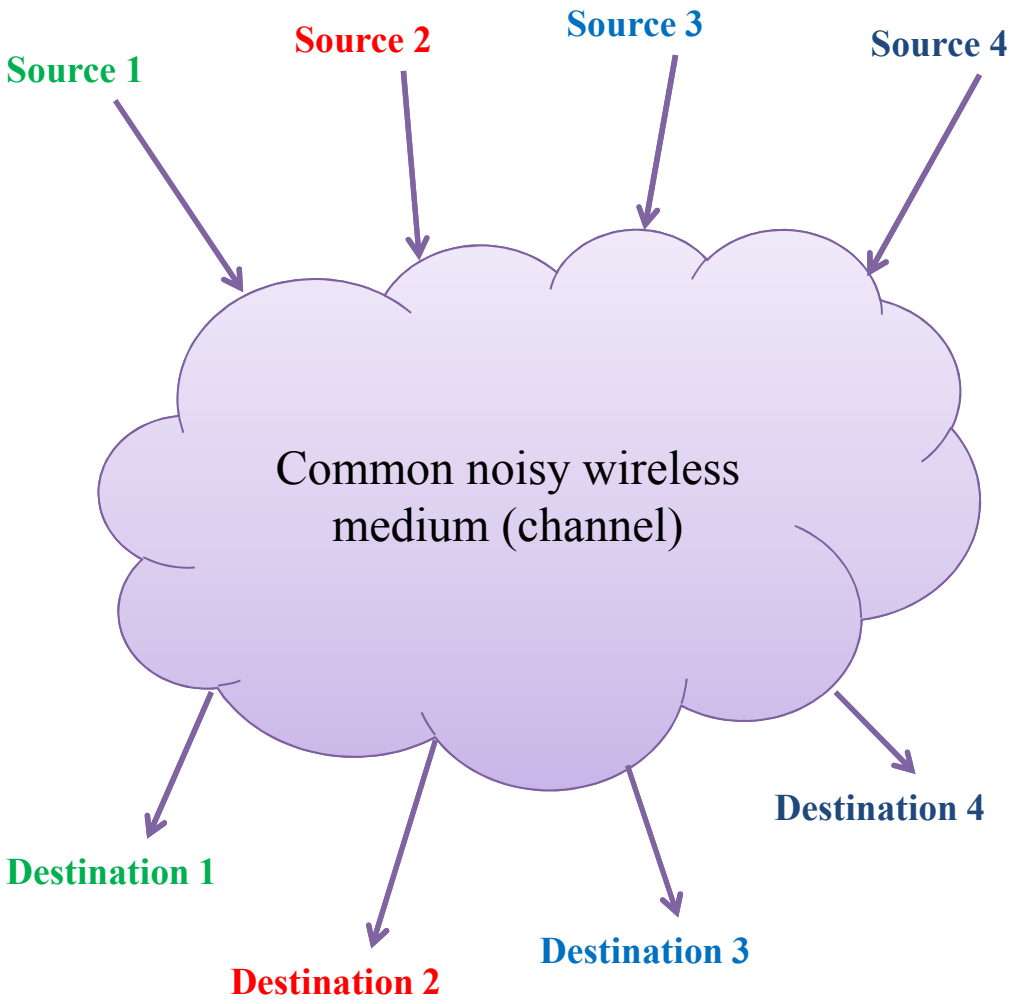

Figure 1.1: Illustration of wireless communication

very short distances (of the order of the wavelength of the transmitted signal) compared to path-loss and shadowing, and as a result the influence of multi-path fading on the signal power is generally referred to as small-scale propagation effect and the influence of path-loss and shadowing is collectively referred to as large-scale propagation effect.

Another fundamental aspect of wireless communication is the interference. The interference in a wireless communication network could be between transmitters communicating with a common receiver (for example, the uplink of a cellular system), between signals from a single transmitter to multiple receivers (like in the downlink of a cellular system), or between different transmitter-receiver pairs as shown in Figure 1.3. Understanding this interference and how to deal with it is central to the design of any wireless communication system.

A wireless communication system (network) is any collection of transmitters and receivers (generally referred to as nodes) that are interconnected wirelessly communicating over the channel to transfer information from the source to the destination. There are several kinds of wireless communication systems that we encounter in our daily lives, the most popular of which are shown in Figure 1.4. The conventional cellular system (or macrocell network) is classically viewed as a network where the given cellular area is divided into regular hexagonal grids (or cells) with a base-station (BS) placed at the center of each hexagonal cell. The arrangement of TV towers could also be associated with a similar regular arrangement in the area of coverage. The wireless LAN network is different from the previous two networks as there is no regular arrangement of the wireless routers or repeaters in general.

1.2 Contributions

The performance or the effectiveness of the above mentioned wireless communication systems are generally assessed by the network operators, system designers and academicians via several metrics such as the outage (or) coverage probability, average rate, spectral efficiency, throughput, network capacity, average load, transmission capacity and the transport capacity. Most of the above mentioned performance metrics appear often in the system design documents, and the last two are of more academic and theoretical importance. We defer the definition of these metrics to the later chapters, as and when they are relevant.

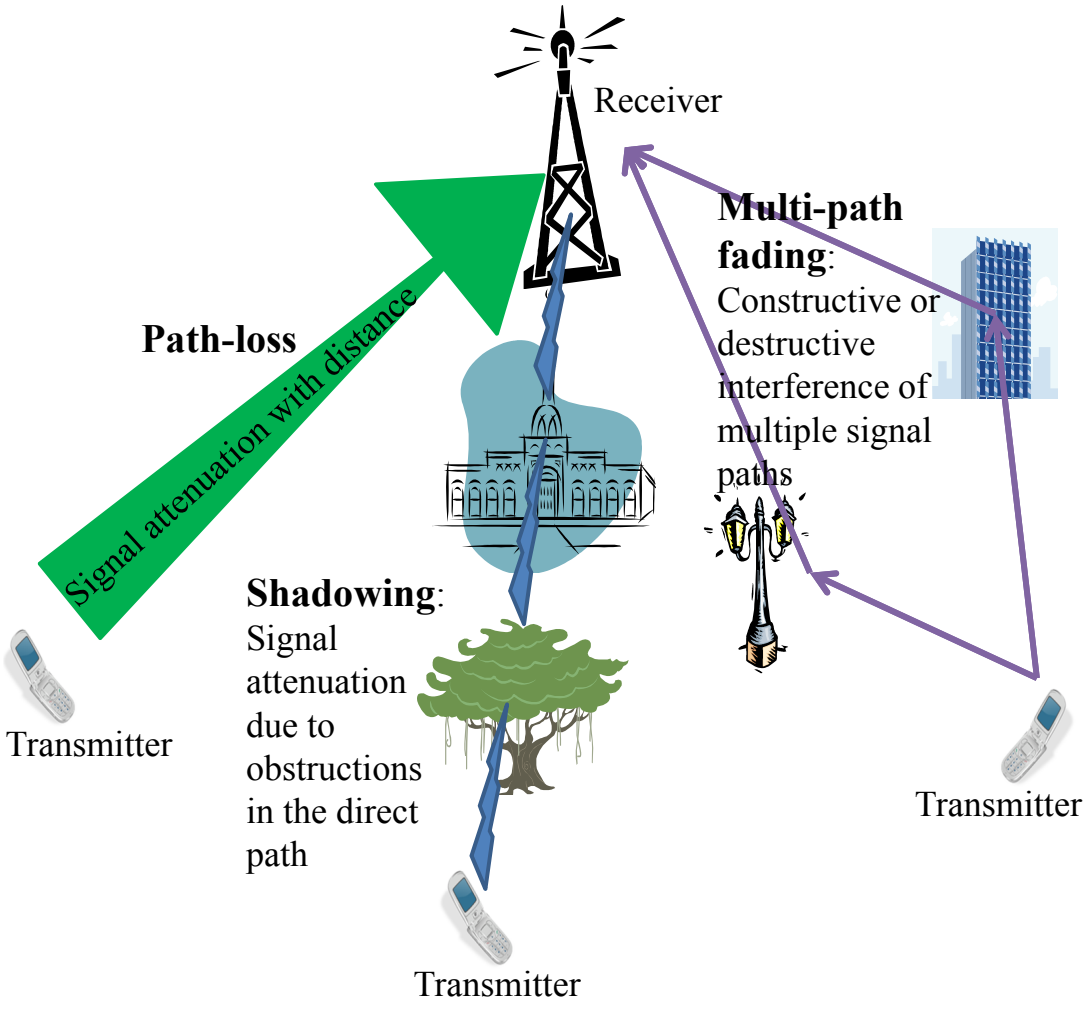

Figure 1.2: Types of fading encountered in wireless communication

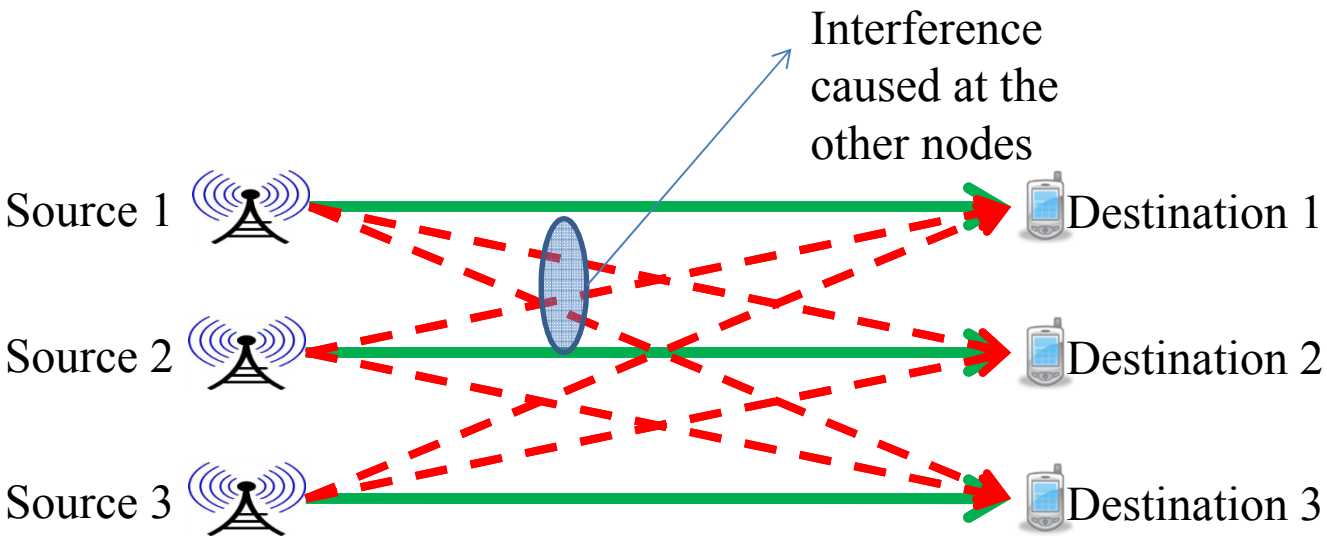

Figure 1.3: Interference in wireless communication

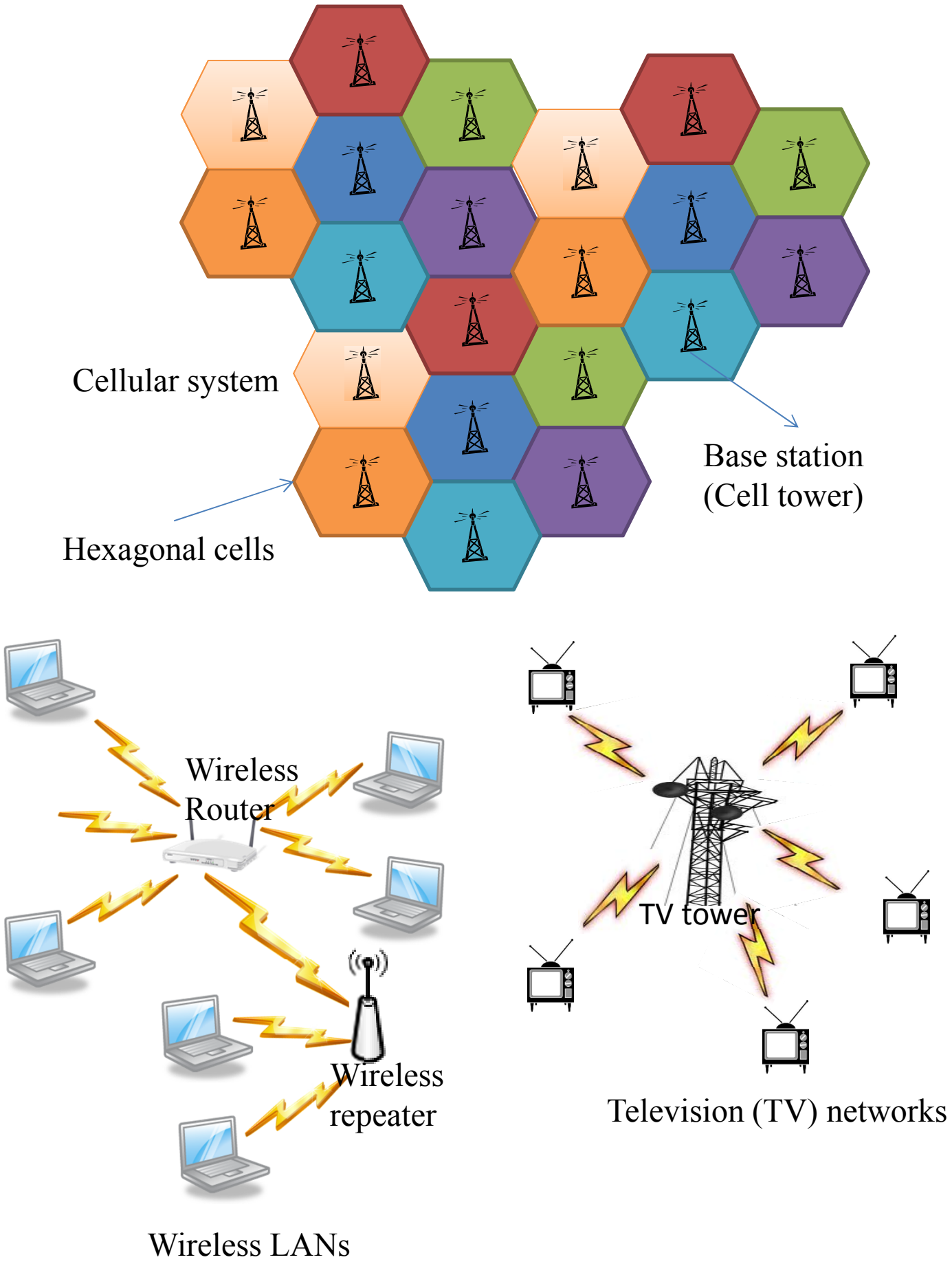

Figure 1.4: Examples of wireless communication systems

Note that all these performance metrics are primarily a function of the signal-to-interference-plus-noise ratio (SINR) at a given node in the system. As a result, in this thesis, we are primarily concerned about the characterization of the SINR in the above mentioned list of wireless communication systems. We further emphasize that once the SINR is characterized for a given system, all the performance metrics listed in the beginning of this paragraph are known. For the sake of clarity, let us define SINR in the context of the cellular system downlink. In the downlink of a cellular system, the MSs act as the receivers and the BSs are the transmitters, and vice versa is true in the uplink of a cellular system. In the cellular downlink, SINR at a given MS is defined as the ratio of the received power from the serving BS to the sum of the interferences from the other transmitting BSs and the background noise. As we have seen previously, the received power at a given MS is equal to the transmitted power of the BS affected by large scale propagation effects such as path-loss and shadow fading and small scale propagation effect called the multipath fading. Path-loss is a decreasing function of the separation between the MS and the transmitting BS and is generally modeled by a power-law path-loss function ($R^{-\varepsilon}$) where R is the separation between the transmitter and the receiver and ε (> 2) is the exponent. Shadow fading and multipath fading are generally modeled as a random variable with a certain distribution. A thorough account of the stochastic as well as the statistical models for the different fading effects in a wireless environment can be found in [4, Chapters 2 and 3]. Further, the location of the MS in the cellular area is random and hence the distances of the BSs (even for the case of regular arrangement as in the hexagonal grid model) from the given MS is subject to randomness. Hence, it is clear that, since the distances of each BS from the MS, the shadow fading and multipath fading coefficients of each BS are all random variables, SINR (which is a function of all these factors) is also a random variable. Hence, the SINR in a wireless system is said to be completely characterized when we have computed either the probability density function (p.d.f), cumulative density function (c.d.f.), tail probability ($= 1 -$ c.d.f.) or the characteristic function of the SINR.

In this report, we characterize the interference and SINR in a variety of wireless communication systems such as the conventional cellular networks, heterogeneous and small-cell networks, cognitive radio networks, massive MIMO networks and interference avoidance or mitigation strategies such as the fractional frequency reuse and relay networks which are used in the fourth generation (4G) long term evolution (LTE)

wireless standards. As the title of this document suggests, we model the above mentioned wireless communications systems using stochastic geometry, characterize and analyze the important performance metrics (primarily the SINR) of these systems in terms of the system parameters. Before we go into further details, a brief introduction to stochastic geometry is provided in the following paragraphs.

1.3 Stochastic Geometric Modeling of Wireless Systems

Stochastic geometry pertains to any random collection of geometric objects such as points, line-segments, spheres etc. in a given space. It is an area of mathematical research that seeks to provide models and statistical methods to study complicated geometric patterns that occur in many area of science and technology, for example in several studies related to ecology, geology, etc. A rigorous account of the popular stochastic geometric models and their applications may be found in [5]. Much like points are the basic ingredients of geometry; random collection of points (point-patterns), also known as point processes play a significant role in stochastic geometry. The simplest and most important random point-pattern is the Poisson point process. An excellent study of the properties of the Poisson point process can be found in [6, 7], and will be presented is this document as and when they are applied.

The aspects of stochastic geometry that shall be witnessed in this thesis are the Poisson point processes and the so-called Boolean model (see Chapter 6). It is well-justified to model certain entities of wireless systems as a Poisson point processes, for example, the distribution of mobile-stations (MSs) in the cellular system, TV receivers in the TV network and the wireless nodes (laptops, notebooks, iPads, etc.) in wireless LANs. Moreover, certain other entities such as BSs in a cellular system can also be modeled as being distributed according to a Poisson point process. The arrangement of BSs is far from the classically studied regular hexagonal grid model due to several reasons including the site-acquisition difficulties, variable traffic load and terrain. Figure 1.5 shows that the actual BS arrangement and the Voronoi tessellations of a major service provider in a relatively flat urban area is visually similar to a BS arrangement according to a Poisson point process than the regular hexagonal grid model. This example serves as a visual justification for why the BS arrangement is also well modeled as being distributed according to a Poisson point process.

Now, we provide a qualitative justification for why the distribution of BSs according to a Poisson

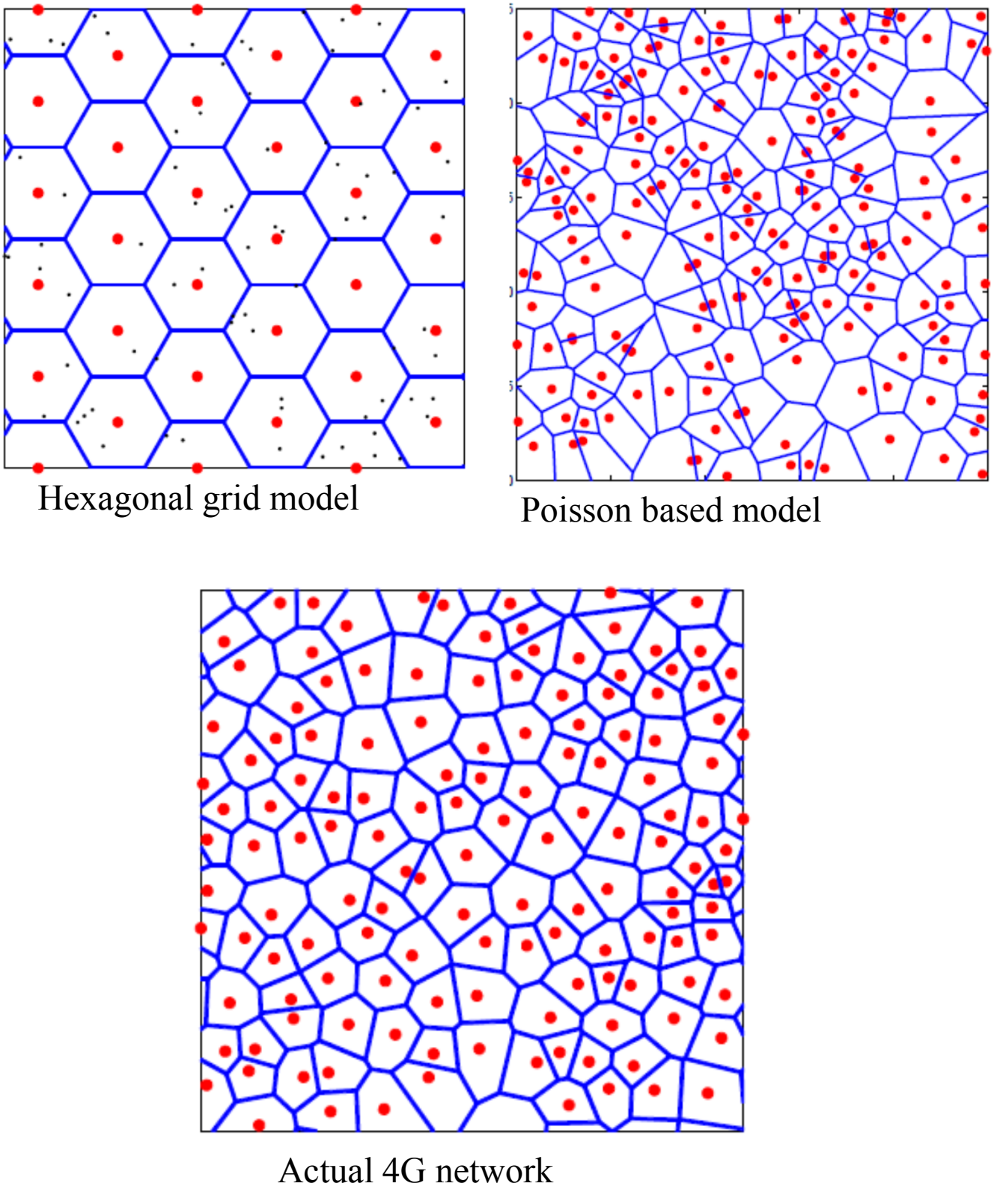

Figure 1.5: Comparison between the BS arrangements and Voronoi tessellations in a regular hexagonal model, Poisson based model and in an actual 4G cellular system [1]

point process is a good model to study the cellular network. In [2, Figure 2], a system simulation compares the signal-to-interference ratio (SIR) at a MS in a cellular system with BS arrangement according to a regular hexagonal grid and another cellular system with Poisson-based BS arrangement. The case when both the cellular systems employ frequency reuse with a reuse factor of 4, a power-law path-loss with a path-loss exponent 4 and a zero-mean log-normal distribution for the shadow fading is considered for the large scale propagation effects in Figure 1.6. It can be seen that the SIR at the 95th percentile of a hexagonal cellular system converges to that of a cellular system with the Poisson-based BS arrangement in the limit of strong shadow fading standard deviation. Moreover, shadow fading standard deviations of 8-15 dB have been reported in indoor environments, in which case SIR performance of the two systems have a small gap. Further, the performance of any practical BS arrangement lies between these two extremes, where on one hand, the hexagonal grid model is the ideal arrangement for maximizing the coverage and on the other hand, the Poisson-based model corresponds to BS arrangement with the maximum entropy for a given mean number of BSs in a given cellular area [8, 9].

Recently, in [10, Theorem 3], it is proved that, in the limit of the shadow fading standard deviation tending to infinity, the set of received powers at any given MS from all the BSs in a cellular system distributed according to a regular arrangement converges to a Poisson point process with a given intensity measure or a density function. This is a very important theoretical result that justifies the modeling of the previously mentioned wireless communication systems as a Poisson point processes for the study of the important metrics that quantify the system performance. It should be noted that all the wireless communication systems that we are concerned with, in this thesis, have been studied so far primarily via large system simulations. Furthermore, while catering to the rapidly growing data demands of the end users as a result of the tremendous improvement in information technology, these wireless communication systems have grown to be extremely complex networks that even system simulation is computationally infeasible. Such systems are often studied by isolating and analyzing small sections of the entire network. The immediate shortcomings of such studies are that they do not represent the overall behavior of the system as a whole, and they provide limited insights about the dependence of the performance on various system parameters. In this thesis, we model various popular and important wireless communication systems, previously studied solely through

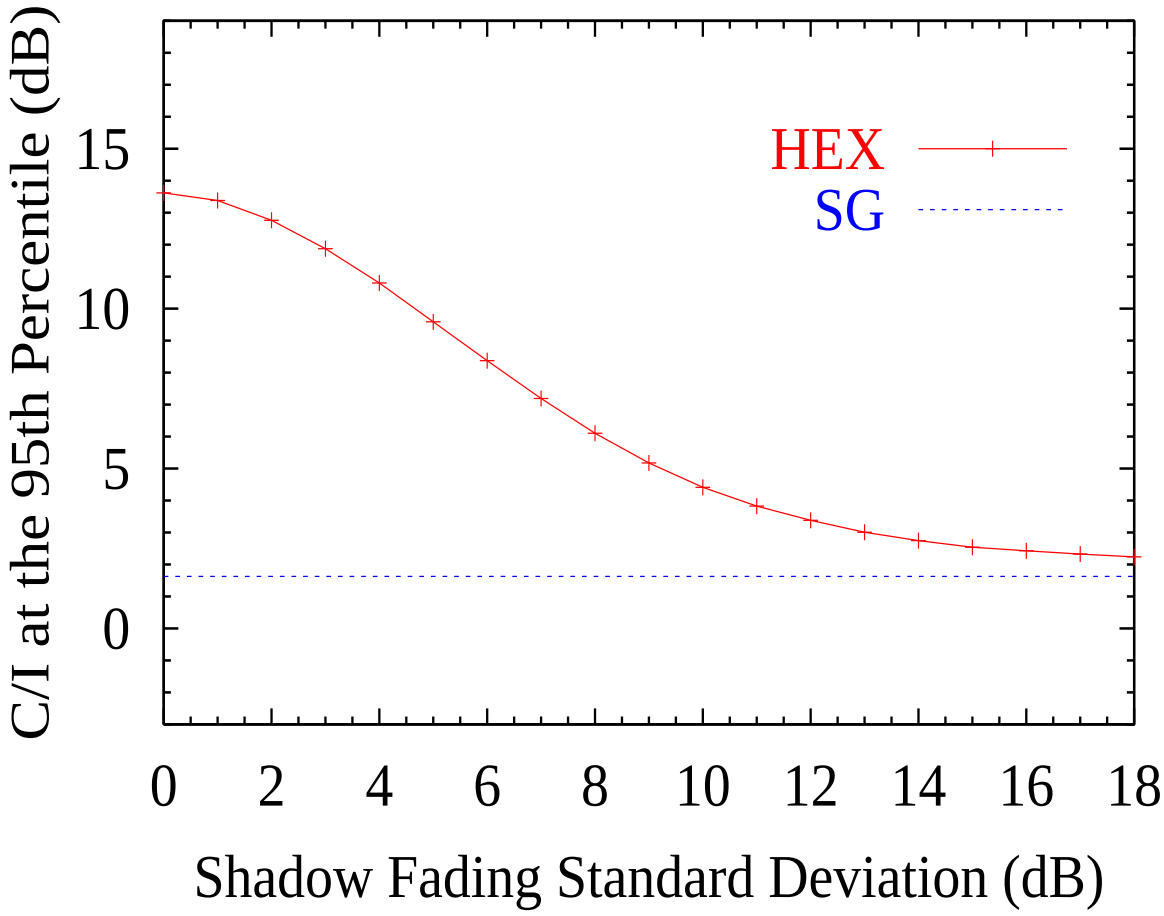

Figure 1.6: Comparison of the SIR (equivalently $\frac{C}{I}$) of the hexagonal grid model (HEX) and the Poisson-based model (SG) [2]

system simulations, using appropriate stochastic geometric models and demonstrate the extent of analytical tractability that can be achieved in terms of characterizing the performance of these systems in terms of the relevant system parameters. In the following section, we list the contributions of this thesis and the organization of the various topics covered.

1.4 Organization of this thesis

Having motivated the idea of modeling the wireless communication systems to be a collection of nodes according to a Poisson point process, we begin with the exploration of the interference characteristics and SINR of the wireless system that has seen most development and growth, namely the cellular network. We dedicate Chapters 2 and 3 to study the downlink performance characteristics of the so-called macrocell network which is composed of large cell towers distributed in a given cellular area to provide coverage to the MSs in the area.

As the number of MSs in the system grows, the traffic and the demand for data in the system increases. In order to cope with the demand and improve the data rate while not adversely affecting the quality-of-service, several techniques are proposed and incorporated, for example, introducing more spectrum, incorporating advanced modulation and coding schemes and spectral reuse. Figure 1.7 lists these methods that the factor of capacity increase that they have been able to achieve since 1950. It is clear that the spectrum-reuse or the spatial frequency reuse has been the dominant factor for achieving the capacity increases.

Spatial frequency reuse means having smaller cell sizes compared to the large hexagonal grids representing the macrocells and a large number of low power BSs. As a result, the cellular system now consists of multiple tiers of small cell networks such as the microcell, picocell and femtocell networks introduced on top of the macrocell network, and the entire cellular networks is now called the heterogeneous network (see Figure 1.8 and Figure 1.9). The modeling and analysis of the heterogeneous network is the subject of Chapter 4, and it is demonstrated that improved coverage and data rate at the MS is achievable with the help of hetnets.

Chapters 2 - 4 characterize the downlink SINR of a MS which is generally referred to as an interior-

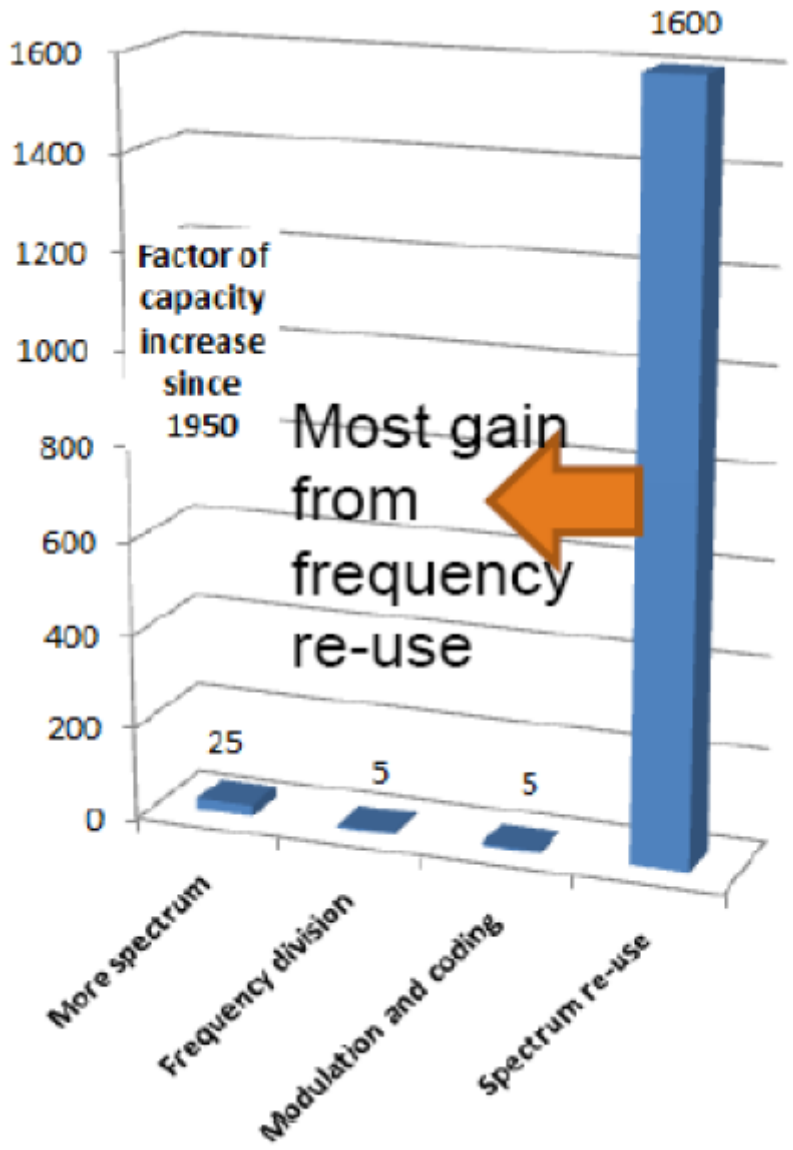

Figure 1.7: Methods to improve the cellular network capacity and their contribution in terms of factors of capacity increase achieved.

user. A MS is said to be an cell-interior user if there exists at least one BS in the entire cellular system, the received SINR from which is above a given threshold to obtain connectivity with the BS. A MS to which there is no BS with a received SINR above the threshold is called the cell-edge user. In a classical hexagonal grid based cellular system, a cell-edge user is a MS at the edge of a given cell. This MS typically sees a poor SINR from the serving BS because there exist a BS at approximately same distance from the MS as the serving BS causing harmful interference at the MS. In the 4G LTE standard, fractional frequency reuse is introduced as an interference mitigation (avoidance) technique to ensure uniformly high data-rates at both the cell-interior user and the cell-edge user. In Chapter 5, we explore the SINR characteristics of a cellular system modeled as a Poisson point process and employing fractional frequency reuse to improve the signal quality at the cell-edge user.

Notice in Figure 1.7 that adding more frequency spectrum also leads to some capacity improvements. Frequency spectrum is an extremely scarce resource and the majority of the spectrum is already allocated for the existing radio application. Nevertheless, Federal Communications Commission (FCC) has identified the licensed televisions (TV) bands to have a very poor spectral efficiency, and has allowed the operation of unlicensed devices called the cognitive radio devices in the television (TV) band along with the legacy users of this band with the goal of improving the spectral efficiency. The cognitive radio network is a collection of cognitive radio devices, that have the ability to search for unused frequency bands and communicate over those bands. The TV band is occupied by the legacy users that are the TV transmitter-receiver pairs and the wireless microphone systems. In Chapter 6, we study the interference caused by the cognitive radio network on the legacy network in the TV white spaces, and characterize the SINR at the legacy users.

In Chapter 7, we consider the study of the so-called massive multiple input multiple output (MIMO) cellular network which is a cellular network where each BS in the network has infinitely many antennas and each MS is equipped with a single antenna. In this chapter, unlike in Chapters 2 - 5, we analyze the SINR distribution and the system performance of the cellular system in both the uplink and the downlink. Finally, the concluding remarks and directions for future research are briefly pointed out in Chapter 8.

In the following subsection, the summary of results corresponding to each chapter is given.

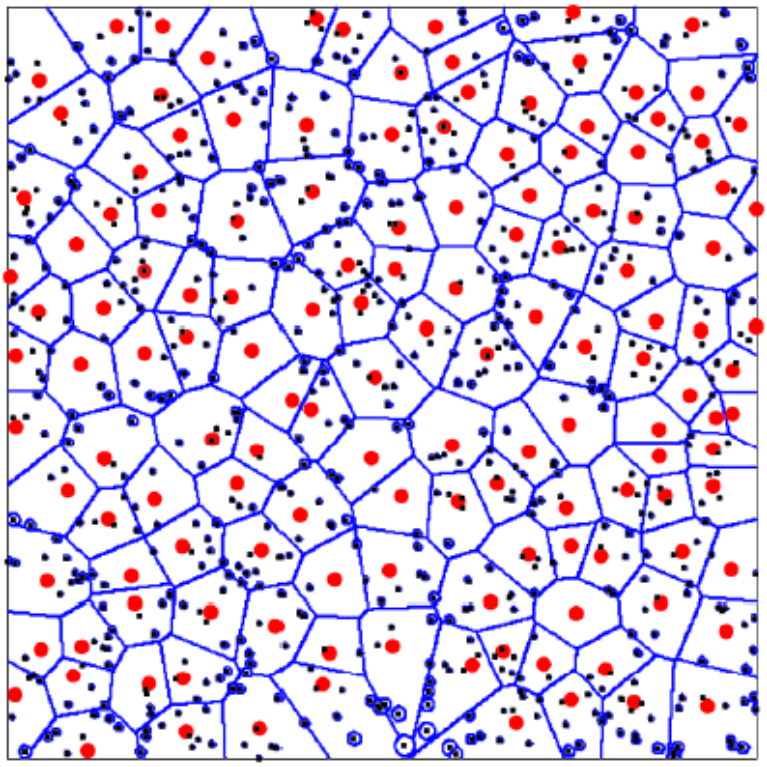

Figure 1.8: Hetnet snapshot showing the macrocell BSs (red dots) and the femtocell BSs (black dots) [3]

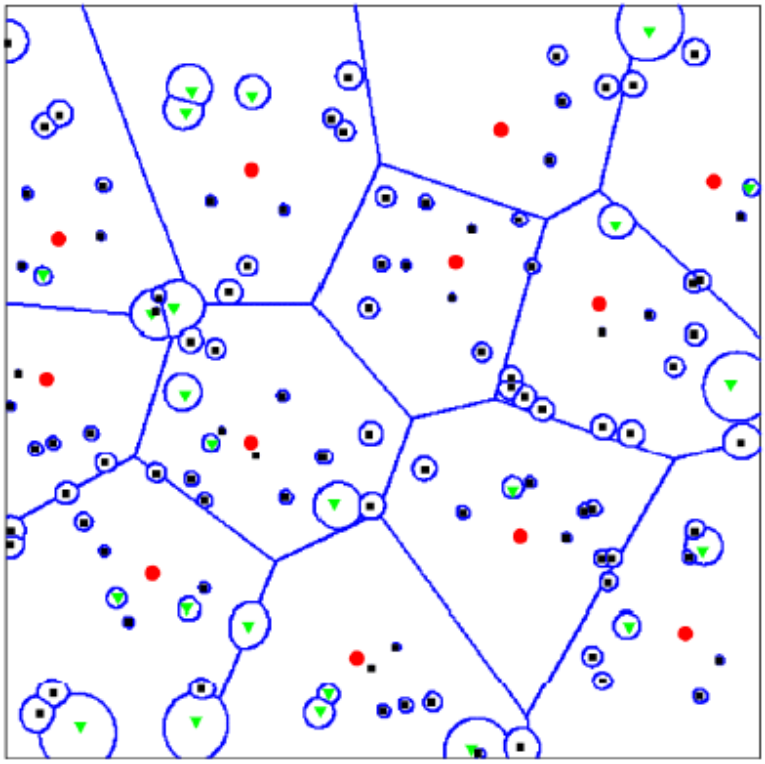

Figure 1.9: Hetnet snapshot (closeup of a section in Figure 1.8) consisting of the macrocell BSs (red), microcell BSs (green) and the femtocell BSs (black). [3]

1.4.1 Summary of Chapter 2

Here, we analyze the SINR performance at a MS in a random cellular network. The cellular network is formed by BSs placed in a one, two or three dimensional space according to a possibly non-homogeneous Poisson point process, which is a generalization of the so-called shotgun cellular system. We develop a sequence of equivalence relations for the SCSs and use them to derive semi-analytical expressions for the distribution of SINR and the coverage probability at the MS when the transmissions from each BS may be affected by random fading with arbitrary distributions as well as attenuation following arbitrary path-loss models. For homogeneous Poisson point processes in the interference-limited case with power-law path-loss model, we show that the SINR distribution is the same for all fading distributions and is not a function of the base station density. In addition, the influence of random transmission powers, power control, multiple channel reuse groups on the downlink performance are also discussed. The techniques developed for the analysis of SINR have applications beyond cellular networks and can be used in similar studies for cognitive radio networks, femtocell networks and other heterogeneous and multi-tier networks.

1.4.2 Summary of Chapter 3

Though a semi-analytical expression for the distribution of SINR is obtained for a cellular system modeled as a non-homogeneous Poisson point process, insights obtained from the expression about the system performance is limited. As a result, an analytical tool based on usual stochastic ordering is developed to compare the distributions of SIR at the MS of cellular systems where the base stations are distributed randomly according to certain non-homogeneous Poisson point processes. The comparison is done by studying the base station densities without having to solve for the distributions of the SIR, which are often hard to obtain.

1.4.3 Summary of Chapter 4

In this chapter, we consider the downlink SINR analysis in a hetnet with $\mathbf{K}$ open-access tiers and a closed-access tier. Each tier is characterized by a BS arrangement according to a homogeneous Poisson point process with certain BS density, random transmission power and random shadow fading factor with

an arbitrary joint distribution, arbitrary path-loss exponent for the power-law path-loss model. The MS can connect to any BS belonging to the open-access tiers, and is not allowed access to the closed-access tier. We characterize the SINR distribution at the MS for both the max-SINR connectivity model and the nearest-BS connectivity model. Further, analytical expressions for the coverage probability and ergodic average rate at the MS, and the average fraction of users that are served by a given tier are also computed.

1.4.4 Summary of Chapter 5

In this chapter, we analyze the downlink SIR performance in an OFDMA cellular network where the BSs are distributed according to a homogeneous Poisson point process on the two-dimensional plane. We study two popular adaptive fractional frequency reuse (FFR) mechanisms, namely strict-FFR and soft frequency reuse (SFR). We compute the coverage probability at the MS which chooses to communicate with the BS with the maximum instantaneous SIR for the two FFR techniques. Comparison of these results with those of the nearest BS connectivity model by Novlan et. al. show a surprising result that the maximum SIR connectivity, which is known to be coverage optimal for static and no frequency reuse scenarios, is not optimal anymore with FFR techniques. This shift from conventional wisdom demands further exploration on which BS should the MS connects to for optimal downlink performance.

1.4.5 Summary of Chapter 6

In this chapter, we study the cognitive radio (CR) network where the CR devices opportunistically communicate in the frequency bands occupied by the primary users in order to improve the spectral efficiency in these bands. By detecting the beaconing signals emitted by the primary users (both the television (TV) transmitter-receiver pairs and the wireless microphone systems), each CR device determines whether or not to operate in the band. The CR devices, due to erroneous detection capabilities, either misses the beaconing signals causing excessive interference at the primary user or false-alarms causing it to remain silent in a white-space band leading to poor spectrum utility. The impact of these imperfections on the primary user operations in terms of the coverage probability (= 1 - outage probability) is characterized where the primary users and the CR devices are distributed according to independent homogeneous Poisson point processes on

the plane. The coverage probability at a TV receiver is the probability that there exists at least one TV transmitter that has a signal-to-interference ratio (SIR) above a given threshold. At the wireless microphone receiver (WMR), it is the probability that the transmitter corresponding to the WMR has an SIR above a given threshold.

1.4.6 Summary of Chapter 7

We study a multiple input multiple output (MIMO) cellular system where each base-station (BS) is equipped with a large antenna array and serves some single antenna mobile stations (MSs). With the same setup as in [11], the influence of orthogonal and non-orthogonal pilot sequences on the system performance is analytically characterized when each BS has infinitely many antennas. Using stochastic geometric modeling of the BS and MS locations, closed-form expressions are derived for the distribution of signal-to-interference-ratio (SIR) for both uplink and downlink. Moreover, they are shown to be equivalent for the orthogonal pilots case. Further, it is shown that the downlink SIR is greatly influenced by the correlations between the pilot sequences in the non-orthogonal pilots case. Finally, the mathematical tools can be used to study system performances with other general channel estimation methods and transmission-reception schemes.

Chapter 2

Downlink Performance Analysis for a Generalized Shotgun Cellular System

2.1 Introduction

The modern cellular communication network is a complex overlay of heterogeneous networks such as macrocells, microcells, picocells, and femtocells. The BS deployment for these network can be planned, unplanned, or uncoordinated. Even when planned, the BS placement in a region typically deviates from the ideal regular hexagonal grid due to site-acquisition difficulties, variable traffic load, and terrain. The coexistence of heterogeneous networks has further added to these deviations. As a result, the BS distribution appears increasingly irregular as the BS density grows and is outside standard performance analysis.

Two approaches of modeling have been widely adopted in the literature. At one end, the BSs are located at the centers of regular hexagonal cells to form an ideal hexagonal cellular system. At the other end, the BS deployments are modeled according to a Poisson point process which we refer to as shotgun cellular system (SCS). In [2], we make a connection between these two models on a homogeneous two dimensional (2-D) plane. It is shown that the SIR of the SCS lower bounds that of the ideal hexagonal cellular system and, moreover, the two models converge in the strong fading regime. The BS deployment in the practical cellular system lies somewhere in between these two extremes, and as noted in [2,12,13], significant insights about the cellular performance can be gained by thoroughly understanding the hexagonal cellular system and the SCSs, especially in the strong fading regime. The hexagonal cellular systems are difficult to study analytically and hence, vast literature on the performance studies of such systems is purely simulation-based. On the other hand, here we demonstrate that the SCSs are extremely amenable to mathematical analysis

even for a very general system model. An in-depth analysis of the downlink performance of the SCS is conducted by considering three levels of generality. Firstly, the BS arrangement in the SCS is according to a non-homogeneous Poisson point process in an arbitrary dimension ($l = 1,\ 2,\ 3$), which can mimic the BS arrangement in a real cellular system by the appropriate choice of the intensity function of the point process. Secondly, a general model is considered for the path-loss suffered by the BS transmissions, which covers the most-popular power-law path-loss model as well as other models that more accurately capture indoor propagation losses. Thirdly, the fading undergone by the transmitted signals of each BS is modeled as a random variable with any arbitrary distribution that is independent and identically distributed (i.i.d.) across all the BSs, that covers the most commonly used log-normal and exponential distributions, and more.

2.1.1 Prior work and our contributions

A Poisson point process has been adopted in the literature for the locations of nodes in the study of sensor networks, wireless LANs, cognitive radios, ad hoc networks and other uncoordinated and decentralized networks [14–30]. In the case of ad-hoc networks, bounds on the transmission capacity have been derived in several different contexts [19,20,23–25,31–34]. Finding the optimal bandwidth partitioning in uncoordinated wireless networks is considered in [35]. Similar outage probability analysis in ad-hoc packet radio networks is considered in [36, 37].

An underlying assumption in all the previous work is that the density of transmitters is constant throughout the cellular region, i.e. the Poisson point process is homogeneous; propagation model follows the power law path-loss; and the fading models are log-normal, Rayleigh, or Rician distributions. In this chapter, the three levels of generality mentioned in the previous subsection helps in more accurately modeling the cellular system thereby making the results hold for a wide variety of practical scenarios. Moreover, the region of interest need not be restricted to $\mathbb{R}^2$ as in prior work, and may be $\mathbb{R}^1$ or $\mathbb{R}^3$. Furthermore, the dependence of the downlink performance on the MS location within the cellular region is also characterized. Handoff features and correlations between the fading coefficients corresponding to different BS transmissions are out of the scope of this work.

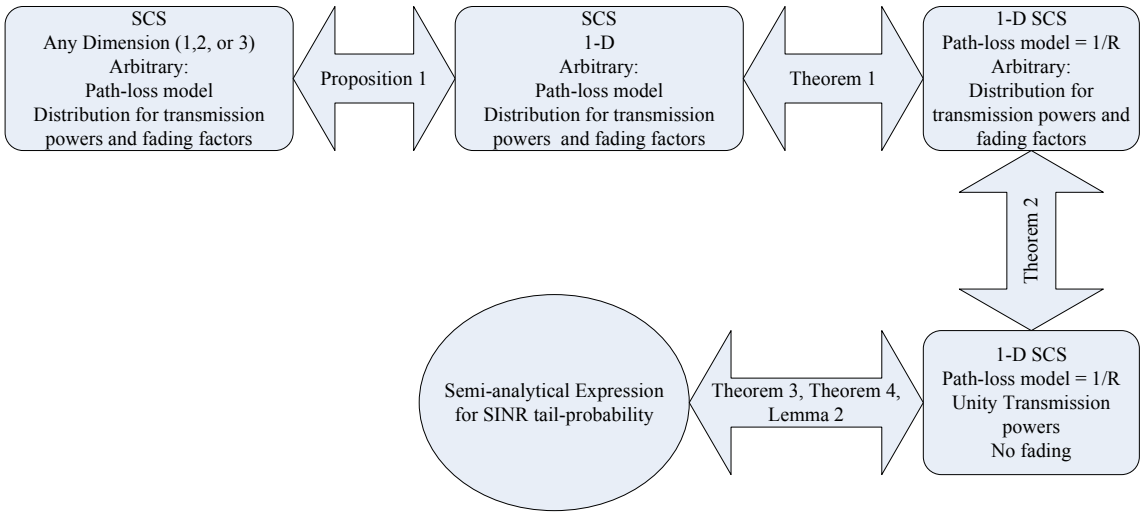

Figure 2.1: Contributions of this chapter: SINR characterization for SCSs. A general SCS is reduced to the simplest SCS (canonical SCS, lower right corner of the figure) using a series of transformations. The double arrows indicate equivalence of the SINR tail-probability of the SCS before and after the transformation (proved in the theorem that label the corresponding arrows). The SINR tail-probability is derived for the canonical SCS, which is the same for the original SCS as a result of the equivalent transformations.

The main results of this chapter are discussed below. As shown in Figure 2.1, we successively reduce the actual SCS to a canonical model that is equivalent in terms of the SINR characteristics, and characterize the SINR distribution for the simplest equivalent system, thereby solving the problem for the most general network. These results are covered in Section 2.3 borrowing ideas from [38] for constructing the equivalent canonical model. In [38], we looked at a qualitative comparison between the SINRs of two SCSs based on usual stochastic ordering without actually computing the distribution of SINR, whereas in this chapter, the main objective is to compute the SINR distribution for any given SCS and to systematically characterize the influence of the model parameters on the downlink performance.

Next, for the special case of homogeneous SCSs, which is the most widely used model for random node locations, the canonical model takes an extremely simple form in which the BS arrangement is according to a unit mean homogeneous Poisson point process and where each BS has unity transmission power and there is no fading. Further, the effect of the system parameters of the actual SCS (e.g., BS density, arbitrary transmission power and fading distributions, background noise power) on the downlink SINR are all captured in the background noise power term in the canonical model. Finally, simple closed form characterizations for the distribution of SINR, downlink coverage (outage) probability, downlink average ergodic rate and several insights about the cellular system are obtainable and are the topic of concern in Section 2.4.

Applications of the above results to specific wireless communication scenarios are briefly described in Section 2.6 where we point out the application of the ideas and results of this chapter to the performance analysis of cognitive radio networks and heterogeneous and small-cell networks. Next, the system model and the performance metric of interest are briefly explained.

2.2 System Model

This section describes the various elements used to model the shotgun cellular system, namely, the BS layout, the radio environment, and the performance metrics of interest.

2.2.1 BS Layout

Definition 1. The *Shotgun Cellular System (SCS)* is a model for the cellular system in which the BSs are placed in a given l-dimensional plane (typically $l = 1, 2,$ and 3) according to a non-homogeneous Poisson point process on $\mathbb{R}^l$ [6, 7].

The intensity function of the Poisson point process is called the BS density function in the context of the SCS. A 1-D SCS models, for example, the BS deployments along a highway. A 2-D SCS models planar BS deployments, and the 3-D SCS models BS deployments in a dense urban area, or wireless LANs in an apartment building. The 1-D, 2-D and 3-D SCSs are described using the BS density functions $d(x)$, $d(r, \theta)$, and $d(r, \theta, \phi)$, where $-\infty \leq x \leq \infty$ represents a point in 1-D, and $r,\ \theta,\ \phi$ are used to represent a point in polar coordinates, in 2-D and 3-D.

A $l-$D SCS is said to be homogeneous if the BS density function is a constant over the entire l-D space. A homogeneous 2-D SCS is a common model for the random node placement in many scenarios.

We consider the most general possible description for the wireless radio environment. Let the received power at a distance $r\ (\geq 0)$ from a given BS be given by

$$P(r) \quad = \quad K\Psi / h(r), \tag{2.1}$$

where K represents the transmission power and the antenna gain of the BS, Ψ captures the channel fading, and the function $h(\cdot)$ represents a path-loss that a signal experiences as it propagates in the wireless environment. The most commonly used path-loss model is the power-law path-loss model, $h(r) = r^{\varepsilon}$, where ε is called the path-loss exponent.

2.2.2 Performance Metric

In this chapter, we focus on the downlink performance of the SCS. In other words, we are concerned with the signal quality at a mobile-station (MS) within the SCS. The MS is assumed to be located at the origin of the l-D SCS unless specified otherwise. The signal quality at the MS is defined as the ratio of the received power from the serving BS to the sum of the interference powers (I or P_I), and the background noise power (η), and is called the signal-to-interference-plus-noise ratio (SINR). In an **interference-limited**

system, $I \gg \eta$ and the signal quality is the signal-to-interference ratio (SIR).

Using (2.1), the SINR at the MS from a BS at a distance, say R_i, is

$$\text{SINR} \quad = \quad \frac{K_i \Psi_i / h(R_i)}{\sum_{\substack{j=1 \\ j \neq i}}^{\infty} K_j \Psi_j / h(R_j) + \eta}, \tag{2.2}$$

where $\{K_j,\ \Psi_j\}_{j=1}^{\infty}$ are independent and identically distributed (i.i.d) pairs of random variables representing the transmission power and the channel gain coefficients, respectively, of the j^{th} BS, and $\{R_j\}_{j=1}^{\infty}$ are random variables that come from underlying Poisson point process that governs the BS placement. Also, the MS associates itself with the BS that has the strongest received signal power (referred to as the serving BS), and can successfully communicate with this BS, only if the corresponding SINR exceeds a certain operating threshold, denoted by γ. In this chapter, we find the tail probability [i.e. the complementary cumulative density function (c.c.d.f.)] of the SINR, which helps characterize an important performance metric for wireless networks, namely, the coverage probability, i.e. the probability that a MS is able to successfully communicate with the desired BS. The following section presents some necessary results that helps simplify and solve the problem.

2.3 SINR Characteristics

As illustrated in Figure 2.1, this section presents several equivalence relations on BS density, path-loss model, transmission power and fading that leads to an equivalent canonical SCS model. Then the equivalence relations are used to simplify the analysis of the SINR. The equivalence is defined below.

Definition 2. Two SCSs are *equivalent* if the joint distribution of the powers from all the BSs of a SCS received at the MS located at the origin is the same as the joint distribution of the other SCS.

As a result, if the noise powers are equal, the SINRs at the MSs in two equivalent SCSs have the same distribution.

The following proposition gives an equivalent 1-D SCS for any l-D SCS. It is a simple consequence of the fact that the path-loss models considered in this chapter is a function of only the distance between the MS and a BS, not of the orientation.

Proposition 1. An l-D SCS, $l = 1,\ 2,$ and 3 is equivalent to a 1-D SCS with a one-sided BS density function $\lambda(r),\ r \geq 0$, calculated below, if other parameters are the same.

- **For a 1-D SCS with density function** $d(x),\ -\infty \leq x \leq \infty$, $\lambda(r) = d(r) + d(-r)$.
  - **For a 2-D SCS with density function** $d(r,\theta),\ \lambda(r) = \int_{\theta=0}^{2\pi} d(r,\theta)\, r d\theta$**.**
  - **For a 3-D SCS with density function** $d(r,\theta,\phi),\ \lambda(r) = \int_{\theta=0}^{\pi}\int_{\phi=0}^{2\pi} d(r,\theta,\phi)\, r^2 \sin(\theta)\, d\theta d\phi$.

Next, we show the equivalence between SCS's with path-loss model $\frac{1}{h(R)}$ and SCS's with path-loss model $\frac{1}{R}$, using the concepts of stochastic ordering [7, 39, 40].

Theorem 1. ***If other parameters are the same, a 1-D SCS with a BS density function*** $\lambda(r)$ ***and path-loss model*** $\frac{1}{h(R)}$ ***is equivalent to a 1-D SCS with a BS density function*** $\bar{\lambda}(r) = \lambda(h^{-1}(r)) \times \frac{d}{dr}h^{-1}(r)$, ***and path-loss model*** $\frac{1}{R}$, ***where*** R ***is the distance between a BS and the MS, as long as*** $h(r),\ r \geq 0$ ***is a monotonically increasing function with a derivative*** $h'(r) > 0,\ \forall\ r > 0$ ***and an inverse*** $h^{-1}(r)$. ***As a result, if the noise powers are the same, the SINRs at the MSs located at the origin in the two SCSs have the same distribution, i.e. the SINR of (2.2) satisfies***

$$\mathrm{SINR}|_{\lambda(r)} \quad =_{\mathrm{st}} \quad \left.\frac{K_i \Psi_i / \tilde{R}_i}{\sum_{\substack{j=1 \\ j\neq i}}^{\infty} K_j \Psi_j / \tilde{R}_j + \eta}\right|_{\bar{\lambda}(r)}, \tag{2.3}$$

where $\left\{\tilde{R}_j\right\}_{j=1}^{\infty}$ ***is the set of distances of BSs from the MS in the 1-D SCS with BS density function*** $\bar{\lambda}(r)$ ***and*** $=_{\mathrm{st}}$ ***represents the equivalence in distribution.***

Proof. See Appendix 2.8.1. □

In the following theorem, we show the equivalence between SCS's with random transmission power and fading and SCS's with deterministic transmission power and fading.

Theorem 2. ***A 1-D SCS with BS density function*** $\lambda(r)$, ***path-loss model*** $\frac{1}{R}$, ***random transmission power*** K ***and random fading*** Ψ ***that are i.i.d. across all BSs, is equivalent to another 1-D SCS with a BS density function*** $\bar{\lambda}(r)$, $\frac{1}{R}$ ***path-loss model, unity transmission power and unity fading . The above is true for arbitrary joint distributions of*** (K, Ψ) ***as long as*** $\bar{\lambda}(r) =$

$\mathbb{E}_{K,\Psi}\left[K\Psi\lambda\left(K\Psi r\right)\right] < \infty$ ***holds for all*** $r \geq 0$***, where*** $\mathbb{E}_{K,\Psi}\left[\cdot\right]$ ***is the expectation operator w.r.t.*** (K, Ψ). ***The distributions of the SINRs at the MSs located at the origin of the two SCS's are the same if the noise powers of the MSs are equal.***

Proof. See Appendix 2.8.2. □

Combining Proposition 1, Theorem 1 and Theorem 2, without loss of generality, we can now restrict our attention to the SINR characterization of the canonical SCS defined below.

Definition 3. A canonical SCS is a 1-D SCS with a BS density function $\lambda\left(r\right),\ r \geq 0$, unity transmission power and unity fading factors for all BSs in the SCS, and a path-loss model of $\frac{1}{R}$.

For a canonical SCS, the BS closest to the origin is the serving BS and the rest of the BSs contribute to the interference power. The following is an interesting fact.

Lemma 1. ***If the noise powers are the same, the distributions of SINRs at the MS in canonical SCSs with BS density function of the form*** $\frac{1}{a}\lambda(\frac{r}{a})$ ***are the same for all*** $a > 0$***. In other words,*** $\mathrm{SINR}|_{\lambda(r)} =_{st} \mathrm{SINR}|_{\frac{1}{a}\lambda(\frac{r}{a})}$.

Proof. See Appendix 2.8.3. □

As a result, the appropriate scaling of the BS density function will not change the p.d.f. of SINR. Next, we derive expressions for the tail probability of the SINR.

Theorem 3. ***The tail probability of SINR at the MS in a canonical SCS,*** $\mathbb{P}\left(\{\mathrm{SINR}_{\mathrm{canonical}} > \gamma\}\right)$ ***is given by***

$$\mathbb{P}\left(\{\mathrm{SINR}_{\mathrm{canonical}} > \gamma\}\right) = \begin{cases} \int_{\omega=-\infty}^{\infty} \Phi_{\frac{1}{\mathrm{SINR}_{\mathrm{canonical}}}}\left(\omega\right)\left(\frac{1-\exp\left(-\frac{i\omega}{\gamma}\right)}{i\omega}\right)\frac{d\omega}{2\pi}, & \gamma > 0 \\ 1, & \gamma = 0 \end{cases}, \tag{2.4}$$

where $\Phi_{\frac{1}{\mathrm{SINR}_{\mathrm{canonical}}}}\left(\omega\right)$ ***is the characteristic function of*** $\frac{1}{\mathrm{SINR}_{\mathrm{canonical}}}$ ***given by***

$$\Phi_{\frac{1}{\mathrm{SINR}_{\mathrm{canonical}}}}\left(\omega\right) = \mathbb{E}_{R_1}\left[\exp\left(i\omega\eta R_1\right) \times \Phi_{P_I|R_1}\left(\omega R_1 |\, R_1\right)\right] \tag{2.5}$$

$$= \mathbb{E}_{R_1}\left[\exp\left(i\omega\eta R_1\right)\exp\left(R_1 \times \int_{u=1}^{\infty}\left(\exp\left(\frac{i\omega}{u}\right) - 1\right)\lambda\left(uR_1\right)du\right)\right], \tag{2.6}$$

where $\mathbb{E}_{R_1}[\cdot]$ ***is the expectation w.r.t. the random variable*** R_1, ***which is the distance of the BS closest to the origin, and with the probability density function (p.d.f.)*** $f_{R_1}(r) = \lambda(r) \times \mathrm{e}^{-\int_{s=0}^{r} \lambda(s) ds}$, $r \geq 0$.

Proof. See Appendix 2.8.4. □

Now, we take a minor detour from studying the canonical SCS and consider a 1-D SCS affected by i.i.d. random fading factor with unity mean exponential distribution. For this case, the following theorem gives a simpler expression for the tail probability of SINR when $\gamma \geq 1$.

Theorem 4. ***For a 1-D SCS with a BS density function*** $\bar{\lambda}(r)$, $\frac{1}{R}$ ***path-loss model, unity transmission power, i.i.d. unity mean exponential random variable for fading at each BS, the tail probability of SINR for*** $\gamma \geq 1$ ***is given by***

$$\mathbb{P}(\{\mathrm{SINR} > \gamma\}) = \int_{r=0}^{\infty} \bar{\lambda}(r) \exp\left(-\eta\gamma r - \int_{s=0}^{\infty} \frac{\bar{\lambda}(s)\, ds}{1 + (\gamma r)^{-1} s}\right) dr. \tag{2.7}$$

Proof. See Appendix 2.8.5. □

The above result can be used for a canonical SCS under certain conditions. We briefly investigate this situation for which we define $\mathcal{L}(f(x), s) \triangleq \int_{x=0}^{\infty} \mathrm{e}^{-sx} f(x)\, dx$ to be the unilateral Laplace transform of the function $f(x)$.

Lemma 2. A canonical SCS with BS density function $\lambda(r)$ is equivalent to the 1-D SCS considered in Theorem 4 if there exists a continuous BS density function $\bar{\lambda}(r) \geq 0$ such that

$$\mathcal{L}\left(\bar{\lambda}(x), \frac{1}{r}\right) = \int_{s=0}^{r} \lambda(s)\, ds, \ \forall\, r \geq 0. \tag{2.8}$$

As a result, the tail probability of SINR for such canonical SCS is equal to (2.7).

Proof. The above result is obtained as a consequence of Theorem 2 which says that the two SCSs considered above are equivalent if $\lambda(r) = \mathbb{E}_{\Psi}\left[\Psi \bar{\lambda}(r\Psi)\right]$, $\forall\, r \geq 0$, where Ψ is the unity mean exponential random variable representing the fading factors in the latter SCS. By rewriting the expectation in the above equation as an integral and simplifying, we obtain

$$\lambda(r) = \int_{x=0}^{\infty} \frac{d}{dr}\left(\mathrm{e}^{-\frac{x}{r}}\right) \bar{\lambda}(x)\, dx \overset{(a)}{=} \frac{d}{dr}\left(\mathcal{L}\left(\bar{\lambda}(x), \frac{1}{r}\right)\right),$$

where (a) is obtained by exchanging the order of integration and differentiation, which is valid since $\bar{\lambda}(r)$ is continuous. Further, the resultant integral can be written in terms of the Laplace transform of $\bar{\lambda}(x)$. Using $\mathcal{L}\left(\bar{\lambda}(x), \frac{1}{r}\right)\big|_{r=0} = 0$ as the initial condition, the above differential equation can be solved to obtain the condition for equivalence between the two SCSs to be (2.8). □

The following shows examples for the existence of BS density functions $\left(\lambda(r), \bar{\lambda}(r)\right)$ that satisfy the condition in (2.8).

Example 1. Polynomial - polynomial equivalence: The pair $\left(\lambda(r), \bar{\lambda}(r)\right) = \left(\alpha_1 r^{\delta}, \alpha_2 r^{\delta}\right)$ satisfy the condition in (2.8) as long as $\delta + 1 > 0$, and $\alpha_1 = \alpha_2 \Gamma(1+\delta) > 0$, where $\Gamma(\cdot)$ is the Gamma function.

Example 2. Rational - exponential equivalence: The pair $\left(\lambda(r), \bar{\lambda}(r)\right) = \left(\frac{1}{(1+\alpha r)^2}, \mathrm{e}^{-\alpha r}\right)$, $\forall\ \alpha > 0$ satisfy the condition in (2.8).

We will see in the following section that the equivalent 1-D BS density function for the homogeneous l-D SCSs are polynomial functions, and using Example 1 and Theorem 4, simple analytical expressions for the tail probability of SINR are obtained.

The results presented in this section can together accurately characterize the SINR in any arbitrary SCS with arbitrary transmission and channel characteristics. The semi-analytical expressions presented above might seem unwieldy at the first glance. But it turns out that several insightful results can be extracted from this representation for a special class of SCSs that are practically important and popular in literature. This special class of SCSs are the homogeneous l-D SCSs, $l \in \{1, 2, 3\}$, and we dedicate the next section to studying this special class in detail.

2.4 Homogeneous l-D SCS

In this section, we focus on the analysis of the homogeneous l-D SCSs with a power-law path-loss model $h(R) = R^{\varepsilon}$. The homogeneous l-D SCS is the most widely used stochastic geometric model in the literature for modeling arrangement of node locations. Especially, its validity in the study of the small-cell networks is extremely appealing. Moreover, this model has the advantage of being analytically amenable for a variety of situations that are of great importance in the modeling and analysis of any type of wireless

network. The results provide several insights about such large-scale networks that can be applied in the design of actual networks in practice. Next, we apply the results of the previous section to the case of the homogeneous l-D SCS.

Corollary 1. ***[of Proposition 1] A homogeneous l-D SCS with a constant BS density λ_0 over the entire space is equivalent to the 1-D SCS with a BS density function $\lambda(r) = \lambda_0 b_l r^{l-1},\ \forall\ r \geq 0$, where $b_1 = 2$, $b_2 = 2\pi$, $b_3 = 4\pi$.***

This is easily proved by letting $d(x)$, $d(r,\theta)$, and $d(r,\theta,\phi)$ be λ_0 in Proposition 1.

For the power-law path-loss model $h(R) = R^{\varepsilon}$, we have the following equivalent SCS using Corollary 1 and Theorem 2.

Corollary 2. ***[of Theorem 2] A homogeneous l-D SCS with BS density λ_0 and path-loss model $\frac{1}{R^{\varepsilon}}$ is equivalent to the 1-D SCS with a BS density function $\bar{\lambda}(r) = \lambda_0 \frac{b_l}{\varepsilon} r^{\frac{l}{\varepsilon}-1},\ r \geq 0$ and the path-loss model $\frac{1}{R}$.***

Next, we characterize the effect of random transmission powers and fading factors, i.i.d. across BSs in the homogeneous l-D SCS.

Corollary 3. ***[of Theorem 2] A homogeneous l-D SCS with BS density λ_0, power-law path-loss model $\left(\frac{1}{R^{\varepsilon}}\right)$, random transmission powers and fading factors that have arbitrary joint distribution and are i.i.d. across all the BSs is equivalent to another homogeneous l-D SCS with a BS density $\bar{\lambda} = \lambda_0 \mathbb{E}\left[(K\Psi)^{\frac{l}{\varepsilon}}\right]$, same power-law path-loss model $\left(\frac{1}{R^{\varepsilon}}\right)$, unity transmission power and unity fading factor at each BS, where K, Ψ have the same joint distribution as the transmission power and fading factors of the original homogeneous l-D SCS and $\mathbb{E}[\cdot]$ is the expectation operator w.r.t. K and Ψ, as long as $\mathbb{E}\left[(K\Psi)^{\frac{l}{\varepsilon}}\right] < \infty$.***

Proof. Using Corollary 1 and Corollary 2, we obtain a 1-D SCS with BS density function $\tilde{\lambda}(r) = \lambda_0 \frac{b_l}{\varepsilon} r^{\frac{l}{\varepsilon}-1}$, with a path-loss model $\frac{1}{R}$. Now, from Theorem 2, the equivalent canonical SCS has a BS density function $\hat{\lambda}(r) = \mathbb{E}\left[(K\Psi)^{\frac{l}{\varepsilon}}\right] \times \tilde{\lambda}(r)$. As a result, this can be traced back to the scaling of the BS density of the original homogeneous l-D SCS by $\mathbb{E}\left[(K\Psi)^{\frac{l}{\varepsilon}}\right]$. □

As a result, we can restrict our attention to SINR characterization when all the BSs of the l-D SCS have unity transmission power and fading factors. Now, we give the expression for the tail probability of SINR in a homogeneous l-D SCS.

Corollary 4. ***[of Theorem 3] In a homogeneous l-D SCS with a BS density λ_0, unity transmission power and fading factor at each BS, if the path-loss exponent of the power-law path-loss model satisfies $\varepsilon > l$, the characteristic function of the reciprocal of SINR is given by***

$$\Phi_{\frac{1}{\mathrm{SINR}}}(\omega) \quad = \quad \mathrm{E}_{R_1}\left[\mathrm{e}^{i\omega\eta R_1} \times \mathrm{e}^{\frac{\lambda_0 b_l}{l} R_1^{\frac{l}{\varepsilon}}\left(1-{}_1F_1\left(-\frac{l}{\varepsilon};1-\frac{l}{\varepsilon};i\omega\right)\right)}\right], \tag{2.9}$$

where the p.d.f. of R_1 is $f_{R_1}(r) = \lambda_0 \frac{b_l}{\varepsilon} r^{\frac{l}{\varepsilon}-1} \cdot \mathrm{e}^{-\lambda_0 \frac{b_l}{l} r^{\frac{l}{\varepsilon}}},\ r \geq 0$. When $\eta = 0$, the SINR is equivalently the signal-to-interference ratio (SIR), and

$$\Phi_{\frac{1}{\mathrm{SIR}}}(\omega) \quad = \quad \frac{1}{{}_1F_1\left(-\frac{l}{\varepsilon};1-\frac{l}{\varepsilon};i\omega\right)}, \tag{2.10}$$

where ${}_1F_1(\dots)$ is the confluent hypergeometric function of the first kind [41]. The tail probability of SINR is given by (2.4).

Proof. From Corollary 2, the SINR distribution is equivalent to the canonical SCS with BS density function $\lambda(r) = \lambda_0 \frac{b_l}{\varepsilon} r^{\frac{l}{\varepsilon}-1},\ r \geq 0$. Now, by solving for (2.6), in Theorem 3, we obtain (2.9). Further, the expectation in (2.9) reduces to (2.10). □

Due to Corollary 3, the homogeneous l-D SCS satisfies the conditions in Theorem 4 and hence a simple expression for the tail probability of SINR for $\gamma \geq 1$ can be derived below.

Corollary 5. [of ***Theorem 4***] For a homogeneous l-D SCS with BS density λ_0, path-loss model $\frac{1}{R^\varepsilon},\ \varepsilon > l$, with unity transmission power and fading factor at each BS, the tail probability of SINR for $\gamma \geq 1$ is

$$\mathbb{P}(\{\mathrm{SINR} > \gamma\}) \quad = \quad \int_{r=0}^{\infty} \frac{\lambda_0 b_l r^{l-1}}{\Gamma\left(1+\frac{l}{\varepsilon}\right)} \exp\left(-\eta\gamma r^{\varepsilon} - \frac{\lambda_0 b_l r^l \pi \gamma^{\frac{l}{\varepsilon}}}{\varepsilon\Gamma\left(1+\frac{l}{\varepsilon}\right)\sin\left(\frac{l\pi}{\varepsilon}\right)}\right) dr, \tag{2.11}$$

and when $\eta = 0$, the tail probability of SIR is

$$\mathbb{P}(\{\mathrm{SIR} > \gamma\}) \quad = \quad \frac{\sin\left(\frac{l\pi}{\varepsilon}\right)\gamma^{-\frac{l}{\varepsilon}}}{\left(\frac{l\pi}{\varepsilon}\right)} = \mathrm{sinc}\left(\frac{l}{\varepsilon}\right)\gamma^{-\frac{l}{\varepsilon}}. \tag{2.12}$$

Proof. Due to Corollary 3, the homogeneous l-D SCS is equivalent to another homogeneous l-D SCS with the same path-loss model and transmission powers as the former, and with a BS density $\frac{\lambda_0}{\Gamma\left(1+\frac{l}{\varepsilon}\right)}$ and i.i.d. unity mean exponential random fading factors at each BS. Using Corollary 2, the BS density function of the 1-D SCS with $\frac{1}{R}$ path-loss model that is equivalent to the latter homogeneous l-D SCS is $\bar{\lambda}(r) = \frac{\lambda_0 b_l r^{\frac{l}{\varepsilon}-1}}{\varepsilon\Gamma\left(1+\frac{l}{\varepsilon}\right)},\ r \geq 0$. An alternate approach to obtain the expression for $\bar{\lambda}(r)$ is using Lemma 2 and Example 1.

For the 1-D SCS, Theorem 4 is used to obtain the expression for the tail probability of SINR to be (2.11), using the identity $\int_{s=0}^{\infty} \frac{s^{\frac{l}{\varepsilon}-1} ds}{1+(\gamma r)^{-1} s} = \frac{\pi(\gamma r)^{\frac{l}{\varepsilon}}}{\sin\left(\frac{l\pi}{\varepsilon}\right)}$. Finally, (2.12) is obtained by substituting $\eta = 0$ in (2.11) and evaluating the outer integral. This completes the proof. □

Using Corollaries 4 and 5, the expression for the tail probability of SINR in a homogeneous l-D SCS with random transmission power and fading factor with an arbitrary joint distribution that are i.i.d. across the BSs of the SCS can be obtained by merely scaling the BS density λ_0 with an appropriate constant that is given in Corollary 3.

The following lemma shows another interesting property of the SINR distribution in a homogeneous l-D SCS.

Lemma 3. ***The SINR distribution in a homogeneous l-D SCS with a constant BS density λ_0, path-loss model $\frac{1}{R^{\varepsilon}}$, unity transmission power and fading factor at each BS with a background noise power η is the same as in a homogeneous l-D SCS with the same path-loss model, unity BS density, unity transmission power and fading factor at each BS and a background noise power $\eta\lambda_0^{-\frac{\varepsilon}{l}}$. Equivalently,***

$$\mathrm{SINR}|_{(\lambda_0,\varepsilon,\eta)} \quad =_{\mathrm{st}} \quad \mathrm{SINR}|_{\left(1,\varepsilon,\eta\lambda_0^{-\frac{\varepsilon}{l}}\right)}. \tag{2.13}$$

Proof. $\mathrm{SINR}|_{(\lambda_0,\varepsilon,\eta)} \overset{(a)}{=} \left.\frac{R_1^{-\varepsilon}}{\sum_{k=2}^{\infty} R_k^{-\varepsilon}+\eta}\right|_{\lambda_l(r)} \overset{(b)}{=}_{\mathrm{st}} \left.\frac{(\alpha R_1)^{-\varepsilon}}{\sum_{i=2}^{\infty}(\alpha R_i)^{-\varepsilon}+\eta\alpha^{-\varepsilon}}\right|_{\lambda_l(r)} \overset{(b)}{=}_{\mathrm{st}} \left.\frac{\left(R_1'\right)^{-\varepsilon}}{\sum_{k=2}^{\infty}\left(R_k'\right)^{-\varepsilon}+\bar{\eta}}\right|_{\frac{1}{\alpha}\lambda_l\left(\frac{r}{\alpha}\right)}$, where $\alpha = \lambda_0^{\frac{1}{l}}$; $\bar{\eta} = \eta\alpha^{-\varepsilon}$; (a) is obtained by expressing SINR in terms of the equivalent 1-D SCS with $\lambda_l(r) = \lambda_0 b_l r^{l-1},\ r \geq 0$, and multiplying numerator and denominator with $\alpha^{-\varepsilon}$; (b) follows from Corollary 6; and finally, (2.13) is obtained by noting that the 1-D SCS with BS density function $\frac{1}{\alpha}\lambda_l\left(\frac{r}{\alpha}\right)$ in (b) corresponds to a homogeneous l-D SCS with BS density 1. □

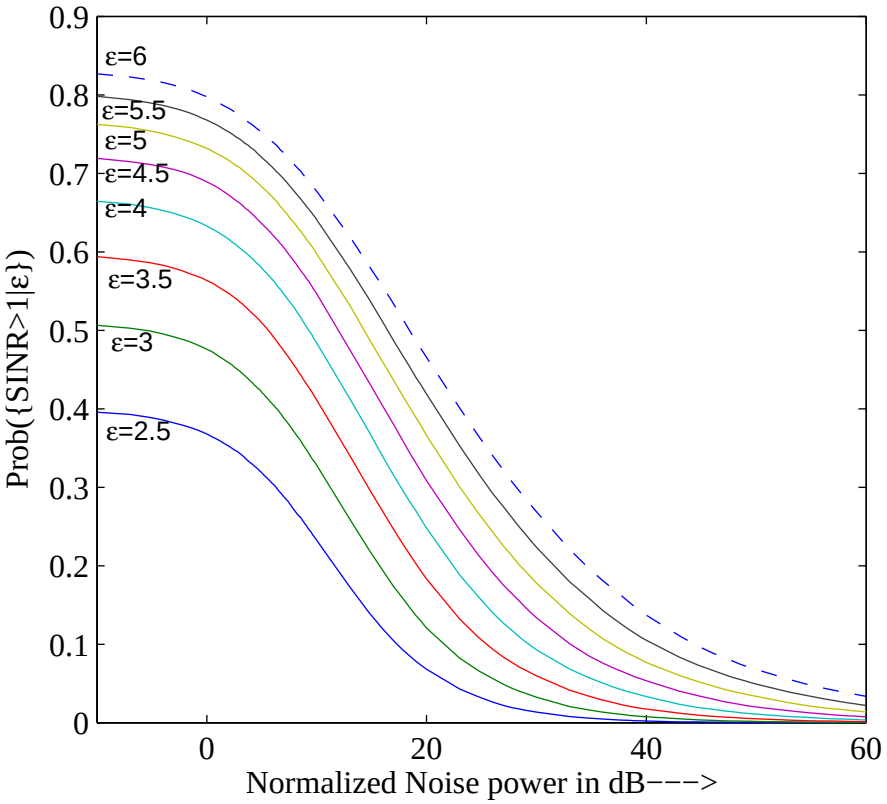

Figure 2.2: Plot of Prob $(\{\text{SINR} > 1\})$ vs Noise power

Therefore, it is sufficient to analyze a ***homogeneous*** l-D SCS with BS density $\lambda_0 = 1$ and maintain a lookup table for the tail probability of SINR for different values of the noise powers and path-loss exponents using (2.4). The lookup table is presented for a ***homogeneous*** 2-D SCS in Figure 2.2 as a plot of $\mathbb{P}(\{\text{SINR} > 1\})$ against noise powers for different values of path-loss exponents. Further, in a ***homogeneous*** l-D SCS with a high BS density λ_0, the equivalent noise power $\eta\lambda_0^{-\frac{\varepsilon}{l}}$ is small according to Lemma 3. Hence, in an *interference-limited system* (large λ_0), the signal quality can be measured in terms of SIR. Further remarks on SIR of a homogeneous l-D SCS based on Corollaries 4 are given below.

Remark 1. The characteristic function of the $\frac{1}{\text{SIR}}$ does not depend on λ_0, and hence the tail probability of SIR at a MS in a homogeneous l-D SCS does not depend on λ_0.

Remark 2. From Corollary 1 and Remark 1, the tail probability of SIR is invariant to random transmission powers and fading factors with arbitrary joint distribution and i.i.d. across the BSs.

Remark 3. The expression for the characteristic function of $\frac{1}{\text{SIR}}$ for a *homogeneous* 2-D and 3-D SCS is same as that of a *homogeneous* 1-D SCS with path-loss exponents $\frac{\varepsilon}{2}$ and $\frac{\varepsilon}{3}$, respectively.

Remark 3 helps build an intuition of why the *homogeneous* 1-D SCS has a higher tail probability of SIR than *homogeneous* 2-D and 3-D SCSs. As the path-loss exponent decreases, the BSs farther away from the MS have a greater contribution to the total interference power at the MS, and this leads to a poorer SIR at the MS and a smaller tail probability. Next, Figure 2.3a shows the tail probabilities of SIR in a *homogeneous* 1-D SCS as a function of the path-loss exponent ε; the squares ($\square$) and the pluses ($+$) represent the values computed analytically and by Monte-Carlo simulations, respectively. According to Remark 3, the same figure can be used for 2-D and 3-D systems using the scaling of $\frac{\varepsilon}{2}$, and $\frac{\varepsilon}{3}$ respectively.

In the following, we present an approximation to SIR based on modeling the interference due to the strongest few BSs accurately and the interference due to the rest by their ensemble average. The approximation is expected to be tight for low BS densities. Due to Remark 1, the same approximation will be tight for all BS densities. Now, we define the so-called *few BS approximation* and derive closed form expressions for the tail probability of SIR at MS in a *homogeneous* l-D SCS for both the SIR regions $[0, 1)$ and $[1, \infty)$.

Definition 4. *The few BS approximation* corresponds to modeling the total interference power at the MS in a SCS as the sum of the contributions from the strongest few interfering BSs and an ensemble average of the contributions of the rest of the interfering BSs.

Recall that the total interference power is $P_I = \sum_{i=2}^{\infty} R_i^{-\varepsilon}$, where $\{R_i\}_{i=1}^{\infty}$ is the set of distances of BSs arranged in the ascending order of their separation from the MS. The arrangement also corresponds to the descending order of their contribution to P_I, due to path-loss. In the few BS approximation, P_I is approximated by $\tilde{P}_I(k) = \sum_{i=2}^{k} R_i^{-\varepsilon} + \mathbb{E}\left[\sum_{i=k+1}^{\infty} R_i^{-\varepsilon} \middle| R_k\right]$, for some k, where $\mathbb{E}[\cdot]$ is the expectation operator and corresponds to the ensemble average of the contributions of BSs beyond R_k. The SIR at the MS obtained by the few BS approximation is denoted by SIR_k. The expectation is calculated as follows.

Lemma 4. ***For a homogeneous l-D SCS, with BS density λ_0 and $\varepsilon > l$, for*** $k = 1,\ 2,\ 3, \cdots$,

$$\mathbb{E}\left[\sum_{i=k+1}^{\infty} R_i^{-\varepsilon} \middle| R_k\right] = \frac{\lambda_0 b_l R_k^{l-\varepsilon}}{\varepsilon - l}. \tag{2.14}$$

Proof. Firstly, use Corollary 1 to reduce the l-D SCS to an equivalent 1-D SCS with BS density function $\lambda(r) = \lambda_0 b_l r^{l-1},\ \forall\ r \geq 0$. Next, given k, using the Superposition theorem of Poisson processes, the original Poisson process is equivalent to the union of two independent Poisson processes defined in the non-overlapping regions $[0, R_k]$ and (R_k, ∞), respectively, with the same BS density function. Now, using Campbell's theorem [6, Page 28] to the Poisson process defined in (R_k, ∞), we obtain (2.14). □

The following theorem gives the SIR tail probability approximation, using $k = 2$.

Theorem 5. ***In a homogeneous l-D SCS with BS density λ_0 and path-loss exponent ε, satisfying $\varepsilon > l$, the tail probability of*** SIR_2 ***at the MS is given by***

$$\mathbb{P}(\{\mathrm{SIR}_2 > \gamma\}) = \begin{cases} \gamma^{-\frac{l}{\varepsilon}} C_{\frac{\varepsilon}{l}}, & \gamma \geq 1 \\ 1 - e^{-u(\gamma)}(1 + u(\gamma)) + \gamma^{-\frac{l}{\varepsilon}} D_{\frac{\varepsilon}{l}}(\gamma), & \gamma \leq 1 \end{cases}, \tag{2.15}$$

where $C_{\frac{\varepsilon}{l}} = G(0)$ ***and*** $D_{\frac{\varepsilon}{l}}(\gamma) = G(u(\gamma))$ ***with*** $G(a) = \int_{v=a}^{\infty} \frac{v e^{-v}}{\left(1 + v\left(\frac{\varepsilon}{l} - 1\right)^{-1}\right)^{\frac{l}{\varepsilon}}} dv$, ***and*** $u(\gamma) \equiv \left(\frac{\varepsilon}{l} - 1\right)\left(\frac{1}{\gamma} - 1\right)$.

Proof. See Appendix 2.8.6. □

The above approximation can be further tightened by recalling that we already have a simple closed-form expression in (2.12) for the tail probability of SIR for values in the range $[1, \infty)$. Hence, the new approximation is as follows

$$\mathbb{P}\left(\{\mathrm{SIR}_{approx} > \gamma\}\right) = \begin{cases} \mathbb{P}\left(\{\mathrm{SIR} > \gamma\}\right) & , \ \gamma \geq 1 \\ \mathbb{P}\left(\{\mathrm{SIR}_2 > \gamma\}\right) & , \ \gamma \leq 1 \end{cases}, \tag{2.16}$$

where the relevant quantities are obtained from (2.12) and Theorem 5.

Notice that $\mathbb{P}\left(\{\mathrm{SIR} > \gamma\}\right) = \frac{\mathrm{sinc}\left(\frac{l}{\varepsilon}\right)}{C_{\frac{\varepsilon}{l}}} \mathbb{P}\left(\{\mathrm{SIR}_2 > \gamma\}\right)$ for $\gamma \geq 1$. Figure 2.3a shows that the few BS approximation ($\bullet$) closely follows the actual behavior ($\square$). Figure 2.3b shows the comparison of the tail probabilities of SIR (computed using Corollaries 4 and 5) and SIR_2 for a *homogeneous* 2-D SCS with path-loss exponent 4. Notice that the gap between the two tail probability curves is negligible in the region $\gamma \in [0, 1]$, and further, both the curves are straight lines parallel to each other in the region $\gamma \in [1, \infty)$, when the tail probability is plotted against γ, both in the logarithmic scale. This shows that the few BS approximation characterizes the signal quality in closed form and is a good approximation for the actual SIR.

Now, having characterized the SIR for the homogeneous l-D SCS, we look closely into what happens when $\varepsilon \leq l$. We will restrict ourselves to the case when $l = 2$, and the steps are similar for $l = 1$, and $l = 3$.

Theorem 6. ***A homogeneous 2-D SCS with BS density*** λ, ***where the signal decays according to a power-law path-loss function with a path-loss exponent*** $\varepsilon \leq 2$, ***the SIR at the MS is 0 with probability 1.***

Proof. See Appendix 2.8.7 for the case $\varepsilon = 2$. From [27, Corollary 5], $\mathbb{P}\left(\{\mathrm{SIR} > \gamma\}\right)|_{\varepsilon<2} \leq \mathbb{P}\left(\{\mathrm{SIR} > \gamma\}\right)|_{\varepsilon=2} = 0, \ \forall \ \gamma \geq 0$. Hence we have proved the above result. □

Note that once we have characterized the SINR distribution, the outage probability at the MS is known. The event that the MS is in coverage is given by $\{\mathrm{SINR} > \gamma\}$, where γ is the SINR threshold that the MS should satisfy to be in coverage. Consequently, the coverage probability, $\mathbb{P}\left(\{\mathrm{SINR} > \gamma\}\right)$ is precisely the tail probability of SINR computed at γ. Next, we study the average ergodic reception

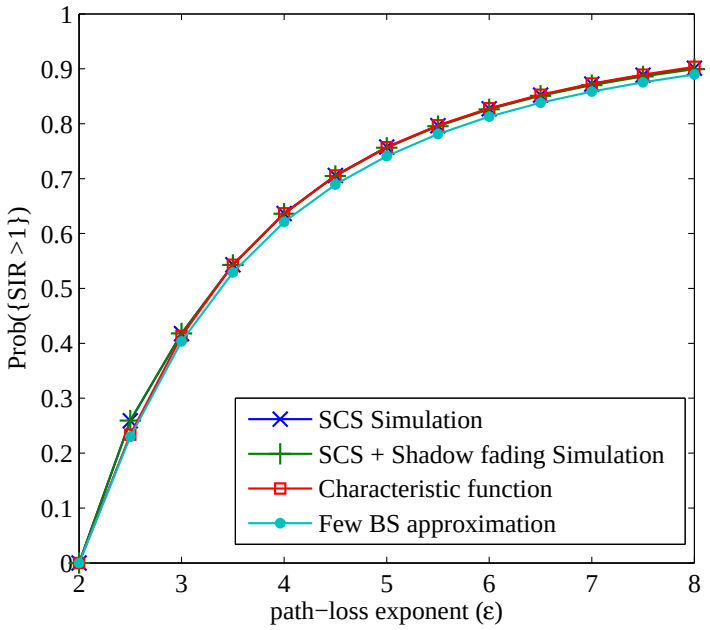

(a)

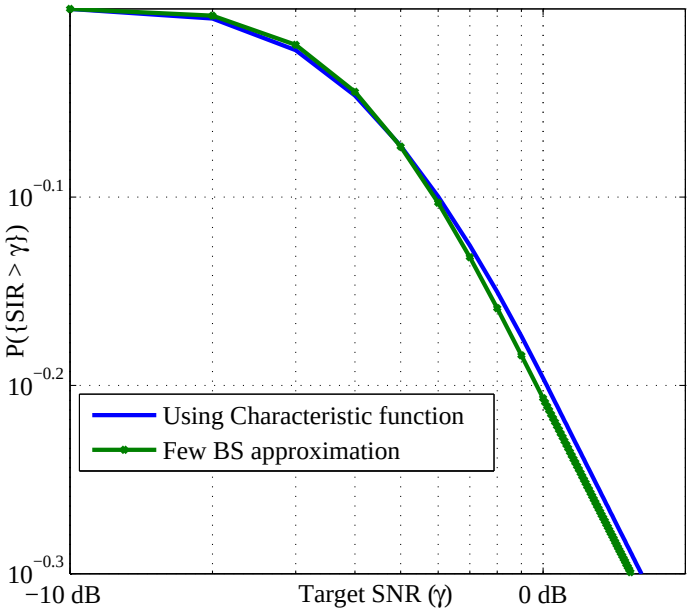

(b)

Figure 2.3: (a) Comparison of Simulations with the analytical results, (b) Homogeneous 2-D SCS: Comparing exact SIR and the few BS approximation for path-loss $\varepsilon = 4$.

rate for an MS in coverage. This quantity, termed as the coverage conditional average rate, is given by $\mathcal{R} = \mathbb{E}\left[\log\left(1+\text{SINR}\right)|\left\{\text{SINR} > \gamma\right\}\right]$ and is the average of the instantaneous rate achievable at the MS when the interference is considered as noise. The coverage conditional average rate at the MS simplifies to the following expression.

$$\mathcal{R} \quad = \quad \log\left(1+\gamma\right) + \int_{t=\Gamma}^{\infty} \frac{\mathbb{P}\left(\left\{\text{SINR} > t\right\}\right)}{\left(1+t\right)\mathbb{P}\left(\left\{\text{SINR} > \gamma\right\}\right)} dt.$$

As a result, based on Proposition 1 and Theorems 1 - 4, we can compute the coverage conditional average rate for any SCS. Specifically, in the interference-limited case, the following proposition provides the expression for a homogeneous l-D SCS and when the popular power-law path-loss model is assumed. For this case, the SIR characteristics are invariant to the randomness in the transmission powers and the fading factors due to Remark 2. Hence, without loss of generality, we restrict our attention to the case of constant transmission powers at all BSs and no fading.

Proposition 2. ***The ergodic average rate at the MS in a homogeneous 2-D SCS under the power-law path-loss model, with constant transmission powers at all BSs and no fading is given by***

$$\mathcal{R} = \log\left(1+\gamma\right) + \int_{x=\gamma}^{\alpha} \frac{\mathbb{P}\left(\left\{\text{SIR} > x\right\}\right)}{\mathbb{P}\left(\left\{\text{SIR} > \gamma\right\}\right)\left(1+x\right)} dx + \alpha^{-\frac{2}{\varepsilon}} \frac{\varepsilon}{2} \cdot {}_2F_1\left(1, \frac{2}{\varepsilon}; 1+\frac{2}{\varepsilon}; -\alpha^{-1}\right),$$

where $\alpha = \max\left(\gamma, 1\right)$, ***where*** ${}_2F_1\left(1, \frac{2}{\varepsilon}; 1+\frac{2}{\varepsilon}; -\alpha^{-1}\right)$ ***is the Gauss hypergeometric function and the probabilities are computed using*** (4). ***Note that for*** $\gamma \geq 1$, ***the middle term drops out.***

2.5 Numerical Example and Discussion

In the first example, we consider a homogeneous 2-D SCS with $\lambda = 0.01$, a power-law path-loss model with path-loss exponent 4, and a background noise power of -10 dB and unity transmission powers. We compare the SINR tail probabilities for several cases where we vary the distributions of the fading factors as well as the background noise power. Notice in Figure 2.4a that in the case when there is background noise, the distribution of the fading greatly affects the SINR performance at the MS. We consider two examples for the i.i.d. fading factors: one of them has an exponential distribution and the other has a log-normal

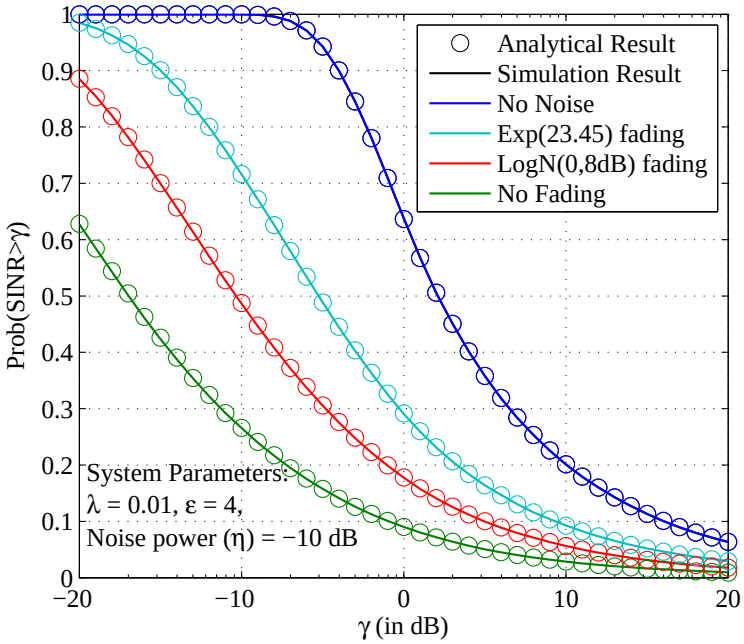

(a)

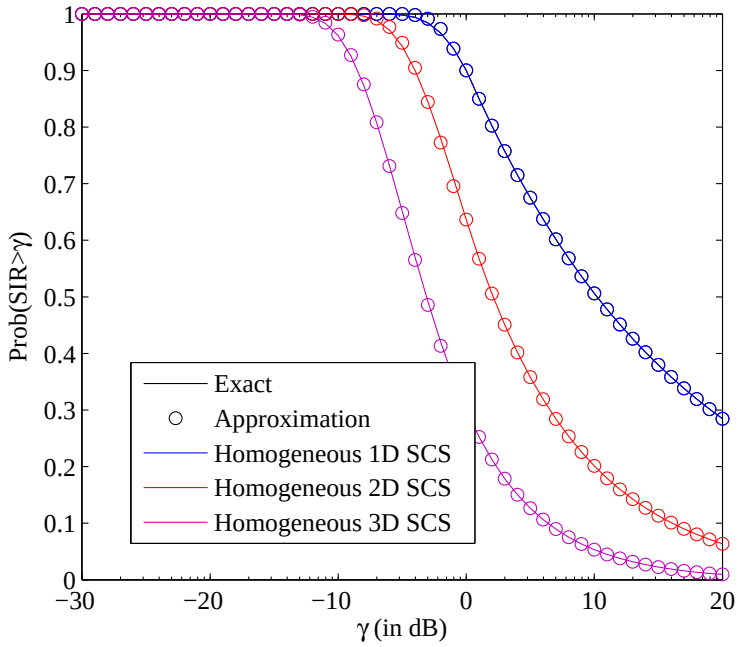

(b)

Figure 2.4: (a) Comparing the SINR distributions for various fading distributions and noise profiles (Exp(23.45) refers to an exponential random variable with mean 23.45, logN(0,8dB) refers to a log-normal random variable whose natural logarithm has a mean and variance of 0 and 8 dB, respectively.), (b) Evaluating the tightness of the few-BS approximation

distribution, and keep the same mean (=23.45) for both the cases, for a fair comparison. In the presence of the background noise, the MS sees a better SINR performance for the exponential case compared to the log-normal case and the SINR performance in both is far more superior than that without fading. This is justified by Corollary 3 and Corollary 3 where the equivalent homogeneous 2-D SCS with unity BS density has an equivalent background noise power for the log-normal fading case that is strictly greater than that for the exponential fading distributions. Further, in the no noise case, the SINR performance is invariant to the fading distribution and is the same as in the no fading case. This is also depicted in Figure 2.4a.

In Figure 2.4b, we assess the few-BS approximation for the SIR characterization in the homogeneous l-D SCS. This figure shows that the SIR approximation derived in Section 2.4 based on the few-BS approximation (Equation (2.16)) closely follows the exact SIR characterization. Moreover, this relationship holds for a wide range of scenarios of interest such as for arbitrary fading and transmission power distributions, and for all BS densities. In the following section, we discuss the usage of the results obtained thus far in the analysis of other useful wireless communication scenarios.

2.6 Applications in wireless communications

We discuss several scenarios where the wireless communication systems are modeled by the *homogeneous* l-D SCS with BS density λ_0, where $l = 1$, 2, and 3 correspond to highway, suburban, and dense urban deployments, respectively.

2.6.1 BSs with sectorized antennas

In this example, we give a practical scenario where the transmission powers of the BSs are i.i.d. random variables. For example, consider the case where each BS has an ideal sectorized antenna with gain G and beam-width θ, such that BS's antenna faces the MS with probability $\frac{\theta}{2\pi}$, in which case $K_i = G$, and otherwise $K_i = 0$. In this case, in the absence of fading, from Corollary 3, $\overline{\lambda}_0 = \lambda_0 G^{\frac{2}{\varepsilon}} \frac{\theta}{2\pi}$ is the BS density of the equivalent *homogeneous* l-D SCS.

2.6.2 Multiple Access Techniques

Next, we study the signal quality at the MS in a cellular system employing different multiple access techniques. For example, in a code division multiple access (CDMA) system, the goal is to maintain a constant voice signal quality at the MS, which is done by power control. This goal is achievable by having the serving BS increase its transmission power by $\alpha = \gamma \mathrm{SIR}^{-1}$, where α is the power control factor or the processing gain, SIR is the instantaneous signal quality at the MS, and γ is the desired constant signal quality. In this formulation, α for each BS is a random variable and in general, the α's of nearby BSs are correlated. But if the correlation is small, the SIR distribution computed here enables radio designers to approximately model the power needs to communicate with a MS in a SCS. In another formulation, if α is a constant factor by which the power of the serving BS is improved, its effect on the tail probability SIR at the MS is obtained by straightforward manipulations as $\mathbb{P}\left(\{\alpha \times \mathrm{SIR} > \gamma | \, \varepsilon, l\}\right) = \mathrm{sinc}\left(\frac{l}{\varepsilon}\right)\left(\frac{\gamma}{\alpha}\right)^{-\frac{l}{\varepsilon}}$ if $\gamma > \alpha$.

Then, consider frequency division multiple access (FDMA) and time division multiple access (TDMA) based cellular systems. Let the available spectrum (in frequency for FDMA and in time-slots for TDMA) be divided into N channel reuse groups (CG), and indexed as $k = 1, 2, \cdots, N$. Then, each BS is assigned one of the N CGs, such that the k^{th} CG is assigned with probability p_k. In such a system, the MS chooses a CG that corresponds to the best SIR; the BS in the CG that corresponds to the strongest received power is the *desired* BS, and the MS chooses it as the serving BS. The SIR at the MS in such a SCS is of interest to us. Note that this *homogeneous* l-D SCS is equivalent to N independent *homogeneous* l-D SCSs with constant BS densities $\lambda_0 p_1, \cdots, \lambda_0 p_N$, by the properties of Poisson point processes. The tail probability of SIR at the MS in such a system is given by $\mathbb{P}\left(\{\mathrm{SIR} > \gamma | \, \varepsilon, N\}\right) = 1 - \left[1 - \mathbb{P}\left(\{\mathrm{SIR} > \gamma | \, \varepsilon\}\right)\right]^N$, where the tail probability on the right hand side is computed using Corollary 4.

2.6.3 Cognitive Radios

In cognitive radio technology, the cognitive radio devices (or *secondary users*) opportunistically operate in licensed frequency bands occupied by *primary users*. The interference caused by *secondary user* transmissions is harmful for *primary users* operation, and is not acceptable beyond certain limits. Studying the nature of these interferences and formulating methods for addressing them has been an active area of

research (see [42–45]). The results in this chapter are a rich source of mathematical tools for such studies. In [28, 46, 47], we have extensively applied the ideas and results developed here to understand the role of cooperation between the *secondary users* in ensuring that the interference caused by the *secondary users* are within the acceptable limits. The *secondary users* are modeled analogous to BS placement in *homogeneous* 1-D and 2-D SCS, and the tail probability of $\frac{C}{I}$ at the *primary user* is characterized. Further, in the context of radio environment map (REM, [28, and references therein]), we have highlighted the practical significance of the study of 1-D SCS.

2.6.4 Overlay Networks

The modern cellular communication network is a complex overlay of heterogeneous networks, such as macrocells, microcells, picocells and femtocells. This complex overlay network is seldom studied as is, due to the analytical intractabilities. In [14, 48], cellular systems consisting of macrocell and femtocell networks are analyzed. Using the results in this chapter, the cumulative effect of all the networks constituting the overlay network, on the signal quality at the MS can be studied. A detailed study on this is set aside as a future work, while the preliminary results are presented in [29, 30, 49]. Other efforts on the downlink performance characterization for heterogeneous networks can be found in [3, 50–55].

2.7 Conclusions

In this chapter, we study the characterization of the SIR and SINR at the MS in shotgun cellular systems where a SCS is defined as a cellular system where the BS deployment in a given region is according to a Poisson point process. A sequence of equivalent SCSs are derived to show that it is sufficient to study the canonical SCS that has unity transmission power and unity fading factors, and a path-loss model of $\frac{1}{R}$. Analytical expressions for the tail probabilities of the SIR and SINR at the MS are obtained for 1-D, 2-D and 3-D SCSs, where the 1-D, 2-D and 3-D SCS are mathematical models for BS deployments along the highway (1-D), in planar regions (2-D) and in urban areas (3-D), respectively. Further, a closed form expression for the tail probability of SIR is derived for the homogeneous cases of 1-D, 2-D and 3-D SCS. The results are applicable for general fading distributions and arbitrary path-loss models. This makes the results useful

for analyzing many different wireless scenarios that are characterized by uncoordinated deployments. The application of the results has been demonstrated in the study of the impact of cooperation between cognitive radios in the low power primary user detection and can be found in [28], and in the study of heterogeneous networks in [29]. Future work will further explore the applications of the SCS model in the context of indoor femtocells, cognitive radios, and multi-tier or overlay networks.

2.8 Appendix

2.8.1 Proof for Path-loss Equivalence Theorem (Theorem 1)

Let $\bar{R} = h(R)$ be the equivalent BS location. Using the *Mapping Theorem* in [6], BS with locations $\bar{R}$ is also a Poisson point process, whose density is obtained below. For any non-homogeneous 1-D Poisson point process, $\mathbb{E}\left[N\left(r+s\right)-N\left(r\right)\right] = \int_r^{r+s} \lambda(z)dz$ is the expected number of occurrences in the interval $(r, r+s)$. Thus,

$$\begin{aligned} \mathbb{E}\left[N\left(r+s\right)-N\left(r\right)\right] &= \mathbb{E}\left[\text{Number of BSs with } \bar{R} \in (r, r+s)\right] \\ &= \mathbb{E}\left[\text{Number of BSs with } R \in \left(h^{-1}\left(r\right), h^{-1}\left(r+s\right)\right)\right] \\ &= \int_{z=h^{-1}(r)}^{h^{-1}(r+s)} \lambda\left(z\right) dz \;=\; \int_{z=r}^{r+s} \frac{\lambda\left(h^{-1}\left(z\right)\right)}{h'\left(h^{-1}\left(z\right)\right)} dz. \end{aligned} \tag{2.17}$$

Hence, the 1-D SCS with path-loss model $\frac{1}{h(R)}$ and a BS density function $\lambda(r)$ is equivalent to the 1-D SCS with path-loss model $\frac{1}{R}$ and BS density function $\bar{\lambda}\left(r\right)$.

2.8.2 Proof for Arbitrary Fading Equivalence Theorem (Theorem 2)

Let $\bar{R} = R\left(K\Psi\right)^{-1}$, where R is the random variable representing the distance from the MS to a BS in the 1-D SCS with a BS density function $\lambda\left(r\right)$, K, Ψ are the transmission power and the fading factor corresponding to the BS, respectively, and $\bar{R}$ is the corresponding equivalent distance. Using the *product space representation* and *Marking Theorem* in [6], $\bar{R}$ also corresponds to the 1-D SCS with a BS density function derived following (2.17) :

$$\mathbb{E}\left[N\left(r+s\right)-N\left(r\right)\right] \overset{(a)}{=} \mathbb{E}_{K,\Psi}\left[\int_{rK\Psi}^{(r+s)K\Psi} \lambda\left(z\right) dz\right] \overset{(b)}{=} \int_r^{(r+s)} \mathbb{E}_{K,\Psi}\left[K\Psi\lambda\left(K\Psi z\right)\right] dz,$$

where (a) is obtained by rewriting the expectation with respect to each realization of Ψ and K, and (b) is obtained by exchanging the order of integration and expectation in (b) as $\mathbb{E}_{K,\Psi}\left[K\Psi\lambda\left(K\Psi z\right)\right] < \infty$. Hence, $\bar{R}'s$ corresponds to the 1-D SCS with a BS density function $\bar{\lambda}\left(r\right) = \mathbb{E}_{K,\Psi}\left[K\Psi\lambda\left(K\Psi r\right)\right]$.

2.8.3 Proof for Corollary 6

Let $\{R_k\}_{k=1}^{\infty}$ correspond to the 1-D SCS with BS density function $\lambda(r)$. Then, since the ordered base station locations R_k's are determined by inter-base station distances, it follows that $\left.\mathrm{SINR}\right|_{\lambda(r)} \overset{(a)}{=} \left.\frac{(aR_1)^{-1}}{\sum_{k=2}^{\infty}(aR_k)^{-1}+\eta}\right|_{\lambda(r)} \overset{(b)}{=}_{\mathrm{st}} \left.\frac{\left(R_1'\right)^{-1}}{\sum_{k=2}^{\infty}\left(R_k'\right)^{-1}+\eta}\right|_{\frac{1}{a}\lambda\left(\frac{r}{a}\right)}$, where the SINR expression is obtained using (2.2) with $h\left(R\right) = R$, (a) is obtained by multiplying the numerator and denominator by $\frac{1}{a}$, $a > 0$ (b) follows from from the properties of Poisson point processes. Further, $\left\{R_k'\right\}_{k=1}^{\infty}$ in (b) correspond to 1-D SCS with BS density $\frac{1}{a}\lambda\left(\frac{r}{a}\right)$, $a > 0$.

2.8.4 Proof for the Tail Probability of SINR (Theorem 3)

The following are the sequence of step to derive the expression in (2.4).

$$\begin{aligned}\mathbb{P}\left(\{\mathrm{SINR}_{\mathrm{canonical}} > \gamma\}\right) &= \mathbb{P}\left(\left\{\frac{1}{\mathrm{SINR}_{\mathrm{canonical}}} < \frac{1}{\gamma}\right\}\right)\\ &\overset{(a)}{=} \int_{x=0}^{\frac{1}{\gamma}}\int_{\omega=-\infty}^{\infty}\Phi_{\frac{1}{\mathrm{SINR}_{\mathrm{canonical}}}}\left(\omega\right)\mathrm{e}^{-i\omega x}\frac{d\omega}{2\pi}dx,\end{aligned}$$

where (a) is obtained by rewriting the c.d.f. of $\frac{1}{\mathrm{SINR}_{\mathrm{canonical}}}$ in terms of the characteristic function of $\frac{1}{\mathrm{SINR}_{\mathrm{canonical}}}$, where the inner integration computes the p.d.f. of $\frac{1}{\mathrm{SINR}_{\mathrm{canonical}}}$, and the outer integration gives the c.d.f. at $\frac{1}{\gamma}$. When $\gamma = 0$, the above event occurs with probability 1, and otherwise, it is expressed in terms of the integration in (2.4) which is obtained by exchanging the order of integrations in (a), which is valid in this case, and then evaluating the integral w.r.t. x. In the rest of this section, we derive the expression for $\Phi_{\frac{1}{\mathrm{SINR}_{\mathrm{canonical}}}}\left(\omega\right)$, by first noting that $\mathrm{SINR}_{\mathrm{canonical}} = \frac{R_1^{-1}}{\sum_{k=2}^{\infty}R_k^{-1}+\eta}$.

$$\begin{aligned}&\Phi_{\frac{1}{\mathrm{SINR}_{\mathrm{canonical}}}}\left(\omega\right) \overset{(a)}{=} \mathbb{E}_{R_1}\left[\Phi_{\frac{1}{\mathrm{SINR}_{\mathrm{canonical}}}|R_1}\left(\omega|\, R_1\right)\right] \overset{(b)}{=} \mathbb{E}_{R_1}\left[\mathrm{e}^{i\omega\eta R_1}\Phi_{\frac{\sum_{k=2}^{\infty}R_k^{-1}}{R_1^{-1}}\Big|R_1}\left(\omega|\, R_1\right)\right]\\ &= \mathbb{E}_{R_1}\left[\mathrm{e}^{i\omega\eta R_1}\Phi_{\sum_{k=2}^{\infty}R_k^{-1}|R_1}\left(\omega R_1|\, R_1\right)\right] \overset{(c)}{=} \mathbb{E}_{R_1}\left[\mathrm{e}^{i\omega\eta R_1}\mathbb{E}\left[\prod_{k=2}^{\infty}\mathrm{e}^{i\omega R_1 R_k^{-1}}\Big|\, R_1\right]\right]\\ &\overset{(d)}{=} \mathbb{E}_{R_1}\left[\mathrm{e}^{i\omega\eta R_1}\cdot\exp\left(-\int_{r=R_1}^{\infty}\left(1-\mathrm{e}^{i\omega R_1 r^{-1}}\right)\lambda\left(r\right)dr\right)\right],\end{aligned}$$

where (a) is obtained due to the properties of expectation, and R_1 is the random variable for the distance of the closest BS from the origin, (b) is obtained by using the properties of the characteristic functions and noting that in $\frac{1}{\text{SINR}_{\text{canonical}}} = \frac{\sum_{k=2}^{\infty} R_k^{-1} + \eta}{R_1^{-1}}$, conditioned on R_1, the term $\frac{\eta}{R_1^{-1}}$ is a constant and hence separates out as $\mathrm{e}^{i\omega\eta R_1}$ from the original conditional characteristic function expression in (a), (c) is obtained by rewriting the exponential of summation in the characteristic function term in (b) as a product of exponentials, (d) is obtained by first noting that conditioned on R_1, the events in the two disjoint regions $[0,\ R_1]$ and $(R_1,\ \infty)$ are independent of each other, and hence by the Restriction theorem [6, Page 17], all the points beyond R_1, represented by the set $\{R_k\}_{k=1}^{\infty}$ can be regarded to be associated with a Poisson point process in 1-D restricted to the region (R_1, ∞), and with a density function $\lambda(r)$. As a result, now we can apply Campbell's theorem [6, Page 28] to the inner expectation in (c) to obtain (d), which is further simplified to obtain (2.6).

2.8.5 Proof for Theorem 4

Here, we derive the expression for the tail probability of SINR for values greater than or equal to 1. Due to [50, Lemma 1], there exists a unique BS within the 1-D SCS such that $\gamma \geq 1$ holds true. Let the index of this unique BS be i. The expression for the tail probability of SINR is derived as follows.

$$\begin{aligned}
\mathbb{P}\left(\{\text{SINR} > \gamma\}\right) &\overset{(a)}{=} \mathbb{P}\left(\left\{\frac{\Psi_i R_i^{-1}}{\sum_{j=1,\ j\neq i}^{\infty} \Psi_j R_j^{-1} + \eta} > \gamma\right\}\right) \\
&\overset{(b)}{=} \mathbb{E}\left[\exp\left(-\eta\gamma R_i\right) \prod_{j=1,\ j\neq i}^{\infty} \exp\left(-\gamma R_i \Psi_j R_j^{-1}\right)\right] \\
&\overset{(c)}{=} \mathbb{E}\left[\exp\left(-\eta\gamma R_i\right) \exp\left(-\int_{r=0}^{\infty} \left(1 - \mathbb{E}_{\Psi}\left[\mathrm{e}^{-\gamma R_i \Psi r^{-1}}\right]\right) \bar{\lambda}(r)\, dr\right)\right] \\
&\overset{(d)}{=} \mathbb{E}\left[\exp\left(-\eta\gamma R_i\right) \exp\left(-\int_{r=0}^{\infty} \left(1 - \frac{1}{1+\gamma R_i r^{-1}}\right) \bar{\lambda}(r)\, dr\right)\right],
\end{aligned}$$

where (a) is the expression for the tail probability of SINR of the 1-D SCS with BS density $\bar{\lambda}(r)$ for which $\{R_j\}_{j=1}^{\infty}$ is the set of distances of BSs from the MS and 'i' is the index of the unique BS that can satisfy the constraint $\{\text{SINR} > \gamma\}$, (b) is obtained by evaluating the expectation w.r.t. Ψ_i and the expectation operator $\mathbb{E}$ is w.r.t. to all other random variables in (a), (c) is obtained by first conditioning w.r.t. R_i and noting that the Palm distribution of the BSs represented by $\{R_j\}_{j=1,\ j\neq i}^{\infty}$ given a BS at R_i is still a Poisson point process with density function $\bar{\lambda}(r)$, then applying the Marking theorem [6, Page 55] and Campbell's

theorem [6, Page 28] where Ψ is the unity mean exponential random variable, (d) is obtained by evaluating the expectation in (c), and finally (2.7) is obtained by simplifying (d).

2.8.6 Proof for the Few-BS Approximation Theorem (Theorem 5)

First, using Corollary 4, $\mathrm{SIR}_2 = \frac{KR_1^{-\varepsilon}}{\tilde{P}_I(2)}$, with $\tilde{P}_I(2) = KR_2^{-\varepsilon}\left(1 + \frac{\lambda_0 b_l}{\varepsilon - l} R_2^l\right)$. Next, notice that the event $\{\mathrm{SIR}_2 > \gamma\}$ is equivalent to the joint event $\left\{R_1 \le R_2,\ R_1 < \left(\frac{\gamma \tilde{P}_I(2)}{K}\right)^{-\frac{1}{\varepsilon}}\right\}$ and thus, $\mathbb{P}\left(\left\{\frac{C}{I_2} > \gamma\right\}\right) = \mathbb{P}\left(\left\{R_1 \le \min\left(R_2, \left(\frac{\gamma \tilde{P}_I(2)}{K}\right)^{-\frac{1}{\varepsilon}}\right)\right\}\right)$, where

$$\min\left(R_2, \left(\frac{\gamma \tilde{P}_I(2)}{K}\right)^{-\frac{1}{\varepsilon}}\right) = \begin{cases} \left(\frac{\gamma \tilde{P}_I(2)}{K}\right)^{-\frac{1}{\varepsilon}}, & \gamma \ge 1 \\ \left(\frac{\gamma \tilde{P}_I(2)}{K}\right)^{-\frac{1}{\varepsilon}}, & \gamma < 1,\ R_2 > \left(\frac{l \times u(\gamma)}{\lambda_0 b_l}\right)^{\frac{1}{l}} \\ R_2 & , \gamma < 1,\ R_2 \le \left(\frac{l \times u(\gamma)}{\lambda_0 b_l}\right)^{\frac{1}{l}} \end{cases}.$$

Finally, (2.15) is obtained using the joint p.d.f., $f_{R_1,R_2}(r_1, r_2) = (\lambda_0 b_l)^2 (r_1 r_2)^{l-1} \exp\left(-\frac{\lambda_0 b_l}{l} r_2^l\right)$, $0 \le r_1 \le r_2 \le \infty$, due to the properties of Poisson point processes.

2.8.7 Proof for Theorem 6

Let us consider the probability of the event that the interference due to all the BSs beyond the signal BS at a given distance R_1 is below a certain value, say, δ, for the case $\varepsilon = 2$.

$$\begin{aligned} &\mathbb{P}\left(\left\{\sum_{k=2}^{\infty} R_k^{-2} \le \delta \,\middle|\, R_1\right\}\right) = \mathbb{P}\left(\left\{\mathrm{e}^{-s\sum_{k=2}^{\infty} R_k^{-2}} \ge \mathrm{e}^{-s\delta} \,\middle|\, R_1\right\}\right) \\ &\overset{(a)}{\le} \mathrm{e}^{s\delta}\mathbb{E}\left[\mathrm{e}^{-s\sum_{k=2}^{\infty} R_k^{-2}} \,\middle|\, R_1\right] \overset{(b)}{=} \mathrm{e}^{s\delta}\mathrm{e}^{-\lambda\int_{r=R_1}^{\infty}\left(1-\mathrm{e}^{-sr^{-2}}\right)2\pi r dr} \\ &\overset{(c)}{=} \mathrm{e}^{s\delta}\mathrm{e}^{\lambda\int_{r=R_1}^{\infty}\sum_{k=1}^{\infty}\frac{\left(-sr^{-2}\right)^k}{k!}2\pi r dr} \\ &= \mathrm{e}^{s\delta}\mathrm{e}^{-\lambda s 2\pi\cdot\log(r)|_{r=R_1}^{\infty} + \lambda 2\pi\sum_{k=2}^{\infty}\frac{(-s)^k}{k!}\frac{\left(R_1^{2-k\varepsilon}\right)}{k\varepsilon-2}} \\ &= \mathrm{e}^{s\delta} \times 0 \times \mathrm{e}^{\alpha(R_1)} = 0, \end{aligned}$$

where (a) is obtained by applying Markov's inequality, (b) is obtained by applying Campbell's theorem to the homogeneous Poisson point process defined in the 2-D plane beyond R_1 from the origin, (c) is obtained after the Taylor's series expansion of the exponential function in (b), and finally the result is obtained by

noting that the exponential of a sum of functions is a product of exponential and by showing that one of the terms in the product is 0 while the others evaluate to a finite number.

As a result,

$$\begin{aligned}\mathbb{P}\left(\{SIR > \gamma\}\right) &= \mathbb{E}_{R_1}\left[\mathbb{P}\left(\left\{\sum_{k=2}^{\infty} R_k^{-\varepsilon} < \left(\gamma R_1^{\varepsilon}\right)^{-1} \middle| R_1\right\}\right)\right] \\ &= 0, \ \forall\, \gamma \geq 0.\end{aligned}$$

and hence we have proved the result.

2.8.8 Simulation Methods

In this section, the details of simulating the SCS are presented. A single trial in simulating the BS placement for the 1-D SCS with BS density function $\lambda(r)$ in the region of interest which is a subset of the 1-D plane denoted by S, involves the following steps:

1) Generate a random number M, according to a Poisson distribution with mean $\int_S \lambda(s)\, ds$, which is the number of BSs to be placed in S for the given trial.

2) *BS placement:* For *homogeneous* 1-D SCS, generate M random numbers according to a uniform distribution in the range of S. If $\lambda(s)$ does not correspond to a *homogeneous* 1-D SCS, if $\lambda_{\max} = \sup_{s \in S} \lambda(s)$, then general a random number y which is uniformly distributed in the range $[0, \lambda_{\max}]$ and another random number x according to a uniform distribution in the range of S. A BS is placed uniformly at x, only if $y < \lambda_0(x)$. This process is repeated until M BS are placed.

3) Compute the received power at the MS for each BS using the path-loss exponent ε. The fading in the SCS is incorporated by multiplying each of the received powers with i.i.d. random number generated according to the distribution of the fading factor. Finally, SINR at the MS corresponding to this trial, is computed according to (2.2).

For all the simulations in this chapter $T = 100,000$ trials are used unless specified otherwise.

Chapter 3

Stochastic Ordering based SIR Analysis for the Shotgun Cellular Systems

3.1 Introduction

In the previous chapter, we have modeled the BS arrangement by non-homogeneous Poisson point processes in $\mathbb{R}^l$, $l = 1, 2,$ and 3, and derived semi-analytical expressions for the distribution of SIR at a given MS. This helped in quantifying the outage probability in a very general setting involving arbitrary fading distribution and path-loss models, random BS transmission powers and user mobility. However, in the absence of results in closed form, alternate approaches need to be explored to develop a clearer understanding of such networks. Furthermore, growing interests in understanding networks like femtocells, cognitive radios and heterogeneous networks have created a demand to consider more complex stochastic geometric models, with little hope for complete analytical characterization.

Here, we pose the question: Is it possible to qualitatively compare two SIR distributions by only examining the BS densities without having to obtain the SIR distributions? This chapter answers the question affirmatively for certain BS densities by developing a usual stochastic ordering based tool.

Concepts of stochastic ordering have been previously applied to scenarios of interest in wireless communications. Recently, in [56], performances of communication systems are explored solely using stochastic ordering. Further, [57] focuses on the study of directionally convex ordering of shot-noise fields, and establishes the ordering of interferences in networks with nodes distributed according to different point processes. This chapter focuses on establishing usual stochastic ordering between the SIR at the MS in non-homogeneous Poisson point process based BS arrangements, where the MS connects to the strongest BS, which is different

than the setup considered in [56, 57]. More examples on multi-tier networks and cognitive radios can be found in [28, 29].

The next section gives the system model. The main result of this chapter is Theorem 7 in Section 3.3. The utility of this result is explored in Section 3.4, by considering several scenarios of interest in wireless networks. Section 3.5 concludes the chapter.

3.2 System Model

The *Shotgun Cellular System (SCS)* is a model for the cellular system in which the BSs are distributed in a l-dimensional plane ($l-$D, typically $l = 1, 2,$ and 3) according to a non-homogeneous Poisson point process in $\mathbb{R}^l$. The intensity function of the Poisson point process is called the BS density function.

Without loss of generality, we restrict our attention to 1-D SCSs, because for the SIR analysis, the l-D SCSs can be reduced to an equivalent 1-D SCS [58, Lemma 2] with a BS density function $\lambda(r)$, where $r \geq 0$ is the distance of the BS from a mobile-station (MS) located at the origin. For example, a **homogeneous** l-D SCS with density $\lambda_0\,(>0)$ is equivalent to a 1-D SCS with density function $\lambda\,(r) = \lambda_0 b_l r^{l-1},\ r \geq 0,\ b_1 = 2,\ b_2 = 2\pi,$ and $b_3 = 4\pi$ [58, Corollary 2].

The BSs are assumed to have independent and identically distributed (i.i.d.) random transmission powers K_i's and shadow fadings Ψ_i's across BSs. The path-loss is $R^{-\varepsilon},\ \varepsilon > 0$, where R denotes the distance between the BS and the receiver. We assume an interference limited system and omit thermal noise. We focus on the signal quality of a MS at the origin. The MS chooses to communicate with the BS, referred to as the "serving BS," that corresponds to the **strongest** received signal power, or equivalently strongest SIR. All other BSs are the "interfering BSs". The signal quality at the MS is measured by $\text{SIR} = \frac{K_S \Psi_S R_S^{-\varepsilon}}{\sum_{i=1}^{\infty} K_i \Psi_i R_i^{-\varepsilon}}$, where S indexes the serving BS, i indexes the interfering BSs and the random variables $R_S \leq R_1 \leq R_2 \leq \cdots$ are ordered BS locations.

3.3 The Stochastic Ordering of SIR

In this section, we present the theoretical tools that are used to compare SIR tail probability by comparing the equivalent 1-D BS densities. Since the effect of i.i.d. shadow fading factors and i.i.d. transmission

powers can be captured by modifying the BS density as shown in Section 3.4.4, they are assumed to be 1 for all BSs. The generalization to arbitrary path loss model is given in [58, Section VI], which is also equivalent to modifying the BS density $\lambda(r)$. As a result, SIR $= \frac{R_1^{-\varepsilon}}{\sum_{i=2}^{\infty} R_i^{-\varepsilon}}$.

Definition 5. Let X and Y be two random variables such that $\mathbb{P}(\{X > x\}) \leq \mathbb{P}(\{Y > x\}),\ \forall\, x \in (-\infty, \infty)$, then X is *smaller than Y in the usual stochastic order* and this is denoted by $X \leq_{\text{st}} Y$. Further, $X =_{\text{st}} Y$ means $\mathbb{P}(\{X > x\}) = \mathbb{P}(\{Y > x\}),\ \forall\, x \in (-\infty, \infty)$. [39, p. 3]

If X and Y are the $\frac{C}{I}$ at the MS in two different SCSs, $X \leq_{\text{st}} Y$ implies that the MS in the SCS corresponding to Y is more likely to achieve better signal quality than in the SCS corresponding to X. Let $\{R_k\}_{k=1}^{\infty}$ represent the set of distances of BSs from the MS, indexed in the ascending order of the distance, and let $D_{k+1} = R_{k+1} - R_k$ be the distance between two adjacent BSs, and $f_{D_{k+1}|R_k}(d|\, r; \lambda(s))$ be the probability density function (p.d.f.) of D_{k+1} conditioned on $R_k = r$, as a function of the BS density $\lambda(s)$.

Lemma 5.

$$\begin{aligned} f_{D_{k+1}|R_k}(d\,|r; \lambda(s)) &\overset{(A)}{=} e^{-\int_r^{r+d} \lambda(s)ds} \lambda(r+d), \text{ and} \\ f_{aD_{k+1}|aR_k}(d'\,|r'; \lambda(s)) &\overset{(B)}{=} f_{D_{k+1}|R_k}\left(d' \,\middle|\, r'; \frac{1}{a}\lambda\left(\frac{s}{a}\right)\right). \end{aligned}$$

Proof. Equation (A) follows from the properties of Poisson processes [6, 7]. Equation (B) is proved by

$$\begin{aligned} & f_{aD_{k+1}|aR_k}(d'|r'; \lambda(s)) \\ & \overset{(a)}{=} \frac{1}{a} f_{D_{k+1}|R_k}\left(\frac{d'}{a}|\frac{r'}{a}; \lambda(s)\right) \\ & \overset{(b)}{=} \frac{1}{a}\lambda\left(\frac{r'+d'}{a}\right) \exp\left(-\int_{\frac{r'}{a}}^{\frac{r'+d'}{a}} \lambda(s)ds\right) \\ & \overset{(c)}{=} \frac{1}{a}\lambda\left(\frac{r'+d'}{a}\right) \exp\left(-\int_{r'}^{r'+d'} \frac{1}{a}\lambda\left(\frac{s'}{a}\right) ds'\right), \end{aligned}$$

where (a) is obtained by a variable change; (b) follows from (A); and (c) is obtained by a variable change and gives (B). □

Lemma 5 means that scaling D_{k+1} and R_k by a is equivalent to scaling the BS density as $\frac{1}{a}\lambda(\frac{r}{a})$. The significance of Lemma 5 is presented next, using the notation defined below.

Definition 6. $\mathrm{SIR}|_{\lambda(r)}$ **denotes the random variable of the** SIR **at the MS of a 1-D SCS with BS density function** $\lambda(r)$.

Corollary 6. $\mathrm{SIR}|_{\lambda(r)} =_{st} \mathrm{SIR}|_{\frac{1}{a}\lambda(\frac{r}{a})}$, $\forall\ a > 0$.

Proof. Let $\{R_k\}_{k=1}^{\infty}$ correspond to the 1-D SCS with BS density function $\lambda(r)$. Then, since the ordered BS locations R_k's are determined by inter-BS distances, it follows from Lemma 5 that

$$\mathrm{SIR}|_{\lambda(r)} \quad = \quad \frac{(aR_1)^{-\varepsilon}}{\sum_{k=2}^{\infty}(aR_k)^{-\varepsilon}}\bigg|_{\lambda(r)} =_{\mathrm{st}} \frac{\left(R_1'\right)^{-\varepsilon}}{\sum_{k=2}^{\infty}\left(R_k'\right)^{-\varepsilon}}\bigg|_{\frac{1}{a}\lambda(\frac{r}{a})},$$

where R_k''s corresponding to $\frac{1}{a}\lambda(\frac{r}{a})$ have the same distribution as aR_k's corresponding to $\lambda(r)$. □

The following special case is a direct corollary of the above result.

Corollary 7. ***In a*** *homogeneous* l***-D SCS,*** SIR ***is not a function of the BS density.***

Proof. Firstly, recall that the SIR at the MS in a **homogeneous** $l-$D SCS with BS density λ_0 is the same as that in a $1-$D SCS with a BS density function $\lambda(r) = \lambda_0 b_l r^{l-1}$. Next, from Corollary 6, the distribution of SIR in this SCS is the same as that in a 1-D SCS with the BS density function $\frac{1}{a}\lambda\left(\frac{r}{a}\right) = \lambda_0 \alpha b_l r^{l-1}$, $\alpha = a^{-l}$, $a > 0$. Thus, distributions of SIR corresponding to $\alpha\lambda_0$ and λ_0 are the same. □

The above result was also observed in [58], but Corollary 7 provides a simpler and more fundamental proof. Next, we define a notation used in Theorem 7.

Definition 7. For BS density function $\lambda(r)$, the cumulative BS density function is defined as $\mu(r) \triangleq \int_0^r \lambda(s)ds$, and its inverse function is defined as $\mu^{-1}(q) \triangleq \sup\{r : \mu(r) \leq q\}$.

Since $\lambda(r) \geq 0$, $\mu(r)$ is a non-decreasing function of r. In general, the inverse function is not injective since $\lambda(r)$ can be zero in arbitrary intervals of $r \in [0, \infty)$. The above definition makes it injective. For certain BS densities, it is possible to compare two $\frac{C}{I}$'s by comparing the densities without solving for the distributions. This is facilitated by Theorem 7.

Theorem 7. ***Let*** $\left\{\lambda_1(r), \mu_1(r), \mu_1^{-1}(q)\right\}$ ***and*** $\left\{\lambda_2(r), \mu_2(r), \mu_2^{-1}(q)\right\}$ ***be the BS density functions, cumulative BS density functions and their inverse functions for two 1-D SCSs, respectively.***

The SIR at the MS follows the usual stochastic order $\text{SIR}|_{\lambda_1(r)} \leq_{st} \text{SIR}|_{\lambda_2(r)}$, ***if for each*** $q > 0$ ***and*** $a = \frac{\mu_2^{-1}(q)}{\mu_1^{-1}(q)}$, $\frac{1}{a}\lambda_1\left(\frac{r}{a}\right) \geq \lambda_2(r)$, $\forall\ r \geq \mu_2^{-1}(q)$.

Proof. See Appendix 3.6.1 for the proof. □

Outage probability $P\{\text{SINR} < \gamma\}$ and ergodic rate $\mathbb{E}\left[\log\left(1 + \text{SINR}\right)\right]$ are often used to measure the performance for slowly varying and fast varying systems, respectively. For interference dominated systems, if $\text{SIR}|_{\lambda_1(r)} \leq_{\mathbf{st}} \text{SIR}|_{\lambda_2(r)}$, it is obvious that $P\left\{\text{SIR}|_{\lambda_1(r)} < \gamma\right\} \geq P\left\{\text{SIR}|_{\lambda_2(r)} < \gamma\right\}$, $\forall\gamma$. In addition, for $u\left(\text{SIR}\right) = \log\left(1 + \text{SIR}\right)$ or any other non-decreasing function, $\mathbb{E}\left[u\left(\text{SIR}|_{\lambda_1(r)}\right)\right] \leq \mathbb{E}\left[u\left(\text{SIR}|_{\lambda_2(r)}\right)\right]$. Applications of the above theorem are in the next section.

3.4 Applications of the SIR stochastic ordering

3.4.1 Comparison of Homogeneous $l-$D SCSs ($l = 1, 2,$ and 3)

Here, we show that the signal quality degrades as the dimension l of the **homogeneous** l-D SCS increases, for which we need the following corollaries.

Corollary 8. ***For each*** $q > 0$ ***and*** $a = \frac{\mu_2^{-1}(q)}{\mu_1^{-1}(q)}$, ***if*** $\Delta(r) \triangleq \frac{1}{a}\lambda_1(\frac{r}{a}) - \lambda_2(r)$ ***is a non-decreasing function for all*** $r \geq 0$, ***then*** $\text{SIR}|_{\lambda_1(r)} \leq_{st} \text{SIR}|_{\lambda_2(r)}$.

Proof. Note that

$$\int_0^{\mu_2^{-1}(q)} \frac{1}{a}\lambda_1\left(\frac{s}{a}\right) ds \quad = \quad q = \int_0^{\mu_2^{-1}(q)} \lambda_2(s) ds.$$

Hence, $\int_0^{\mu_2^{-1}(q)} \Delta(s) ds = 0$. Suppose $\Delta(\mu_2^{-1}(q)) < 0$, then $\Delta(r) < 0$, $r \in [0, \mu_2^{-1}(q)]$, since $\Delta(r)$ is non-decreasing. This is a contradiction. Thus, $\Delta(\mu_2^{-1}(q)) \geq 0$. Using Theorem 7, the corollary is proved. □

Corollary 9. ***For a*** *homogeneous* l***-D SCS with BS density*** λ_0 ***and its equivalent 1-D BS density function*** $\lambda_l\left(r\right) = \lambda_0 b_l r^{l-1}$, $r \geq 0$, ***multiplying*** $\lambda_l\left(r\right)$ ***with a non-increasing function*** $\beta(r) > 0$ ***improves the*** SIR, ***i.e.,*** $\text{SIR}|_{\lambda_l(r)} \leq_{st} \text{SIR}|_{\beta(r)\lambda_l(r)}$. ***The inequality reverses if*** $\beta(r)$ ***is non-decreasing.***

Proof. If $\beta(r)$ is non-increasing, for any $a > 0$, the density difference

$$\Delta(r) \quad = \quad \frac{1}{a}\lambda_l(\frac{r}{a}) - \beta(r)\lambda_l(r) = \lambda_0 b_l \left(\frac{1}{a^{l-2}} - \beta(r)\right) r^{l-1}$$

is non-decreasing. By Corollary 8, $\text{SIR}|_{\lambda_l(r)} \leq_{\text{st}} \text{SIR}|_{\beta(r)\lambda_l(r)}$ holds. If $\beta(r)$ is non-decreasing, the same proof applies with $\Delta(r) = \beta(r)\lambda_l(r) - a\lambda_l(\frac{r}{a})$. □

Hence,

$$\text{SIR}|_{\lambda_1(r)} \overset{(a)}{\geq}_{\text{st}} \text{SIR}|_{\lambda_2(r)} \overset{(b)}{\geq}_{\text{st}} \text{SIR}|_{\lambda_3(r)}$$

by plugging $l = 1, 2, 3$ in $\lambda_l(r)$, respectively; (a) holds because $\lambda_2(r) = \beta(r)\lambda_1(r)$, where $\beta(r) = \frac{b_2}{b_1} r$ is a non-decreasing function; and similarly (b) also holds. Thus, the comparison between SIRs is done without finding their distributions.

3.4.2 A Qualitative Comparison between Two 1-D SCSs

Consider a **homogeneous** 1-D SCS with a BS density function $\lambda_1(r) = \lambda,\ r \geq 0$, and another 1-D SCS with a BS density function $\lambda_2(r) = \begin{cases} \alpha & 0 \leq r \leq \rho \\ \beta & r > \rho \end{cases}$, where $\alpha < \beta$ (see inset of Figure 3.1). Such $\lambda_2(r)$ might describe, for example, a highway passing through a region of small population (BS density of α) and then a region of greater population (BS density of β). Usually, such a scenario is approximated by a constant BS density throughout the highway, which is represented by $\lambda_1(r)$. Corollary 9 gives the intuitive result $\text{SIR}|_{\lambda_1(r)} \geq_{\text{st}} \text{SIR}|_{\lambda_2(r)}$ and puts the intuition on solid foundation. Further, Figure 3.1 shows this stochastic ordering using simulations, the steps for which can be found in [58, Appendix D]. On the other hand, if $\alpha > \beta$, $\text{SIR}|_{\lambda_1(r)} \leq_{\text{st}} \text{SIR}|_{\lambda_2(r)}$. Using Corollary 9, similar scenarios can be studied for 2-D and 3-D.

3.4.3 Comparison of Path-loss Models

Here, we compare the SIR at the MS in two 1-D SCSs with BS density functions $\lambda_i(r)$ and path-loss models $\frac{1}{h_i(r)}$, $\forall\ r \geq 0$, for $i \in \{1, 2\}$. Assume the derivative $h_i'(r)$ exists and $h_i'(r) > 0\ \forall\ r > 0$. In the proof of the following corollaries, we use [58, Theorem 4] to reduce the 1-D SCS with BS density function $\lambda_i(r)$

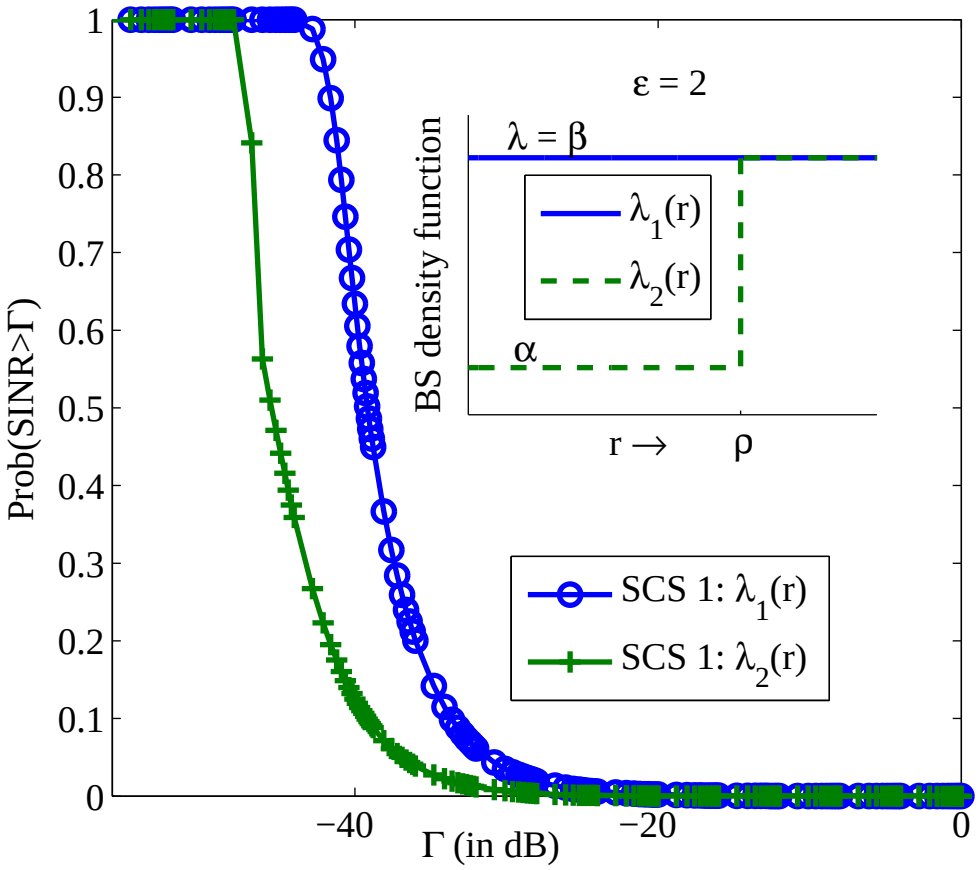

Figure 3.1: Comparison of $\frac{C}{I}$ tail probability of two 1-D SCSs

and path-loss model $\frac{1}{h_i(r)}$ to an equivalent 1-D SCS with BS density function

$$\bar{\lambda}_i(r) = \begin{cases} \frac{\lambda_i\left(h_i^{-1}(r)\right)}{h_i'\left(h_i^{-1}(r)\right)} & r \geq h_i(0) \\ 0 & r < h_i(0) \end{cases}$$

and a path-loss model, $\frac{1}{r}$, where $h_i^{-1}(\cdot)$ is the inverse function. Although $\frac{1}{r}$ is singular at the origin, this conversion works for any non-singular path-loss models $\frac{1}{h(r)}$, such as $\frac{1}{h(r)} = \frac{1}{1+r^{\varepsilon}}$, $\varepsilon > l$, for which $\bar{\lambda}(r) = 0$ for $0 \leq r \leq h(0) = 1$, avoiding the singular point.

Corollary 10. ***In a*** *homogeneous* $l-$***D SCS, if the path-loss follows a power-law parametrized by a path-loss exponent,*** ε***, the SIR at the MS improves as the path-loss exponent increases. In other words, if*** $h_i(r) = r^{\varepsilon_i}$, $i = 1, 2$, ***such that*** $\varepsilon_1 > \varepsilon_2 > l$, ***then*** $\mathrm{SIR}_1 \geq_{\mathrm{st}} \mathrm{SIR}_2$, ***where*** SIR_i ***corresponds to the path-loss model*** $\frac{1}{h_i(r)}$.

Proof. Using [58, Theorem 4], the equivalent 1-D SCSs with a path-loss model $\frac{1}{r}$ have the BS density functions $\bar{\lambda}_i(r) = \frac{\lambda_0 b_l}{\varepsilon_i} r^{\frac{l}{\varepsilon_i}-1}$. Further, $\bar{\lambda}_2(r) = \beta(r)\,\bar{\lambda}_1(r)$, where $\beta(r) = \frac{\varepsilon_1}{\varepsilon_2} r^{\frac{l}{\varepsilon_2}-\frac{l}{\varepsilon_1}}$, $r \geq 0$ is a non-decreasing function. Hence, Corollary 9 applies and $\mathrm{SIR}|_{\bar{\lambda}_1(r)} \geq_{\mathrm{st}} \mathrm{SIR}|_{\bar{\lambda}_2(r)}$. □

Hence, a simple proof that does not require solving the distribution of SIR gives the expected result that a system with a greater path-loss exponent has a better SIR. The following corollary establishes a similar result between two popularly used path-loss models [59].

Corollary 11. ***In a*** *homogeneous* $l-$***D SCS with a BS density*** λ_0***, the received signal of a MS located at the origin satisfies*** $\mathrm{SIR}_1 \leq_{\mathrm{st}} \mathrm{SIR}_2$, ***where*** SIR_1 ***corresponds to path-loss*** $\frac{1}{h_1(r)}$ ***with*** $h_1(r) = r^{\varepsilon_1}$, $r \geq 0$ ***and*** SIR_2 ***corresponds to the path-loss*** $\frac{1}{h_2(r)}$ ***with***

$$h_2(r) = \begin{cases} r^{\varepsilon_1} & , \ r \leq 1 \\ & \\ r^{\varepsilon_2} & , \ r > 1 \end{cases},$$

where $\varepsilon_2 > \varepsilon_1 > l$. ***The opposite conclusion holds when*** $\varepsilon_1 > \varepsilon_2 > l$.

Proof. Using [58, Theorem 4], $\bar{\lambda}_1(r) = \frac{\lambda_0 b_l}{\varepsilon_1} r^{\frac{l}{\varepsilon_1}-1}$, $r \geq 0$, and $\bar{\lambda}_2(r)$ satisfies the equation $\bar{\lambda}_2(r)\,\beta(r) =$

$\bar{\lambda}_1(r)$, where

$$\beta(r) = \begin{cases} 1 & , r \leq 1 \\ \frac{\varepsilon_1}{\varepsilon_2} r^{\frac{l}{\varepsilon_2} - \frac{l}{\varepsilon_1}} & , r > 1 \end{cases}.$$

Since $\varepsilon_2 > \varepsilon_1 > l$, $\beta(r)$ is a non increasing function. As a result, Corollary 9 holds and hence $\text{SIR}|_{\bar{\lambda}_1(r)} \leq_{\text{st}} \text{SIR}|_{\bar{\lambda}_2(r)}$. Thus, the system with the path-loss model $\frac{1}{h_2(r)}$ has a better signal quality compared to that of $\frac{1}{h_1(r)}$. When $\varepsilon_1 > \varepsilon_2 > l$, $\beta(r)$ is a non decreasing function and $\text{SIR}|_{\bar{\lambda}_1(r)} \geq_{\text{st}} \text{SIR}|_{\bar{\lambda}_2(r)}$. □

3.4.4 Shadow Fading and Random Transmission Powers

Shadow fading, random transmission powers, and arbitrary path-loss models together can be captured by modifying the BS density function as follows [58, Theorem 3, 4]. Consider a 1-D SCS with BS density function $\lambda(r)$, path-loss model $\frac{1}{h(r)}$, random shadow fading factors $\{\Psi_i\}_{i=1}^{\infty}$, and transmission powers $\{K_i\}_{i=1}^{\infty}$. Ψ_i and K_i can be correlated but are i.i.d. across i. For the $\frac{C}{I}$ analysis, the SCS is equivalent to another 1-D SCS with BS density function $\bar{\lambda}(r) = \mathbb{E}_{\Psi,K}\left[K\Psi\tilde{\lambda}(K\Psi r)\right]$, where $\tilde{\lambda}(r) = \begin{cases} \frac{\lambda\left(h^{-1}(r)\right)}{h'(h^{-1}(r))} & r \geq h(0) \\ 0 & r < h(0) \end{cases}$; $\mathbb{E}$ is the expectation operator w.r.t. Ψ and K; $\Psi =_{\text{st}} \Psi_i$ and $K =_{\text{st}} K_i$, $\forall\, i$. This holds as long as the expectation converges.

Thus, after modifying the BS density function, Theorem 7 applies. The following corollary shows a scenario where SIR distribution is unaffected by shadow fading and random transmission powers.

Corollary 12. ***In a** homogeneous $l-$**D SCS with a BS density** λ_0**, and a path-loss model** $\frac{1}{r^{\varepsilon}}$, $\varepsilon > l$, **the SIR distribution at the MS does not depend on the random shadow fading factors** $\{\Psi_i\}_{i=1}^{\infty}$ **and transmission powers** $\{K_i\}_{i=1}^{\infty}$, **if they are i.i.d. across BSs and** $\left|\mathbb{E}_{\Psi,K}\left[(\Psi K)^{\frac{l}{\varepsilon}}\right]\right| < \infty$.*

Proof. The equivalent 1-D density function $\lambda(r) = \lambda_0 b_l r^{l-1}$, and the path-loss model $h(r) = r^{\varepsilon}$ gives $\tilde{\lambda}(r) = \frac{\lambda_0 b_l}{\varepsilon} r^{\frac{l}{\varepsilon}-1}$. We have

$$\text{SIR}_{\frac{1}{r^{\varepsilon}},\text{random } \Psi_i,K_i,\lambda(r)} \overset{(a)}{=}_{\text{st}} \text{SIR}|_{\frac{1}{r},\Psi_i=K_i=1,\bar{\lambda}(r)} \overset{(b)}{=}_{\text{st}} \text{SIR}|_{\frac{1}{r},\Psi_i=K_i=1,\frac{1}{\alpha}\tilde{\lambda}\left(\frac{r}{\alpha}\right)} \overset{(c)}{=}_{\text{st}} \text{SIR}|_{\frac{1}{r},\Psi_i=K_i=1,\tilde{\lambda}(r)}$$

, where (a) is obtained with

$$\bar{\lambda}(r) = \mathbb{E}_{\Psi,K}\left[\Psi K\tilde{\lambda}(\Psi K r)\right] = \mathbb{E}_{\Psi,K}\left[(\Psi K)^{\frac{l}{\varepsilon}}\right]\tilde{\lambda}(r)$$

; (b) is obtained by rewriting $\bar{\lambda}(r)$ as $\frac{1}{\alpha}\tilde{\lambda}\left(\frac{r}{\alpha}\right)$ where $\alpha = \left(\mathbb{E}_{\Psi,K}\left[(\Psi K)^{\frac{l}{\varepsilon}}\right]\right)^{-\frac{\varepsilon}{l}}$; (c) is obtained by applying Corollary 6. Thus, the $\frac{C}{I}$ distribution is unaffected by shadow fading and transmission powers. □

This result was already proved in [58, Remark 4(a)]. Here, however, we have shown an alternative proof that is based only on the concepts of usual stochastic ordering.

3.5 Conclusions

This chapter is an extension to our work in characterizing the SIR of SCS in [58]. We have developed a tool based on stochastic ordering to compare the SIR at the MS in non-homogeneous Poisson processes. With Theorem 7, we show that, by just comparing certain BS density functions of the SCSs, we can make strong inferences such as, a MS in a given SCS achieves a SIR that is at least as good as that achieved in another SCS without having to solve for the SIR distributions. Moreover, as a consequence of Theorem 7, simple proofs are given to show that in a homogeneous l-D SCS, (1) a MS sees decreasing signal quality as dimension l increases; (2) the SIR at the MS improves as the path-loss exponent of the channel increases; and (3) SIR distribution is unaffected by shadow fading and random transmission powers.

3.6 Appendix

3.6.1 Proof of Theorem 7

Consider the 1-D SCS specified by the set $\left\{\lambda(r), \mu(r), \mu^{-1}(q)\right\}$, as in Definition 7. The following remark relates SIR to the cumulative BS density.

If R_1 denotes the distance between the serving BS and MS in the 1-D SCS,

$$\begin{aligned}
&\mathbb{P}\left(\{\text{SIR} > y\}\right) \\
&\overset{(a)}{=} \int_{r_1=0}^{\infty} \mathbb{P}\left(\text{SIR} > y | \, R_1 = r\right) f_{R_1}(r) dr \\
&\overset{(b)}{=} \int_{q=0}^{\infty} \mathbb{P}\left(\text{SIR} > y | \, Q = q\right) f_Q(q) dq,
\end{aligned}$$

where $Q \triangleq \mu(R_1)$, and Q is an exponential random variable with mean 1.

Equation (a) is obtained by conditioning w.r.t. R_1. Equation (b) is obtained by expressing (a) in terms of Q, where the p.d.f. of R_1 at $R_1 = \mu^{-1}(q)$ is

$$f_{R_1}(r)dr|_{r=\mu^{-1}(q)} \quad = \quad e^{-\int_0^r \lambda(s)ds}\lambda(r)dr\Big|_{r=\mu^{-1}(q)} = e^{-q}dq = f_Q(q)dq,$$

which does not depend on $\lambda(r)$.

To show that the BS density $\lambda_1(r)$ gives a worse SIR than $\lambda_2(r)$ does, one needs to show that

$$\mathrm{SIR}|_{R_1=\mu_1^{-1}(q),\ \lambda_1(r),\ r\geq\mu_1^{-1}(q)} \leq_{\mathrm{st}} \mathrm{SIR}|_{R_1=\mu_2^{-1}(q),\ \lambda_2(r),\ r\geq\mu_2^{-1}(q)}$$

for all $q > 0$, where the condition of the domain of the BS density is because the locations of interfering BSs only depend on the BS density in that domain. Next, define $a = \frac{\mu_2^{-1}(q)}{\mu_1^{-1}(q)}$. By Corollary 6, where R_k''s are the ordered BS locations of the SCS with BS density $\frac{1}{a}\lambda\left(\frac{r}{a}\right)$. The equation means that the conditional SIR of the SCS with a BS density $\lambda_1(r)$ is equivalent to an SCS with BS density $\frac{1}{a}\lambda_1(\frac{r}{a})$ with the same location of the serving BS as the SCS with BS density $\lambda_2(r)$.

With the locations of the serving BSs equal and fixed, $\frac{C}{I}$ is a decreasing function of the interference. Theorem 1.A.3.(a) of [39] says that decreasing functions reverse the usual stochastic order. So, one only needs to show that the interferences satisfy

$$\begin{aligned}&\sum_{k=2}^{\infty} R_k^{-\varepsilon}|_{R_2\geq\mu_2^{-1}(q),\ \frac{1}{a}\lambda_1(\frac{r}{a}),\ r\geq\mu_2^{-1}(q)}\\ &\geq_{\mathrm{st}} \sum_{k=2}^{\infty} R_k^{-\varepsilon}|_{R_2\geq\mu_2^{-1}(q),\ \lambda_2(r),\ r\geq\mu_2^{-1}(q)}.\end{aligned} \tag{3.1}$$

As shown in [58, Appendix B], the total interference power can be expressed as $\sum_{k=2}^{\infty} R_k^{-\varepsilon} = \lim_{r_B\to\infty}\lim_{N\to\infty}\sum_{i=2}^{N} X_i$, where X_i is a Bernoulli random variable defined by

$$\begin{aligned}\mathbb{P}\left(\{X_i = 0|\, R_1 = r_1\}\right) &= 1 - p_i,\\ \mathbb{P}\left(\left\{X_i = r_i^{-\varepsilon} + o(\Delta r)\right|\, R_1 = r_1\right\}\right) &= p_i,\end{aligned}$$

$p_i = \lambda(r_i)\Delta r + o(\Delta r)$, $r_i = r_1 + (i-1)\Delta r$, $\Delta r = \frac{r_B - r_1}{N}$, and $r_1 = \mu_2^{-1}(q)$. Since the condition $\frac{1}{a}\lambda_1(\frac{r}{a}) \geq \lambda_2(r)$ holds for all $r \geq \mu_2^{-1}(q)$, we have $X_i|_{\frac{1}{a}\lambda_1(\frac{r}{a})} \geq_{\mathrm{st}} X_i|_{\lambda_2(r)}$, $\forall i \geq 2$. As summation preserves stochastic order [39, Theorem 1.A.3.(b)], (3.1) is proved, completing the proof.

Chapter 4

Downlink Analysis for a Heterogeneous Cellular Network

4.1 Introduction

The modern cellular communication network is an overlay of multiple contributing subnetworks such as the macrocell, microcell, picocell and femtocell networks, collectively called the heterogeneous network (or, in short, hetnets). The hetnets have been shown to sustain greater end-user data-rates and throughput as well as provide indoor and cell-edge coverage, further leading to their inclusion as an important feature to be implemented under the fourth-generation (4G) cellular standards [60–66].

Until recently, the analysis of such networks has been done solely through system simulations. Since the hetnets consist of a combination of regularly spaced macrocell networks along with irregularly spaced microcell and picocell networks and often randomly placed end-user deployed femtocell networks, it is difficult to study the entire network at once using simulations. Further, the base-stations (BSs) in each of these networks have different transmit powers, traffic-load carrying capabilities and different radio environment that is based on the locations in which they are deployed. The many parameters involved in the design and modeling of the individual networks makes it difficult to narrow all the possibilities down to a limited set of simulation scenarios based on which one can make the design decisions for the entire network. Under these circumstances, the development of an analytical model that captures all the design scenarios of interest is of great importance.

Towards this goal, a stochastic geometric model has been identified as a plausible analytical model as well as the most widely used one in academia. There is a rich set of results for studying the behavior of

large systems with nodes deployed randomly (especially according to a homogeneous Poisson point process on the plane) and can be found in [67–70]. For the cellular network, a strong motivation for viewing the BS arrangement as a homogeneous Poisson point process can be drawn from the study of the cellular systems in [2,12,13] which suggests that significant insights can be gained by bounding the downlink cellular performance between the ideal hexagonal grid model and the homogeneous Poisson point process based model. More interestingly, in [2, Fig.2.], it is claimed with the help of Monte-Carlo simulations that in the limit of strong log-normal shadow fading (standard deviation of the fading coefficient $\sigma \to \infty$), the downlink performance of an ideal hexagonal cellular system approaches the performance in a cellular system with randomly deployed base-stations according to a homogeneous Poisson point process. Recently, the above convergence has been analytically proved in [10, Theorem 3]. It is shown that the downlink performance of a cellular network with any deterministic arrangement of BSs (not just the ideal hexagonal grid model) converges to that of a Poisson point process based model as $\sigma \to \infty$, and moreover even for realistic values of σ that are observed in the indoor environments, the latter model is a good approximation for the deterministic model. Results in [27, 58, 71] demonstrates that, with the Poisson point process based BS arrangement, the study of the cellular system sees a distinctive advantage of being analytically tractable, unlike the studies based on the hexagonal grid model that are purely simulation-based.

In light of the above motivations, it is well-justified to study the hetnet performance by viewing the hetnet as composed of multiple tiers of networks (e.g. macrocell, microcell, picocell and femtocell networks), each modeled as an independent homogeneous Poisson point process, and such studies have been done in [3, 50–55, 72] and by us in [29, 30, 49]. These studies mathematically characterize important performance metrics such as coverage probability (= 1 - outage probability), average ergodic rate, average load carried by BSs of each tier and load-awareness. Furthermore, such studies have facilitated the characterization of the improvements that techniques such as fractional frequency reuse and carrier aggregation bring to cellular performance as well as hetnet performance. In the following subsection, we differentiate our work from the other prior work on hetnets and list the contributions of this chapter.

4.1.1 Prior work and Contributions of the chapter

In [3,50], the coverage probability results are obtained for the hetnets under the max-SINR connectivity, but are restricted to the case where the fading coefficients corresponding to all the BS transmissions are independent and identically distributed (i.i.d.) exponential random variables, and the path-loss exponents are the same for all the tiers. Using an entirely different approach, [54, 55, 72] derived the coverage probability for the hetnet with max-SINR and nearest BS connectivity models, but were again restricted to the i.i.d. exponential distributed fading coefficients for all BSs. In [53], the authors study the hetnet coverage probability for the maximum average received power (MARP) connectivity model (which is a special case of the nearest-BS connectivity model, as will be seen later), and again for the exponential fading assumption for all BS transmissions. In [29, 30, 49], we derived the hetnet coverage probability for the case when the i.i.d. fading coefficients have an arbitrary distribution and the path-loss exponents are different for different tiers, for the maximum instantaneous received power (MIRP) connectivity model, which is a special case for the max-SINR connectivity model, as will be discussed later.

In this chapter, the hetnet is modeled to consist of open and closed access networks formed by the arrangement of BSs according to homogeneous Poisson point process with a certain density for each tier, and independent of the other tiers. The focus is on the downlink performance analysis, and the MS can connect to one of the open-access networks; and the closed access networks only cause interference. Hence, without loss of generality, we study the downlink performance where the hetnet consists of K tiers of open access networks and a single closed access network. Signals from BSs of a given tier have a constant transmit power, random fading coefficient that is i.i.d. across all the BSs of the same tier and independent of those of the other tiers with any arbitrary distribution, arbitrary path-loss exponent that is constant for all BSs of the same tier and different across different tiers, and the SINR threshold for connectivity to a given k^{th} open-access tier's BS is $\beta_k,\ k = 1, \cdots, K$. For such a general setting, expressions for the coverage probability at the MS are derived for both the max-SINR connectivity model and the nearest-BS connectivity model. In the former connectivity model, the MS is said to be in coverage if there exists at least one open-access BS with an SINR above the corresponding threshold, and under the latter connectivity model, the MS is

said to be in coverage if at least one among the nearest BSs of each open-access tier has an SINR above the corresponding threshold.

When the SINR thresholds of all the tiers are above 1, the hetnet coverage probability under max-SINR connectivity and MIRP connectivity are identical, nearest-BS connectivity and the MARP connectivity are identical. Further, in these special cases, simple analytical expression are derived for the coverage probability, average rate and the load carried by the BSs of each tier. The following section describes the system model in detail.

4.2 System Model

This section describes the various elements used to model the wireless network, namely, the BS layout, the radio environment, and the performance metrics of interest.

4.2.0.1 BS Layout

The hetnet is composed of K open-access tiers and one closed-access tier, and the BS layout in each tier is according to an independent homogeneous Poisson point process in $\mathbb{R}^2$ with density λ_k for the k^{th} open-access tier ($k = 1, \cdots, K$) and a density λ_c for the closed-access tier. The MS is allowed to communicate with any BS of the open-access tiers, but cannot communicate with any of the closed-access BSs.

4.2.0.2 Radio Environment and downlink SINR

The signal transmitted from each BS undergoes shadow fading and path-loss. The SINR at an arbitrary MS in the system from the i^{th} BS of the k^{th} open-access tier is the ratio of the received power from this BS to the sum of the interferences from all the other BSs in the system and the constant background noise η, and is expressed as

$$\text{SINR}_{ki} = \frac{P_k \Psi_{ki} R_{ki}^{-\varepsilon_k}}{\sum_{\substack{m=1 \\ (m,l)\neq(k,i)}}^{K} \sum_{l=1}^{\infty} P_m \Psi_{ml} R_{ml}^{-\varepsilon_m} + \sum_{n=1}^{\infty} P_c \Psi_{cn} R_{cn}^{-\varepsilon_c} + \eta}, \tag{4.1}$$

where $\{P_m, \Psi_{ml}, \varepsilon_m, R_{ml}\}_{m=1,\ l=1}^{m=K,\ l=\infty}$ are the constant transmit power, random shadow fading factor, constant path-loss exponent and the distance from the MS of the l^{th} BS of the m^{th} open-access tier. Similarly,

Symbol	Description
K	Number of open-access tiers
$\{P_l\}_{l=1}^{K},\ P_c$	Constant transmission powers of the BSs of the K open-access tiers and closed access tier, respectively
$\{\varepsilon_l\}_{l=1}^{K},\ \varepsilon_c$	Path-loss exponents of the open and closed - access tiers (> 2).
$\{\Psi_l\}_{l=1}^{K}, \Psi_c$	i.i.d. fading gains of the open and closed-access tiers $\left(\mathbb{E}\Psi_l^{\frac{2}{\varepsilon_l}},\ \mathbb{E}\Psi_c^{\frac{2}{\delta}} < \infty\right)$
$\{\beta_l\}_{l=1}^{K}$	SINR thresholds for connectivity to a BS in the l^{th} open-access tier
η	Background noise power
$\{\gamma_l\}_{l=1}^{K}$	$=\left\{1+\frac{1}{\beta_l}\right\}_{l=1}^{K}$

Table 4.1: List of symbols used in the chapter

$\{P_c, \Psi_{cn}, \varepsilon_c, R_{cn}\}_{n=1}^{\infty}$ lists the constant transmit power, random shadow fading factor, and the constant path-loss exponent of the n^{th} BS of the closed-access tier. The fading coefficients $\{\Psi_{ml}\}_{l=1}^{\infty}$ are i.i.d. random variables with the same distribution as Ψ_m, $m = 1, \cdots, K$, and similarly, $\{\Psi_{cl}\}_{l=1}^{\infty}$ are i.i.d. with the same distribution as Ψ_c. Further, it is assumed that $\left\{\mathbb{E}\left[\Psi_m^{\frac{2}{\varepsilon_m}}\right]\right\}_{m=1}^{K}$, $\mathbb{E}\left[\Psi_c^{\frac{2}{\delta}}\right] < \infty$. Finally, R_{ml} (R_{cl}) is the distance of the l^{th} nearest BS belonging to the m^{th} open-access (closed-access) tier, and $\{R_{ml}\}_{l=1}^{\infty}$, $\{R_{cl}\}_{l=1}^{\infty}$ represents the sets of points distributed according to the homogeneous Poisson point process with density $\lambda_m,\ \lambda_c$, respectively, where $m = 1, \cdots, K$, as seen in Section 5.2.0.1. The various symbols introduced in this section are listed in Table 4.1 for quick reference.

4.2.0.3 BS connectivity models

A MS is able to communicate with a BS of the k^{th} open-access tier if the SINR corresponding to the BS is above a certain threshold $\beta_k,\ k = 1, \cdots, K$, in which case, the MS is said to be in coverage. The BS connectivity models provide a rule to determine which BS to connect to, and in this chapter, we focus on the max-SINR connectivity model and the nearest-BS connectivity model. The MIRP connectivity model and the MARP connectivity model are special cases of the max-SINR and nearest-BS connectivity models, respectively, and will be discussed in detail in the later sections.

Under the max-SINR connectivity model, the MS is said to be in coverage if there exists at-least one BS among all the open-access tiers that has an SINR at the MS above the corresponding threshold, and is

mathematically expressed as follows.

$$\begin{aligned}\mathbb{P}_{\text{coverage}}^{\max-\text{SINR}} &= \mathbb{P}\left(\bigcup_{k=1}^{K}\bigcup_{i=1}^{\infty}\{\text{SINR}_{ki} > \beta_k\}\right) = 1 - \mathbb{P}\left(\bigcap_{k=1}^{K}\bigcap_{i=1}^{\infty}\{\text{SINR}_{ki} \leq \beta_k\}\right) \\ &= \mathbb{P}\left(\bigcup_{k=1}^{K}\{\text{SINR}_k\,(\max) > \beta_k\}\right), \end{aligned} \tag{4.2}$$

where SINR_{ki} corresponds to the i^{th} BS of the k^{th} tier as defined in (4.1) and $\text{SINR}_k\,(\max)$ is the maximum SINR observed by the MS among all the k^{th} open-access tier BSs. In other words, MS is in coverage under the max-SINR connectivity model if there exists at least one of the K open-access tiers in which the maximum SINR at the MS from that tier exceeds the corresponding threshold.

The MS is said to be in coverage under the nearest-BS connectivity model if there exists at least one of the nearest BSs of the K open-access tiers with SINR at the MS above the corresponding threshold. This is mathematically expressed as

$$\mathbb{P}_{\text{coverage}}^{\text{nearest}} = \mathbb{P}\left(\bigcup_{k=1}^{K}\{\text{SINR}_{k1} > \beta_k\}\right), \tag{4.3}$$

where SINR_{k1} (see (4.1)) is the SINR at the MS from the nearest BS among the k^{th} tier BSs. In the following section, we derive expressions for the hetnet coverage probability for the above mentioned connectivity models.

4.3 Hetnet Coverage Probability

In [70], a technique to compute the downlink coverage probability in a single-tier network with BS arrangement according to homogeneous Poisson point process under max-SINR connectivity model was shown. In [3], the authors utilize this technique to compute the hetnet coverage probability for an open-access case where the fading coefficients for all the BSs in the system are i.i.d. unit mean exponential random variables and the path-loss exponents are the same for all tiers. Here, we generalize the technique developed in [70] to compute the hetnet coverage probability for both the max-SINR and nearest-BS connectivity models for a general system model as explained in Section 4.2.

The coverage probability expressions in (4.2) and (4.3) can be equivalently expressed as follows:

$$\mathbb{P}_{\text{coverage}}^{\text{max-SINR}} = \mathbb{P}\left(\bigcup_{k=1}^{K}\left\{\frac{M_k}{I_o + I_c + \eta - M_k} > \beta_k\right\}\right) = \mathbb{P}\left(\left\{\max_{k=1,\cdots,K} \gamma_k M_k > I_o + I_c + \eta\right\}\right), \quad (4.4)$$

$$\mathbb{P}_{\text{coverage}}^{\text{nearest}} = \mathbb{P}\left(\bigcup_{k=1}^{K}\left\{\frac{N_k}{I_o + I_c + \eta - N_k} > \beta_k\right\}\right) = \mathbb{P}\left(\left\{\max_{k=1,\cdots,K} \gamma_k N_k > I_o + I_c + \eta\right\}\right), \quad (4.5)$$

where $M_k = \max_{l=1,\cdots,\infty} P_k \Psi_{kl} R_{kl}^{-\varepsilon_k}$ is the maximum of the received powers from all the k^{th} tier BSs, $N_k = P_k \Psi_{k1} R_{k1}^{-\varepsilon_k}$ is the received power from the nearest BS among all the k^{th} tier BSs, $I_o = \sum_{k=1}^{K}\sum_{l=1}^{\infty} P_k \Psi_{kl} R_{kl}^{-\varepsilon_k}$ $\left(I_c = \sum_{l=1}^{\infty} P_c \Psi_{cl} R_{cl}^{-\varepsilon_c}\right)$ is the sum of the received powers from all the open-access BSs (closed-access BSs) in the system. In the following lemma, we derive expressions for two Laplace transforms that are useful to obtain semi-analytical expressions for $\mathbb{P}_{\text{coverage}}^{\text{max-SINR}}$ and $\mathbb{P}_{\text{coverage}}^{\text{nearest}}$, respectively.

Lemma 6.

$$\begin{aligned}
&\mathcal{L}_{I_o+I_c+\eta,\ \max_{k=1,\cdots,K}\gamma_k M_k \le u}(s) \triangleq \mathbb{E}\left[\exp\left(-s\left(I_o + I_c + \eta\right)\right) \times \mathcal{I}\left(\max_{k=1,\cdots,K}\gamma_k M_k \le u\right)\right] \\
&= \mathcal{L}_{I_c}(s)\, \mathrm{e}^{-s\eta - \sum_{k=1}^{K} \lambda_k \pi (sP_s)^{\frac{2}{\varepsilon_k}} \mathbb{E}\left[\Psi_k^{\frac{2}{\varepsilon_k}}\right]\left[\Gamma\left(1-\frac{2}{\varepsilon_k}\right) + \frac{2}{\varepsilon_k}\Gamma\left(-\frac{2}{\varepsilon_k}, \frac{su}{\gamma_k}\right)\right]}, \quad (4.6) \\
&\mathcal{L}_{I_o+I_c+\eta,\ \max_{k=1,\cdots,K}\gamma_k N_k \le u}(s) \triangleq \mathbb{E}\left[\exp\left(-s\left(I_o + I_c + \eta\right)\right) \times \mathcal{I}\left(\max_{k=1,\cdots,K}\gamma_k N_k \le u\right)\right] \\
&= \mathcal{L}_{I_c}(s)\, \mathrm{e}^{-s\eta - \sum_{k=1}^{K} \lambda_k \pi (sP_s)^{\frac{2}{\varepsilon_k}} \mathbb{E}\left[\Psi_k^{\frac{2}{\varepsilon_k}}\right]\Gamma\left(1-\frac{2}{\varepsilon_k}\right)} \times \\
&\prod_{k=1}^{K} \mathbb{E}_{\Psi_{k1}}\left[\int_{x=0}^{\frac{su}{\gamma_k \Psi_{k1}}} \lambda_k \frac{2\pi}{\varepsilon_k} (sP_k)^{\frac{2}{\varepsilon_k}} x^{-\frac{2}{\varepsilon_k}-1} \mathrm{e}^{-\Psi_{k1}x - \lambda_k \frac{2\pi}{\varepsilon_k}(sP_k)^{\frac{2}{\varepsilon_k}} \mathbb{E}_{\Psi_k}\left[\Psi_k^{\frac{2}{\varepsilon_k}}\Gamma\left(-\frac{2}{\varepsilon_k}, x\Psi_k\right)\right]} dx\right], \quad (4.7)
\end{aligned}$$

where $\mathcal{L}_{I_c}(s) = \exp\left(-\lambda_c \pi (sP_c)^{\frac{2}{\varepsilon_c}} \mathbb{E}\left[\Psi_c^{\frac{2}{\varepsilon_c}}\right] \Gamma\left(1 - \frac{2}{\varepsilon_c}\right)\right)$, *and the random variables* Ψ_{k1} *and* Ψ_k *are i.i.d. for all* $k = 1, \cdots, K$.

Proof. See Appendix 4.7.1. □

When fading coefficients are i.i.d. unit mean exponential random variables $\mathbb{E}\left[\Psi_k^{\frac{2}{\varepsilon_k}}\right] = \Gamma\left(1 + \frac{2}{\varepsilon_k}\right)$, setting $\lambda_c = 0$ and $\{\varepsilon_k\}_{k=1}^{K} = \alpha$, we get [3, (2)]. Further, using [70, Corollary 4], we get the joint p.d.f. of

$\left(I_o+I_c+\eta,\ \max\limits_{i=1,\cdots,K}\gamma_i M_i\right)$ and $\left(I_o+I_c+\eta,\ \max\limits_{i=1,\cdots,K}\gamma_i N_i\right)$ to be

$$f_{I_o+I_c+\eta,\max\limits_{i=1,\cdots,K}\gamma_i M_i}(x,y)=\int_{\omega=-\infty}^{\infty}\frac{\partial}{\partial u}\mathcal{L}_{I_o+I_c+\eta,\ \max\limits_{i=1,\cdots,K}\gamma_i M_i\le u}(j\omega)\Big|_{u=y}\frac{\mathrm{e}^{j\omega x}}{2\pi}d\omega, \tag{4.8}$$

$$f_{I_o+I_c+\eta,\max\limits_{i=1,\cdots,K}\gamma_i N_i}(x,y)=\int_{\omega=-\infty}^{\infty}\frac{\partial}{\partial u}\mathcal{L}_{I_o+I_c+\eta,\ \max\limits_{i=1,\cdots,K}\gamma_i N_i\le u}(j\omega)\Big|_{u=y}\frac{\mathrm{e}^{j\omega x}}{2\pi}d\omega, \tag{4.9}$$

$$\frac{\frac{\partial}{\partial u}\mathcal{L}_{I_o+I_c+\eta,\ \max\limits_{i=1,\cdots,K}\gamma_i M_i}(s)}{\mathcal{L}_{I_o+I_c+\eta,\ \max\limits_{i=1,\cdots,K}\gamma_i M_i\le u}(s)}=\sum_{k=1}^{K}\lambda_k\frac{2\pi}{\varepsilon_k}(\gamma_k P_k)^{\frac{2}{\varepsilon_k}}\mathbb{E}\left[\Psi_k^{\frac{2}{\varepsilon_k}}\right]u^{-1-\frac{2}{\varepsilon_k}}\mathrm{e}^{-\frac{su}{\gamma_k}}, \tag{4.10}$$

$$\frac{\frac{\partial}{\partial u}\mathcal{L}_{I_o+I_c+\eta,\ \max\limits_{i=1,\cdots,K}\gamma_i N_i\le u}(s)}{\mathcal{L}_{I_o+I_c+\eta,\ \max\limits_{i=1,\cdots,K}\gamma_i N_i\le u}(s)}=\sum_{k=1}^{K}\frac{\frac{\mathbb{E}_{\Psi_{k1}}\left[\Psi_{k1}^{\frac{2}{\varepsilon_k}}\mathrm{e}^{-\lambda_k\frac{2\pi}{\varepsilon_k}(sP_k)^{\frac{2}{\varepsilon_k}}\mathbb{E}_{\Psi_k}\left[\Psi_k^{\frac{2}{\varepsilon_k}}\Gamma\left(-\frac{2}{\varepsilon_k},\frac{su\Psi_k}{\gamma_k\Psi_{k1}}\right)\right]}\right]}{u\mathrm{e}^{\frac{su}{\gamma_k}}}}{\int_{x=0}^{1}\frac{\mathbb{E}_{\Psi_{k1}}\left[\Psi_{k1}^{\frac{2}{\varepsilon_k}}\mathrm{e}^{-\lambda_k\frac{2\pi}{\varepsilon_k}(sP_k)^{\frac{2}{\varepsilon_k}}\mathbb{E}_{\Psi_k}\left[\Psi_k^{\frac{2}{\varepsilon_k}}\Gamma\left(-\frac{2}{\varepsilon_k},\frac{sux\Psi_k}{\gamma_k\Psi_{k1}}\right)\right]}\right]}{x^{\frac{2}{\varepsilon_k}+1}\mathrm{e}^{\frac{sux}{\gamma_k}}}dx}. \tag{4.11}$$

Having computed the expressions for the joint p.d.f.'s in (4.8) and (4.9), the coverage probabilities can be easily obtained, and is shown in the following theorem.

Theorem 8. *The hetnet coverage probability max-SINR connectivity and the nearest-BS connectivity models are as follows:*

$$\mathbb{P}_{\text{coverage}}^{\max-\text{SINR}}=\sum_{i=1}^{K}\lambda_i\frac{2\pi}{\varepsilon_i}(\gamma_i P_i)^{\frac{2}{\varepsilon_i}}\mathbb{E}\left[\Psi_k^{\frac{2}{\varepsilon_k}}\right]\times$$

$$\int_{y=0}^{\infty}\int_{\omega=-\infty}^{\infty}\frac{\mathcal{L}_{I_o+I_c+\eta,\ \max\limits_{i=1,\cdots,K}\gamma_i M_i\le y}(j\omega)\left(\mathrm{e}^{j\omega y\left(1-\gamma_i^{-1}\right)}-\mathrm{e}^{j\omega\left(\eta+y\left(\kappa^{-1}-\gamma_i^{-1}\right)\right)}\right)}{2\pi j\omega y^{1+\frac{2}{\varepsilon_i}}}d\omega dy, \tag{4.12}$$

$$\mathbb{P}_{\text{coverage}}^{\text{nearest}}=\int_{y=0}^{\infty}\int_{\omega=-\infty}^{\infty}\frac{\partial}{\partial u}\mathcal{L}_{I_o+I_c+\eta,\ \max\limits_{i=1,\cdots,K}\gamma_i N_i\le u}(j\omega)\Big|_{u=y}\frac{\mathrm{e}^{j\omega y}-\mathrm{e}^{j\omega\left(\frac{y}{\kappa}+\eta\right)}}{j\omega 2\pi}d\omega dy, \tag{4.13}$$

where $\kappa=\max\limits_{i=1,\cdots,K}\gamma_i$, *all the other symbols are in Table 4.1, and the Laplace transform function in (4.12) and the derivative of the Laplace transform function in (4.13) are given in (4.6) and (4.11), respectively.*

Proof. Once the joint p.d.f. has been obtained (see (4.8) and (4.9)), the probability of the event in (4.4) can be derived as follows:

$$\begin{aligned}\mathbb{P}_{coverage}^{\max-\text{SINR}} &= \mathbb{P}\left(\left\{\frac{1}{\kappa}\times\max_{i=1,\cdots,K}\gamma_i M_i+\eta<I<\max_{i=1,\cdots,K}\gamma_i M_i\right\}\right)\\ &\overset{(a)}{=} \int_{y=0}^{\infty}\int_{x=\frac{y}{\kappa}+\eta}^{y}f_{I,\max\limits_{i=1,\cdots,K}\gamma_i M_i}(x,y)\,dxdy\\ &\overset{(b)}{=} \int_{y=0}^{\infty}\int_{\omega=-\infty}^{\infty}\frac{\partial}{\partial u}\mathcal{L}_{I_o+I_c+\eta,\ \max\limits_{i=1,\cdots,K}\gamma_i M_i\le y}(j\omega)\Big|_{u=y}\frac{\mathrm{e}^{j\omega y}-\mathrm{e}^{j\omega\left(\frac{y}{\kappa}+\eta\right)}}{j\omega 2\pi}d\omega dy,\end{aligned}$$

where (a) expresses the probability of the coverage event in terms of the joint p.d.f., (b) is obtained by substituting for the joint p.d.f. from (4.8), then interchanging the order of integrations of the variables x and ω which is justified by the boundedness of the integrals. Finally, the above expression can be further simplified to obtain (4.12).

The same steps can be followed for obtaining (4.13), and is not shown here. □

Using an alternate approach, expressions for the hetnet coverage probability are obtained in [55], again, when all the fading coefficients are i.i.d. exponential random variables. For a general system model as in this chapter, to the best of our knowledge, the hetnet coverage probability has not been characterized, until now.

Nevertheless, the semi-analytical expressions are extremely complicated even for numerical computations, and little intuition and insights about the hetnet performances are obtainable from these expressions. As a result, a more qualitative study is imperative to better understand these soon-to-be-prevalent cellular networks. From now onwards, we conduct a more systematic study to expose the properties and dependencies of the hetnet performance on the various parameters of the system. To begin with, an interesting observation is made regarding the hetnet downlink performance under the max-SINR connectivity model.

Corollary 13. *The hetnet performance under max-SINR connectivity with an arbitrary fading distribution at each tier is the same as in another hetnet with BS densities* $\left\{ \lambda_i \mathbb{E}\Psi_i^{\frac{2}{\varepsilon_i}} \Big/ \Gamma\left(1+\frac{2}{\varepsilon_i}\right) \right\}_{i=1}^{K}$ *and i.i.d. unit mean exponential distribution for fading at all the BSs in the network.*

The above result is obtained by noting that the effect of fading is equivalent to scaling the density of BSs by the $\frac{2}{\varepsilon}^{\text{th}}$ moment of the fading random variable, due to [58, Corollary 2]. A large body of work involving the stochastic geometric study of networks predominantly assume fading coefficients to be i.i.d. exponential random variables, as this greatly simplifies the analysis and renders itself to closed-form characterization of coverage probabilities and other related performance metrics of several networks including the hetnets (see [50]). A common criticism for all these works has been that the exponential distribution does not accurately capture the slow fading environment. Interestingly, the above corollary shows an example of a scenario wherein studies with the exponential fading assumptions completely characterizes the arbitrary

fading scenario. Unfortunately, the same is not true for the nearest-BS connectivity model. In the following section, we explore more properties for the hetnet downlink performance.

4.4 Qualitative study of hetnet downlink performance

We begin with some simple stochastic ordering results comparing the hetnet coverage probabilities for the two connectivity models.

Proposition 3. *For the same system parameters,* $\mathbb{P}_{\text{coverage}}^{\text{max-SINR}} > \mathbb{P}_{\text{coverage}}^{\text{nearest}}$.

The above result is easily proved by noting from (4.2) and (4.3) that $\bigcup_{k=1}^{K}\bigcup_{i=1}^{\infty}\{\text{SINR}_{ki} > \beta_k\} \supset \bigcup_{k=1}^{K}\{\text{SINR}_{k1} > \beta_k\}$, i.e. the coverage event corresponding to the nearest-BS connectivity is a subset of the max-SINR connectivity model. In the special case when $\{\beta_k\}_{k=1}^{\infty} = \beta$, commonly referred to as the unbiased case in the literature, the hetnet coverage probabilities of the max-SINR and nearest-BS connectivity models are identical to the MIRP connectivity and the MARP connectivity models, respectively. Under the MIRP connectivity, the MS connects to the BS with the maximum received power among all the tiers, and under the MARP connectivity, the MS connects to the BS with the maximum long-term averaged received power obtained by ignoring the fading. As a result, the serving BS for the MIRP and MARP connectivity models is identified as

$$(T, I) = \underset{k=1,\cdots,\ K,\ i=1,\ 2,\cdots}{\text{argmax}} P_k \Psi_{ki} R_{ki}^{-\varepsilon_k}, \text{ and } T = \underset{k=1,\cdots,\ K}{\text{argmax}} P_k R_{k1}^{-\varepsilon_k}, \tag{4.14}$$

respectively, where T refers to the tier-index and I refers to the BS-index. The corresponding hetnet coverage probability expressions are

$$\mathbb{P}_{\text{coverage}}^{\text{MIRP}} = \mathbb{P}\left(\{\text{SINR}_{T,I} > \beta_T\}\right),\ \mathbb{P}_{\text{coverage}}^{\text{MARP}} = \mathbb{P}\left(\{\text{SINR}_{T,1} > \beta_T\}\right), \tag{4.15}$$

where $\text{SINR}_{k,i}$ is defined in (4.1), (T, I) for MIRP and T for MARP are from (4.14), respectively.

When $\{\beta_k\}_{k=1}^{K} = \beta$, $\mathbb{P}_{\text{coverage}}^{\text{max-SINR}} = \mathbb{P}_{\text{coverage}}^{\text{MIRP}}$, $\mathbb{P}_{\text{coverage}}^{\text{nearest}} = \mathbb{P}_{\text{coverage}}^{\text{MARP}}$ and are equal to the complementary cumulative density function (c.c.d.f.) of the corresponding $\text{SINR}_{T,I}$ random variables. We begin with characterizing the c.c.d.f. of $\text{SINR}_{T,I}$ for the MIRP case, and several related important characteristics.

4.4.1 SINR characterization under MIRP connectivity

The following stochastic equivalence helps simplify the SINR characterization.

Lemma 7. *The SINR at the MS is the same as in the two-tier hetnet where the tier to which the MS has an open-access network with a BS density function* $\tilde{\lambda}(r) = \sum_{k=1}^{K} \tilde{\lambda}_k(r)$ *with* $\tilde{\lambda}_k(r) = \lambda_k \frac{2\pi}{\varepsilon_k} P_k^{\frac{2}{\varepsilon_k}} \mathbb{E}\Psi_k^{\frac{2}{\varepsilon_k}} r^{\frac{2}{\varepsilon_k}-1}$, $r \geq 0$ *and a closed-access network with a BS density function* $\hat{\lambda}(r) = \lambda_c \frac{2\pi}{\varepsilon_c} P_c^{\frac{2}{\varepsilon_c}} \mathbb{E}\left[\Psi_c^{\frac{2}{\varepsilon_c}}\right] r^{\frac{2}{\varepsilon_c}-1}$. *All the BSs in the system have unity transmit power and unity fading coefficients. The SINR is stochastically equal to*

$$\mathrm{SINR}_{T,I} =_{\mathrm{st}} \left. \frac{\tilde{R}_{T,1}^{-1}}{\sum_{k=1}^{K}\sum_{\substack{l=1 \\ (k,l)\neq(T,1)}}^{\infty} \tilde{R}_{kl}^{-1} + \sum_{l=1}^{\infty} \hat{R}_l^{-1} + \eta} \right|_{\left(\left\{\tilde{\lambda}_k(r)\right\}_{k=1}^{K}, \hat{\lambda}(r)\right)} =_{\mathrm{st}} \left. \frac{\tilde{R}_1^{-1}}{\sum_{k=2}^{\infty} \tilde{R}_k^{-1} + \sum_{l=1}^{\infty} \hat{R}_l^{-1} + \eta} \right|_{\left(\tilde{\lambda}(r), \hat{\lambda}(r)\right)}, \tag{4.16}$$

where $=_{\mathrm{st}}$ *indicates the equivalence in distribution; and* $\left\{\tilde{R}_i\right\}_{i=1}^{\infty}$ $\left(\left\{\hat{R}_i\right\}_{i=1}^{\infty}\right)$ *is the ascendingly ordered distances of the BSs from the origin, obtained from a non-homogeneous 1-D Poisson point process with BS density function* $\tilde{\lambda}(r)$ $\left(\hat{\lambda}(r)\right)$ *defined above.*

Proof. See Appendix 4.7.2. □

The following lemma shows interesting stochastic equivalences when $\{\varepsilon_k\}_{k=1}^{K} = \varepsilon_c = \varepsilon$.

Lemma 8. *The hetnet SINR under MIRP connectivity has the same distribution as that of a MS at the origin of the following three networks. The first is a hetnet with BS densities* $\left\{\lambda_k P_k^{\frac{2}{\varepsilon}} \mathbb{E}\left[\Psi_k^{\frac{2}{\varepsilon}}\right]\right\}_{k=1}^{K}$, $\lambda_c P_k^{\frac{2}{\varepsilon}} \mathbb{E}\left[\Psi_c^{\frac{2}{\varepsilon}}\right]$ *for the* K *open-access tiers and the closed-access tier, respectively, unity transmit powers and shadow fading factors for all tiers. The other two are two-tier networks with unity transmit powers and shadow fading factors for all their BSs. The first two-tier network has the open-access tier BS density* $\sum_{l=1}^{K} \lambda_l P_l^{\frac{2}{\varepsilon}} \mathbb{E}\left[\Psi_l^{\frac{2}{\varepsilon}}\right]$, *closed-access tier BS density* $\lambda_c P_k^{\frac{2}{\varepsilon}} \mathbb{E}\left[\Psi_c^{\frac{2}{\varepsilon}}\right]$ *and experiences the same background noise as the hetnets. The second two-tier network has a unity open-access tier BS density, closed-access tier BS density* $\hat{\lambda}_c = \frac{\lambda_c P_k^{\frac{2}{\varepsilon}} \mathbb{E}\left[\Psi_c^{\frac{2}{\varepsilon}}\right]}{\sum_{l=1}^{K} \lambda_l P_l^{\frac{2}{\varepsilon}} \mathbb{E}\left[\Psi_l^{\frac{2}{\varepsilon}}\right]}$ *and a background noise* $\bar{\eta} = \eta\left(\sum_{l=1}^{K} \lambda_l P_l^{\frac{2}{\varepsilon}} \mathbb{E}\left[\Psi_l^{\frac{2}{\varepsilon}}\right]\right)^{-\frac{\varepsilon}{2}}$. *Equivalently,*

$$\mathrm{SINR}_{T,I} =_{\mathrm{st}} \mathrm{SINR}\left(K, \left\{\lambda_k P_k^{\frac{2}{\varepsilon}} \mathbb{E}\left[\Psi_k^{\frac{2}{\varepsilon}}\right]\right\}_{k=1}^{K}, \lambda_c P_k^{\frac{2}{\varepsilon}} \mathbb{E}\left[\Psi_c^{\frac{2}{\varepsilon}}\right], \eta, T\right) \tag{4.17}$$

$$=_{\mathrm{st}} \mathrm{SINR}\left(2, \sum_{l=1}^{K} \lambda_l P_l^{\frac{2}{\varepsilon}} \mathbb{E}\left[\Psi_l^{\frac{2}{\varepsilon}}\right], \lambda_c P_c^{\frac{2}{\varepsilon}} \mathbb{E}\left[\Psi_c^{\frac{2}{\varepsilon}}\right], \eta, 1\right) \tag{4.18}$$

$$=_{\mathrm{st}} \mathrm{SINR}\left(2, 1, \hat{\lambda}_c, \bar{\eta}, 1\right), \tag{4.19}$$

where $=_{\text{st}}$ *indicates equivalence in distribution.*

Proof. See Appendix 4.7.3. □

Lemmas 7 and 8 are generalizations of [30, Lemma 1] and [27, Lemma 1], respectively, to the case where the hetnet also contains a closed-access tier. Next, we compute the hetnet coverage probability.

Theorem 9. *The hetnet coverage probability under MIRP is*

$$\mathbb{P}_{\text{coverage}}^{\text{MIRP}} = \sum_{k=1}^{K} \lambda_k P_k^{\frac{2}{\varepsilon_k}} \mathbb{E}\left[\Psi_k^{\frac{2}{\varepsilon_k}}\right] \int_{r=0}^{\infty} 2\pi r \int_{\omega=-\infty}^{\infty} \frac{\mathrm{e}^{j\omega\eta r^{\varepsilon_k}} \left(1-\mathrm{e}^{-\frac{j\omega}{\beta_k}}\right)}{j\omega 2\pi} \times \mathrm{e}^{-\sum_{l=1}^{K} \lambda_l P_l^{\frac{2}{\varepsilon_l}} \mathbb{E}\left[\Psi_l^{\frac{2}{\varepsilon_l}}\right] \pi r^{\frac{2\varepsilon_k}{\varepsilon_l}} {}_1F_1\left(-\frac{2}{\varepsilon_l};1-\frac{2}{\varepsilon_l};j\omega\right) - \lambda_c P_c^{\frac{2}{\varepsilon_c}} \mathbb{E}\left[\Psi_c^{\frac{2}{\varepsilon_c}}\right] \pi r^{\frac{2\varepsilon_k}{\varepsilon_c}} G\left(j\omega,\frac{2}{\varepsilon_c}\right)} d\omega dy, \tag{4.20}$$

where $G\left(j\omega,\frac{2}{\varepsilon_c}\right) = \int_{t=0}^{\infty} \left(1-\mathrm{e}^{j\omega t}\right) \frac{2}{\varepsilon_c} t^{-1-\frac{2}{\varepsilon_c}} dt$.

Proof. The proof is along the same lines as [30, Theorem 1], and is not shown here. □

The above expression can be greatly simplified under certain special cases, and the following results present these cases.

Corollary 14. *When* $\{\varepsilon_k\}_{k=1}^{K} = \varepsilon_c = \varepsilon$*, the hetnet coverage probability is*

$$\mathbb{P}_{\text{coverage}}^{\text{MIRP}} = \sum_{k=1}^{K} \frac{\lambda_k P_k^{\frac{2}{\varepsilon}} \mathbb{E}\left[\Psi_k^{\frac{2}{\varepsilon}}\right] \int_{\omega=-\infty}^{\infty} \frac{\left(1-\mathrm{e}^{-\frac{j\omega}{\beta_k}}\right)}{j\omega 2\pi} H\left(j\omega\right) d\omega}{\sum_{l=1}^{K} \lambda_l P_l^{\frac{2}{\varepsilon}} \mathbb{E}\left[\Psi_l^{\frac{2}{\varepsilon}}\right]}, \tag{4.21}$$

where $H\left(j\omega\right) = \int_{r=0}^{\infty} 2\pi r \mathrm{e}^{j\omega\bar{\eta}r^{\varepsilon} - \pi r^2\left({}_1F_1\left(-\frac{2}{\varepsilon};1-\frac{2}{\varepsilon};j\omega\right) + \hat{\lambda}_c G\left(j\omega,\frac{2}{\varepsilon}\right)\right)} dr$, $H\left(j\omega\right)|_{\bar{\eta}=0} = \frac{1}{{}_1F_1\left(-\frac{2}{\varepsilon};1-\frac{2}{\varepsilon};j\omega\right) + \hat{\lambda}_c G\left(j\omega,\frac{2}{\varepsilon}\right)}$, *$\bar{\eta}$ and $\hat{\lambda}_c$ are from Lemma 8 and $G\left(\cdot,\cdot\right)$ is defined in Theorem 9. When $\{\beta_k\} = \beta$, (4.21) is equal to $\mathbb{P}_{\text{coverage}}^{\text{max-SINR}}$, and further, when there is no closed-access tier $\left(\hat{\lambda}_c = 0\right)$, (4.21) is equal to the single-tier network coverage probability (see [58, Corollary 4]) and is independent of the transmission powers and fading factors of the BSs in the system.*

Proof. The result is obtained by exchanging the order of integrations in (4.20) and simplifying. □

The following theorem shows another scenario when the hetnet coverage probabilities are identical for the max-SINR and MIRP connectivity models.

Theorem 10. *When $\beta_k \geq 1,\ \forall\ k = 1, \cdots, K$, the hetnet coverage probability is given by*

$$\mathbb{P}_{\text{coverage}}^{\max-\text{SINR}} = \mathbb{P}_{\text{coverage}}^{\text{MIRP}} = \sum_{k=1}^{K} \frac{\lambda_k P_k^{\frac{2}{\varepsilon_k}} \mathbb{E}\left[\Psi_k^{\frac{2}{\varepsilon_k}}\right] \beta_k^{-\varepsilon_k}}{\Gamma\left(1+\frac{2}{\varepsilon_k}\right)} \times$$
$$\int_{r=0}^{\infty} 2\pi r \times \mathrm{e}^{-\eta r^{\varepsilon_k} - \frac{\lambda_c \pi P_c^{\frac{2}{\varepsilon_c}} \mathbb{E}\left[\Psi_c^{\frac{2}{\varepsilon_c}}\right] r^{\frac{2\varepsilon_k}{\varepsilon_c}}}{\Gamma\left(1+\frac{2}{\varepsilon_c}\right)\text{sinc}\left(\frac{2\pi}{\varepsilon_c}\right)} - \sum_{l=1}^{K} \frac{\lambda_l \pi P_l^{\frac{2}{\varepsilon_l}} \mathbb{E}\left[\Psi_l^{\frac{2}{\varepsilon_l}}\right] r^{\frac{2\varepsilon_k}{\varepsilon_l}}}{\Gamma\left(1+\frac{2}{\varepsilon_l}\right)\text{sinc}\left(\frac{2\pi}{\varepsilon_l}\right)}} dr, \tag{4.22}$$

and in the interference limited case ($\eta = 0$) when $\{\varepsilon_k\}_{k=1}^{K} = \varepsilon$

$$\mathbb{P}_{\text{coverage}}^{\max-\text{SINR}} = \mathbb{P}_{\text{coverage}}^{\text{MIRP}} = \sum_{k=1}^{K} \frac{\lambda_k P_k^{\frac{2}{\varepsilon}} \mathbb{E}\left[\Psi_k^{\frac{2}{\varepsilon}}\right] \text{sinc}\left(\frac{2\pi}{\varepsilon}\right) \beta_k^{-\varepsilon}}{\lambda_c P_c^{\frac{2}{\varepsilon}} \mathbb{E}\left[\Psi_c^{\frac{2}{\varepsilon}}\right] + \sum_{l=1}^{K} \lambda_l P_l^{\frac{2}{\varepsilon}} \mathbb{E}\left[\Psi_l^{\frac{2}{\varepsilon}}\right]}. \tag{4.23}$$

Proof. Firstly, from [50, Lemma 1], when $\beta_k \geq 1$, there exists at most one open-access BS that can have an SINR above the corresponding threshold. As a result, hetnet coverage probability in (4.2) becomes $\mathbb{P}_{\text{coverage}}^{\max-\text{SINR}} = \sum_{k=1}^{K} \mathbb{P}\left(\{\text{SINR}_k\left(\max\right) > \beta_k\}\right) = \mathbb{P}_{\text{coverage}}^{\text{MIRP}}$. See Appendix 4.7.4 to derive (4.22), which simplifies to (4.23) when $\eta = 0$. □

In the above result, (4.22) is an extremely simple integral to compute and is an extension of [50, Theorem 1] to arbitrary fading and arbitrary path-loss case. The study of the MIRP connectivity has given many interesting insights and simplifications for the max-SINR case. Now, we study the MARP connectivity in further detail, and derive interesting results for the hetnet performance under nearest-BS connectivity.

4.4.2 SINR characterization under MARP connectivity

From the definition of the hetnet coverage probability under MIRP and MARP, the stochastic ordering result can be extended beyond Proposition 3 as follows.

Proposition 4. *For the same system parameters, when $\{\beta_k\}_{k=1}^{K} = \beta$ or $\{\beta_k\}_{k=1}^{K} \geq 1$, $\mathbb{P}_{\text{coverage}}^{\text{MARP}} = \mathbb{P}_{\text{coverage}}^{\text{nearest}} < \mathbb{P}_{\text{coverage}}^{\max-\text{SINR}} = \mathbb{P}_{\text{coverage}}^{\text{MIRP}}$.*

It is clear from equations (4.11) and (4.5) that it is not easy to compute the hetnet coverage probability, even with numerical integration, for arbitrary fading case. With slight modifications to the approach in Theorem 8 and [70, Theorem 1], hetnet coverage probability with MARP can also be derived. These expressions do not simplify significantly beyond that in (4.5) and hence is not presented here. Nevertheless, the following stochastic equivalence is a useful simplification that will be used in the rest of this section.

Corollary 15. *Under MARP connectivity, the following stochastic equivalences hold:*

$$\mathrm{SINR}_{T,1} \quad =_{\mathrm{st}} \quad \left.\frac{\Psi_{T,1}\tilde{R}_{T,1}^{-1}}{\sum_{\substack{m=1\\(m,l)\neq(T,1)}}^{K}\sum_{l=1}^{\infty}\Psi_{ml}\tilde{R}_{ml}^{-1}+\sum_{n=1}^{\infty}\Psi_{cn}\hat{R}_{cn}^{-1}+\eta}\right|_{\left(\left\{\tilde{\lambda}_k(r)\right\}_{k=1}^{K},\hat{\lambda}(r)\right)}, \tag{4.24}$$

where the equivalent hetnet has BS distributions according to non-homogeneous Poisson process with density functions $\left\{\tilde{\lambda}_k(r)=\lambda_k\frac{2\pi}{\varepsilon_k}P_k^{\frac{2}{\varepsilon_k}}r^{\frac{2}{\varepsilon_k}-1}\right\}_{k=1}^{K}$, $\hat{\lambda}(r)=\lambda_c\frac{2\pi}{\varepsilon_c}P_c^{\frac{2}{\varepsilon_c}}r^{\frac{2}{\varepsilon_c}-1}$, $r\geq 0$, *for the* K *open-access tiers and the closed-access tier, respectively. In both the equivalent hetnets, the fading distributions are the same as the original hetnet, all BSs have unity transmit power and hence, MARP is the same as the MS communicating with the nearest BS of the* K *open-access tiers.*

The result is yet another application of the Marking theorem of Poisson process, and can be proved using the same techniques as developed in Lemma 7. In [53], Jo et. al. have demonstrated that simple expressions for the hetnet coverage probability under MARP can be computed when the fading coefficients are i.i.d. exponential random variables. These results are restricted to the open-access case, and are extended for a general hetnet below.

Theorem 11. *The hetnet coverage probability under MARP connectivity with i.i.d. exponential fading distribution at all BSs is*

$$\mathbb{P}_{\mathrm{coverage}}^{\mathrm{MARP}}=\sum_{k=1}^{K}\lambda_k P_k^{\frac{2}{\varepsilon_k}}\beta_k^{-\frac{2}{\varepsilon_k}}\int_{r=0}^{\infty}2\pi r\times \mathrm{e}^{-\eta r^{\varepsilon_k}-\frac{\lambda_c\pi P_c^{\frac{2}{\varepsilon_c}}r^{\frac{2\varepsilon_k}{\varepsilon_c}}}{\mathrm{sinc}\left(\frac{2\pi}{\varepsilon_c}\right)}-\sum_{l=1}^{K}\lambda_l\pi P_l^{\frac{2}{\varepsilon_l}}F(\beta_k,\varepsilon_l)r^{\frac{2\varepsilon_k}{\varepsilon_l}}}dr, \tag{4.25}$$

where $F(\beta_k,\varepsilon_l)=\frac{1}{\mathrm{sinc}\left(\frac{2\pi}{\varepsilon_l}\right)}+\beta_k^{-\frac{2}{\varepsilon_l}}\left[1-\ {}_2F_1\left(1,\frac{2}{\varepsilon_l};1+\frac{2}{\varepsilon_l};-\beta_k^{-1}\right)\right]$. *When* $\{\varepsilon_k\}_{k=1}^{K}=\varepsilon$ *and* $\eta=0$,

$$\mathbb{P}_{\mathrm{coverage}}^{\mathrm{nearest}}=\mathbb{P}_{\mathrm{coverage}}^{\mathrm{MARP}}=\sum_{k=1}^{K}\frac{\lambda_k P_k^{\frac{2}{\varepsilon}}\beta_k^{-\frac{2}{\varepsilon}}\mathrm{sinc}\left(\frac{2\pi}{\varepsilon}\right)}{\lambda_c P_c^{\frac{2}{\varepsilon}}+\sum_{l=1}^{K}\lambda_l P_l^{\frac{2}{\varepsilon}}F(\beta_k,\varepsilon)\,\mathrm{sinc}\left(\frac{2\pi}{\varepsilon}\right)}. \tag{4.26}$$

Proof. See Appendix 4.7.5. □

The above is a generalization of [53, Theorem 1] to closed-access case. Further, comparing (4.23) and (4.26), clearly, $\mathbb{P}_{\mathrm{coverage}}^{\mathrm{MIRP}}\geq\mathbb{P}_{\mathrm{coverage}}^{\mathrm{MARP}}$, when $\{\beta_k\}_{k=1}^{\infty}\geq 1$ since $F(\beta_k,\varepsilon_l)\,\mathrm{sinc}\left(\frac{2\pi}{\varepsilon_l}\right)\geq 1$, $\forall\ \beta_k\geq 0$, $\varepsilon_l>2$.

4.5 Numerical Examples and Discussion

In this section, we provide some numerical examples that complement the theoretical results presented until now. We restrict ourselves to the study of a two tier hetnet consisting of the macrocell and the femtocell

networks, respectively, under the max-SINR connectivity model while reminding the reader that the theory presented in this paper allows a similar analysis for arbitrary number of tiers and also carries over to the nearest-BS connectivity model. Also, please refer to Appendix 4.7.6 for the algorithm to perform the Monte-Carlo simulations. For all the studies in this paper, $\lambda_2 = 5\lambda_1$, $P_1 = 25P_2$, $\varepsilon = 3$, and $\beta_2 = 1$ dB, where the subscripts '1' and '2' correspond to macrocell and femtocell networks, respectively. Further, under the closed-access BS association scheme, the MS has access to the macrocell network only.

In Figures 4.1, 4.2 and 4.3, we study the coverage probability, coverage conditional average rate and the average fraction of users served by the macrocell network, respectively, for various configurations of shadow fading distributions at the macrocell and the femtocell BSs. In all the figures, T1 (T2) stand for tier 1, i.e. the macrocell network (tier 2, i.e. the femtocell network). Further, Exp$(\cdot)$ and LN$(\cdot)$ are abbreviations for exponential distribution with a given mean and log-normal distribution with a zero mean and standard deviation (when the random variable is expressed in dB), respectively, and they represent distribution of the shadow fading factors of the corresponding tiers.

While the expressions in Theorem 10 clearly show that a MS has a better coverage probability under open-access than closed-access, the plots in Figure 4.1 provides a quantitative justification for the same. The coverage probability curve corresponding to the exponential fading distribution at both the tiers 1 and 2 with means 40 and 1, respectively, also corresponds to the case where $P_1 = 1000P_2$, with the shadow fading factors at both the tiers being unit mean exponential distributions. The open and closed access have approximately the same coverage probabilities because the MS is almost always served by a macrocell BS, as can been seen in the corresponding curve in Figure 4.2. As a result, blocking access to the femtocell BSs altogether, has only a marginal influence on the coverage probability at the MS.

The two curves following the aforementioned curve in Figures 4.1-4.3 complement the fact that all the three performance metrics are identical irrespective of the distribution of the shadow fading factors, when the shadow fading factors have the same distribution across all the tiers. The last two curves in Figures 4.1-4.3 show that all the performance metrics are identical as long as the shadow fading coefficients of the corresponding tiers have the same $(2/\varepsilon)^{\text{th}}$ moments. Note that $\mathbb{E}\left[\Psi^{\frac{2}{\varepsilon}}\right]$ is the same when Ψ has a log-normal distribution with zero mean and 6 dB standard deviation or when Ψ is an exponential random variable with

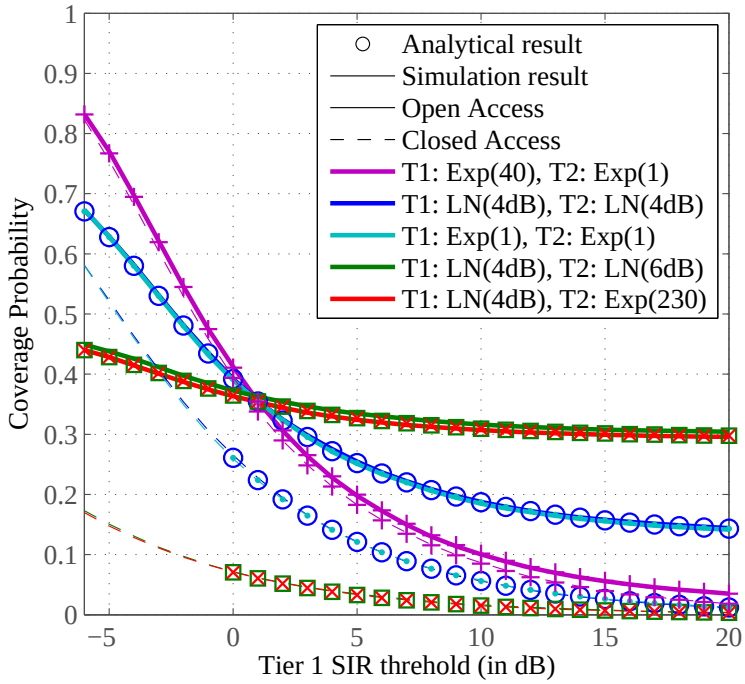

Figure 4.1: Two-tier hetnet: Comparing coverage probabilities for various shadow fading distributions

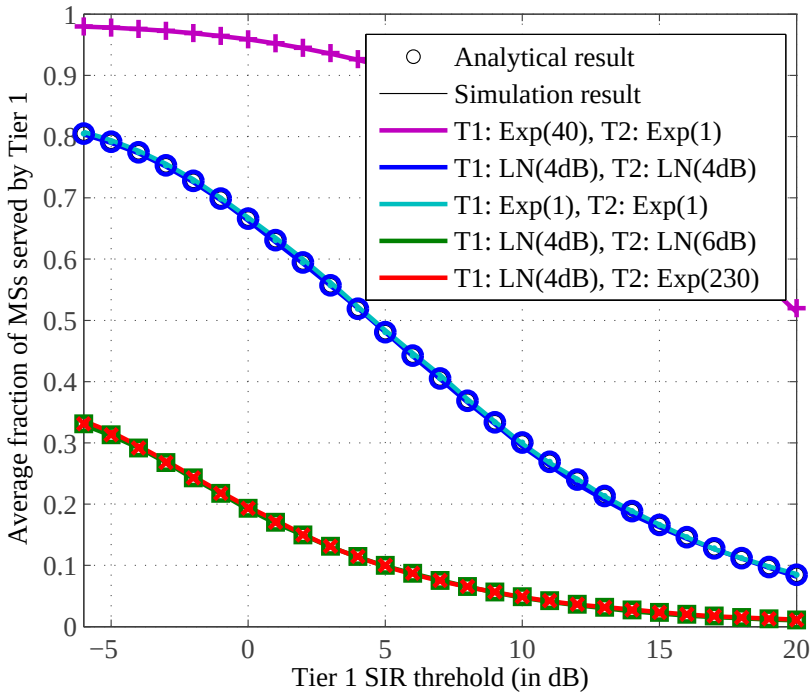

Figure 4.2: Two-tier hetnet: Average fraction of MSs served by macrocell BSs vs macrocell SIR threshold

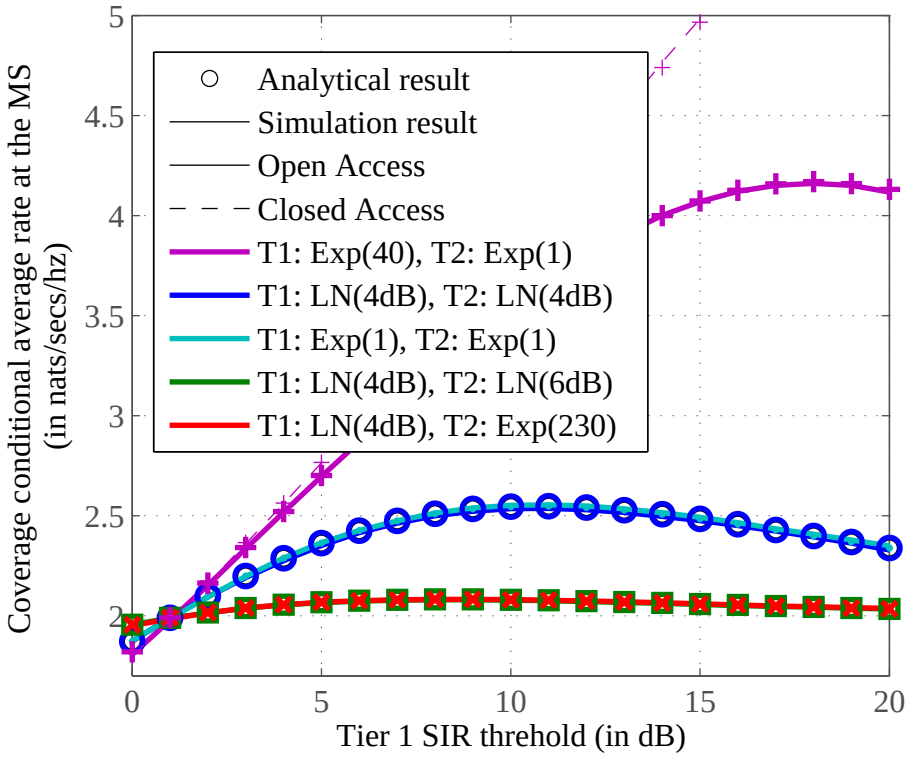

Figure 4.3: Two-tier hetnet: Variation of coverage conditional average rate with Tier 1 SIR threshold and different shadow fading distributions

mean 230.

A log-normal random variable with zero mean and a given standard deviation is a good model for shadow fading factors. Note that the femtocell network is introduced to improve the indoor performance. The shadow fading factors in the indoor environments are known to have a comparable or greater standard deviation than otherwise. Such a situation is represented by last four curves in Figures 4.1-4.3. The gap between the open and closed access coverage probability curves indicate the contribution of the femtocell network in providing coverage to the MS. It is immediately clear that the dense low-power femtocell network has a more critical role in providing coverage in realistic indoor models, when we look at the last 4 curves in Figures 4.1 and 4.2.

Under open-access, the coverage probability and the coverage conditional average rate (see Figures 4.1 and 4.2) for all the 5 curves mentioned above intersect when the SIR threshold for the macrocell network is equal to 1 dB. This brings us to an important point that when the SIR threshold is the same for all the tiers, these metrics become independent of the transmission power and shadow fading factors of the different tiers, and collapses to the corresponding metrics in a single-tier network with the same path-loss exponent and SIR threshold. Along the same lines, the coverage conditional average rate for a two-tier hetnet under closed-access also collapses to that of a single-tier network, and is independent of the transmission power and shadow fading factors of the different tiers.

4.6 Conclusions

In this chapter, for the most general model of the hetnets, the downlink coverage probability and other related performance metrics such as the average downlink rate and average fraction of users served by each tier of the hetnet are characterized. Two important BS connectivity models are studied, namely, the max-SINR and the nearest-BS connectivity, respectively. Semi-analytical expressions for the hetnet coverage probability is obtained for both the cases. Further, several properties pertaining to the hetnet downlink performance are analyzed, which provide great insights about these complex networks. As an example, we identify the MIRP and MARP connectivity models to be equivalent to the former models under certain special conditions. These models are much simpler to analyze and the results for these models

expose interesting properties of the hetnet. The results in this chapter greatly generalize the existing hetnet performance characterization results and are essential for better understanding of the future developments in wireless communications that are heavily based on hetnets.

4.7 Appendix

4.7.1 Proof for Lemma 6

The proof for (4.6) is shown below.

$$
\begin{aligned}
&\mathcal{L}_{I_o+I_c+\eta,\ \max\limits_{k=1,\cdots,K}\gamma_k M_k\leq u}(s)\\
&=\mathbb{E}\left[\exp\left(-s\left(I_o+I_c+\eta\right)\right)\times\mathcal{I}\left(\max_{k=1,\cdots,K}\gamma_k M_k\leq u\right)\right]\\
&\overset{(a)}{=}\mathcal{L}_{I_c}(s)\,\mathrm{e}^{-s\eta}\mathbb{E}\left[\prod_{k=1}^{K}\prod_{l=1}^{\infty}\mathrm{e}^{-sP_k\Psi_{kl}R_{kl}^{-\varepsilon_k}}\mathcal{I}\left(\gamma_k P_k\Psi_{kl}R_{kl}^{-\varepsilon_k}\leq u\right)\right]\\
&\overset{(b)}{=}\mathcal{L}_{I_c}(s)\,\mathrm{e}^{-s\eta}\prod_{k=1}^{K}\mathbb{E}\left[\prod_{l=1}^{\infty}\mathrm{e}^{-sP_k\Psi_{kl}R_{kl}^{-\varepsilon_k}}\mathcal{I}\left(P_k\Psi_{kl}R_{kl}^{-\varepsilon_k}\leq\frac{u}{\gamma_k}\right)\right]\\
&\overset{(c)}{=}\mathcal{L}_{I_c}(s)\,\mathrm{e}^{-s\eta}\prod_{k=1}^{K}\exp\left(-\lambda_k\int_{r=0}^{\infty}\left(1-\mathbb{E}\left[\mathrm{e}^{-sP_k\Psi_k r^{-\varepsilon_k}}\mathcal{I}\left(P_k\Psi_k r^{-\varepsilon_k}\leq\frac{u}{\gamma_k}\right)\right]\right)2\pi r dr\right)\\
&\overset{(d)}{=}\mathcal{L}_{I_c}(s)\,\mathrm{e}^{-s\eta}\prod_{k=1}^{K}\exp\left(-\lambda_k\mathbb{E}_{\Psi_k}\left[\int_{t=0}^{\infty}\left(1-\mathrm{e}^{-t}\mathcal{I}\left(t\leq\frac{su}{\gamma_k}\right)\right)\frac{2\pi}{\varepsilon_k}t^{-\frac{2}{\varepsilon}-1}\left(sP_k\Psi_k\right)^{\frac{2}{\varepsilon_k}}dt\right]\right)\\
&\overset{(e)}{=}\mathcal{L}_{I_c}(s)\,\mathrm{e}^{-s\eta}\prod_{k=1}^{K}\exp\left(-\lambda_k\pi\left(sP_k\right)^{\frac{2}{\varepsilon_k}}\mathbb{E}\left[\Psi_k^{\frac{2}{\varepsilon_k}}\right]\left[\Gamma\left(1-\frac{2}{\varepsilon_k}\right)+\frac{2}{\varepsilon_k}\int_{t=0}^{\infty}\mathrm{e}^{-t}t^{-\frac{2}{\varepsilon}-1}\mathcal{I}\left(t>\frac{su}{\gamma_k}\right)dt\right]\right)
\end{aligned}
\tag{4.27}
$$

where (a) is obtained by noting that I_c is independent of the random variables I_o and $\max\limits_{k=1,\cdots,K}\gamma_k M_k\leq u$, $\mathcal{L}_{I_c}(s)$ is a direct consequence of the Campbell's theorem [6], $\mathrm{e}^{-s\eta}$ is a constant and $\left\{\max\limits_{k=1,\cdots,K}\gamma_k M_k\leq u\right\}\iff\left\{\gamma_k P_k\Psi_{kl}R_{kl}^{-\varepsilon_k}\leq u\right\}$, $\forall\ k=1,\cdots,\ K$ and $l=1,\ 2,\cdots$; (b) is obtained since the random variables corresponding to a given tier are independent of the other tiers; (c) is obtained by applying the Campbell's theorem [6] to each tier of the hetnet; (d) is obtained by changing the variable of integration from r to $t=sP_k\Psi_k r^{-\varepsilon_k}$; (e) is obtained by rewriting the integral in (d) using special functions; and finally (4.6) is obtained by rewriting the integral in (e) in terms of the incomplete Gamma function.

The proof for (4.7) follows along the same lines as above and we provide only a brief outline as follows.

$$\mathcal{L}_{I_o+I_c+\eta,\ \max\limits_{k=1,\cdots,K}\gamma_k N_k\leq u}(s)$$
$$\overset{(a)}{=}\mathcal{L}_{I_c}(s)\,\mathrm{e}^{-s\eta}\mathbb{E}\left[\prod_{k=1}^{K}\prod_{l=1}^{\infty}\mathrm{e}^{-sP_k\Psi_{kl}R_{kl}^{-\varepsilon_k}}\times\mathcal{I}\left(\max_{k=1,\cdots,K}\gamma_k P_k\Psi_{k1}R_{k1}^{-\varepsilon_k}\leq u\right)\right]$$
$$=\mathcal{L}_{I_c}(s)\,\mathrm{e}^{-s\eta}\mathbb{E}\left[\prod_{k=1}^{K}\prod_{l=1}^{\infty}\mathrm{e}^{-sP_k\Psi_{kl}R_{kl}^{-\varepsilon_k}+\ln\left(\mathcal{I}\left(\gamma_k P_k\Psi_{k1}R_{k1}^{-\varepsilon_k}\leq u\right)\right)}\right]$$
$$\overset{(b)}{=}\mathcal{L}_{I_c}(s)\,\mathrm{e}^{-s\eta}\prod_{k=1}^{K}\mathbb{E}_{\Psi_{k1},R_{k1}}\left[\mathrm{e}^{-sP_k\Psi_{k1}R_{k1}^{-\varepsilon_k}}\mathcal{I}\left(\gamma_k P_k\Psi_{k1}R_{k1}^{-\varepsilon_k}\leq u\right)\mathbb{E}\left[\prod_{l=2}^{\infty}\mathrm{e}^{-sP_k\Psi_{kl}R_{kl}^{-\varepsilon_k}\mathcal{I}(R_{kl}>R_{k1})}\middle|R_{k1}\right]\right]$$
$$\overset{(c)}{=}\mathcal{L}_{I_c}(s)\,\mathrm{e}^{-s\eta}\prod_{k=1}^{K}\mathbb{E}_{\Psi_{k1},R_{k1}}\left[\mathrm{e}^{-sP_k\Psi_{k1}R_{k1}^{-\varepsilon_k}}\mathcal{I}\left(\gamma_k P_k\Psi_{k1}R_{k1}^{-\varepsilon_k}\leq u\right)\mathrm{e}^{-\lambda_k\int_{r=R_{k1}}^{\infty}\left(1-\mathbb{E}\left[\mathrm{e}^{-sP_k\Psi_k r^{-\varepsilon_k}}\right]\right)2\pi r dr}\right]$$
$$\overset{(d)}{=}\mathcal{L}_{I_c}(s)\,\mathrm{e}^{-s\eta}\prod_{k=1}^{K}\mathbb{E}_{\Psi_{k1},R_{k1}}\left[\mathrm{e}^{-sP_k\Psi_{k1}R_{k1}^{-\varepsilon_k}}\mathcal{I}\left(\gamma_k P_k\Psi_{k1}R_{k1}^{-\varepsilon_k}\leq u\right)\times\right.$$
$$\left.\mathrm{e}^{-\lambda_k\pi(sP_k)^{\frac{2}{\varepsilon_k}}\mathbb{E}_{\Psi_k}\left[\Psi_k^{\frac{2}{\varepsilon_k}}\int_{t=0}^{sP_k\Psi_k R_{k1}^{-\varepsilon_k}}\left(1-\mathrm{e}^{-t}\right)\frac{2}{\varepsilon_k}t^{-\frac{2}{\varepsilon_k}-1}dt\right]}\right],$$

where the maximization in (a) is only among the nearest BSs of the K tiers of the hetnet, $\mathcal{L}_{I_c}(s)$ is the same as in (4.27); (b) is obtained by exchanging the order of expectation and product since the K tiers of the hetnet are independent of each other, and further conditioning w.r.t. the fading coefficient and the distance of the nearest BS of each tier; (c) is obtained by applying the Campbell's theorem to the set of k^{th} tier BSs beyond R_{k1}, conditioned on R_{k1}; (d) is obtained by further simplifying (c); and finally (4.7) is obtained by evaluating the expectation w.r.t. R_{k1} in (d) where the p.d.f. of R_{k1} is $f_{R_{k1}}(r)=\lambda_k 2\pi r\mathrm{e}^{-\lambda_k\pi r^2},\ r\geq 0$, and further simplifying.

4.7.2 Proof for Lemma 7

Given a BS belonging to the k^{th} open-access tier is at a distance R_k from the origin, then, due to [30, Theorem 2], $\tilde{R}\Big|\,k=(P_k\Psi_k)^{-1}R_k^{\varepsilon_k}$ represents the distance of the BS from the origin where the BS arrangement is according to a non-homogeneous 1-D Poisson point process with BS density function $\lambda^{(k)}(r)$, as long as $\mathbb{E}\left[\Psi_k^{\frac{2}{\varepsilon_k}}\right]<\infty$, for each $k=1,\ 2,\cdots,\ K$. Similarly, for the closed-access tier, $\hat{R}=(P_c\Psi_c)^{-1}R_c^{\varepsilon_c}$ the distance where the BS arrangement is according to a non-homogeneous 1-D Poisson point process with BS density function $\hat{\lambda}(r)$, as long as $\mathbb{E}\left[\Psi_c^{\frac{2}{\varepsilon_c}}\right]<\infty$. This is a consequence of the Mapping theorem [6, Page 18] and the Marking Theorem [6, Page 55] of the Poisson processes. Further, since the BS arrangements

in the different tiers were originally independent of each other, the set of all the BSs in the equivalent 1-D non-homogeneous Poisson process is merely the union of all $\tilde{R}'s \Big| k,\ \forall\ k = 1,\ 2, \cdots,\ K$. By the Superposition Theorem [6, Page 16] of Poisson process, $\tilde{R}$ (notice that it is not conditioned on k) corresponds to the distance from origin of BS arrangement according to non-homogeneous Poisson point process with density function $\tilde{\lambda}(r) = \sum_{k=1}^{K} \lambda^{(k)}(r),\ r \geq 0$.

In summary, we have converted the BS arrangement on a 2-D plane of hetnet to a BS arrangement of the equivalent 2-tier network along 1-D (positive x-axis), and hence, the SINR distributions of both these networks are also equivalent. Further, by our construction, the MIRP BS in the hetnet corresponds to the BS that is nearest to the origin (MS) in the equivalent 2-tier network. As a result, SINR may be written in terms of the $\tilde{R}$'s and $\hat{R}$'s indexed in the ascending order, and we get (4.16).

4.7.3 Proof for Lemma 8

The hetnet SINR under MIRP can be computed as follows. For each tier $m = 1, \cdots,\ K,\ c$ (c refers to the closed-access tier), form the set $\left\{(P_m \Psi_{m,l})^{-\frac{1}{\varepsilon}} R_{m,l}\right\}_{l=1}^{\infty}$ and represent as $\left\{\bar{R}_{m,k}\right\}_{k=1}^{\infty}$ where $\tilde{R}$'s are ascendingly ordered. Now, $\left\{\bar{R}_{m,k}^{-\varepsilon}\right\}_{k=1}^{\infty}$ represents the received powers of all the m^{th} tier BSs in the descending order. Finally, the desired BS's power and tier index (T) can be easily found by identifying the maximum in the set $\left\{\bar{R}_{m,1}^{-\varepsilon}\right\}_{m=1}^{K}$ and the SINR can be computed. Using [58, Corollary 3] which is an application of the Marking theorem [6, Page 55], it can be seen that $\left\{\bar{R}_{m,k}\right\}_{k=1}^{\infty}$ represents the distances from origin of BSs arranged according to homogeneous Poisson point process with BS density $\lambda_m P_m \mathbb{E}\left[\Psi_m^{\frac{2}{\varepsilon}}\right]$, where Ψ_m has the same distribution as the m^{th} tier shadow fading factors. As a result, the set $\left\{\bar{R}_{m,l}^{-\varepsilon}\right\}_{m=1,\ l=1}^{m=K,\ l=\infty}$ represents the set of received powers at the origin of the hetnet composed of K open-access tiers and a closed-acess tier with BS densities $\left\{\lambda_k P_k \mathbb{E}\left[\Psi_k^{\frac{2}{\varepsilon}}\right]\right\}_{k=1}^{K}$, $\lambda_c P_c \mathbb{E}\left[\Psi_c^{\frac{2}{\varepsilon}}\right]$, respectively, with unity transmit powers and shadow fading factors at each BS. This is equivalent to the original hetnet and has the same SINR distribution, hence proving (4.17).

Further, using the Superposition theorem [6, Page 16], the K open-access tiers of the equivalent hetnet can be combined to form a single tier network with a BS density equal to $\sum_{l=1}^{K} \lambda_l P_l^{\frac{2}{\varepsilon}} \mathbb{E}\Psi_l^{\frac{2}{\varepsilon}}$, thus proving the SINR equivalence in (4.18). The distribution of SINR of this two-tier network is the same as that of an MS

in another two-tier network where the open-access tier has unity BS density, the closed-access tier has a BS density $\frac{\lambda_c P_c \mathbb{E}\left[\Psi_c^{\frac{2}{\varepsilon}}\right]}{\sum_{l=1}^{K} \lambda_l P_l^{\frac{2}{\varepsilon}} \mathbb{E}\Psi_l^{\frac{2}{\varepsilon}}}$, unity transmit power and shadow fading factors at all BSs and a background noise $\frac{\eta}{\left(\sum_{l=1}^{K} \lambda_l P_l^{\frac{2}{\varepsilon}} \mathbb{E}\Psi_l^{\frac{2}{\varepsilon}}\right)^{-\frac{\varepsilon}{2}}}$, due to [58, Lemma 3] and hence we get the relation (4.19).

4.7.4 Proof for Theorem 10

From Corollary 13 and Lemma 7, we get the following stochastic equivalence:

$$\mathrm{SINR}_{T,I} \quad =_{\mathrm{st}} \quad \left. \frac{h_{T,I}\tilde{R}_{T,I}^{-1}}{\sum_{\substack{k=1}}^{K}\sum_{\substack{(k,l)\neq(T,I)}}^{\infty} h_{kl}\tilde{R}_{kl}^{-1} + \sum_{l=1}^{\infty} g_l \hat{R}_l^{-1} + \eta} \right|_{\left(\left\{\tilde{\lambda}_k(r)\right\}_{k=1}^{\infty}, \hat{\lambda}(r)\right)},$$

where h_{kl}'s and g_l's are i.i.d. unit mean exponential random variables, $J = \underset{k=1,2,\cdots}{\operatorname{argmax}} h_{T,k}\tilde{R}_{T,k}^{-1}$, $\left\{\tilde{R}_{kl}\right\}_{l=1}^{\infty}$ and $\left\{\hat{R}_l\right\}_{l=1}^{\infty}$ are from non-homogeneous 1-D Poisson processes with density functions $\tilde{\lambda}_k(r) = \lambda_k \frac{2\pi}{\varepsilon_k} P_k^{\frac{2}{\varepsilon_k}} r^{\frac{2}{\varepsilon_k}-1}$, $k = 1, \cdots, K$ and $\hat{\lambda}(r) = \lambda_c \frac{2\pi}{\varepsilon_c} P_c^{\frac{2}{\varepsilon_c}} r^{\frac{2}{\varepsilon_c}-1}$, respectively. The following steps derive the hetnet coverage probability and closely follows the proof techniques for [30, Theorem 4] and [50, Theorem 1]

$$\begin{aligned}
\mathbb{P}_{\text{coverage}}^{\text{max-SINR}} = \mathbb{P}_{\text{coverage}}^{\text{MIRP}} &= \sum_{i=1}^{K} \mathbb{P}\left(\left\{\frac{h_{ij}\tilde{R}_{ij}^{-1}}{\sum_{\substack{k=1}}^{K}\sum_{\substack{(k,l)\neq(i,j)}}^{\infty} h_{kl}\tilde{R}_{kl}^{-1} + \sum_{l=1}^{\infty} g_l \hat{R}_l^{-1} + \eta} > \beta_i\right\}\right) \\
&\overset{(a)}{=} \sum_{i=1}^{K} \mathbb{E}_{\tilde{R}_{ij}}\left[\mathrm{e}^{-\beta_i \tilde{R}_{ij}\eta}\mathbb{E}\left[\mathrm{e}^{-\beta_i \tilde{R}_{ij}\sum_{\substack{k=1}}^{K}\sum_{\substack{(k,l)\neq(i,j)}}^{\infty} h_{kl}\tilde{R}_{kl}^{-1}}\middle|\tilde{R}_{ij}\right]\mathbb{E}\left[\mathrm{e}^{-\beta_i \tilde{R}_{ij}\sum_{l=1}^{\infty} g_l \hat{R}_l^{-1}}\middle|\tilde{R}_{ij}\right]\right] \\
&\overset{(b)}{=} \sum_{i=1}^{K} \int_{r=0}^{\infty} \tilde{\lambda}_i(r)\, \mathrm{e}^{-\eta\beta_i r - \sum_{l=1}^{K} \frac{\lambda_l \pi (P_l \beta_i r)^{\frac{2}{\varepsilon_l}} \mathbb{E}\left[\Psi_l^{\frac{2}{\varepsilon_l}}\right]}{\Gamma\left(1+\frac{2}{\varepsilon_l}\right)\mathrm{sinc}\left(\frac{2\pi}{\varepsilon_l}\right)} - \frac{\lambda_c \pi (P_c \beta_i r)^{\frac{2}{\varepsilon_c}} \mathbb{E}\left[\Psi_c^{\frac{2}{\varepsilon_c}}\right]}{\Gamma\left(1+\frac{2}{\varepsilon_c}\right)\mathrm{sinc}\left(\frac{2\pi}{\varepsilon_c}\right)}} dr,
\end{aligned}$$

where $\tilde{R}_{ij}$ is the distance from the origin of an arbitrary point in the non-homogeneous Poisson process with density function $\tilde{\lambda}_i(r)$, (a) is obtained by computing the probability of w.r.t. h_{ij} conditioned on all the other involved random variables and noting that the two Poisson processes are independent of each other, (b) is obtained by evaluating the inner expectations by applying Campbell's theorem [6] (same steps as in the proof of [30, Theorem 4]) and expressing the expectation w.r.t. $\tilde{R}_{ij}$ by the integral where $\tilde{\lambda}(r)\, dr$ is the probability that there exists a point in the interval $(r, r+dr)$, and finally (4.22) is obtained by simplifying the integral in (b).

4.7.5 Proof for Theorem 11

Along the same lines as [30, Lemma 4], the c.c.d.f. and the p.d.f. of the distance from the MS of the serving BS of the k^{th} open-access tier is

$$\mathbb{P}\left(\left\{\tilde{R}_{k1} > r\right\} \bigcap \bigcap_{l=1,\ l\neq k}^{K} \left\{\tilde{R}_{l1} > \tilde{R}_{k1}\right\}\right) = \mathbb{E}_{\tilde{R}_{k1}}\left[\mathcal{I}\left(\tilde{R}_{k1} > r\right)\mathbb{P}\left(\bigcap_{l=1,\ l\neq k}^{K} \left\{\tilde{R}_{l1} > \tilde{R}_{k1}\right\} \middle| \tilde{R}_{k1}\right)\right]$$

$$= \int_{t=r}^{\infty} \tilde{\lambda}_k(t)\, \mathrm{e}^{-\sum_{l=1}^{K}\int_{s=0}^{t}\tilde{\lambda}_l(s)ds} dt, \tag{4.28}$$

$$f_{T,\tilde{R}_{T1}}(k,r) = \tilde{\lambda}_k(r)\cdot \mathrm{e}^{-\sum_{l=1}^{K}\lambda_l \pi P_l^{\frac{2}{\varepsilon_l}} t^{\frac{2}{\varepsilon_l}}},\ k=1,\cdots,\ K,\ r\geq 0, \tag{4.29}$$

where $\tilde{\lambda}_l(r)$ for $l=1,\cdots,\ K$ is from Corollary 15 and the p.d.f. of $\tilde{R}_{l1}$ is $f_{T,\tilde{R}_{T,1}}(l,r) = \tilde{\lambda}_l(r)\cdot \mathrm{e}^{-\int_{s=0}^{r}\tilde{\lambda}_l(s)ds}$, $r\geq 0$ using the properties of Poisson process. Then, the calculation of the expectation in the first equality to obtain (4.28), and the derivative of (4.28) to obtain (4.29) are both straight forward. The the hetnet coverage probability is

$$\mathbb{P}^{\text{MARP}}_{\text{coverage}} \overset{(a)}{=} \sum_{k=1}^{K} \mathbb{E}_{T,\tilde{R}_{T1}}\left[\mathbb{P}\left(\left\{\frac{\Psi_{T1}\tilde{R}_{T1}^{-1}}{\sum_{m=1}^{K}\sum_{\substack{l=1\\(m,l)\neq(T,1)}}^{\infty}\Psi_{ml}\tilde{R}_{ml}^{-1} + \sum_{n=1}^{\infty}\Psi_{cn}\hat{R}_{cn}^{-1} + \eta} > \beta_T\right\}\middle| T,\tilde{R}_{T1}\right)\right]$$

$$\overset{(b)}{=} \sum_{k=1}^{K} \mathbb{E}_{T,\tilde{R}_{T1}}\left[\mathrm{e}^{-\eta\beta_k\tilde{R}_{T1}}\mathbb{E}\left[\prod_{n=1}^{\infty}\mathrm{e}^{\frac{-\beta_k\tilde{R}_{T1}\Psi_{cn}}{\hat{R}_{cn}}}\middle| T,\tilde{R}_{T1}\right]\prod_{m=1}^{K}\mathbb{E}\left[\prod_{l=1}^{\infty}\mathrm{e}^{\frac{-\beta_k\tilde{R}_{T1}\Psi_{ml}}{\tilde{R}_{ml}}}\mathcal{I}\left(\tilde{R}_{ml} > \tilde{R}_{T1}\right)\middle| T,\tilde{R}_{T1}\right]\right],$$

where (a) is from the stochastic equivalence in Corollary 15, (b) is obtained due to the independence of each tier in the hetnet given (T, R_{T1}). Finally, (4.25) is obtained by computing each expectation in (b) by applying the Campbell-Mecke theorem.

For $\{\varepsilon_k\}_{k=1}^{K} = \varepsilon$ and $\eta = 0$, the integral in (4.25) simplifies to (4.26).

4.7.6 Simulation Method

The k^{th} tier of the hetnet with K tiers is identified by the following set of system parameters: $(\lambda_k,\ P_k,\ \Psi_k,\ \varepsilon_k,\ \beta_k)$, where the symbols have all been defined in Section 4.2, and $k=1,\ 2,\cdots,\ K$, where K is the total number of tiers. Now we illustrate the steps for simulating the hetnet in order to obtain the SINR distribution and the coverage probability assuming the MS is at the origin. The algorithm for the Monte-Carlo simulation is as follows:

1) Generate N_k random variables according to a uniform distribution in the circular region of radius R_B for the locations of all the k^{th} tier BSs, where $N_k \sim \text{Poisson}\left(\lambda_k \pi R_B^2\right)$.

3) Compute the SINR at the desired BS according to Section 4.2.0.3 and record the tier index I of the desired BS.

Repeat the same procedure T (typically, $>$ 50000) times. Finally, the tail probability of SINR at η is given by $\frac{\{\#\text{ of trials where SINR} > \eta\}}{T}$, and the coverage probability is given by $\sum_{k=1}^{K} \frac{\{\#\text{ of trials where } I=k \text{ and } SINR>\beta}{T}$

Chapter 5

OFDMA Cellular Network with Fractional Frequency Reuse under Maximum SIR Connectivity

5.1 Introduction

The high data-rate targets at the MSs set by the ever-growing demands on the cellular networks to support data-intensive applications have created the need for the development and deployment of orthogonal frequency division multiplexing (OFDM) based 4G cellular networks like the third generation partnership project - long term evolution (3GPP - LTE) and the worldwide interoperability for microwave access (WiMAX) systems.

These 4G systems have recognized aggressive frequency reuse (which involves the simultaneous transmissions on all time-frequency resource blocks by all the BSs) as an approach to increase the system capacity. Associated with this improved network capacity due to the availability of the entire operable frequency band for transmission, is the issue of SIR degradation at all the MSs due to the interference from all the BSs in the multi-cellular system. This inter-cell interference renders the operation of MSs at the edge of the cell (referred to as cell-edge users) that already see a weak SIR, practically impossible unless proper interference cancellation or mitigation techniques are adopted. Discussion and evaluation of the various interference management techniques for the 4G systems can be found in [73, 74].

In this chapter, we focus on one of the several inter-cell interference coordination techniques to manage radio resources through adaptive fractional frequency reuse (FFR) mechanisms. The analysis of the FFR mechanisms and their impact on the network throughput have been studied mainly through simulations.

In [75, 76], Novlan et. al. have developed an analytical framework to study the impact of the two popular FFR techniques, namely, the strict-FFR and the soft frequency reuse (SFR) on the downlink performance by characterizing the coverage probability and average rate at any given MS within the cellular system.

The analysis in [75, 76] is based on the assumption that the MS associates itself with a BS that is the geographically closest one, which we refer to as nearest BS connectivity. Here, we consider the maximum SIR connectivity where the MS chooses to associate itself with the BS with the best channel quality index (CQI), which in turn corresponds to the BS with the highest SIR at the MS. In this chapter, using the framework developed by Novlan et. al. and assuming an interference-limited system, we compute the coverage probabilities of the cell-edge users and the cell-interior users (formally defined in Section 5.2.0.1) with strict-FFR and SFR for the maximum SIR connectivity model. Further, we show that, unlike the case of conventional cellular systems with static or no frequency reuse, where the maximum SIR connectivity provides the best coverage probability for the MS, when the FFR techniques are employed, the coverage probability for the MS is better with nearest BS connectivity (considered in [75, 76]) thereby posing a question, what is the ideal BS to connect to in order to achieve the best coverage with FFR.

In Section 5.2, we describe the two adaptive FFR techniques and the system model. The coverage probabilities for the cell-interior and cell-edge users with strict-FFR and SFR are computed in Sections 5.3 and 5.4, respectively. Finally, we provide the discussion of the results by taking relevant examples in Section 5.5.

5.2 System Model

This section briefly describes the various elements in the downlink of a cellular system necessary for our analysis.

5.2.0.1 BS and MS Layout

The BS arrangement in the cellular network is according to a homogeneous Poisson point process on the two-dimensional (2-D) plane with density λ. The MS uses the maximum SIR connectivity criterion where it chooses to communicate with the BS to which it has the highest SIR. The MS experiencing an

SIR above a certain threshold, denoted by T_{FR}, is termed as a cell-interior user. Otherwise, the MS is termed as a cell-edge user. Further, we assume $T_{FR} > 0$ dB for the sake of simplicity of analysis. For the cell-edge user, the BS invokes the FFR mechanism to ensure that the MS experiences a reduced inter-cell interference and therefore a better SIR. A MS with an SIR that exceeds a certain threshold denoted by T is said to be in coverage. In this chapter, we are interested in characterizing the coverage probability. The coverage probability for the cell-interior user is $\mathbb{P}_{cov}\left(\text{int}\right) = \mathbb{P}\left(\{\text{SIR} > T | \text{SIR} > T_{FR}\}\right)$ and for the cell-edge user is $\mathbb{P}_{cov}\left(\text{edge}\right) = \mathbb{P}\left(\{\text{SIR}_{FFR} > T | \text{SIR} \leq T_{FR}\}\right)$, where SIR_{FFR} is the SIR experienced by the MS due to the use of the FFR mechanism by the serving BS. The following paragraph briefly explains the two FFR mechanisms.

5.2.0.2 Adaptive FFR techniques

The two FFR techniques considered, that improve the cell-edge user's coverage, are strict-FFR and SFR, respectively. These techniques ensure a greater spectrum utilization in addition to the advantage of the traditional (or static) frequency reuse mechanisms of mitigating the inter-cell interference at the MS.

In strict-FFR, the entire available spectrum is divided into two partitions to serve the cell-interior and the cell-edge users, respectively. In the spectrum allocated for the cell-interior users, the BS operates with a frequency reuse of 1, justified by the notion that the strong signal from the chosen BS at the MS is capable of coping with the inter-cell interference from all the other BSs. In the second partition, the BS uses the traditional frequency reuse with a reuse factor of Δ (> 1) to talk to the MS. The cell-edge user experiences reduced interference because each BS transmits in only one of the Δ subbands such that the adjacent BSs do not operate in the same subbands. This leads to an improved SINR and better coverage for the cell-edge user, though at the expense of less efficient spectrum usage.

In the SFR case, while the BS's interaction with the cell-edge user is the same as in the strict-FFR case; in the unused $\Delta - 1$ subbands, the BS transmits with a smaller power which may be used to provide coverage to cell-interior users. In this approach, the BSs of the adjacent cells cause lesser interference to the cell-edge users due to the reduced transmit power. This approach is more bandwidth efficient than strict-FFR, but is inferior in terms of providing coverage to the cell-edge users. Please refer [73–75] (and

references therein) for further details on the FFR techniques.

5.2.0.3 Radio Environment

The received power at the MS from a BS at a distance D (> 0) from the MS is given by $P\Psi D^{-\varepsilon}$, where P is the constant transmit power, Ψ is the random channel gain coefficient which is an exponential random variable with mean 1 and ε (> 2) is the exponent of the power-law path-loss model. Further, the channel gain coefficients for all the BSs in the system are independent and identically distributed (i.i.d.) random variables across all BSs in the cellular system, and across all subbands.

5.2.0.4 Performance Metric

Without loss of generality, the MS is assumed to be at the origin. We consider an interference-limited system where the background noise power is assumed to be zero. The corresponding performance metric is the signal-to-interference ratio (SIR) at the MS defined as the ratio of the received signal power from the desired BS to the sum of the powers from all interfering BSs. As a result, for the strict-FFR technique,

$$\text{SIR} = \frac{\frac{P\Psi_i}{R_i^{\varepsilon}}}{\sum_{\substack{j=1 \\ j\neq i}}^{\infty} \frac{P\Psi_j}{R_j^{\varepsilon}}}, \ \text{SIR}_{sFFR} = \frac{\frac{P\hat{\Psi}_i}{R_i^{\varepsilon}}}{\sum_{\substack{j=1 \\ j\neq i}}^{\infty} \frac{P\hat{\Psi}_j \mathcal{I}(\delta_j=\delta_i)}{R_j^{\varepsilon}}} \tag{5.1}$$

where i is the index of the BS with the maximum received power at the MS in the frequency band with unity reuse factor; $\left\{R_j, \Psi_j, \hat{\Psi}_j\right\}$ contains the list of distances from origin of each BS and its channel gains in the cell-interior user's subband and the cell-edge user's subband, respectively; SIR is used to determine whether the MS is a cell-interior/ cell-edge user based on the criteria mentioned in Section 5.2.0.1; SIR_{sFFR} is the SIR experienced at the cell-edge user when the chosen BS uses strict-FFR technique and $\{\delta_j\}_{j=1}^{\infty}$ are i.i.d. random variables uniformly distributed in $\{1,\ 2, \ldots,\ \Delta\}$; and $\mathcal{I}(\cdot)$ is the indicator function. The random frequency assignment considered for the cell-edge user subband assignment for each BS ensures analytical tractability and is a popular assumption made in such work. For the SFR technique, we use the same model as in [75, 76] where the BSs use only one of the Δ subbands for transmitting to a cell-edge users, and the others for cell-interior users. Additionally, since the BS transmits on all subbands, it adopts a coarse power control where it transmits at a constant power βP when communicating with the cell-edge user and at a

constant power P otherwise, where β (>1) is a design parameter. Consequently,

$$\text{SIR} = \frac{\frac{P\Psi_i}{R_i^{\varepsilon}}}{\sum_{\substack{j=1 \\ j\neq i}}^{\infty} \frac{\eta P\Psi_j}{R_j^{\varepsilon}}},\ \text{SIR}_{SFR} = \frac{\frac{\beta P\hat{\Psi}_i}{R_i^{\varepsilon}}}{\sum_{\substack{j=1 \\ j\neq i}}^{\infty} \frac{\eta P\hat{\Psi}_j}{R_j^{\varepsilon}}}, \tag{5.2}$$

where $\eta = \beta/\Delta + 1 - 1/\Delta$, and the other symbols are the same as in (5.1). Again, a cell-interior user experiences a signal quality given by SIR from the desired BS and the cell-edge user experiences SIR_{SFR} from the desired BS in its assigned cell-edge frequency with a greater transmission power, βP. In the following section, we delve into the coverage probability computations for the cell-interior and the cell-edge users for the strict-FFR technique.

5.3 Coverage probability for Strict FFR

Recall from Section 5.2.0.1 that we assume $T_{FR} > 1$, while T can take any arbitrary value. The coverage probability for the cell-interior user is

$$\mathbb{P}_{cov}^{sFFR}(\text{int}) \quad = \quad \mathbb{P}\left(\{\text{SIR} > T | \text{SIR} > T_{FR}\}\right), \tag{5.3}$$

where SIR is defined in (5.1) and the following proposition gives the closed form expression for the same. It is a direct consequence of the Baye's rule and the result $\mathbb{P}(\{SIR > t\}) = \frac{\sin\left(\frac{2\pi}{\varepsilon}\right)t^{-\frac{2}{\varepsilon}}}{\left(\frac{2\pi}{\varepsilon}\right)}$, $\forall\, t \geq 1$ from [30,50,58].

Proposition 5. For $T_{FR} \geq 1$ and $T \geq 0$,

$$\mathbb{P}_{cov}^{sFFR}(\text{int}) = \left(\frac{\max(T, T_{FR})}{T_{FR}}\right)^{-\frac{2}{\varepsilon}}. \tag{5.4}$$

Next, we move on to obtaining an analytical expression for the coverage probability for the cell-edge user, denoted as

$$\mathbb{P}_{cov}^{sFFR}(\text{edge}) \quad = \quad \mathbb{P}\left(\{\text{SIR}_{sFFR} > T | \text{SIR} \leq T_{FR}\}\right), \tag{5.5}$$

where SIR and SIR_{sFFR} are defined in (5.1) . The derivation of the expression for $\mathbb{P}_{cov}^{sFFR}(\text{edge})$ is the central part of this chapter. The expression for the coverage probability for $T_{FR} > 1$ is

$$\begin{aligned}
&\mathbb{P}_{cov}^{sFFR}(\text{edge}) \\
&= \left(1 - \frac{\sin\left(\frac{2\pi}{\varepsilon}\right) T_{FR}^{-\frac{2}{\varepsilon}}}{\left(\frac{2\pi}{\varepsilon}\right)}\right)^{-1} \left[\mathbb{P}\left(\{\text{SIR}_{sFFR} > T\}\right)\right. \\
&\left. -\mathbb{P}\left(\{\text{SIR}_{sFFR} > T,\ \text{SIR} > T_{FR}\}\right)\right],
\end{aligned} \tag{5.6}$$

as a direct consequence of Baye's rule. The following theorems derive expressions for the two probability terms in (5.6).

Theorem 12. The tail probability of SIR at the MS when strict-FFR is employed is

$$\begin{aligned}\mathbb{P}\left(\{\mathrm{SIR}_{sFFR} > T\}\right) &= \int_{t=0}^{\infty} \frac{t^{\frac{2}{\varepsilon}}\mathrm{e}^{-t}}{\Gamma\left(1+\frac{2}{\varepsilon}\right)+\frac{1}{\Delta}g\left(Tt,\varepsilon\right)}dt \\ &\triangleq \overline{F}\left(T,\Delta,\varepsilon\right), \end{aligned} \tag{5.7}$$

where $g\left(a,\varepsilon\right) = \frac{2\pi/\varepsilon a^{\frac{2}{\varepsilon}}}{\sin(2\pi/\varepsilon)} - \frac{2}{\varepsilon}\int_{t=0}^{\infty}\frac{\mathrm{e}^{-t}t^{\frac{2}{\varepsilon}-1}}{1+a^{-1}t}$, $a,\ T \geq 0$.

Proof. Firstly, note that the numerator in the expression for SIR_{sFFR} in (5.1) is the received power in the cell-edge user subband from the BS indexed i that was chosen as best for communicating on the cell-interior frequency subband. Taking care of the above fact, the expression for the tail probability of SIR_{sFFR} becomes $\mathbb{P}\left(\{\mathrm{SIR}_{sFFR} > T\}\right) = \mathbb{P}\left(\mathcal{E}_1 \bigcap \mathcal{E}_2\right)$, where the event $\mathcal{E}_1 = \left\{\bigcap_{j=1,\ j\neq i}^{\infty}\left\{\Psi_j R_j^{-\varepsilon} < \Psi_i R_i^{-\varepsilon}\right\}\right\}$ corresponds to the event that the BS indexed i has the strongest received power at the MS in the frequency reuse 1 subband. Event $\mathcal{E}_2 = \left\{\frac{\hat{\Psi}_i R_i^{-\varepsilon}}{\sum_{j=1,\ j\neq i}^{\infty}\hat{\Psi}_j R_j^{-\varepsilon}\mathcal{I}(\delta_j=\delta_i)} > T\right\}$ corresponds to the event that the SIR at the MS from the i^{th} BS in the subband allocated for the BSs transmissions to the cell-edge user exceeds the threshold T; where $\left\{R_j, \Psi_j, \hat{\Psi}_j\right\}_{j=1}^{\infty}$ is the set containing the distances of BSs from the origin, and the corresponding channel gain coefficients in the reuse factor 1 frequency subband and the cell-edge user frequency subband. The evaluation of the probability of $\mathcal{E}_1 \bigcap \mathcal{E}_2$ is shown in Appendix 5.7.1. □

Theorem 13. When $T_{FR} \geq 1$,

$$\mathbb{P}\left(\{\mathrm{SIR}_{sFFR} > T,\ \mathrm{SIR} > T_{FR}\}\right) = \frac{\sin\left(\frac{2\pi}{\varepsilon}\right)/\frac{2\pi}{\varepsilon}}{E\left(T_{FR},T,\Delta,\varepsilon\right)}, \tag{5.8}$$

where $T \geq 0$, $\varepsilon > 2$, and $E\left(T_{FR},T,\Delta,\varepsilon\right) = \begin{cases} \left(1+\frac{2}{\varepsilon\Delta}\right)T_{FR}^{\frac{2}{\varepsilon}} & ,\ T = T_{FR} \\ \left(1-\frac{1}{\Delta}\right)T_{FR}^{\frac{2}{\varepsilon}} + \frac{T^{1+\frac{2}{\varepsilon}} - T_{FR}^{1+\frac{2}{\varepsilon}}}{\Delta(T-T_{FR})} & ,\ T \neq T_{FR} \end{cases}$.

Proof. Recall the definition of SIR and SIR_{sFFR} from (5.1). Note from [50, Lemma 1] that there exists a unique R_i that satisfies the condition $\mathrm{SIR} > T_{FR}$, if $T_{FR} \geq 1$, where R_i is the distance of the MS and the BS that it chooses to communicate with, in the frequency band with reuse factor 1. As a result, it must be the same BS that must cause the event $\{\mathrm{SIR}_{sFFR} > T,\ \mathrm{SIR} > T_{FR}\}$ to happen. Based on the above justification, Appendix 5.7.2 proves the derivation of the expression for the probability of the aforementioned event. □

Proposition 6. The coverage probability of the cell-edge user under strict FFR is

$$\mathbb{P}_{cov}^{sFFR}(\text{edge}) = \frac{\overline{F}(T,\Delta,\varepsilon) - \frac{\sin\left(\frac{2\pi}{\varepsilon}\right)}{\frac{2\pi}{\varepsilon}E(T_{FR},T,\Delta,\varepsilon)}}{1-\sin\left(\frac{2\pi}{\varepsilon}\right)T_{FR}^{-\frac{2}{\varepsilon}}\Big/\left(\frac{2\pi}{\varepsilon}\right)}, \tag{5.9}$$

and is obtained by using Theorem 12 and 13 in (5.6).

5.4 Coverage probability for SFR

In this section, we derive the coverage probabilities for the cell-interior user and the cell-edge user when the SFR technique is employed by the BSs. The coverage probability for the cell-interior user is

$$\mathbb{P}_{cov}^{SFR}(\text{int}) = \mathbb{P}(\{\text{SIR} > T | \text{SIR} > T_{FR}\}), \tag{5.10}$$

where SIR is defined in (5.2). The following remark shows a connection between the cell-interior user's coverage probability for the strict FFR and SFR techniques.

Remark 4. The cell-interior user's coverage probability with SFR is the same as that with strict FFR as shown in (5.1) in which $T,\ T_{FR}$ are replace with $\eta T,\ \eta T_{FR}$, respectively.

The following result is an immediate consequence of the above remark.

Proposition 7. For $T_{FR} \geq 1$, the cell-interior user has the same coverage probability for both strict FFR and SFR techniques, i.e.

$$\mathbb{P}_{cov}^{SFR}(\text{int}) = \mathbb{P}_{cov}^{sFFR}(\text{int}), \tag{5.11}$$

where $\mathbb{P}_{cov}^{sFFR}(\text{int})$ is given in (5.4), and does not depend on the reuse factor Δ, and the power control factor β corresponding to the SFR scheme defined in Section 5.2.0.4.

Next, let us denote the cell-edge user's coverage probability under SFR as

$$\mathbb{P}_{cov}^{SFR}(\text{edge}) = \mathbb{P}(\{\text{SIR}_{SFR} > T | \text{SIR} \leq T_{FR}\}), \tag{5.12}$$

where SIR and SIR_{SFR} are defined in (5.2). Notice that the expression for SIR given in (5.2) for the SFR scheme differs from that in (5.1) by a scaling factor of $\frac{1}{\eta}$. Similarly, the expression for SIR_{SFR} in (5.2) is the same as that for SIR_{sFFR} in (5.1) with a unity frequency reuse factor ($\Delta = 1$) and the latter is scaled by a factor $\frac{\beta}{\eta}$. As a result, we obtain the following result.

Remark 5. The cell-edge user's coverage probability under SFR is the same as that under strict FFR where (T, T_{FR}, Δ) is replaced with $\left(\frac{\eta T}{\beta}, \eta T_{FR}, 1\right)$.

Thus, we get the expression for the coverage probability in (5.12) as follows.

Corollary 16. The cell-edge user's coverage probability under SFR technique when $T_{FR} \geq 1$ is

$$\mathbb{P}_{cov}^{sFFR}(\text{edge}) = \frac{\overline{F}\left(\frac{\eta T}{\beta}, 1, \varepsilon\right) - \frac{\sin\left(\frac{2\pi}{\varepsilon}\right)/\frac{2\pi}{\varepsilon}}{E(\eta T_{FR}, \eta T/\beta, 1, \varepsilon)}}{1 - \sin\left(\frac{2\pi}{\varepsilon}\right)(\eta T_{FR})^{-\frac{2}{\varepsilon}} \Big/ \left(\frac{2\pi}{\varepsilon}\right)}, \tag{5.13}$$

where the function $\overline{F}$ is defined in Theorem 12, and the function $E()$ is defined in Theorem 13.

Hence, in Sections 5.3 and 5.4, we have completely characterized the SIR at the MS when the desired BS employs strict-FFR and SFR. Further, we have derived cell-interior user and cell-edge user coverage probabilities for both FFR techniques when $T_{FR} \geq 1$. With these results, the average ergodic rate expressions can also be characterized. Due to lack of space, we leave the rate and resource allocation related discussions to future work.

5.5 Numerical Examples and Discussion

In this section, we present some numerical examples to illustrate the coverage probability trends with FFR. For all the examples, we assume $\lambda = 1$, $P = 1$, frequency reuse factor $\Delta = 3$, and $T_{FR} = 1$ dB.

The cell-interior user coverage probability is the same for both strict-FFR and SFR, and independent of β. The transition in the cell-interior user's coverage probability in Figure 5.1 happens at $T = T_{FR}$, beyond which the curve follows a log-linear behavior as pointed out in (5.4).

The cell-edge user experiences a superior coverage probability with strict-FFR because the overall interference at the MS is reduced by a factor of Δ, the frequency reuse factor for the cell-edge user frequencies. In contrast, with SFR, all the BSs in the cellular system cause interference and the power control factor β needs to be adjusted to achieve a certain coverage probability. Further, Figure 5.1 shows that SFR attains cell-edge user coverage probability comparable to that of strict-FFR only when the desired BS transmits in the cell-edge user subband at a transmit power at least 10 dB above the value it would transmit for a cell-interior user, i.e. for $\beta > 10$, where the typical values for β are in the range 2-20. The main advantage

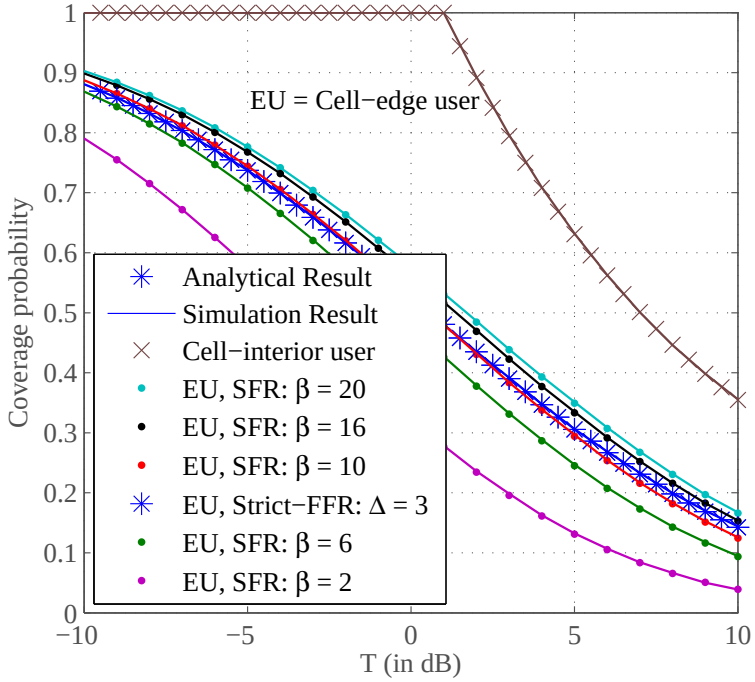

Figure 5.1: Comparison between Strict-FFR and SFR based on the cell-interior and cell-edge user coverage probabilities

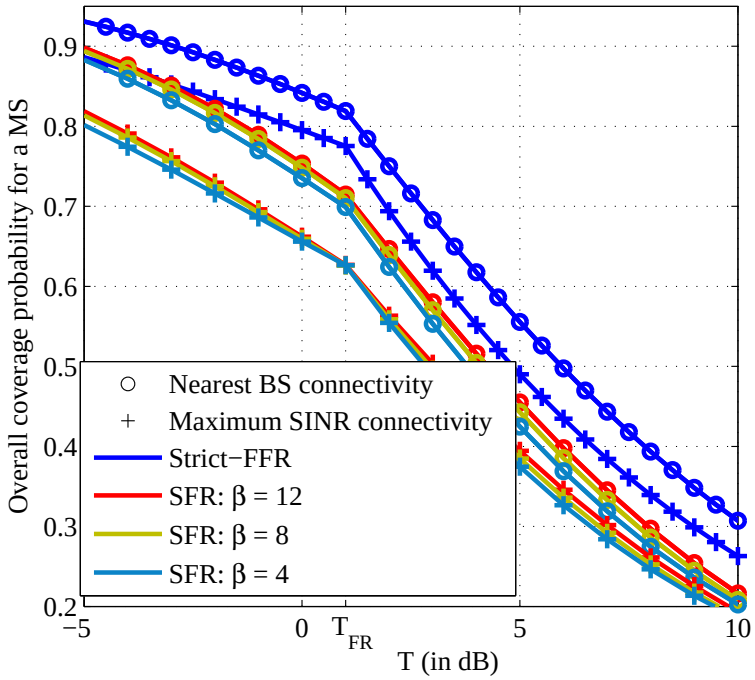

Figure 5.2: Comparison between the maximum SINR connectivity model and the nearest BS connectivity model

of SFR is in the efficient spectral utilization front and the design of β in order to strike a balance between the coverage probability and spectrum utilization for the model studied will be considered in the future.

The overall coverage probability for a given MS with strict-FFR and SFR, denoted by $\mathbb{P}_{cov}^{sFFR}(\text{MS})$ and $\mathbb{P}_{cov}^{SFR}(\text{MS})$, respectively, are given below.

$$\mathbb{P}_{cov}^{sFFR}(\text{MS}) = \mathbb{P}(\{\text{SIR} > T\})\,\mathbb{P}_{cov}^{sFFR}(\text{int}) + (1 - \mathbb{P}(\{\text{SIR} > T\}))\,\mathbb{P}_{cov}^{sFFR}(\text{edge}), \text{ and} \quad (5.14)$$

$$\mathbb{P}_{cov}^{SFR}(\text{MS}) = \mathbb{P}(\{\text{SIR} > \eta T\})\,\mathbb{P}_{cov}^{SFR}(\text{int}) + (1 - \mathbb{P}(\{\text{SIR} > \eta T\}))\,\mathbb{P}_{cov}^{SFR}(\text{edge}), \quad (5.15)$$

where $\mathbb{P}(\{\text{SIR} > T\})$ $(\mathbb{P}(\{\text{SIR} > \eta T\}))$ is the probability that the MS is determined to be a cell-interior user for strict-FFR (SFR), and its expression is given in Section 5.3. Further, the overall coverage probability for a given MS is also superior for the strict-FFR technique compared to SFR, for all practical values of β, as can be seen in Figure 5.2, by observing the plots corresponding to the maximum SIR connectivity.

In Figure 5.2, we also compare the overall coverage probabilities with strict-FFR and SFR between the maximum SIR connectivity model considered in this chapter, and the nearest BS connectivity model considered by Novlan et. al. using the results in [75, Section 3], respectively. Note the strictly better coverage provided to the typical MS by the nearest BS connectivity model for both strict-FFR and SFR techniques. This is surprising because the maximum SIR connectivity model, which is coverage optimal for static or no frequency reuse cases, is not optimal with FFR.

A heuristic explanation for such a behavior is as follows. Since we assume that the channel gains for the cell-interior and the cell-edge frequencies are i.i.d. random variables, this gives us two chances to get a favorable channel. Under the maximum SIR connectivity model, the desired BS is likely to have an above average channel gain. Further, by the principle of return to mean, the channel gain in the cell-edge frequency is not likely to be better than the average. In other words, if the desired BS does not satisfy the SIR constraint in the cell-interior frequency, then it is less likely that the desired BS do so in the cell-edge frequency. On the other hand, under the nearest BS connectivity model, the desired BS not satisfying the SIR constraint in the cell-interior frequencies is likely a below average channel gain scenario, and so, by going to the cell-edge frequency, the desired BS is likely to see a better channel gain. Nevertheless, there is a need to explore other connectivity models and assess the coverage and rate achieved at the MS with the available

results.

For instance, the following BS connectivity models may be considered. Firstly, one in which the MS uses the maximum SIR connectivity criterion to communicate with the desired BSs in the cell-interior and cell-edge user subbands may be considered. In such a model, there is a handoff between BSs when the MS switches from the cell-interior user subband to the cell-edge user subband, when the SIR is insufficient for coverage in the former frequency band. Another model may be considered where the MS chooses to connect to a BS that has the maximum SIR in its cell-edge user subband, instead of the maximum SIR connectivity criterion being used in the cell-interior user subband. While it is clear that this strategy ensures maximum coverage to the cell-edge user, its impact on the cell-interior user's performance is still not known.

The above mentioned approaches are merely two of the perhaps many such approaches conceivable, but we lack adequate understanding in this front due to analytical intractability. The proof techniques shown in this chapter will be useful for characterizing the coverage probability and average rate for the MS when such connectivity models are employed, and this shall be considered in greater detail elsewhere.

5.6 Conclusions

We have studied the coverage probability at the MS in an OFDMA cellular network where the BS, distributed according to a homogeneous Poisson point process on the plane, employ FFR to provide improved coverage to the cell-edge users. The MS chooses to connect to the BS with the maximum SIR. The distribution of SIR at the MS when the chosen BS employs FFR is completely characterized for both the strict-FFR and SFR techniques (Theorem 12). Further, the cell-edge user's coverage probability as well as the overall coverage probability for a typical MS are computed for the case when $T_{FR} > 0$ dB, thereby characterizing the improvement in the coverage experienced by the MS with strict-FFR compared to SFR.

By comparing the results in this chapter with the corresponding ones for the nearest BS connectivity model considered in [75], we obtain a surprising result that the nearest BS connectivity model provides better coverage than the maximum SIR connectivity with FFR. For the design of the OFDMA cellular system with FFR, this poses an additional requirement to choose the right BS for optimal downlink performance, which is no more the BS chosen based on the conventional maximum SINR connectivity criterion. Further, the

analytical tools developed in this chapter make the study of such networks with different connectivity models including those with handoff possible and this shall be considered elsewhere.

5.7 Appendix

5.7.1 Derivation for the tail probability of SIR_{sFFR}

The sequence of steps for the derivation of the expression for $\mathbb{P}\left(\{\mathcal{E}_1 \bigcap \mathcal{E}_2\}\right)$ is given below.

$$
\begin{aligned}
&\mathbb{P}\left(\left\{\mathcal{E}_1 \bigcap \mathcal{E}_2\right\}\right) = \mathbb{P}\left(\mathcal{E}_1 \bigcap \mathcal{E}_2 \middle| \delta_i = 1\right) \\
&\overset{(a)}{=} \mathbb{P}\left(\left\{\frac{\hat{\Psi}_i R_i^{-\varepsilon}}{\sum_{j=1,\ j\neq i}^{\infty} \hat{\Psi}_j R_j^{-\varepsilon} \mathcal{I}\left(\delta_j = 1\right)} > T\right\} \bigcap \bigcap_{j=1,\ j\neq i}^{\infty} \left\{\Psi_i R_i^{-\varepsilon} \geq \Psi_j R_j^{-\varepsilon}\right\} \middle| \delta_i = 1\right) \\
&\overset{(b)}{=} \mathbb{E}\left[\prod_{j=1,\ j\neq i}^{\infty} \mathbb{P}\left(\left\{\Psi_j R_j^{-\varepsilon} \leq \Psi_i R_i^{-\varepsilon}\right\}\right) \cdot \mathrm{e}^{-T R_i^{\varepsilon} \hat{\Psi}_j R_j^{-\varepsilon} \mathcal{I}(\delta_j = 1)}\right] \\
&\overset{(c)}{=} \mathbb{E}\left[\prod_{j=1,\ j\neq i}^{\infty} \left(1 - \mathrm{e}^{-\Psi_i R_i^{-\varepsilon} R_j^{\varepsilon}}\right)\left(1 - \frac{1/\Delta}{1 + \left(T R_i^{\varepsilon}\right)^{-1} R_j^{\varepsilon}}\right)\right] \\
&\overset{(d)}{=} \mathbb{E}_{\Psi_i, R_i}\left[\exp\left(-\lambda \int_{r=0}^{\infty} \frac{1/\Delta\left(1 - \mathrm{e}^{-\Psi_i R_i^{-\varepsilon} r^{\varepsilon}}\right) 2\pi r dr}{1 + \left(T R_i^{\varepsilon}\right)^{-1} r^{\varepsilon}} - \lambda \int_{r=0}^{\infty} \mathrm{e}^{-\Psi_i R_i^{-\varepsilon} r^{\varepsilon}} 2\pi r dr\right)\right] \\
&\overset{(e)}{=} \mathbb{E}_{\Psi_i, R_i}\left[\exp\left(-\lambda\pi R_i^2 \Psi_i^{-\frac{2}{\varepsilon}}\left(\Gamma\left(1 + \frac{2}{\varepsilon}\right) + \frac{g\left(T\Psi_i, \varepsilon\right)}{\Delta}\right)\right)\right] \overset{(f)}{=} \mathbb{E}_{\Psi_i}\left[\int_{r=0}^{\infty} \lambda 2\pi r \mathrm{e}^{-\lambda\pi \mathrm{R_i^2} \Psi_i^{-\frac{2}{\varepsilon}}\left(\Gamma\left(1+\frac{2}{\varepsilon}\right) + \frac{g(T\Psi_i, \varepsilon)}{\Delta}\right)} dr\right] \\
&\overset{(g)}{=} \mathbb{E}_{\Psi_i}\left[\frac{\Psi_i^{\frac{2}{\varepsilon}}}{\Gamma\left(1 + \frac{2}{\varepsilon}\right) + \frac{g(T\Psi_i, \varepsilon)}{\Delta}}\right],
\end{aligned}
\tag{5.16}
$$

where (a) is obtained by first noting $\mathbb{P}\left(\{\mathcal{E}_1 \bigcap \mathcal{E}_2\}\right)$ is the same for all realizations of δ_i and then recalling the definitions of $\mathcal{E}_1$ and $\mathcal{E}_2$, (b) is obtained by noting that $\mathcal{E}_1$ and $\mathcal{E}_2$ are independent events conditioned on $\{R_j\}_{j=1}^{\infty}$, and $\left\{\hat{\Psi}_j, \delta_j\right\}_{j=1,\ j\neq i}^{\infty}$, and then computing the probability for $\hat{\Psi}_i$ after conditioning w.r.t. the above mentioned random variables, (c) is obtained by evaluating the expectation w.r.t. δ_j's, $\hat{\Psi}_j$'s, and Ψ_j's, $j \neq i$, (d) is obtained by first conditioning on (R_i, Ψ_i) and noting that the Palm distribution of the BSs represented by R_j's $(j \neq i)$ given a BS at R_i is still a homogeneous Poisson point process with density λ, then applying the Campbell's theorem [6, Page 28] and simplifying, (e) is obtained by evaluating the integrals in (f) where $\int_{r=0}^{\infty} \frac{2\pi r dr}{1+\alpha^{-1} r^{\varepsilon}} = \frac{\pi \alpha^{\frac{2}{\varepsilon}}}{\mathrm{sinc}\left(\frac{2}{\varepsilon}\right)}$, $\mathrm{sinc}\left(x\right) = \frac{\sin(x)}{x}$, and $\Gamma\left(\cdot\right)$ is the Gamma function, (f) represents the expectation w.r.t. R_i, which is the distance of any point in a homogeneous Poisson point process on

the plane, (g) is obtained by evaluating the integral in (f) and finally (5.7) is obtained by rewriting the expectation w.r.t. to Ψ_i (exponential random variable with mean 1) in terms of the integral.

5.7.2 Proof for Theorem 13

The sequence of steps for the derivation of the expression for $\mathbb{P}\left(\{\mathrm{SIR}_{sFFR} > T,\ \mathrm{SIR} > T_{FR}\}\right)$ is provided below.

$$\mathbb{P}\left(\{\mathrm{SIR}_{sFFR} > T,\ \mathrm{SIR} > T_{FR}\}\right) \overset{(a)}{=} \mathbb{E}_{R_i}\left[\mathbb{P}\left(\{\mathrm{SIR}_{SFFR} > T,\ \mathrm{SIR} > T_{FR} | \,\delta_i = 1\}\right)\right]$$

$$\overset{(b)}{=} \mathbb{P}\left(\left\{\frac{\hat{\Psi}_i R_i^{-\varepsilon}}{\sum_{\substack{j=1\\ j\neq i}}^{\infty} \hat{\Psi}_j R_j^{-\varepsilon} \mathcal{I}\left(\delta_j = 1\right)} > T,\ \frac{\Psi_i R_i^{-\varepsilon}}{\sum_{\substack{j=1\\ j\neq i}}^{\infty} \Psi_j R_j^{-\varepsilon}} > T_{FR}\right\}\right)$$

$$\overset{(c)}{=} \mathbb{E}\left[\mathbb{P}\left(\left\{\hat{\Psi}_i > \sum_{j=1,\ R_j\neq R_i}^{\infty} T R_i^{\varepsilon} \hat{\Psi}_j R_j^{-\varepsilon} \mathcal{I}\left(\delta_j = 1\right)\right\}\right) \times \mathbb{P}\left(\left\{\Psi_i > \sum_{j=1,\ R_j\neq R_i}^{\infty} T_{FR} R_i^{\varepsilon} \Psi_j R_j^{-\varepsilon}\right\}\right)\right]$$

$$\overset{(d)}{=} \mathbb{E}\left[\prod_{j=1,\ R_j\neq R_i}^{\infty} \mathrm{e}^{-R_i^{\varepsilon} R_j^{-\varepsilon}\left(T\hat{\Psi}_j \mathcal{I}(\delta_j=1) + T_{FR}\Psi_j\right)} \middle| R_i\right]$$

$$\overset{(e)}{=} \mathbb{E}\left[\prod_{j=1,\ R_j\neq R_i}^{\infty} \left(1 - \frac{1}{1 + \left(T_{FR} R_i^{\varepsilon}\right)^{-1} R_j^{\varepsilon}}\right)\left(1 - \frac{1/\Delta}{1 + \left(T R_i^{\varepsilon}\right)^{-1} R_j^{\varepsilon}}\right)\right]$$

$$\overset{(f)}{=} \mathbb{E}_{R_i}\left[\exp\left(-\lambda \int_{r=0}^{\infty} \left[\frac{1}{1 + \left(T_{FR} R_i^{\varepsilon}\right)^{-1} r^{\varepsilon}} + \frac{1/\Delta}{1 + \left(T R_i^{\varepsilon}\right)^{-1} r^{\varepsilon}} - \frac{1/\Delta}{\left(1 + \left(T R_i^{\varepsilon}\right)^{-1} r^{\varepsilon}\right)\left(1 + \left(T_{FR} R_i^{\varepsilon}\right)^{-1} r^{\varepsilon}\right)}\right] 2\pi r dr\right)\right]$$

$$\overset{(g)}{=} \mathbb{E}_{R_i}\left[\exp\left(-\frac{\lambda \pi R_i^2}{\mathrm{sinc}\left(2\pi/\varepsilon\right)}\left[\left(1 - \frac{1}{\Delta}\right) T_{FR}^{\frac{2}{\varepsilon}} + \frac{T^{1+\frac{2}{\varepsilon}} - T_{FR}^{1+\frac{2}{\varepsilon}}}{\Delta\left(T - T_{FR}\right)}\right]\right)\right] \overset{(h)}{=} \mathbb{E}_{R_i}\left[\exp\left(-\frac{\lambda \pi R_i^2 E\left(T, T_{FR}, \Delta, \varepsilon\right)}{\mathrm{sinc}\left(\frac{2\pi}{\varepsilon}\right)}\right)\right] \quad (5.17)$$

where (a) follows due to the same argument as in $(5.16 - a)$, (b) rewrites (a) using (5.1), (c) is obtained by first taking the expectation w.r.t. all the random variables except $\hat{\Psi}_i$ and Ψ_i, which are themselves independent of each other, (d) is obtained by evaluating the expectations w.r.t. $\hat{\Psi}_i$ and Ψ_i which are independent exponential random variables with mean 1, (e) is obtained by first evaluating the expectation w.r.t. $\delta_j's$ and then w.r.t. Ψ_j's and $\hat{\Psi}_j$'s, (f) is obtained by applying the Campbell's theorem [6, Page 28] to (e), and (g) is obtained by simplifying the last fraction in (f) using partial fraction expansions assuming $T \neq T_{FR}$, and then evaluating the integrals using $\int_{r=0}^{\infty} \frac{2\pi r dr}{1+\alpha^{-1} r^{\varepsilon}} = \frac{\pi \alpha^{\frac{2}{\varepsilon}}}{\mathrm{sinc}\left(\frac{2\pi}{\varepsilon}\right)}$. Further, note that the result of the integral in (f) when $T = T_{FR}$ is obtained by evaluating the corresponding expression in (g) in the limit $T \to T_{FR}$, using L'Hospital's rule. Then, (h) rewrites (g) in terms of the function $E\left(\right)$ defined in Theorem

13 and finally (5.7) is obtained by evaluating the expectation w.r.t. R_i in the same way as in $(5.16 - f, g)$.

Chapter 6

On the Primary User Coverage Probability and Faulty Cognitive Radios

6.1 Introduction

The FCC has allowed the operation of cognitive radio (CR) devices in the ultra high frequency (UHF) television (TV) bands which have been identified to have a low spectrum usage and excellent propagation characteristics. The operation of these unlicensed CR devices is allowed under the condition that they do not cause harmful interference to the operation of the primary users [77–79]. The primary users of these bands are the TV transmitter-receiver pairs, radio astronomy service and the low-power wireless microphones systems, among other incumbent services [80]. Further, the CRs can operate in the same band as the primary users only if they are located outside the protected region of the primary users, so as to not hinder the primary user operations.

The CR devices sense for white spaces (or available channels) via spectrum sensing or beaconing techniques or by geo-location and database lookup techniques. Under spectrum sensing, the CRs use a threshold-based hypothesis testing of the primary user signals to find the white spaces [81]. Under the beaconing approach, the beacons can either be explicitly attached to the primary receivers [82–84] or some indirect means. For instance, the cognitive radio might be detecting the TV receiver local oscillator [85] which acts like a beacon. Further, the geo-location and database schemes provides general information for usage in a region. Notice that, in all these schemes, the CRs are prone to make mistakes in identifying the white spaces, such as failing to detect the primary user operation while being located inside the protected region of the primary user (referred to as miss-detection), or falsely concluding that an available channel

is busy while being outside the protection region of all primary users (referred to as false-alarm). Further, miss-detection causes harmful interference to the primary users and false-alarms lead to inefficient usage of the white spaces. In this chapter, we adopt a stochastic geometric approach to study the interference characteristics at the primary users in the presence of CR devices with imperfect detection capabilities.

6.1.1 Literature survey and Contributions of the chapter

By modeling the CR arrangement as a homogeneous Poisson point process, a characteristic function based interference analysis at the primary receiver has been considered in [28, 45, 86, 87]. For a similar system model, [42] derives expressions for the primary user outage probability due to the interference by the CRs in the system employing various dynamic spectrum sharing techniques. All these studies are restricted to a single primary user case.

Models where the CRs and the primary users are both distributed over the plane according to independent homogeneous Poisson point processes have been studied extensively for establishing transmission capacity bounds for the coexistence of the primary users and CRs [88–90], but these do not consider the scenario that the CRs perform spectrum sensing.In [43], the CRs perform a location based sensing, and engages in transmission over the channel only when they detect a free channel, and is the most realistic of the models. Closed form lower bounds and an approximations for outage probability at the primary receiver and the CR receiver are computed for the case when the transmitter-receiver pairs corresponding to both the primary users and the CRs are collocated. Notice that, although these studies hold relevance for the wireless microphone system where the transmitters and the receivers are separated by a small distance, they do not necessarily represent the scenarios involving the TV transmitters and receiver, whose arrangement in an area are essentially independent of each other, and could be separated by large distance, as a TV transmitter typically provide coverage for TV receivers in a large geographical area, much like the macrocell base-stations in the conventional cellular system.

In this chapter, we introduce some important features into the system model which makes the study more generally applicable. Firstly, we introduce imperfections to the CR detection capability which have not been studied before. Secondly, these studies also include the case where the primary receiver is provided

coverage by some transmitter in the entire system which has a signal-to-interference ratio (SIR) at the receiver above a given specified threshold, instead of a collocated transmitter which is the subject of all the prior studies. Further, we develop a systematic approach to study the various characteristics of the interference to a given primary user due to the presence of the other primary users and the CRs in the network and obtain a series of bounds for the same (see Section 6.3). Specifically, in Theorem 15, we decompose the original spatial point process of the interfering CRs with imperfect detection capabilities to two independent spatial point processes that are easy to study, and the CRs in these have perfect detection capabilities. Further, we obtain tight upper and lower bounds for the coverage probability at a typical primary receiver (see Section 6.4 for the TV receiver case and Section 6.5 for the WMR case). Finally, Section 6.7 discusses the various bounds derived in the chapter with numerical examples. The following section describes the system setup.

6.2 System Model

Firstly, we describe the arrangement of the primary users and the cognitive radio transceivers. We focus on the spatial arrangement of the two types of primary users, namely, the television (TV) transmitter-receiver pairs and the wireless microphone systems, respectively.

The TV transmitters and the TV receivers are assumed to be distributed in the entire two-dimensional (2-D) plane according to independent homogeneous Poisson point processes with densities λ_t and λ_r, respectively. Further, any TV transmitter that has a signal-to-interference ratio (SIR, defined later) at the TV receiver above a given threshold, say β is said to provide coverage to the TV receiver. In other words, the TV receiver is in coverage if there exists at least one TV transmitter with an SIR above β, which happens if-and-only-if the TV transmitter with the strongest signal at the TV receiver has an SIR above β.

Next, in the case of the wireless microphone systems, the receivers are distributed according to a homogeneous Poisson point process on the 2-D plane with the density λ_r and the transmitter corresponding to each receiver is located at a fixed distance r_t from the receiver in an arbitrary direction. The cognitive radio transceivers are assumed to be distributed according to another independent homogeneous Poisson point process on the 2-D plane with a density λ_s, where 's' stands for the secondary users.

Figures 6.1 and 6.2 gives a pictorial representation of the primary user and cognitive radio arrangement.

Note that the mutual interferences caused by TV systems and the wireless microphone systems on each other is not considered here. It is assumed that the wireless microphone systems are operating in the TV white spaces corresponding to their locations. If necessary, the interference between these systems could also be considered, but is not done here for the sake of simplicity. In Figures 6.1 and 6.2, the green arrows represent the signals from the serving primary transmitter(s), and the red arrows represent the interferences at any arbitrary primary receiver. The total interference power at any given primary receiver is the sum of the powers from the rest of the primary transmitters and all the secondary transmitters.

6.2.1 Primary receiver beaconing and Detection range

In order to protect the primary receiver from the harmful interference caused by the secondary user operations, each primary receiver transmits a beacon signal that can be detected by all the cognitive radios (CRs) that are upto a distance d from the receiver. In essence, each primary receiver at $\xi_i \in \mathbb{R}^2$ has a corresponding detection region $\xi_i \oplus \mathcal{S}_i$, where $\mathcal{S}_i = \{x | \|x\|_2 \leq d\}$ and $\oplus$ represents the Minkowski sum of the two sets involved. In Figures 6.1 and 6.2, this is represented by the dotted circular patch around each primary receiver. Each CR has an imperfect detection capability. In other words, any CR lying with the detection region misses detecting the beacon signal from the primary receivers in its range with a probability p_{MD} and any CR lying outside the detection regions of all the primary users stops operating in the band with a false-alarm probability p_{FA}. Upon the (true/ false) detection of the beacon signals, the CR switches to a different channel and hence does not cause interference at the primary receiver. In Figures 6.1 and 6.2, the solid red arrows from the CRs correspond to those CRs that are transmitting in the same band, and the dashed red arrows correspond to those CRs that have switch to a different channel and do not cause any interference at the primary receivers. Ideally, when all the CRs have a perfect detection capability ($p_{MD} = p_{FA} = 0$), the CRs lying within the detection region of some primary user switches to a different channel in order to protect the primary user operations, and all the other CRs communicate in the same band leading to improved spectrum usage.

Note that the beacons described here can either be explicit beacons attached to the receivers [82] or some indirect means. For instance, there may be no explicit beacon but the cognitive radio might be

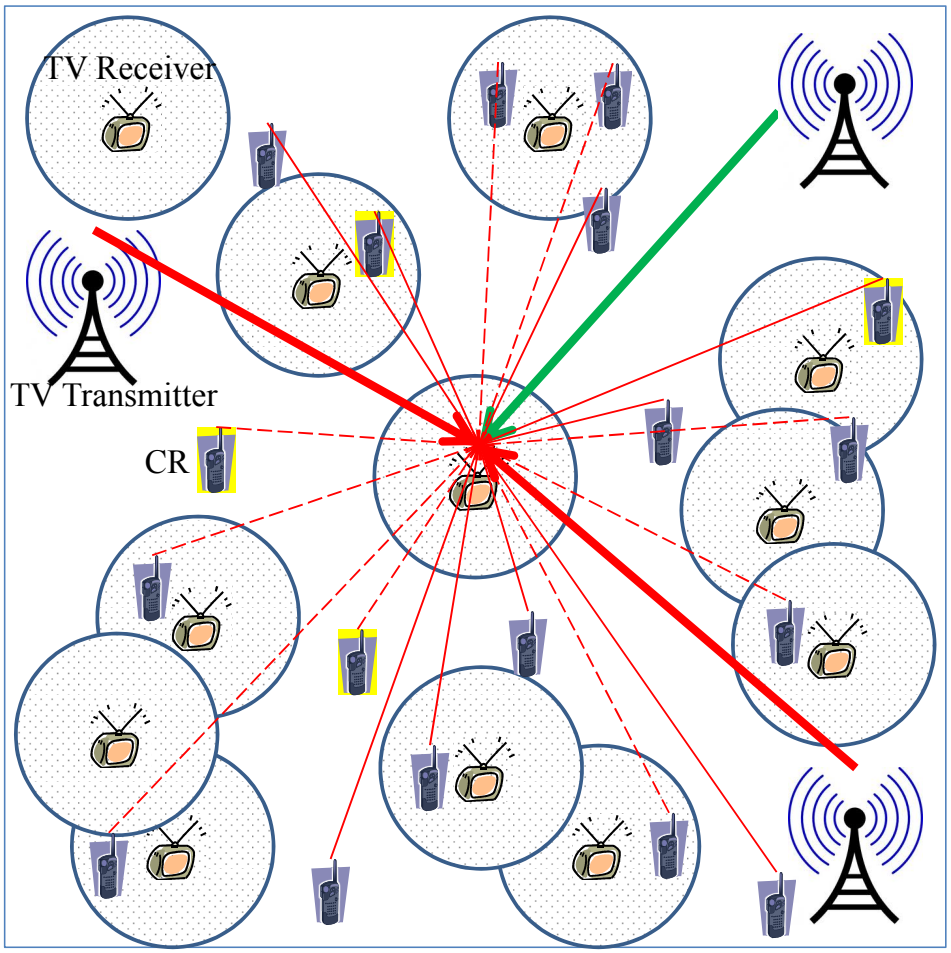

Figure 6.1: Primary user and cognitive radio arrangement with TV transmitter-receiver pairs as the primary users

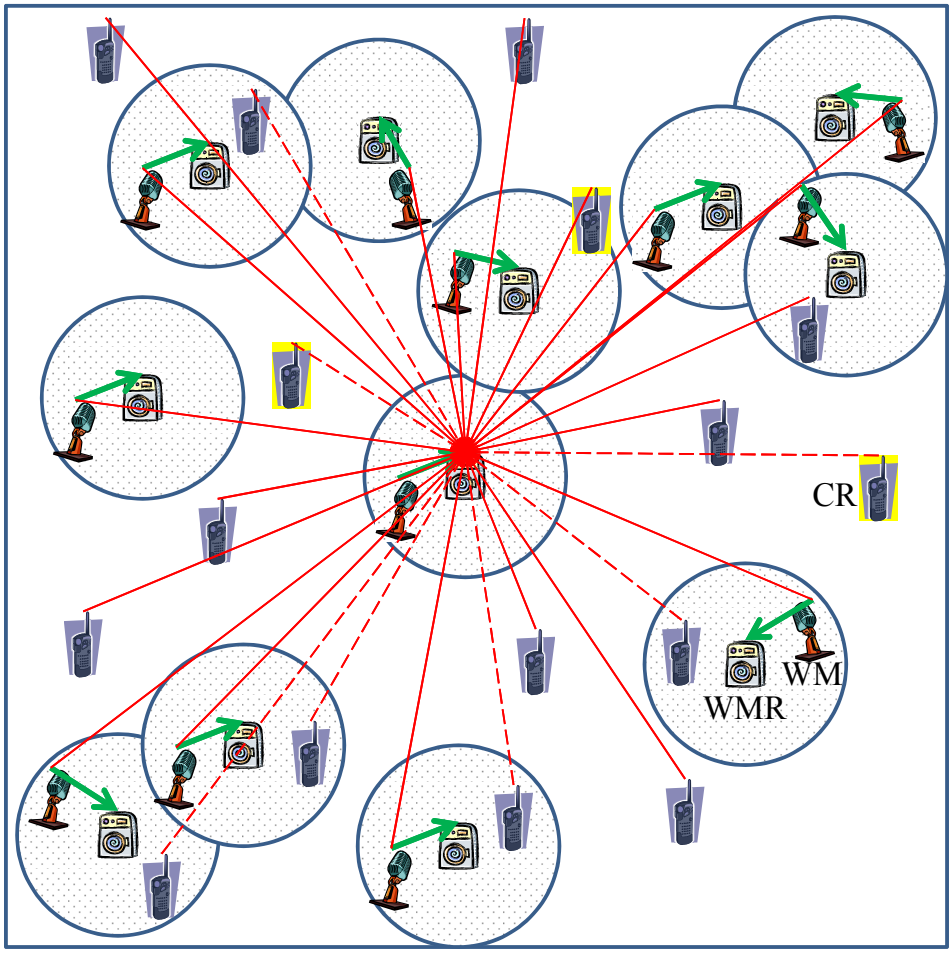

Figure 6.2: Primary user and cognitive radio arrangement with wireless microphone systems as the primary users

detecting the TV receiver local oscillator [85] which acts similar to a beacon. Or, a large 'd' can model a geo-location and database scheme that provides general information for usage in a region. In this chapter, errors in this scheme are labeled as misdetection. Further, we are concerned with computing the probability of successful communication between the primary transmitter-receiver pairs in the presence of the additional interfering cognitive radios with imperfect operational capabilities. In the following subsection, we formally set up the problem.

6.2.2 Interference Modeling and Coverage (Success) Probability

Firstly, the received power at the primary receiver from any given transmitter in the system is modeled as $P = K\Psi R^{-\varepsilon}$ where K captures the transmission power and the antenna gains of the transmitter at a distance R from the receiver. The signal from the transmitter is subjected to a power-law path-loss $R^{-\varepsilon}$, with ε (> 2) as the path-loss exponent, and fading represented by the multiplicative factor Ψ which is independent across the transmitters and identically distributed according to a unit mean exponential distribution. For convenience, we restrict ourselves to the interference-limited case and assume that the background noise power is zero. All the results presented in this chapter can be easily extended to the non-zero background noise power case easily as done in [47]. The performance metric of interest is the SIR at the primary receiver. For the case where the primary receivers are the TV receivers, the SIR is

$$\mathrm{SIR}_{TVR} = \frac{P_t h_k \left\|x_k\right\|_2^{-\varepsilon}}{I_{TV} + I_{CR}}, \tag{6.1}$$

$$I_{TV} = \sum_{l \neq k} P_t h_l \left\|x_l\right\|_2^{-\varepsilon}, \text{ and} \tag{6.2}$$

$$I_{CR} = \sum_{m=1}^{\infty} P_s g_m \left\|y_m\right\|_2^{-\varepsilon} \left(\mathcal{I}\left(y_m \in \mathcal{B}\bigcup \mathcal{S},\ M_m = 1\right) + \mathcal{I}\left(y_m \notin \mathcal{B}\bigcup \mathcal{S},\ F_m = 0\right)\right) \tag{6.3}$$

where I_{TV} is the sum of received powers from the interfering TV transmitters, $\left\{P_t h_l \left\|x_l\right\|_2^{-\varepsilon}\right\}_{l=1}^{\infty}$ represents the set of received powers at the TV receiver located at the origin from the TV transmitters located at x_l's in $\mathbb{R}^2$ with constant transmission power P_t and i.i.d. random fading gains h_l's with unit mean exponential distribution. The subscript 'k' in the numerator of (6.1) corresponds to the TV transmitter with the strongest signal at the TV receiver. Further, I_{CR} is the total received power from all the interfering CRs, and $\left\{P_s g_m \left\|y_m\right\|_2^{-\varepsilon}\right\}_{m=1}^{\infty}$ is the corresponding set of received powers at the TV receiver from all the CRs in $\mathbb{R}^2$.

Further, $\{x_l\}_{l=1}^{\infty}$ and $\{y_m\}_{m=1}^{\infty}$ are points drawn from independent homogeneous Poisson point processes with densities λ_t and λ_s, respectively.

The imperfect operational capabilities of the CRs are modeled as follows. The cognitive radios in the system are assigned i.i.d. random marks $\{M_m,\ F_m\}_{m=1}^{\infty}$ where M_m is Bernoulli(p_{MD}) and F_m is Bernoulli(p_{FA}) random variable, respectively.

The set of miss-detecting cognitive radios may be represented as $\{y_m |\, y_m \in \mathcal{B} \bigcup \mathcal{S},\ M_m = 1\}$, where $\mathcal{B} = \bigcup_{n=1}^{\infty} \{z_n \oplus S_n\}$ is the union of the detection regions of all the primary receivers in the system, and is the random set corresponding to the popular Boolean model [5, 91] in stochastic geometry. Further, the Palm distribution of the Boolean model $\mathcal{B}$ conditioned on the typical primary receiver is the same as the set $\mathcal{B} \bigcup \mathcal{S}$ [91, Page 202], where $\mathcal{S}$ is the detection region corresponding to the primary receiver at the origin. The set of false-alarming cognitive radios may be represented as $\{y_m |\, y_m \notin \mathcal{B} \bigcup \mathcal{S},\ F_m = 1\}$. In Figures 6.1 and 6.2, the miss-detecting and false-alarming CRs have a yellow background. Finally, (6.3) represents the interference from all the CRs that have either miss-detected or have not false-alarmed. In the special case when the CRs have perfect detection capability ($p_{MD} = p_{FA} = 0$), I_{CR} is the sum of the interference powers from all the CRs belonging to the set $\{y_m |\, y_m \notin \mathcal{B} \bigcup \mathcal{S}\}$. Further, I_{TV} as well as the signal power at the TV receiver at the origin (numerator in (6.1)) are both independent of I_{CR}.

Next, for the case when the primary receivers are the wireless microphone receivers, the SIR is

$$\mathrm{SIR}_{WMR} = \frac{P_t h_k r_s^{-\varepsilon}}{I_{WM} + I_{CR}}, \tag{6.4}$$

$$I_{WM} = \sum_{n \neq k} P_t h_n \left\| z_n + \tilde{x}_n \right\|_2^{-\varepsilon}, \tag{6.5}$$

and I_{CR} is the same as in (6.3), $\left\{ P_t h_n \left\| z_n + \tilde{x}_n \right\|_2^{-\varepsilon} \right\}_{m=1}^{\infty}$ is the set of interference powers from all the wireless microphones. Recall that the wireless microphones are located at a distance r_s from the corresponding wireless microphone (or primary) receiver in a uniformly randomly chosen direction. Further, as in the case of the TV transmitter-receiver pairs, the sets $\mathcal{B}$ and $\mathcal{S}$ have the same meaning, except that the primary receivers here are the wireless microphones receivers and their locations are given by the set $\{z_n\}_{n=1}^{\infty}$. Notice that, unlike the TV transmitter-receiver case, the interferences I_{WM} and I_{CR} are not independent. Further, notice that the interference I_{WM} is not considered in SIR_{TVR} and the interference from the TV transmitters

is not considered in SIR_{WMR}.

Finally, the success probability (or the coverage probability) at the primary receivers are defined as $\mathbb{P}_{coverage}\left(\mathrm{TVR}\right) = \mathbb{P}\left(\{\mathrm{SIR}_{TVR} > \beta\}\right)$, $\mathbb{P}_{coverage}\left(\mathrm{WMR}\right) = \mathbb{P}\left(\{\mathrm{SIR}_{WMR} > \beta\}\right)$ at the TV receiver and the wireless microphone receiver, respectively, where β is the SIR threshold.

In [43, 46], we have seen that characterizing the interference exactly is not possible, and the SIR can be characterized only via approximations and tight upper and lower bounds. Here, we delve further on the notions developed in the above mentioned references to the case when the cognitive radios have imperfect detection capabilities. Towards this goal, in the following section, we study the characteristics of the interferences at the primary receiver in detail by computing bounds on the mean, variance and the moment generating function (or Laplace transform) of each interference term individually.

6.3 Interference characteristics

We first consider the Laplace transform of I_{WM}, denoted as $\mathcal{L}_{I_{WM}}\left(s\right) = \mathbb{E}\left[\mathrm{e}^{-sI_{WM}}\right]$, $s > 0$. This quantity can be computed in closed form (see [43]) and can be expressed as

$$\begin{aligned} \mathcal{L}_{I_{WM}}\left(s\right) &= \exp\left(-\lambda_s G\left(\left(sP_t\right)^{-1}, \varepsilon, 0\right)\right), && (6.6) \\ G\left(\alpha, \varepsilon, \delta\right) &\triangleq \int_{r=\delta}^{\infty} \frac{2\pi r dr}{1+\alpha r^{\varepsilon}} \\ &= \frac{2\pi^2 \alpha^{-\frac{2}{\varepsilon}}}{\varepsilon \sin\left(\frac{2\pi}{\varepsilon}\right)} - \pi\delta^2 \times \ {}_2F_1\left(1, \frac{2}{\varepsilon}; 1+\frac{2}{\varepsilon}; -\alpha\delta^{\varepsilon}\right), && (6.7) \end{aligned}$$

where ${}_2F_1\left(\cdot,\cdot;\cdot;\cdot\right)$ is the Gauss hypergeometric function. Further, the variance of the random variable $\mathrm{e}^{-sI_{WM}}$ is

$$\mathrm{var}\left(\mathrm{e}^{-sI_{WM}}\right) = \mathcal{L}_{I_{WM}}\left(2s\right) - \left[\mathcal{L}_{I_{WM}}\left(s\right)\right]^2. \quad (6.8)$$

Lemma 9. *The probability that an arbitrary CR located at $\xi \in \mathbb{R}^2$ does not lie in the detection region of any primary receiver in the system is $\mathbb{P}\left(\{\xi \notin \mathcal{B}\}\right) = \exp\left(-\lambda_p \pi d^2\right) = \rho$ and is the same irrespective of the location of the CR.*

Proof.

$$\begin{aligned}\mathbb{P}\left(\{\xi \notin \mathcal{B}\}\right) &= \mathbb{P}\left(\{\text{no primary receiver in } \xi \oplus \mathcal{S}_\xi\}\right) \\ &= \exp\left(-\lambda_p \left\|\mathcal{S}_\xi\right\|\right) = \exp\left(-\lambda_p \pi d^2\right),\end{aligned}$$

where $\xi \oplus \mathcal{S}_\xi$ is the set of all points upto a distance d from ξ, $\left\|\mathcal{S}_\xi\right\|$ is the measure of the set which is exactly the area occupied by the set. □

Now, we characterize the Laplace transform of I_{CR}, denoted as $\mathcal{L}_{I_{CR}}(s)$. As this quantity cannot be characterized in closed form, we obtain lower and upper bounds for the same. When we study the interference from the CRs, we are interested in the interference from CRs belonging to two disjoint sets $\mathcal{B}\bigcup\mathcal{S}$ and $(\mathcal{B}\bigcup\mathcal{S})^c$, where the interference due to the CRs in the former set is due to those that have missed detecting the presence of primary users in its vicinity, and the CRs belonging to the latter set that correctly detect the absence of any primary user in its vicinity and are transmitting.

If (p_{FA}, p_{MD}) corresponds to the tuple with the false-alarm and missed-detection probabilities for each cognitive radio, it is clear that the case $1 - p_{FA} < p_{MD}$ is practically irrelevant since this corresponds to extremely faulty cognitive radios. The above scenario means that cognitive radios in the detection region are more likely to communicate than those outside the detection region. This leads to harmful interferences as well as inefficient utilization of the white-spaces by the CRs. As a result, we will focus on the case $1 - p_{FA} \geq p_{MD}$.

Theorem 14. *The lower-bounds for $\mathcal{L}_{I_{CR}}(s)$ are listed below:*

$$\begin{aligned}\mathcal{L}^{l1}_{I_{CR}}(s) &= \exp\Big(-\lambda_s p_{MD}\left[G\left(\left(sP_s\right)^{-1}, \varepsilon, 0\right) - p_{FA} G\left(\left(sP_s\right)^{-1}, \varepsilon, d\right)\right] \\ &\quad -\lambda_s p_{MD} p_{FA} G\left(\left(sP_s\left(1-\rho\right)\right)^{-1}, \varepsilon, d\right) \\ &\quad -\lambda_s \left(1-p_{MD}\right)\left(1-p_{FA}\right) G\left(\left(sPs\rho\right)^{-1}, \varepsilon, d\right)\Big). \qquad (6.9)\end{aligned}$$

When $1 - p_{FA} \geq p_{MD}$,

$$\begin{aligned}\mathcal{L}^{l2}_{I_{CR}}(s) &= \exp\Big(-\lambda_s\left[p_{MD} G\left(\left(sP_s\right)^{-1}, \varepsilon, 0\right) + \left(1-p_{MD}-p_{FA}\right) G\left(\left(sP_s\right)^{-1}, \varepsilon, d\right)\right]\Big) \times \\ &\quad \left[1 + \lambda_s \left(1-p_{FA}-p_{MD}\right)\left(1-\rho\right) G\left(\left(sP_s\right)^{-1}, \varepsilon, d\right)\right]. \qquad (6.10)\end{aligned}$$

Proof. Equation (6.9) is obtained by applying Jensen's inequality. Equation (6.10) is obtained by suitable lower-bounding the conditional Laplace transform of I_{CR} conditioned on $\mathcal{B}$ leading to a simple closed form expression. See Appendix 6.9.1 for the complete proof. □

The following theorem uses the basic properties of a homogeneous Poisson point process to translate the original system where the cognitive radios have imperfect detection capability to an equivalent system where all the cognitive radios have perfect detection capability.

Theorem 15. *Let* $\Pi_{MD} \triangleq \{x_i | \, x_i \in \mathrm{PPP}(\lambda_s), \; x_i \in \mathcal{B} \bigcup \mathcal{S}, \; M_i = 1\}$ *be the set of cognitive radios in the system that cause interference at the origin due to missed detection where* $M_i \overset{\text{i.i.d.}}{\sim} \mathrm{Bernoulli}(p_{MD})$. *Similarly, let* $\Pi_{FA^c} \triangleq \{x_i | \, x_i \in \mathrm{PPP}(\lambda_s), \; x_i \notin \mathcal{B} \bigcup \mathcal{S}, \; F_i = 0\}$ *be the set of cognitive radios that communicate in the regions where there are no primary receivers in the vicinity and cause interference at the origin, with* $F_i \overset{\text{i.i.d.}}{\sim} \mathrm{Bernoulli}(p_{FA})$ *such that* $1 - p_{FA} \geq p_{MD}$. *Then,*

$$\Pi_{MD} \bigcup \Pi_{FA^c} \;\; = \;\; \Pi_1 \bigcup \Pi_2, \tag{6.11}$$

where $\Pi_1 \triangleq \{x_i | \, x_i \in \mathrm{PPP}(\lambda_1)\}$, $\Pi_2 \triangleq \{x_i | \, x_i \in \mathrm{PPP}(\lambda_2), \; x_i \notin \mathcal{B} \bigcup \mathcal{S}\}$, $\lambda_1 = p_{MD}\lambda_s$, $\lambda_2 = (1 - p_{FA} - p_{MD})\lambda_s$, Π_1 *and* Π_2 *are independent of each other and cognitive radios represented by the sets* Π_1 *and* Π_2 *all have perfect detection capabilities.*

Proof. See Appendix 6.9.2 for the proof. □

Corollary 17. *The total interference at the primary receiver due to the CRs,* I_{CR} *has the same distribution as the sum of the interferences due to points belonging to two independent spatial point processes* Π_1 *and* Π_2 *(defined in Theorem 15), denoted by* I_1 *and* I_2, *respectively. In other words,* $I_{CR} =_{\text{st}} I_1 + I_2$ *where* $I_1 = \sum_{x_i \in \Pi_1} P_s g_{1i} \|x_i\|_2^{-\varepsilon}$, $I_2 = \sum_{x_i \in \Pi_2} P_s g_{2i} \|x_i\|_2^{-\varepsilon}$ *are independent of each other,* g_{1i}, g_{2i} *are i.i.d. unit mean exponential random variables* $\forall \; i$ *and* $=_{\text{st}}$ *corresponds to equivalence in distribution.*

Due to Theorem 15, the original stochastic geometric model (or spatial point process) can be decomposed into two independent stochastic geometric models that are relatively easy to study. Further, it follows from Corollary 17 that $\mathcal{L}_{I_{CR}}(s) = \mathcal{L}_{I_1}(s)\mathcal{L}_{I_2}(s)$, where $\mathcal{L}_{I_1}(s)$ can be obtained in closed form along the

same lines as $\mathcal{L}_{I_{WM}}(s)$ in (6.6). A new set of bounds for $\mathcal{L}_{I_{CR}}(s)$ are obtained by deriving bounds for $\mathcal{L}_{I_2}(s)$ in the following two theorems.

Theorem 16. *Another lower-bound for $\mathcal{L}_{I_{CR}}(s)$ is listed below:*

$$\mathcal{L}^{l3}_{I_{CR}}(s) \quad = \quad \mathcal{L}_{I_1}(s) \times \max\left(\mathbb{E}\left[\mathrm{e}^{-sI_2^{'}}\right], \mathrm{e}^{-s\mathbb{E}[I_2]}\right) \tag{6.12}$$

where $\mathcal{L}_{I_1}(s) = \exp\left(-\lambda_1 G\left(\left(sP_s\right)^{-1}, \varepsilon, 0\right)\right)$, $\mathbb{E}\left[\mathrm{e}^{-sI_2^{'}}\right] = \mathrm{e}^{-\lambda_2 G\left(\left(sP_s\right)^{-1}, \varepsilon, d\right)}$ *and* $\mathbb{E}[I_2] = \frac{\lambda_2 \rho P_s 2\pi d^{2-\varepsilon}}{\varepsilon - 2}$.

Finally, we have

$$\mathcal{L}^{l}_{I_{CR}}(s) \quad = \quad \max\left(\left\{\mathcal{L}^{li}_{I_{CR}}\right\}_{i=1}^{3}\right). \tag{6.13}$$

Proof. Note that $\Pi_2 \subseteq \Pi_2^{'} = \{x_i | \, x_i \in \mathrm{PPP}(\lambda_2), \; x_i \notin \mathcal{S}\}$ by definition. As a result, the total interference power corresponding to Π_2 is upper bounded by the total interference power corresponding to $\Pi_2^{'}$. This implies $I_2 \leq_{st} I_2^{'} = \sum_{x_i \in \Pi_2^{'}} P_s g_{1i} \left\|x_i\right\|_2^{-\varepsilon}$ and hence $\mathcal{L}_{I_2}(s) \geq \mathcal{L}_{I_2^{'}}(s)$, and $\mathcal{L}_{I_2^{'}}(s)$ can be computed in closed-form along the same lines as $\mathcal{L}_{I_{WM}}(s)$ in (6.6). The second lower bound for $\mathcal{L}_{I_2}(s)$ can be obtained using Jensen's inequality. Combining these two bounds, we get a new lower bound for $\mathcal{L}_{I_{CR}}(s)$ in (6.12). □

Theorem 17. *The upper bounds for $\mathcal{L}_{I_{CR}}(s)$ are listed below:*

$$\mathcal{L}^{u1}_{I_{CR}}(s) = \begin{cases} \mathcal{L}_{I_1}(s)\left(1 - \frac{\lambda_2 \rho G\left(\frac{1}{sP_s}, \varepsilon, d\right)}{2}\right) & , 0 \leq \lambda_2 G\left(\frac{1}{sP_s}, \varepsilon, d\right) \leq 1.5916 \\ \mathcal{L}_{I_1}(s) & , \text{ otherwise} \end{cases}, \tag{6.14}$$

$$\mathcal{L}^{u2}_{I_{CR}}(s) = \mathcal{L}_{I_1}(s) \prod_{i=1}^{2}\left(1 - \rho H_i\left(\lambda_2, \left(2sP_s\right)^{-1}, \varepsilon, d\right)\right)^{\frac{1}{2}}, \tag{6.15}$$

$$\mathcal{L}^{u3}_{I_{CR}}(s) = \mathcal{L}_{I_1}(s)\left[1 - \sum_{i=1}^{2} \frac{\rho H_i\left(\lambda_2, \left(2sP_s\right)^{-1}, \varepsilon, d\right)}{2}\right], \tag{6.16}$$

$$\mathcal{L}^{u4}_{I_{CR}}(s) = \mathcal{L}_{I_1}(s)\left[1 - \rho H_1\left(\lambda_2, \left(sP_s\right)^{-1}, \varepsilon, d\right)\right], \tag{6.17}$$

$$\mathcal{L}^{u}_{I_{CR}}(s) = \min\left(\left\{\mathcal{L}^{ui}_{I_{CR}}(s)\right\}_{i=1}^{4}\right), \tag{6.18}$$

where $\mathbb{E}\left[\mathrm{e}^{-sI_2^{'}}\right]$ ***is as in Theorem 16,*** $\rho = \mathrm{e}^{-\lambda_r \pi d^2}$ ***from Corollary 9,***

$$H_k\left(\lambda, \left(2sP_s\right)^{-1}, \varepsilon, d\right) \quad = \quad \int_{r=d}^{\infty} \frac{\left(\lambda\pi\right)^k 2r \times \left(r^2 - d^2\right)^{k-1} dr}{\left(1 + \left(2sP_s\right)^{-1} r^{\varepsilon}\right) \mathrm{e}^{\lambda\pi\left(r^2 - d^2\right)}}. \tag{6.19}$$

Proof. As in Theorem 16, upper bounds for $\mathcal{L}_{I_{CR}}(s)$ are obtained by deriving upper bounds for $\mathcal{L}_{I_2}(s)$ due to Theorem 15 and Corollary 17. The upper bound (6.14) is obtaining using the inequality, $\exp(-x) \leq 1-\frac{x}{2}$, $\forall\ x \in [0, 1.5916]$. The upper bounds (6.39) - (6.41) are obtained by lower bounding I_2 by the interference caused by the nearest few active CRs. See Appendix 6.9.3 for the complete proof. □

Finally, based on the upper and lower bounds for $\mathcal{L}_{I_{CR}}(s)$, we can derive the corresponding upper and lower bounds for $\text{var}\left(\text{e}^{-sI_{CR}}\right)$ as shown below.

Proposition 8. ***Upper and lower bounds for*** $\text{var}\left(\text{e}^{-sI_{CR}}\right)$ ***are***

$$\text{var}_u\left(\text{e}^{-sI_{CR}}\right) = \max\left(0, \mathcal{L}^u_{I_{CR}}(2s) - \left[\mathcal{L}^l_{I_{CR}}(s)\right]^2\right), \tag{6.20}$$

$$\text{var}_l\left(\text{e}^{-sI_{CR}}\right) = \max\left(0, \mathcal{L}^l_{I_{CR}}(2s) - \left[\mathcal{L}^u_{I_{CR}}(s)\right]^2\right). \tag{6.21}$$

The max operation ensures that the bounds are non-negative. Further, the upper (lower) bound is obtained by upper (lower) bounding each term in $\text{var}\left(\text{e}^{-sI_{pc}}\right) = \mathcal{L}_{I_{pc}}(2s) - \left[\mathcal{L}_{I_{pc}}(s)\right]^2$, which is due to the definition of variance of a random variable.

Now, we study the characteristics of an approximation for I_{CR}, denoted by $\bar{I}_{CR}$ which is obtained by independent thinning of the points belonging to $\Pi_2^{'}$ (defined in the proof of Theorem 16) with a probability ρ, the probability that an arbitrary point lies outside the detection region of all primary receivers. The following remark defines $\bar{I}_{CR}$ and computes its Laplace transform.

Remark 6. $\bar{I}_{CR} = I_1 + \bar{I}_2$, where $\bar{I}_2 = \sum_{x_i \in \Pi_2^{'}} P_s g_{2i} \left\|x_i\right\|_2^{-\varepsilon} T_i$, and T_i's are i.i.d. Bernoulli(ρ) random variables. As a result, the Laplace transform of $\bar{I}_{CR}$ is

$$\mathcal{L}_{\bar{I}_{CR}}(s) = \mathcal{L}_{I_1}(s)\,\mathcal{L}_{\bar{I}_2}(s) = \mathcal{L}_{I_1}(s) \times \exp\left(-\lambda_2 \rho G\left(\left(sP_s\right)^{-1}, \varepsilon, d\right)\right). \tag{6.22}$$

The independent thinning of the points in $\Pi_2^{'}$ is represented by T_i's. The above approximation is motivated by the fact that the higher order statistics, that captures the effects of two or more points belonging to the detection region of the same primary receiver, become less significant, as demonstrated in [43, 92]. Further, the Laplace transform is easily derived by noting that I_1 and $\bar{I}_2$ are, by construction, independent of each other, $\mathcal{L}_{I_1}(s)$ is derived in Theorem 16, and $\mathcal{L}_{\bar{I}_2}(s)$ can be derived along the same lines as $\mathcal{L}_{I_{WM}}(s)$ in (6.6).

Having studied the characteristics of the individual interferences that affect the primary user at the origin (both the wireless microphone receiver and the TV receiver), we move on to characterizing the success probabilities at any given primary receiver. We begin with characterizing the success probability for the TV receivers.

6.4 Coverage probability bounds for the TV receiver

Recall that (6.1) gives the expression for the coverage probability where the interferences to the TV receiver, namely, I_{TV} and I_{CR} are both independent of each other. The bounds for the Laplace transform of I_{CR} (Equations (6.13) and (6.18)) derived in the previous section shall be utilized to bound the coverage probability denoted by $\mathbb{P}_{coverage}\left(\text{TVR}\right) = \mathbb{P}\left(\{\text{SIR}_{TVR} > \beta\}\right)$ in the following theorems.

Theorem 18. *The lower bound for the coverage probability at the TV receiver located at the origin is*

$$\begin{aligned}\mathbb{P}^{l}_{coverage}\left(\text{TVR}\right) &= \lambda_t \frac{2\pi}{\varepsilon}\left(\gamma P_t\right)^{\frac{2}{\varepsilon}}\Gamma\left(1+\frac{2}{\varepsilon}\right)\times \\ &\quad \int_{y=0}^{\infty}\int_{\omega=-\infty}^{\infty}\mathcal{L}_{I_1}\left(j\omega\right)\mathbb{E}\left[\mathrm{e}^{-j\omega I_2^{'}}\right]\mathcal{L}_I^{y}\left(j\omega\right)\left(\frac{\mathrm{e}^{\frac{j\omega y}{\beta}}-1}{2\pi j\omega y^{1+\frac{2}{\varepsilon}}}\right)d\omega dy, \qquad (6.23)\\ \mathcal{L}_I^{y}\left(s\right) &= \mathrm{e}^{-\lambda_t\pi(sP_t)^{\frac{2}{\varepsilon}}\Gamma\left(1+\frac{2}{\varepsilon}\right)\left[\Gamma\left(1-\frac{2}{\varepsilon}\right)+\frac{2}{\varepsilon}\Gamma\left(-\frac{2}{\varepsilon},\frac{sy}{\gamma}\right)\right]}, \qquad (6.24)\end{aligned}$$

where $\gamma = 1+\beta^{-1}$, $\mathcal{L}_{I_1}\left(j\omega\right)$ *and* $\mathbb{E}\left[\mathrm{e}^{-sI_2^{'}}\right]$ *are obtained from Theorem 16 and* I *is the sum of the received powers from all the TV transmitters in the system. Further, based on Remark 6, an approximation for the coverage probability, denoted by* $\mathbb{P}^{approx}_{coverage}\left(\text{TVR}\right)$ *can be obtained by replacing* $\mathbb{E}\left[\mathrm{e}^{-j\omega I_2^{'}}\right]$ *with* $\mathcal{L}_{\bar{I}_2}\left(j\omega\right)$ *shown in (6.22).*

Proof. We use [70, Theorems 2 and 3] to show this result. See Appendix 6.9.4 for the proof. □

Theorem 19. *For* $\beta \geq 1$,

$$\mathbb{P}_{coverage}\left(\text{TVR}\right) = \mathbb{P}\left(\{\text{SIR}_{TVR} > \beta\}\right) = \beta^{-\frac{2}{\varepsilon}}\mathbb{P}\left(\{\text{SIR}_{TVR} > 1\}\right). \qquad (6.25)$$

By bounding $\mathbb{P}\left(\{\text{SIR}_{TVR} > 1\}\right)$*, the upper and lower bounds for the coverage probability (*$\mathbb{P}^{u}_{coverage}\left(\text{TVR}\right)$ *and* $\mathbb{P}^{l}_{coverage}\left(\text{TVR}\right)$ *respectively) at the TV receiver located at the origin are obtained as shown below.*

$$\mathbb{P}^{u}_{coverage}\left(\text{TVR}\right) = \beta^{-\frac{2}{\varepsilon}}\int_{r=0}^{\infty}\lambda_t 2\pi r\mathcal{L}^{u}_{I_{CR}}\left(\frac{r^{\varepsilon}}{P_t}\right)\exp\left(-\frac{\lambda_t\pi r^2}{\text{sinc}\left(\frac{2\pi}{\varepsilon}\right)}\right)dr, \qquad (6.26)$$

where $\mathcal{L}^u_{I_{CR}}(s)$ is obtained from Theorem 17. The lower bound for the coverage probability at the TV receiver is given by replacing $\mathcal{L}^u_{I_{CR}}(s)$ in (6.26) with $\mathcal{L}^l_{I_{CR}}(s)$ that can be obtained from Theorem 14 and Theorem 16. Further, $\mathbb{P}^{approx}_{coverage}(\text{TVR})$ also reduces to the simple form shown in (6.26) where $\mathcal{L}^u_{I_{CR}}\left(\frac{r^\varepsilon}{P_t}\right)$ is replaced with $\mathcal{L}_{\bar{I}_{CR}}\left(\frac{r^\varepsilon}{P_t}\right)$ derived in (6.22).

Proof. See Appendix 6.9.5 for the proof. □

Notice that the integral in the above equation is not a function of β, the SIR threshold, which means that they need to be computed only once each for the upper bounds, lower bounds and the approximation respectively. Also, the results in this section hold for unit mean exponential fading distributions at the TV transmitters. Next, we generalize these results for arbitrary fading distributions at the TV transmitters using the following corollary.

Corollary 18. *When the i.i.d. fading factors corresponding to each TV transmitter in the system has an arbitrary distribution, same as that of a random variable, Ψ, the coverage probability at the TV receiver is the same as in the case where the i.i.d. fading factors at the TV transmitters are unit mean exponential random variables, and the density of the TV transmitters is $\frac{\lambda_t \mathbb{E}\left[\Psi^{\frac{2}{\varepsilon}}\right]}{\Gamma\left(1+\frac{2}{\varepsilon}\right)}$, as long as $\mathbb{E}\left[\Psi^{\frac{2}{\varepsilon}}\right] < \infty$.*

Proof. This result is a direct consequence of [58, Corollary 3]. □

As a result, by appropriately scaling λ_t, Theorems 18 and 19 provide the coverage probability bounds for arbitrary fading distributions at the TV transmitters.

6.5 Coverage probability bounds for the wireless microphone receiver

The probability of successful communication between the wireless microphone receiver and its wireless microphone transmitter separated by a distance r_s is

$$\mathbb{P}_{coverage}(\text{WMR}) = \mathbb{P}\left(\{\text{SIR}_{WMR} > \beta\}\right) = \mathbb{P}\left(\left\{\frac{P_t h_k r_s^{-\varepsilon}}{I_{WM} + I_{CR}} > \beta\right\}\right) \overset{(a)}{=} \mathbb{E}\left[\mathrm{e}^{-s(I_{WM}+I_{CR})}\right], \tag{6.27}$$

where I_{WM} is defined in (6.5), I_{CR} is defined in (6.3), $s = \frac{\beta}{P_t r_t^{-\varepsilon}}$ and (a) is obtained when the fading gains for all the wireless microphone transmitters and the cognitive radio transmitters are i.i.d. unity mean exponential random variables. Unlike the TV receiver case, the interferences I_{WM} and I_{CR} at the wireless

microphone receiver are correlated random variables, and again the Laplace transform of their sum cannot be characterized in closed form. As a result, we focus on finding their upper and lower bounds.

Theorem 20. *Upper bounds for* $\mathbb{P}_{coverage}\left(\text{WMR}\right)$ *are*

$$\mathbb{P}^{u1}_{coverage}\left(\text{WMR}\right) = \min\left(\mathcal{L}_{I_{WM}}\left(s\right), \mathcal{L}^{u}_{I_{CR}}\left(s\right), \sqrt{\mathcal{L}_{I_{WM}}\left(2s\right) \times \mathcal{L}^{u}_{I_{CR}}\left(2s\right)}\right), \tag{6.28}$$

$$\mathbb{P}^{u2}_{coverage}\left(\text{WMR}\right) = \mathcal{L}_{I_{WM}}\left(s\right)\mathcal{L}^{u}_{I_{CR}}\left(s\right) + \sqrt{\text{var}\left(\text{e}^{-sI_{WM}}\right)\text{var}_{u}\left(\text{e}^{-sI_{CR}}\right)}, \tag{6.29}$$

$$\mathbb{P}^{u}_{coverage}\left(\text{WMR}\right) = \min\left(\mathbb{P}^{u1}_{coverage}\left(\text{WMR}\right), \mathbb{P}^{u2}_{coverage}\left(\text{WMR}\right)\right), \tag{6.30}$$

where $s = \frac{\beta}{P_t r_t^{-\varepsilon}}$, $\mathcal{L}_{I_{WM}}\left(s\right)$ *and* $\text{var}\left(\text{e}^{-sI_{WM}}\right)$ *are from (6.6) and (6.8),* $\mathcal{L}^{u}_{I_{CR}}\left(s\right)$ *and* $\text{var}_{u}\left(\text{e}^{-sI_{CR}}\right)$ *are from Theorem 17 and (6.20), respectively.*

Proof. Firstly, notice that $I_{WM}+I_{CR} \geq \max\left(I_{WM},\ I_{CR}\right)$, and as a result, $\mathbb{P}_{coverage}\left(\text{WMR}\right) \leq \min\left(\mathcal{L}_{I_{WM}}\left(s\right), \mathcal{L}^{u}_{I_{CR}}\left(s\right)\right)$. Next, $\mathbb{P}_{coverage}\left(\text{WMR}\right) \leq \sqrt{\mathbb{E}\left[\text{e}^{-2sI_{WM}}\right]\mathbb{E}\left[\text{e}^{-2sI_{CR}}\right]}$ using the Cauchy-Schwartz inequality. By upper bounding the second expectation term in the product and combining the above mentioned bounds, we get (6.28).

Further, from the definition of the correlation coefficient between two dependent random variables X and Y, we get

$$-1 \leq \frac{\mathbb{E}\left[XY\right] - \mathbb{E}\left[X\right]\mathbb{E}\left[Y\right]}{\sqrt{\text{var}\left(X\right) \times \text{var}\left(Y\right)}} \leq 1. \tag{6.31}$$

Hence, using the upper bound in (6.31), we get

$$\mathbb{P}_{coverage}\left(\text{WMR}\right) \leq \mathcal{L}_{I_{WM}}\left(s\right)\mathcal{L}_{I_{CR}}\left(s\right) + \sqrt{\text{var}\left(\text{e}^{-sI_{WM}}\right)\text{var}\left(\text{e}^{-sI_{CR}}\right)}$$

and by further upper bounding $\mathcal{L}_{I_{CR}}\left(s\right)$ and $\text{var}\left(\text{e}^{-sI_{CR}}\right)$, we get (6.29). Finally, (6.30) is obtained since the minimum of (6.28) and (6.29) is a tighter upper bound. □

Theorem 21. *Lower bounds for* $\mathbb{P}_{coverage}\left(\text{WMR}\right)$ *are*

$$\mathbb{P}^{l1}_{coverage}\left(\text{WMR}\right) = \max\left(0, \mathcal{L}_{I_{WM}}\left(s\right)\mathcal{L}^{l}_{I_{CR}}\left(s\right) - \sqrt{\text{var}\left(\text{e}^{-sI_{WM}}\right)\text{var}_{u}\left(\text{e}^{-sI_{CR}}\right)}\right), \tag{6.32}$$

$$\mathbb{P}^{l2}_{coverage}\left(\text{WMR}\right) = \mathcal{L}_{I_{WM}}\left(s\right)\mathcal{L}_{I_{1}}\left(s\right)\mathbb{E}\left[\text{e}^{-sI_{2}^{'}}\right], \tag{6.33}$$

$$\mathbb{P}^{l}_{coverage}\left(\text{WMR}\right) = \max\left(\mathbb{P}^{u1}_{coverage}\left(\text{WMR}\right), \mathbb{P}^{u2}_{coverage}\left(\text{WMR}\right)\right), \tag{6.34}$$

where $s = \frac{\beta}{P_t r_t^{-\varepsilon}}$, $\mathcal{L}_{I_{WM}}\left(s\right)$ *and* $\text{var}\left(\text{e}^{-sI_{WM}}\right)$ *are from (6.6) and (6.8),* $\mathcal{L}^{l}_{I_{CR}}\left(s\right)$ *is from Theorem 14 and Theorem 16,* $\text{var}_{u}\left(\text{e}^{-sI_{CT}}\right)$ *is from (6.20), and* $\mathbb{E}\left[\text{e}^{-sI_{2}^{'}}\right]$ *is as in Theorem 16.*

Proof. Equation (6.32) is proved along the same lines as (6.28) using the lower bound in (6.31). A tight lower bound for $\mathbb{P}_{coverage}(WMR)$ is obtained as follows. $I_{WM}+I_{CR} \overset{(a)}{=} I_{WM}+I_1+I_2 \overset{(b)}{\leq} I_{WM}+I_1+I_2^{'}$ where (a) is obtained by applying Theorem 15 where I_1 and I_2 are the total interferences from the points belonging to Π_1 and Π_2 in Theorem 15 and $I_2^{'}$ upper bounds I_2. Notice that I_{WM}, I_1 and $I_2^{'}$ are all independent of each other and their respective Laplace transforms can be obtained in closed form, we get (6.33). Further, since the maximum of the lower bounds is also a lower bound, we get (6.34). □

Due to Remark 6, an approximation for the $\mathbb{P}_{coverage}$(WMR), denoted by $\mathbb{P}^{approx}_{coverage}$(WMR) can be computed as follows.

Theorem 22. *An approximation for the coverage probability at an arbitrary wireless microphone receiver is* $\mathbb{P}^{approx}_{coverage}(\text{WMR}) = \mathcal{L}_{I_{WM}}(s)\,\mathcal{L}_{I_1}(s)\,\mathcal{L}_{\bar{I}_2}(s)$, *where* $s = \frac{\beta}{P_t r_t^{-\varepsilon}}$, *and is obtained by replacing* I_{CR} *in (6.27) with* $\bar{I}_{CR}$, *and noting that* I_{WM} *and* $\bar{I}_{CR}$ *are independent random variables by construction. The above expression follows from (6.6) and Remark 6.*

Having thoroughly studied the interference characteristics and the coverage probabilities at the TVR and the WMR, we take a closer look at the primary user performance in the presence of CRs with imperfect operational capabilities.

6.6 CR Imperfections

From the discussion so far, we realize that, with increase in p_{MD}, the amount of harmful interference increases as the CRs becomes more likely to operate within the detection region of the primary receivers. On the other hand, with increase in p_{FA}, more and more CRs that see a white-space frequency band fail to make use of the opportunity, thereby leading to lowered spectrum utilization. Let us define a spectrum utilization figure-of-merit, F as the fraction of active CRs operating in the white space bands. Further, $F = \frac{\rho(1-p_{FA})}{\rho(1-p_{FA})+(1-\rho)p_{MD}}$, where the numerator is the probability that an arbitrary CR that is outside the detection region of all the primary receivers operates, and the denominator is the probability that an arbitrary CR operates, either because of successful identification of a white space or due to missed detection. Accordingly, possible values taken by the tuple $(p_{MD},\ p_{FA})$ can be divided into 4 quadrants as shown in Figure 6.3.

In the previous sections, we have characterized the coverage probabilities for the case when $p_{FA} + p_{MD} \leq 1$. It turns out that, for extremely faulty CRs i.e. when $p_{FA} + p_{MD} > 1$, a simple strategy can cause the CRs to operate in more practically desirable region of $p_{FA} + p_{MD} \leq 1$, as explained in the following remark.

Remark 7. When $0.5 \leq p_{FA}\ (p_{MD}) < 1$, each CR can incorporate the strategy of switching its decisions. As a result, each CR now false-alarms (miss-detects) with a probability $0 < 1 - p_{FA}\ (1 - p_{MD}) \leq 0.5$. Also, the analysis in the previous sections now provide us the coverage probability characterizations.

Also, for the special case that $p_{FA} + p_{MD} = 1$, the coverage probability at the primary receivers can be computed in closed form. The following corollary lists the results.

Corollary 19. *When $p_{FA} + p_{MD} = 1$, $\Pi_2 = \{\phi\}$ with probability 1. As a result, $I_2 = I_2^{'} = 0$ with probability 1, in which case (6.23) gives the expression for the exact coverage probability. Further, when $\beta \geq 1$,*

$$\mathbb{P}_{coverage}\left(\text{TVR}\right) \quad = \quad \frac{\lambda_t P_t^{\frac{2}{\varepsilon}} \beta^{-\frac{2}{\varepsilon}} \text{sinc}\left(\frac{2\pi}{\varepsilon}\right)}{\lambda_t P_t^{\frac{2}{\varepsilon}} + \lambda_s p_{MD} P_s^{\frac{2}{\varepsilon}}}. \tag{6.35}$$

The exact coverage probability at the WMR is $\mathbb{P}_{coverage}\left(\text{WMR}\right) = \mathcal{L}_{I_{WM}}\left(\frac{\beta}{P_t r_t^{-\varepsilon}}\right) \mathcal{L}_{I_1}\left(\frac{\beta}{P_t r_t^{-\varepsilon}}\right)$.

Notice that the coverage probability could not be characterized exactly in general because the interference I_2 could not be characterized exactly. In the above special case, I_2 has a point mass at 0 and hence the coverage probabilities can be computed exactly. The above results can also be proved by showing that the upper and lower bounds for coverage probabilities coincide for $p_{FA} + p_{MD} = 1$.

Now, we will consider some numerical examples for some realistic scenarios.

6.7 Numerical Examples and Discussion

We begin with assessing the Laplace transforms of the various interference terms that were studied in Section 6.3. Recall that the interference from the other primary transmitters can be characterized exactly, and the closed-form expression $\mathcal{L}_{I_{WM}}(s)$ is shown in (6.6). In the case of the interference at the primary receiver due to CRs, a series of upper and lower bounds are derived for $\mathcal{L}_{I_{CR}}(s)$. The lower bound for $\mathcal{L}_{I_{CR}}(s)$ based on $I_2^{'}$ (see Theorem 16) ignores the effect of the multiple primary users in the system, and

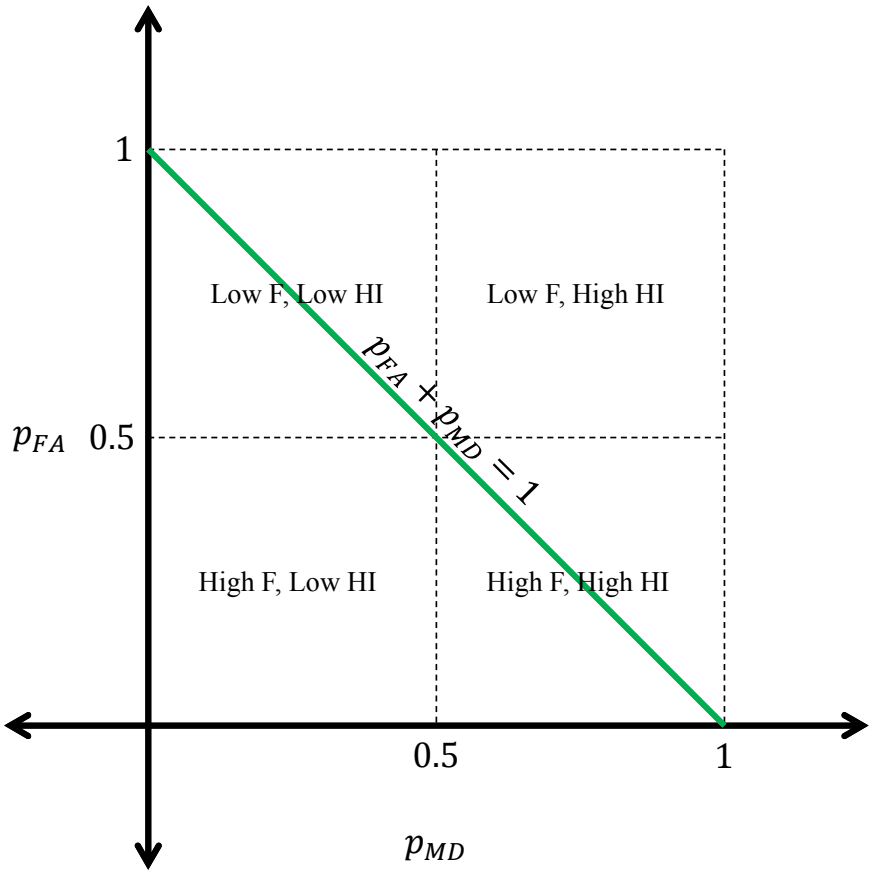

Figure 6.3: Spectrum utilization figure-of-merit (F) and harmful interference (HI) trade-offs based on CR imperfection parameters

is a good estimate only for small λ_r, while the other lower bounds dominate in the high λ_r regime. Next, $\mathcal{L}^{u1}_{I_{CR}}(s)$ is a good upper bound when λ_r is small. As λ_r increases, more primary receivers are likely to lie near the origin expanding the effective detection region around the origin. Given that signals decay sharply with distance, the interference caused by a few strong CRs contributing to I_2 can be a good estimate for I_2. This premise is used to derive $\mathcal{L}^{u2}_{I_{CR}}(s)$, $\mathcal{L}^{u3}_{I_{CR}}(s)$, and $\mathcal{L}^{u4}_{I_{CR}}(s)$. Further, the approximation $\bar{I}_{CR}$ studied in Remark 6 well-models I_{CR}, and $\mathcal{L}_{\bar{I}_{CR}}(s)$ closely follows $\mathcal{L}_{I_{CR}}(s)$ for all cases. Moreover, this approximation gives a simple intuitive way of understanding the interference caused by the CRs.

Now, we move on to studying the coverage probability at the TVR and the WMR, respectively. We provide some simulation results and verify the bounds and approximations for the coverage probability that we have derived in Sections 6.4 and 6.5 against the simulation results. For the study of the coverage probability at the TVR, the system parameters for the Monte-Carlo simulations are $\lambda_r = 0.1$, $\lambda_t = 0.01$, $\lambda_s = .1$, $P_t = 250$, $P_s = .1$, and $d = 1$. For the WMR case, the system parameters are $P_t = 1$, $P_s = .2$, $r_t = .5$, $\varepsilon = 4$, $d = 5$, $\lambda_t = \frac{1}{\pi d^2}$ and $\lambda_s = .5$. From Figures 6.4 and 6.5, notice that the coverage probability at the TVR is more robust to imperfect operations of the CRs compared to the WMR, which shows erratic changes in performance with varying imperfections at the CRs. Further, notice that the coverage probability approximation at the TVR and the WMR are uniformly tight for all cases. Also, notice from the curves in Figure 6.5 that, with a small increase in p_{MD}, the nearby CRs are more likely to interfere with the primary receiver and cause harmful interference, and therefore causes a significant reduction in the coverage probability. Further, when $p_{FA} + p_{MD} = 1$, coverage probability can be characterized in closed form as soon in the last two curves of Figure 6.5.

Next, for a given system parameters, a system designer may be interested to find the SIR that a primary user can expect to see with a high reliability, say with a coverage probability of 95%. Notice from Figure 6.5 that the bounds for the coverage probability are tight especially at the 95^{th} percentile. As a result, system design decisions made based on the bounds and approximation studies in this chapter are likely to be of reasonable accuracy.

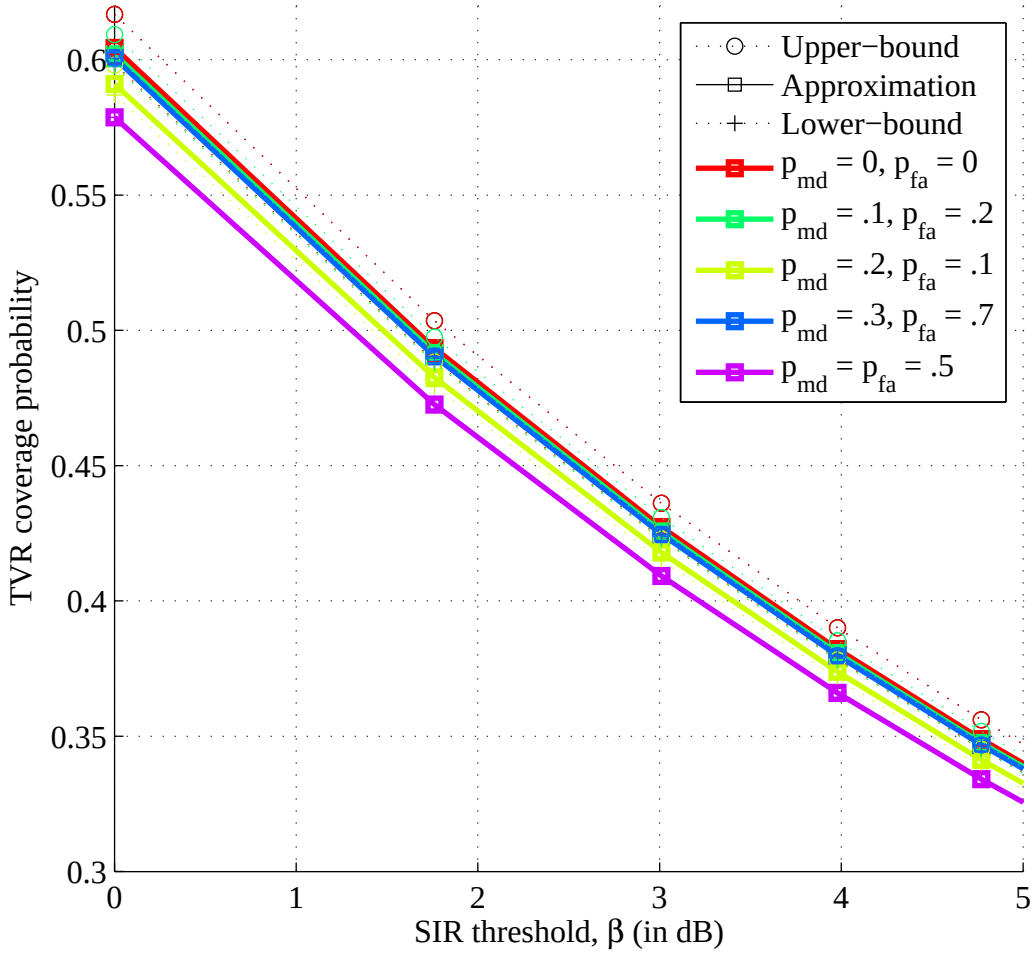

Figure 6.4: Coverage probability comparison for different imperfect detection configurations for the TVR case

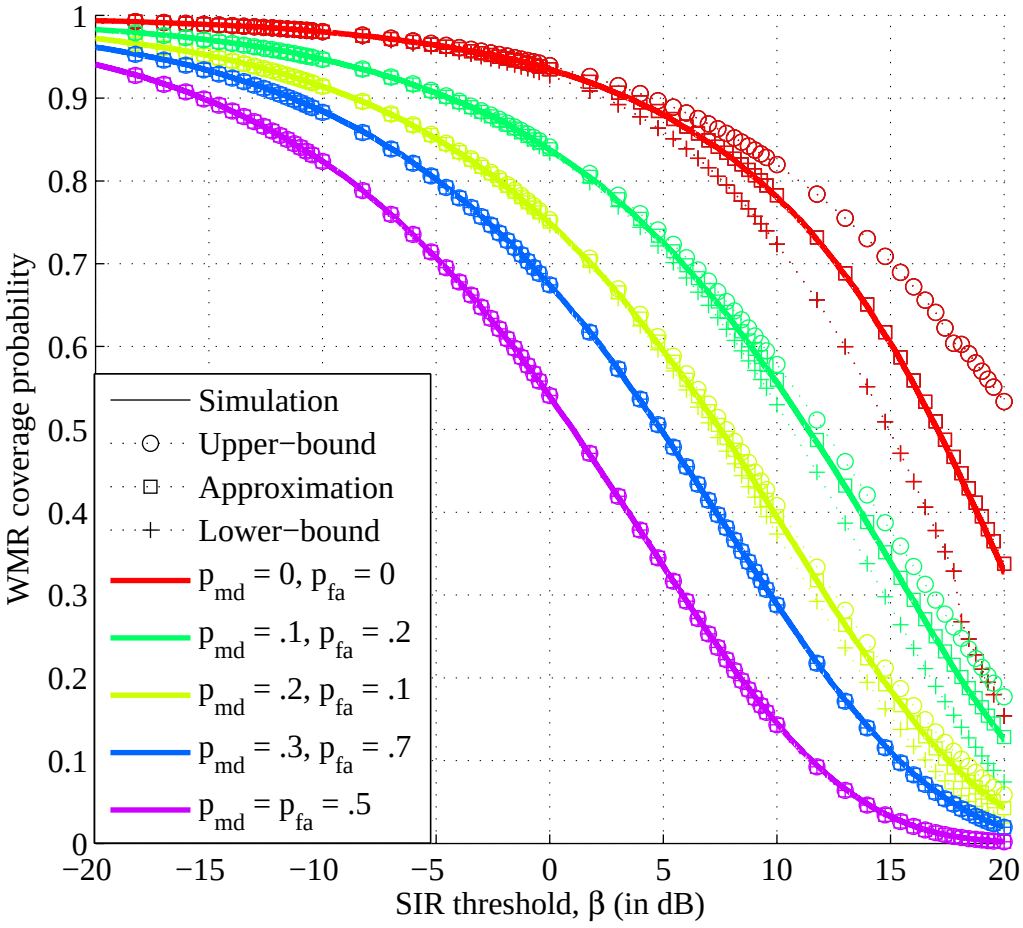

Figure 6.5: Coverage probability comparison for different imperfect detection configurations for the WMR case.

6.8 Conclusions

In this chapter, we study the impact of imperfections in the ability of the CRs in detecting primary user operations by characterizing the interference characteristics and coverage probability at the primary receivers. The primary users and CRs are assumed to be distributed according to independent homogeneous Poisson point proceses. Further, we study the performance at two types of primary users, namely, the TV transmitter-receiver pairs and the wireless microphone systems. A stochastic-geometry based study of the performance at the TV transmitter-receiver pairs has been done before this. We derive tight upper and lower bounds and an intuitive approximation for the Laplace transforms of the interference. These results, are then used to derive the corresponding bounds and approximation for the coverage probability.

6.9 Appendix

6.9.1 Proof for Theorem 14

The proof for (6.9) is as follows:

$$\begin{aligned}
\mathcal{L}_{I_{CR}}(s) &\overset{(a)}{=} \mathbb{E}\left[\mathrm{e}^{-s\sum_{m=1}^{\infty} P_s g_m \|y_m\|_2^{-\varepsilon}\mathcal{I}(y_m\in\mathcal{S})\mathcal{I}(M_m=1)}\right]\times \\
&\quad \mathbb{E}\left[\mathrm{e}^{-s\sum_{m=1}^{\infty} P_s g_m \|y_m\|_2^{-\varepsilon}\mathcal{I}(y_m\in\mathcal{S}^c)[\mathcal{I}(y_m\in\mathcal{B})\mathcal{I}(M_m=1)+\mathcal{I}(y_m\notin\mathcal{B})\mathcal{I}(F_m=0)]}\right] \\
&\overset{(b)}{\geq} \mathbb{E}\left[\mathrm{e}^{-s\sum_{m=1}^{\infty} P_s g_m \|y_m\|_2^{-\varepsilon}\mathcal{I}(y_m\in\mathcal{S})\mathcal{I}(M_m=1)}\right]\times \\
&\quad \mathbb{E}\left[\mathrm{e}^{-s\sum_{m=1}^{\infty} P_s g_m \|y_m\|_2^{-\varepsilon}\mathcal{I}(y_m\in\mathcal{S}^c)\mathbb{E}_{\mathcal{B}}[\mathcal{I}(y_m\in\mathcal{B})\mathcal{I}(M_m=1)+\mathcal{I}(y_m\notin\mathcal{B})\mathcal{I}(F_m=0)]}\right] \\
&\overset{(c)}{=} T1\times\exp\left(-\lambda_s\int_{r=d}^{\infty}\left(1-\mathbb{E}\left[\mathrm{e}^{-sP_s g r^{-\varepsilon}[(1-\rho)\mathcal{I}(M_m=1)+\rho\mathcal{I}(F_m=0)]}\right]\right)dr\right), \qquad (6.36)
\end{aligned}$$

where (a) is obtained by rewriting $\mathcal{I}(y_m\in\mathcal{B}\bigcup\mathcal{S}) = \mathcal{I}(y_m\in\mathcal{S}) + \mathcal{I}(y_m\in\mathcal{B})\mathcal{I}(y_m\notin\mathcal{S})$ and noting that the Poisson point processes defined in $\mathcal{S}$ and $\mathcal{S}^c$ are independent of each other [7], (b) is obtained applying Jensen's inequality for the second term in (a) w.r.t. $\mathcal{B}$,(c) is obtained by applying Campbell's theorem [6] for the first term to get

$$T1 = \exp\left(-\lambda_s p_{MD}\left[G\left((sP_s)^{-1},\varepsilon,0\right)-G\left((sP_s)^{-1},\varepsilon,d\right)\right]\right),$$

computing the expectation w.r.t. $\mathcal{B}$ in the second term of (b) and then applying Campbell's theorem, and finally, (6.9) is obtained by evaluating the expectation in (c) and then representing the result in terms of the

$G()$.

The proof for (6.10) is as follows:

$$\begin{aligned}
&\mathcal{L}_{I_{CR}}(s) \overset{(a)}{=} T1 \times \mathbb{E}\left[\mathrm{e}^{-s\sum_{m=1}^{\infty} P_s g_m \|y_m\|_2^{-\varepsilon}\mathcal{I}(y_m\in\mathcal{S}^c)[\mathcal{I}(y_m\in\mathcal{B})\mathcal{I}(M_m=1)+\mathcal{I}(y_m\notin\mathcal{B})\mathcal{I}(F_m=0)]}\right] \\
&\overset{(b)}{=} T1 \times \mathbb{E}_{\mathcal{B}}\left[\exp\left(-\lambda_s\int_{y\in\mathbb{R}^2\bigcap\mathcal{S}^c}\left(1-\mathbb{E}\left[\mathrm{e}^{-sP_s g\|y\|_2^{-\varepsilon}[\mathcal{I}(y\in\mathcal{B})\mathcal{I}(M=1)+\mathcal{I}(y\notin\mathcal{B})\mathcal{I}(F=0)]}\right]\right)dy\right)\right] \\
&\overset{(c)}{=} T1 \times \mathbb{E}_{\mathcal{B}}\left[\exp\left(-\lambda_s\int_{y\in\mathbb{R}^2\bigcap\mathcal{S}^c}\mathcal{I}(y\in\mathcal{B})\left(1-\mathbb{E}\left[\mathrm{e}^{-sP_s g\|y\|_2^{-\varepsilon}\mathcal{I}(M=1)}\right]\right)dy\right)\times\right. \\
&\left.\exp\left(-\lambda_s\int_{y\in\mathbb{R}^2\bigcap\mathcal{S}^c}\mathcal{I}(y\notin\mathcal{B})\left(1-\mathbb{E}\left[\mathrm{e}^{-sP_s g\|y\|_2^{-\varepsilon}\mathcal{I}(F=0)}\right]\right)dy\right)\right] \\
&\overset{(d)}{=} T1 \times \mathbb{E}_{\mathcal{B}}\left[\exp\left(-\lambda_s\int_{y\in\mathbb{R}^2\bigcap\mathcal{S}^c}\frac{\mathcal{I}(y\in\mathcal{B})\,p_{MD}+\mathcal{I}(y\notin\mathcal{B})(1-p_{FA})}{1+(sP_s)^{-1}\|y\|_2^{\varepsilon}}dy\right)\right] \\
&\overset{(e)}{=} T1 \times \mathrm{e}^{-\lambda_s(1-p_{FA})G\left((sP_s)^{-1},\varepsilon,d\right)}\mathbb{E}_{\mathcal{B}}\left[\exp\left(\lambda_s(1-p_{FA}-p_{MD})\int_{y\in\mathbb{R}^2\bigcap\mathcal{S}^c}\frac{\mathcal{I}(y\in\mathcal{B})}{1+(sP_s)^{-1}\|y\|_2^{\varepsilon}}dy\right)\right] \\
&\overset{(f)}{\geq} T1 \times \mathrm{e}^{-\lambda_s(1-p_{FA})G\left((sP_s)^{-1},\varepsilon,d\right)}\times \\
&\mathbb{E}_{\mathcal{B}}\left[1+\lambda_s(1-p_{FA}-p_{MD})\int_{y\in\mathbb{R}^2\bigcap\mathcal{S}^c}\frac{\mathcal{I}(y\in\mathcal{B})}{1+(sP_s)^{-1}\|y\|_2^{\varepsilon}}dy\right],\ \text{when } 1-p_{FA}\geq p_{MD} \\
&= T1 \times \mathrm{e}^{-\lambda_s(1-p_{FA})G\left((sP_s)^{-1},\varepsilon,d\right)}\left[1+\lambda_s(1-p_{FA}-p_{MD})(1-\rho)\,G\left((sP_s)^{-1},\varepsilon,d\right)\right], \qquad (6.37)
\end{aligned}$$

where (a) follows from (6.36)-(a), (b) is obtained by evaluating the expectation w.r.t. the Poisson point process conditioned on $\mathcal{B}$, (c) is obtained by rewriting (b), (d) is obtained by applying Campbell's theorem to the second term in (c), (e) is obtained by rewriting $\mathcal{I}(y\notin\mathcal{B}) = 1-\mathcal{I}(y\in\mathcal{B})$ and simplifying, (f) is obtained using the inequality $\mathrm{e}^{\lambda}\geq 1+\lambda,\ \forall\ \lambda\geq 0$.

6.9.2 Proof for Theorem 15

Firstly, notice that Π_{MD} and Π_{FA^c} are independent of each other since restrictions of homogeneous Poisson point processes to disjoint regions are independent of each other. Using the Coloring theorem [6, Page 53], we get

$$\begin{aligned}
\Pi_{MD} &= \left\{x_i |\, x_i\in \mathrm{PPP}\left(\lambda_s p_{MD}\right),\ x_i\in\mathcal{B}\bigcup\mathcal{S}\right\} \\
\Pi_{FA^c} &= \left\{x_i |\, x_i\in \mathrm{PPP}\left(\lambda_s(1-p_{FA})\right),\ x_i\notin\mathcal{B}\bigcup\mathcal{S}\right\},
\end{aligned}$$

where $\mathrm{PPP}(\lambda)$ refers to a homogeneous Poisson point process on the plane with density λ. Further, since the homogeneous Poisson point process is an infinitely divisible point process [93, Page 87], we can rewrite

Π_{FA^c} as a superposition of two independent homogeneous Poisson point processes as shown below.

$$\Pi_{FA^c} = \left\{ x_i | \, x_i \in \text{PPP}\left(\lambda_s p_{MD}\right), \; x_i \notin \mathcal{B} \bigcup \mathcal{S} \right\} \bigcup \Pi_2.$$

Finally,

$$\begin{aligned} \Pi_{MD} \bigcup \Pi_{FA^c} &= \left\{ x_i | \, x_i \in \text{PPP}\left(\lambda_s p_{MD}\right), \; x_i \in \mathcal{B} \bigcup \mathcal{S} \right\} \bigcup \\ &\quad \left\{ x_i | \, x_i \in \text{PPP}\left(\lambda_s p_{MD}\right), \; x_i \notin \mathcal{B} \bigcup \mathcal{S} \right\} \bigcup \Pi_2 \end{aligned}$$

and hence, by applying the Superposition theorem [6, Page 16], we get (6.11) where Π_1 and Π_2 are by construction independent of each other.

6.9.3 Proof for Theorem 17

Recall that $\mathcal{L}_{I_{CR}}(s) = \mathcal{L}_{I_1}(s)\,\mathcal{L}_{I_2}(s)$, and $\mathcal{L}_{I_1}(s)$ is known to us in closed form. In the rest of this section we derive upper bounds for $\mathcal{L}_{I_2}(s)$.

Proof for (6.14):

$$\begin{aligned} \mathcal{L}_{I_2}(s) &= \mathbb{E}_{\mathcal{B}}\left[\mathbb{E}\left[\mathrm{e}^{-\sum_{i=1}^{\infty} s P_s h_i \|x_i\|_2^{-\varepsilon} \mathcal{I}(x_i \in \mathcal{B}^c \bigcap \mathcal{S}^c)} \middle| \, \mathcal{B} \right] \right] \\ &\overset{(a)}{=} \mathbb{E}_{\mathcal{B}}\left[\mathrm{e}^{-\lambda_2 \int_{x \in \mathcal{S}^c} \frac{\mathcal{I}(x \notin \mathcal{B})}{1+(sP_s)^{-1}\|x\|_2^{\varepsilon}} dx} \right], \end{aligned}$$

where the first equality is obtained by rewriting the Laplace transform by first conditioning w.r.t. the random set $\mathcal{B}$, (a) is obtained by applying the Campbell's theorem for the homogeneous Poisson point process defined in the space $\mathcal{B}^{\rfloor} \bigcap \mathcal{S}^{\rfloor}$, and finally, (6.14) is obtained by using the inequality $\exp(-z) \leq 1 - \frac{z}{2}$, $\forall \; z \in [0, 1.5916]$, $\int_{x \in \mathcal{S}^c} \frac{\lambda_2 \mathcal{I}(x \notin \mathcal{B})}{1+(sP_s)^{-1}\|x\|_2^{\varepsilon}} dx \leq z \triangleq \int_{x \in \mathcal{S}^c} \frac{\lambda_2 dx}{1+(sP_s)^{-1}\|x\|_2^{\varepsilon}} = \lambda_2 G\left(\frac{1}{sP_s}, \varepsilon, d\right)$ and then evaluating the expectation w.r.t. $\mathcal{B}$.

Proof for (6.15) – (6.17) : Several upper bounds for $\mathcal{L}_{I_2}(s)$ can be obtained by lower bounding I_2 by considering the interference caused by a few active CRs that are closest to the origin (typical primary receiver) and are the dominant interferers. For this we consider the nearest and the next nearest potential CRs in the region $\mathbb{R}^2 \bigcap \mathcal{S}^c$, and denote their distances from the origin by R_1 and R_2, respectively. The p.d.f. of R_1 and R_2 denoted by $f_{R_k}(r)$, for $r \geq d$ are

$$f_{R_k}(r) = \frac{\left(\lambda_2 \pi \left(r^2 - d^2\right)\right)^{k-1} \lambda_2 2\pi r \mathrm{e}^{-\lambda_2 \pi \left(r^2 - d^2\right)}}{k!}, \tag{6.38}$$

for $k = 1,\ 2$. Now, we can obtain the upper bounds (6.15) and (6.16) by considering only the interference from the nearest two CRs in the region $\mathbb{R}^2 \bigcap \mathcal{S}^c$. The first bound is

$$\begin{aligned}
\mathcal{L}_{I_2}(s) &\overset{(a)}{\leq} \mathbb{E}\left[\mathrm{e}^{-\sum_{i=1}^{2} sP_s h_i \|x_i\|_2^{-\varepsilon} \mathcal{I}(x_i \notin \mathcal{B} \bigcup \mathcal{S})}\right] \\
&\overset{(b)}{\leq} \sqrt{\prod_{i=1}^{2} \mathbb{E}\left[\mathrm{e}^{-2sP_s h_i \|x_i\|_2^{-\varepsilon} \mathcal{I}(x_i \notin \mathcal{B} \bigcup \mathcal{S})}\right]} \\
&\overset{(c)}{=} \sqrt{\prod_{i=1}^{2} \mathbb{E}\left[\frac{1}{1 + 2sP_s \|x_i\|_2^{-\varepsilon} \mathcal{I}(x_i \notin \mathcal{B} \bigcup \mathcal{S})}\right]} \\
&\overset{(d)}{=} \sqrt{\prod_{i=1}^{2} 1 - \rho + \rho \mathbb{E}\left[\frac{1}{1 + 2sP_s \|x_i\|_2^{-\varepsilon}}\right]},
\end{aligned} \tag{6.39}$$

where x_i in (a) corresponds to the i^{th} nearest CR in $\mathbb{R}^2 \bigcap \mathcal{S}^c$, with $\|x_i\| = R_i$, whose p.d.f. is given in (6.38), (b) is obtained by applying Cauchy-Schwartz inequality on (a), (c) is obtained by evaluating the expectation with respect to the i.i.d. unit mean exponential random variables h_1 and h_2, respectively, (d) is obtained by evaluating the expectation w.r.t. the random set $\mathcal{B}$, with $\mathbb{P}(\{x_i \notin \mathcal{B}\}) = \rho$ from Lemma 9 and finally (6.15) is obtained by evaluating the expectations w.r.t. the random variables R_1 and R_2, and rewriting in terms of the function $H_k(\cdot)$ as defined in (6.19). The second upper bound based on the same idea is as follows.

$$\mathcal{L}_{I_2}(s) \overset{(a)}{\leq} \mathbb{E}\left[\frac{1}{2}\sum_{i=1}^{2} \mathrm{e}^{-2sP_s h_i \|x_i\|_2^{-\varepsilon} \mathcal{I}(x_i \notin \mathcal{B} \bigcup \mathcal{S})}\right], \tag{6.40}$$

where the expression in $(6.39) - (a)$ is now upper bounded by applying the Young's inequality to obtain (a), and the upper bound in (6.40) is obtained by taking the expectation inside the summation, repeating the steps $(6.39) - (c)$ and (d), and representing the result in terms of the $H_k(\cdot)$ function.

Next, the upper bound in (6.17) is obtained by considering the interference caused by only the nearest CR in $(\mathcal{B} \bigcup \mathcal{S})^c$.

$$\mathcal{L}_{I_2}(s) \leq \mathbb{E}\left[\mathrm{e}^{-sP_s h_1 \|x_1\|_2^{-\varepsilon} \mathcal{I}(x_1 \notin \mathcal{B} \bigcup \mathcal{S})}\right], \tag{6.41}$$

and the expression in (6.41) is obtained by evaluating the above expectation in the same way as shown in (6.39) and (6.40).

Finally, minimum of the upper bounds $(6.14) - (6.17)$ is also an upper bound which is tighter than all of these, and hence we get (6.18).

6.9.4 Proof for Theorem 18

Recall that the TV receiver connects to the strongest TV transmitter in the system and the interference at the TV receiver is due to the other TV transmitters and the active cognitive radios. Let us denote $I = \sum_{l=1}^{\infty} P_t h_l \left\|x_l\right\|_2^{-\varepsilon}$ and $M = \max_{l=1,2,\cdots} P_t h_l \left\|x_l\right\|_2^{-\varepsilon}$ denote the sum of the received powers from all the TV transmitters and the received power from the TV transmitter communicating with the TV receiver, respectively. The expression for the coverage probability is $\mathbb{P}\left(\{\mathrm{SIR}_{TVR} > \beta\}\right) = \mathbb{P}\left(\left\{\frac{M}{I-M+I_{CR}} > \beta\right\}\right) = \mathbb{P}\left(\{\gamma M > I + I_{CR}\}\right) \geq \mathbb{P}\left(\left\{\gamma M > I + I_1 + I_2^{'}\right\}\right)$, where I_{CR} is defined in (6.3), $\gamma = 1 + \frac{1}{\beta}$, $I + I_{CR} = I + I_1 + I_2 \leq I + I_1 + I_2^{'}$ where the equality is obtained due to Theorem 15 with I_1 and I_2 representing the total received power from all the points in Π_1 and Π_2, respectively and the inequality is apparent from the definition of $I_2^{'}$ in Theorem 16. Further, I, $I_1$and $I_2^{'}$ are all independent of each other. Consider the following Laplace transform term:

$$\begin{aligned}
\mathcal{L}_{\frac{I+I_1+I_2^{'}}{\gamma}, M \leq z}(s) &= \mathbb{E}\left[\mathrm{e}^{-\frac{s}{\gamma}\left(I+I_1+I_2^{'}\right)} \mathcal{I}\left(M \leq z\right)\right] \\
&\overset{(a)}{=} \mathcal{L}_{I_1}\left(\frac{s}{\gamma}\right) \mathcal{L}_{I_2^{'}}\left(\frac{s}{\gamma}\right) \mathbb{E}\left[\mathrm{e}^{-\frac{s}{\gamma} I} \mathcal{I}\left(M \leq z\right)\right] \\
&\overset{(b)}{=} \mathcal{L}_{I_1}\left(\frac{s}{\gamma}\right) \mathcal{L}_{I_2^{'}}\left(\frac{s}{\gamma}\right) \mathcal{L}_I^z\left(s\right) \qquad (6.42)
\end{aligned}$$

where $\mathcal{L}_I^z\left(s\right)$ is defined in (6.24), $(a)(M, I)$ are independent of $\left(I_1, I_2^{'}\right)$ and (b) is obtained by evaluating the expectation in (a) using [70, Theorem 1].

6.9.5 Proof for Theorem 19

The following steps derive the steps to obtain the upper bound for the coverage probability.

$$\begin{aligned}
\mathbb{P}\left(\{\mathrm{SIR}_{TVR} > \beta\}\right) &= \mathbb{P}\left(\left\{\frac{P_t h_k \left\|x_k\right\|_2^{-\varepsilon}}{I_{TV}+I_{CR}} > \beta\right\}\right) \\
&\overset{(a)}{=} \mathbb{E}\left[\exp\left(-\frac{\beta\left\|x_k\right\|_2^{\varepsilon}}{P_t}\left(I_{TV}+I_{CR}\right)\right)\right] \\
&\overset{(b)}{=} \mathbb{E}_{x_k}\left[\mathcal{L}_{I_{CR}}\left(\frac{\beta\left\|x_k\right\|_2^{\varepsilon}}{P_t}\right)\mathbb{E}\left[\prod_{l=1,}^{\infty}\exp\left(-\beta\left\|x_k\right\|_2^{\varepsilon}h_l\left\|x_l\right\|_2^{-\varepsilon}\right)\middle| x_k\right]\right] \\
&\overset{(c)}{=} \mathbb{E}_{x_k}\left[\mathcal{L}_{I_{CR}}\left(\frac{\beta\left\|x_k\right\|_2^{\varepsilon}}{P_t}\right)\exp\left(-\lambda_t\int_{x\in\mathbb{R}^2}\left(1-\mathbb{E}\left[\mathrm{e}^{-\beta\|x_k\|_2^{\varepsilon}h\|x\|_2^{-\varepsilon}}\middle| x_k\right]\right)dx\right)\right] \\
&\overset{(d)}{=} \mathbb{E}_{x_k}\left[\mathcal{L}_{I_{CR}}\left(\frac{\beta\left\|x_k\right\|_2^{\varepsilon}}{P_t}\right)\exp\left(-\frac{\lambda_t\pi\beta^{\frac{2}{\varepsilon}}\left\|x_k\right\|_2^2}{\mathrm{sinc}\left(\frac{2\pi}{\varepsilon}\right)}\right)\right] \\
&\overset{(e)}{=} \int_{r=0}^{\infty}\lambda_t 2\pi r\mathcal{L}_{I_{CR}}\left(\frac{\beta r^{\varepsilon}}{P_t}\right)\exp\left(-\frac{\lambda_t\pi\beta^{\frac{2}{\varepsilon}}r^2}{\mathrm{sinc}\left(\frac{2\pi}{\varepsilon}\right)}\right)dr
\end{aligned} \tag{6.43}$$

where (a) is obtained by noting that there exists a unique TV transmitter that can satisfy the SIR constraint ($\beta \geq 1$) according to [50, Lemma 1], (b) is obtained by recalling that I_{CR} is independent of (I_{TV}, x_k) and then by upper bounding the resulting Laplace transform term $\mathcal{L}_{I_{CR}}\left(\frac{\beta\|x_k\|_2^{\varepsilon}}{P_t}\right)$, (c) is obtained by applying the Campbell's theorem [6], (d) evaluates the integral in (c) and finally, (e) is obtained by rewriting the expectation in (d), and upon simplication, we get (6.25).

Further, since $\mathcal{L}_{I_{CR}}(s)$ is not known exactly, the upper bound, lower bound and approximation for the coverage probability are obtained by replacing $\mathcal{L}_{I_{CR}}\left(\frac{\beta\|x_k\|_2^{\varepsilon}}{P_t}\right)$ with $\mathcal{L}^{u}_{I_{CR}}\left(\frac{\beta\|x_k\|_2^{\varepsilon}}{P_t}\right)$, $\mathcal{L}^{l}_{I_{CR}}\left(\frac{\beta\|x_k\|_2^{\varepsilon}}{P_t}\right)$ and $\mathcal{L}_{\bar{I}_{CR}}\left(\frac{\beta\|x_k\|_2^{\varepsilon}}{P_t}\right)$, derived in Section 6.3, respectively.

Chapter 7

Stochastic Geometric Modeling and Interference Analysis for Massive MIMO Systems

7.1 Introduction

Massive multiple input multiple output (MIMO) systems are multiuser MIMO cellular systems where each BS is equipped with a large number of antennas compared to the number of MSs it serves. The study of such systems has gained immense attention due to their potential for achieving high data rates and throughput gains while ensuring a low transmission powers in both the forward link and reverse link [11, 94, 95].

In [11], a low complexity transmission-reception scheme is studied for the uplink and downlink performance of such a system. All BSs reuse the same set of orthogonal pilot sequences that they assign to the MSs for reverse link pilot signaling. Using these pilot sequences, the BSs estimate the reverse link channel to the corresponding MS, and extract the subsequent data symbols via maximum ratio combining. Further, due to channel reciprocity enforced by time division duplexing (TDD) operation, the BS also has an estimate of the forward channel, using which the BS does linear precoding prior to downlink data transmission. In the limit as the the number of BS antennas tend towards infinity, in both the uplink and downlink, it was observed that the effect of uncorrelated noise and fast fading is completely eliminated and the desired signal is only corrupted by the interferences caused by a phenomena termed 'pilot contamination', which is due to the reuse of the same set of pilot sequences by all the BSs. Consequently, the distributions of SIR and rate achievable for a given BS-MS pair in both uplink and downlink is studied for the ideal hexagonal cellular system using

Monte-Carlo simulations. Further studies in this topic have analyzed different precoder/detector designs with the goal of minimizing the pilot contamination to as low as possible and to analyze the resulting SIR and rate expressions obtained in the uplink and the downlink [96–98].

In this chapter, we study the massive MIMO system of [11] under stochastic geometric settings and demonstrate that the uplink and downlink performance can be analytically characterized in terms of the key system parameters. Towards this goal, the BS arrangement is modeled according to a homogeneous Poisson point process on the plane, the MSs served by a given BS are uniformly distributed within a circle of a certain fixed radius centered at the BS location and the number of MSs served by each BS is an i.i.d. Poisson random variable with a given mean. This system is depicted in Fig. 7.1.

The stochastic geometric modeling and analysis of wireless networks has gained increased popularity since they are amenable to rigorous analytical studies [27, 30, 43, 50, 58, 70, 83]. For the cellular network, a strong motivation for viewing the BS arrangement as a homogeneous Poisson point process can be drawn from the study of the cellular systems in [2, 12, 13] which suggests that significant insights can be gained by bounding the downlink cellular performance between the ideal hexagonal grid model and the homogeneous Poisson point process based model. More interestingly, in [2, Fig. 2.], it is shown with the help of Monte-Carlo simulations that in the limit of strong log-normal shadow fading (standard deviation of the fading coefficient $\sigma \to \infty$), the downlink SIR distribution of an ideal hexagonal cellular system approaches that of a cellular system with BSs deployed according to a homogeneous Poisson point process.

Recently, the above convergence has been analytically proved in [10, Theorem 3]. It is shown that the downlink performance of a cellular network with any deterministic arrangement of BSs (not just the ideal hexagonal grid model) converges to that of a Poisson point process based model as $\sigma \to \infty$, and moreover even for realistic values of σ (i.e. 8 dB) that are observed in cluttered environments, the latter model is a good approximation for the deterministic model. In the massive MIMO system, the uplink-downlink performance is completely determined by the shadow fading coefficients and the location of the BSs and the MSs in the cellular system, thus making a strong case for a rigorous study of these performance metrics using stochastic geometric models.

The contributions of this chapter are briefly described here. Note that the transmission-reception

schemes studied in [11] are restricted to the case where all the pilot sequences were orthogonal to each other. In practice, orthogonality between pilot sequences is hard to ensure in the uplink (downlink) as the MS (BS) transmissions are never perfectly synchronized. In Section 7.3, we have extended it to the more practical case when the pilot sequences have a small correlation with each other, and derived the expressions for the SIR and the achievable rate in both the uplink and downlink for an arbitrary BS-MS pair. Next, in Section 7.4, closed-form expressions for the distribution of SIR and rate are derived based on the stochastic geometric model. Further, when all the pilot sequences are orthogonal to each other, it is shown that the distribution of SIR and rate in the uplink and downlink are identical. This analytical result is consistent with [94, Fig. 4-7] where the uplink and downlink SIR and rate have nearly identical behavior (see Section 7.4.1). For the non-orthogonal pilot sequence case (see Section 7.4.2), closed form expressions for the distribution of the downlink SIR and rate are derived and simple approximations are derived for the corresponding uplink performance. It is shown that the downlink SIR is strictly upper-bounded by the inverse of total pilots correlation.

Next, we introduce the system model.

7.2 System Model

The cellular system is composed of BSs distributed according to a homogeneous Poisson point process on the plane with BS density λ_b. The BSs employ Δ-frequency reuse (Δ =1, 3, 4, 7 etc.) where each BS is randomly assigned one of the $\{1,\ 2, \cdots,\ \Delta\}$ frequency bands with equal probability and the BSs in different bands do not interfere with each other [59]. Further, the MSs served by a BS are assumed to be uniformly distributed in a circle of radius R centered at the BS and independent of the other MS or BS arrangements. The number of MSs served by a given BS is a Poisson random variable with mean $\lambda_u \pi R^2$, where λ_u is the average number of MSs per cell area. Each MS has a single antenna and each BS is equipped with M antennas ($M \to \infty$). Fig. 7.1 illustrates the scenario.

All the BSs in the system share the same set of P pilot sequences and can serve at most P MSs simultaneously. Each pilot sequence is a K length unit-norm vector denoted as $\mathbf{a}_i \in \mathbb{C}^{K\times 1}$, $i = 1,\ 2, \cdots, P$, and the correlation between two pilot sequences $\mathbf{a_i},\ \mathbf{a_j}$ is $\mathbf{a_i^\dagger a_j} = \alpha_{ij}$, such that $0 \leq |\alpha_{ij}| \leq 1$ and $\alpha_{ii} = 1$,

$\forall\ i = 1, \cdots,\ P$. The pilots are said to be orthogonal if the correlation is zero for $i \neq j$ and non-orthogonal otherwise. The BSs and the MSs communicate with each other via time division duplexing (TDD) such that the in-band uplink and downlink transmissions are sufficiently separated in time and do not cause interference to one another. Further, the TDD operation induces channel reciprocity causing the forward and reverse-link channels for a given BS-MS pair to be identical.

7.3 Transmission-Reception Schemes

This section generalizes the results in [11] to the case when the pilot sequences are non-orthogonal and when the number of MSs in each cell is an independent and identically distributed (i.i.d.) random variable as mentioned in Section 7.2.

7.3.1 Pilot signaling and channel estimation

The communication begins with the training phase when all the MSs in the cell transmit their respective pilot sequences to the serving BS. The BSs utilize the reverse-link pilot transmissions to estimate the reverse-link channel to each of its MSs. We denote the kth BS by BS_k and its nth MS by MS_{kn}. The received signal at BS_k corresponding to one pilot sequence transmission period (consisting of K symbols) may be represented by $\mathbf{Y}_k \in \mathbb{C}^{M\times K}$:

$$\mathbf{Y}_k = \sqrt{\rho_{\text{P}}} \sum_{l=1}^{\infty} \sum_{n=1}^{P} b_{kl} \mathbf{h}_{kln} \mathbf{a}_n^{\dagger} \mathcal{I}(n,l) + \mathbf{W}_k \tag{7.1}$$

where M is the number of BS antennas, K is the length of a pilot sequence, $b_{kl} = 1$ if BS_l operates in the same frequency band as BS_k and $b_{kl} = 0$ otherwise, $\mathbf{h}_{kln} \in \mathbb{C}^{M\times 1}$ is the channel corresponding to the wireless link from MS_{ln} to BS_k, ρ_{P} is the pilot signal-to-noise ratio (SNR), $\mathbf{W}_k$ is the i.i.d. zero-mean noise at BS_k, and $\mathcal{I}(n,l)$ is the indicator function

$$\mathcal{I}(n,l) = \begin{cases} 1, & n^{\text{th}} \text{ pilot is used in } l^{\text{th}} \text{ cell} \\ 0, & \text{otherwise} \end{cases}.$$

Further, $\mathbf{h}_{kln} = \beta_{kln}^{\frac{1}{2}} R_{kln}^{-\frac{\varepsilon}{2}} \mathbf{g}_{kln}$, $\mathbf{g}_{kln} \in \mathbb{C}^{M\times 1}$ represents the fast fading coefficients between the MS_{ln} and the antennas of BS_k with i.i.d. zero mean and unit variance entries, β_{kln} is the shadow fading coefficient,

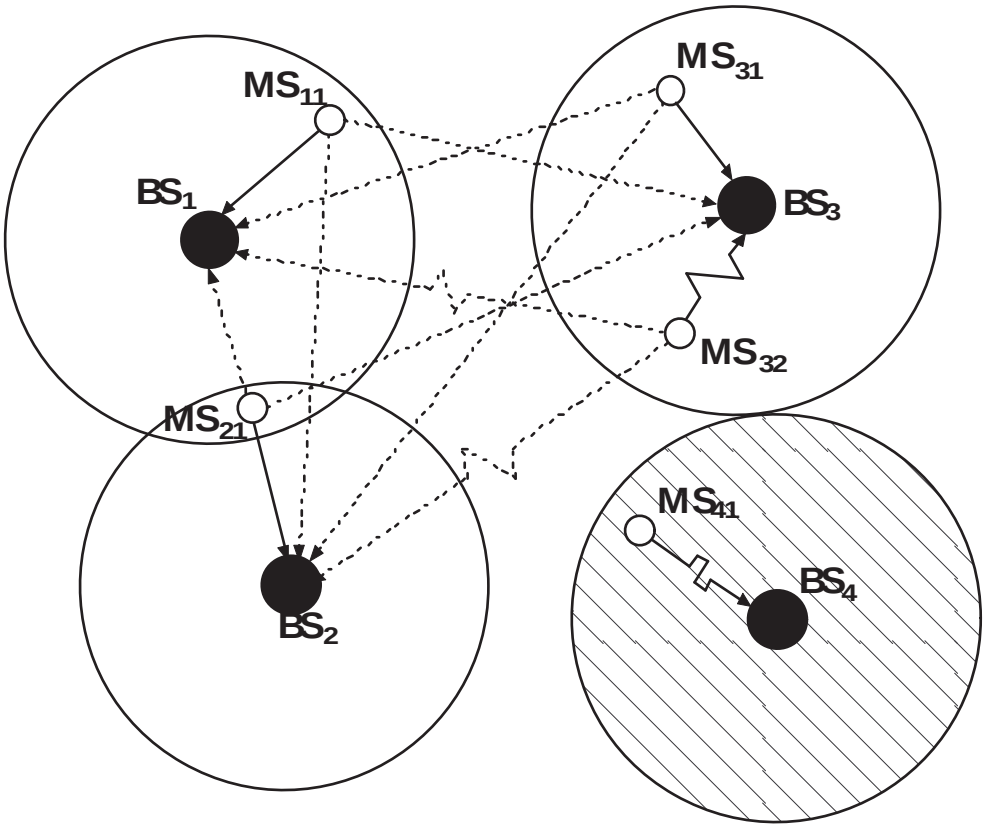

Figure 7.1: User distribution and pilots assignments. BSs in the circles with different background patterns operate in different frequency bands. The different pilot sequences assigned to MSs are indicated by different line patterns. Solid line represents desired signal while dotted line represents interference to others.

generally modeled as a log-normal random variable with 0 mean and variance σ^2 dB, R_{kln} is the distance between MS_{ln} and BS_k and ϵ $(\epsilon > 2)$ is the path-loss exponent of the power-law path-loss model.

From the received signal in (7.1), BS_k estimates the channel to the MS transmitting the m^{th} pilot sequence as

$$\hat{\mathbf{h}}_{kkm} = \frac{\mathbf{Y}_k \mathbf{a}_m}{\sqrt{\rho_{\text{P}}}} = h_{kkm} + \sum_{n=1,\ n\neq m}^{P} \alpha_{nm} \mathbf{h}_{kkn} \mathcal{I}(n,k)$$
$$+ \sum_{\substack{l=1 \\ l\neq k}}^{\infty} \sum_{n=1}^{P} \alpha_{nm} b_{kl} \mathbf{h}_{kln} \mathcal{I}(n,l) + \frac{\mathbf{W}_k \mathbf{a}_m}{\sqrt{\rho_{\text{P}}}}, \tag{7.2}$$

where $m = 1,\ 2, \cdots,\ P$, the first term is the desired channel, the second term is the contamination due to non-orthogonal pilots used by other MSs served by BS_k, the third term is the contamination due to the pilot transmissions of the MSs belonging to the other cells and the last term corresponds to the background noise. Next, we focus on the uplink data transmission and decoding scheme used by each BS to recover the data transmitted by each of its MSs.

7.3.2 Uplink Data Transmission and Maximum Ratio Combining

Following the pilot signaling stage is the reverse link data transmission stage, when all the MSs transmit data symbols to their corresponding BS, and the composite signal as received by BS_k is given by

$$\mathbf{y}_k = \sqrt{\rho_{\text{U}}} \sum_{l=1}^{\infty} \sum_{n=1}^{P} b_{kl} \mathbf{h}_{kln} d_{ln} \mathcal{I}(n,l) + \mathbf{w}_k, \tag{7.3}$$

where ρ_{U} is the uplink SNR, d_{ln} is the data symbol transmitted by MS_{ln}, and $\mathbf{w}_k$ is the i.i.d. zero mean and unit variance background noise at BS_k's antennas and all other symbols are the same as in (7.1). From the above received signal, BS_k recovers the symbols corresponding to each of its MSs using maximum-ratio combining, by left-multiplying the received signal by the conjugate-transpose of the channel estimate of the corresponding MS. Further, in the limit as $M \to \infty$, the recovered data symbol $\hat{d}_{km}$ corresponding to MS_{km}

takes a relatively simple form as shown below.

$$\begin{aligned}
\hat{d}_{km} &= \lim_{M\to\infty} \frac{\hat{\mathbf{h}}_{kkm}^{\dagger}\mathbf{y}_k}{M\sqrt{\rho_{\mathrm{U}}}} \\
&\overset{(a)}{=} \lim_{M\to\infty} \frac{1}{M}\left(\sum_{l=1}^{\infty}\sum_{n=1}^{P}\alpha_{nm}^{*}b_{kl}\mathbf{h}_{kln}^{\dagger}\mathcal{I}\left(n,l\right)+\frac{\mathbf{a}_m^{\dagger}\mathbf{W}_k^{\dagger}}{\sqrt{\rho_{\mathrm{P}}}}\right) \\
&\cdot\left(\sum_{s=1}^{\infty}\sum_{t=1}^{P}\mathbf{h}_{kst}b_{ks}d_{st}\mathcal{I}\left(t,s\right)+\frac{\mathbf{w}_k}{\sqrt{\rho_{\mathrm{U}}}}\right) \\
&\overset{(b)}{=} \frac{\beta_{kkm}d_{km}}{R_{kkm}^{\epsilon}}+\sum_{n=1,\ n\neq m}^{P}\frac{\alpha_{nm}^{*}\beta_{kkn}d_{kn}}{R_{kkn}^{\epsilon}}\mathcal{I}\left(n,k\right) \\
&+\sum_{l=1,\ l\neq k}^{\infty}\sum_{n=1}^{P}\frac{\alpha_{nm}^{*}b_{kl}\beta_{kln}d_{ln}}{R_{kln}^{\epsilon}}\mathcal{I}\left(n,l\right), \qquad (7.4)
\end{aligned}$$

where $m=1,\ 2,\cdots,\ P$, (a) is obtained by substituting for $\hat{\mathbf{h}}_{kkm}$ and $\mathbf{y}_k$ from (7.2) and (7.3), respectively, and (b) is obtained by noting that $\lim_{M\to\infty}\frac{\mathbf{h}_{kln}^{\dagger}\mathbf{h}_{kst}}{M}=\sqrt{\frac{\beta_{kln}\beta_{kst}}{R_{kln}^{\frac{\epsilon}{2}}R_{kst}^{\frac{\epsilon}{2}}}}\lim_{M\to\infty}\frac{\mathbf{g}_{kln}^{\dagger}\mathbf{g}_{kst}}{M}=b_{kl}\beta_{kln}R_{kln}^{-\epsilon}\delta\left(l=s,n=t\right)$, $\lim_{M\to\infty}\frac{\mathbf{h}_{kln}^{\dagger}\mathbf{w}_k}{M}=0$, $\lim_{M\to\infty}\frac{\mathbf{W}_k^{\dagger}\mathbf{h}_{kst}}{M}=0$, and $\lim_{M\to\infty}\frac{\mathbf{W}_k^{\dagger}\mathbf{w}_k}{M}=0$ by applying the law of large numbers, since $\mathbf{g}_{kln}$, $\mathbf{w}_k$, $\mathbf{W}_k$ all contain i.i.d. zero mean unit variance entries. Further, the first term in (b) is the desired data symbol, the second is the intra-cell interference term and the third is the inter-cell interference term. Next, we study the downlink transmission scheme in detail.

7.3.3 Precoding and Downlink Data Transmission

In the downlink, the BS precodes the data symbol intended for each MS with the channel estimate of the corresponding wireless link, and transmits the sum of the precoded signals of all its MSs through the M antennas. The received signal at MS_{km} is

$$y_{km} \quad = \quad \sqrt{\rho_{\mathrm{D}}}\sum_{l=1}^{\infty}b_{kl}\mathbf{h}_{lkm}^{\dagger}x_l+w_{km},$$

where ρ_{D} is the downlink SNR, $x_l=\sum_{n=1}^{P}\hat{\mathbf{h}}_{lln}d_{ln}\mathcal{I}\left(n,l\right)$ is the signal transmitted by BS_l, d_{ln} is the data symbol intended to MS_{ln} and is precoded by the corresponding channel estimate $\hat{\mathbf{h}}_{lln}$. Due to channel reciprocity induced by the TDD operation, the channel between BS_l and MS_{km} is $\mathbf{h}_{lkm}^{\dagger}$, and lastly, w_{km} is a zero mean, unit variance random variable representing the background noise. Each MS performs a relatively simple processing to recover the data symbol transmitted by the serving BS. The recovered data symbol in

the downlink is

$$\begin{aligned}\hat{d}_{km} &= \lim_{M\to\infty} \frac{y_{km}}{M\sqrt{\rho_{\mathrm{D}}}} \\ &= \lim_{M\to\infty} \frac{1}{M} \sum_{l=1}^{\infty} \mathbf{h}_{lkm}^{\dagger} \sum_{n=1}^{P} \hat{\mathbf{h}}_{lln} d_{ln} \mathcal{I}(n,l) + \frac{w_{km}}{M\sqrt{\rho_{\mathrm{D}}}} \\ &= \sum_{l=1}^{\infty} \left(\sum_{n=1}^{P} \alpha_{nm}^{*} d_{ln} \mathcal{I}(n,l) \right) b_{kl} \beta_{lkm} R_{lkm}^{-\epsilon}, \end{aligned} \tag{7.5}$$

where $m = 1,\ 2, \cdots,\ M$, $\lim_{M\to\infty} \frac{\mathbf{h}_{lkm}^{\dagger} \hat{\mathbf{h}}_{lln}}{M} = \alpha_{mn} \beta_{lkm} R_{lkm}^{-\epsilon}$, $\alpha_{mn} = \alpha_{nm}^{*}$, and $\lim_{M\to\infty} \frac{w_{km}}{M\sqrt{\rho_{\mathrm{D}}}} = 0$. Notice that the resultant system is again interference-limited and the following lemma provides the expressions for the uplink and downlink SIR for a given BS-MS pair.

Lemma 10. *The uplink and downlink SIRs are*

$$SIR_{km}^{(UL)} = \frac{\beta_{kkm}^2 R_{kkm}^{-2\epsilon}}{I_{km}^{(UL)}} \text{ and } SIR_{km}^{(DL)} = \frac{\beta_{kkm}^2 R_{kkm}^{-2\epsilon}}{I_{km}^{(DL)}}, \tag{7.6}$$

where $I_{km}^{(UL)} = \sum_{l=1}^{\infty} \sum_{\substack{n=1 \\ (l,n)\neq(k,m)}}^{P} b_{kl} |\alpha_{nm}|^2 \beta_{kln}^2 R_{kln}^{-2\epsilon} \mathcal{I}(n,l)$ *and* $I_{km}^{(DL)} = \sum_{l=1}^{\infty} \Big(\sum_{\substack{n=1 \\ (l,n)\neq(k,m)}}^{P} |\alpha_{nm}|^2 \mathcal{I}(n,l) \Big) b_{kl} \beta_{lkm}^2 R_{lkm}^{-2\epsilon}$ *are the corresponding interference powers.*

Notice that, when each BS serves a fixed number of user equal to P using a set of P orthogonal pilot sequences, the resultant expressions for $\mathrm{SIR}_{km}^{(UL)}$ and $\mathrm{SIR}_{km}^{(DL)}$ are identical to those obtained in [11].

In the following section, we systematically evaluate the system performance in the uplink and downlink.

7.4 Interference characteristics and SIR

In this section, we derive closed-form expressions for the Laplace transform of interference and the SIR distribution for both uplink and downlink. We first consider the case when all the P pilot sequences are orthogonal to each other. Since each pilot sequence is of length K, at most K orthogonal pilot sequences can be designed, and hence $P \leq K$.

7.4.1 Case of orthogonal pilot sequences

In this case, the pilot sequences $a_1, \cdots,\ a_P$ are such that the correlation $\alpha_{ij} = 1$, if $i = j$ and 0 otherwise. From Lemma 10, it can be seen that the intra-cell interference is completely eliminated and the

inter-cell interference is only due to the transmissions corresponding to the same pilot sequence as the desired signal.

Theorem 23. *With orthogonal pilot sequences, the Laplace transform of the interference in the uplink and downlink are*

$$\mathcal{L}_{I_{km}^{(UL)}} = \mathcal{L}_{I_{km}^{(DL)}}(s) = \exp\left(-\frac{\lambda_b \pi \eta \mathbb{E}\left[\beta^{\frac{2}{\epsilon}}\right] s^{\frac{1}{\epsilon}}}{\Gamma\left(1+\frac{1}{\varepsilon}\right)\Delta \mathrm{sinc}\left(\frac{\pi}{\epsilon}\right)}\right), \tag{7.7}$$

where $\Gamma(\cdot)$ *is the Gamma function,* $I_{km}^{(UL)}$ *and* $I_{km}^{(DL)}$ *are obtained from Lemma 10,* $\eta = \sum_{n=1}^{P-1} \frac{n}{P} \frac{\left(\lambda_u \pi R^2\right)^n}{n!} e^{-\lambda_u \pi R^2} + \sum_{n=P}^{\infty} \frac{\left(\lambda_u \pi R^2\right)^n}{n!} e^{-\lambda_u \pi R^2}$ *is the probability that two BSs in the system use the same pilot sequence,* β *is the random variable with the same distribution as the set of i.i.d. random variables* $\{\beta_{klm}\}_{l=1}^{\infty}$, $\mathbb{E}\left[\beta^{\frac{2}{\epsilon}}\right] < \infty$, Δ *is the frequency reuse factor and* $\mathrm{sinc}(x) = \frac{\sin(x)}{x}$. *Also,*

$$SIR_{km}^{(UL)} \quad =_{st} \quad SIR_{km}^{(DL)}, \tag{7.8}$$

where $=_{\mathrm{st}}$ *is the equivalence in distribution. Further, in the special case when* $\{\beta_{klm}\}_{l=1}^{\infty}$ *is a set of i.i.d. unit mean exponential random variables, the complementary cumulative density function (c.c.d.f.) of SIR is*

$$\mathbb{P}\left(\left\{\mathrm{SIR}_{km}^{(UL)} > \gamma\right\}\right) = \mathbb{P}\left(\left\{\mathrm{SIR}_{km}^{(DL)} > \gamma\right\}\right) = \frac{1-\mathrm{e}^{-T}}{T}, \tag{7.9}$$

where $\gamma \geq 0$ *and* $T = \frac{\eta \lambda_b \pi R^2 \gamma^{\frac{1}{\epsilon}}}{\Delta \mathrm{sinc}\left(\frac{\pi}{\epsilon}\right)}$.

Proof. See Appendix 7.7.1. □

Further, when the number of users in each cell is equal to K at all times, all $P = K$ orthogonal pilot sequences are used by each BS, η (defined in Theorem 23) is 1 and hence the c.c.d.f. of SIR is obtained using (7.9) with $\eta = 1$. Note that the above is exactly the scenario considered in [11] where the uplink and downlink SIRs could only be analyzed via Monte-Carlo simulations. Here, with the help of stochastic geometry, we are able to obtain closed form expressions for the relevant performance metrics in terms of the critical system parameters. In Section 7.5, we further demonstrate its significance with numerical examples.

7.4.2 Case of non-orthogonal pilot sequences

Now, we consider the case when the pilot sequences are not orthogonal to each other. Such a scenario arises under two conditions. Firstly, when the pilot signaling by various transmitters are not perfectly synchronized. Secondly, in an overloaded system where the BS serves a large number of users. Particularly when $P > K$, all P pilot sequences of length K cannot be orthogonal to each other. In this section, we consider an extreme case when all the P pilot sequences are used by each BS. The uplink and downlink interferences ar

$$I_{km}^{(UL)} = \sum_{\substack{l=1 \\ (l,n)\neq(k,m)}}^{\infty} \sum_{n=1}^{P} b_{kl} \left|\alpha_{nm}\right|^2 \beta_{kln}^2 R_{kln}^{-2\epsilon}, \tag{7.10}$$

$$I_{km}^{(DL)} = \frac{\bar{\alpha}_m \beta_{kkm}^2}{R_{kkm}^{2\epsilon}} + (\bar{\alpha}_m + 1) \sum_{l=1,\ l\neq k}^{\infty} \frac{b_{kl}\beta_{lkm}^2}{R_{lkm}^{2\epsilon}}, \tag{7.11}$$

where $\bar{\alpha}_m \triangleq \sum_{\substack{n=1 \\ n\neq m}}^{P} |\alpha_{nm}|^2$. By substituting in (7.6), we obtain the corresponding SIR expressions. The following theorem derives the Laplace transform of interference and the distribution of SIR in the downlink.

Theorem 24. *When all BSs in the system serve P MSs using the P non-orthogonal pilot sequences, the Laplace transform of the $I_{km}^{(DL)}$ is*

$$\mathcal{L}_{I_{km}^{(DL)}}(s) = \mathbb{E}_\beta \left[\frac{\left(s\bar{\alpha}_m\beta^2\right)^{\frac{1}{\epsilon}} \Gamma\left(-\frac{1}{\epsilon}, \frac{s\bar{\alpha}_m\beta^2}{R^{2\epsilon}}\right)}{\epsilon R^2} \right] \times$$
$$\exp\left(-\frac{\lambda_b \pi \mathbb{E}\left[\beta^{\frac{2}{\epsilon}}\right] s^{\frac{1}{\epsilon}} (\bar{\alpha}_m + 1)^{\frac{1}{\epsilon}}}{\Gamma\left(1+\frac{1}{\varepsilon}\right) \Delta \mathrm{sinc}\left(\frac{\pi}{\epsilon}\right)} \right), \tag{7.12}$$

where $\Gamma(\cdot,\cdot)$ is the incomplete Gamma function, $\Gamma(\cdot)$ is the Gamma function, β is a random variable with the same distribution as the i.i.d. random variables β_{klm}'s in (7.11), Δ and $\mathrm{sinc}(\cdot)$ are as in Theorem 23.

When $\{\beta_{klm}\}_{l=1}^{\infty}$ is a set of i.i.d. unit mean exponential random variables, the c.c.d.f. of downlink SIR is

$$\mathbb{P}\left(\left\{\mathrm{SIR}_{km}^{(DL)} > \gamma\right\}\right) = \frac{\Delta \mathrm{sinc}\left(\frac{\pi}{\epsilon}\right)}{\lambda_b \pi R^2 \bar{\gamma}^{\frac{1}{\epsilon}}} \left[1 - \mathrm{e}^{-\frac{\lambda_b \pi R^2 \bar{\gamma}^{\frac{1}{\epsilon}}}{\Delta \mathrm{sinc}\left(\frac{\pi}{\epsilon}\right)}}\right], \tag{7.13}$$

$\forall\ 0 \leq \gamma \leq \bar{\alpha}_m^{-1}$ *and* $\bar{\gamma} = \frac{\gamma(1+\bar{\alpha}_m)}{1-\bar{\alpha}_m\gamma}$.

Proof. See Appendix 7.7.2. □

An important implication of Theorem 24 is that the downlink SIR in the non-orthogonal case cannot exceed $\frac{1}{\bar{\alpha}_m}$ as can be seen from (7.19), and hence shows how the design of the set of pilot sequences determines the system performance.

Next, we characterize the uplink performance with non-orthogonal pilot sequences. Accurate closed-form characterizations of the performance metrics in the uplink is not possible, and hence, we consider the following approximations to (7.10) that make the analysis tractable.

(1) Replace the instantaneous correlation between the pilot sequences with the average of the correlations with all pilot sequences, i.e. replace $|\alpha_{nm}|^2$ of the intra-cell interference terms with $\frac{\bar{\alpha}_m}{P-1}$ and $|\alpha_{nm}|^2$ of the inter-cell interference terms with $\frac{\bar{\alpha}_m+1}{P}$.

(2) Upper bound the distance between MS_{ln} and BS_k, R_{kln} with $R_{kl}+R$, for $(l,n) \neq (k,m)$, where R_{kl} is the radial distance between BS_k and BS_l. By doing so, it can be shown that the point process of the resultant inter-cell interferer is a homogeneous Poisson point process in the entire plane except the circle of radius R about the origin. Further, the resultant interference after this operation is a lower bound for the actual uplink interference.

(3) In order to achieve a mathematically tractable approximation, we extend the interferer point process obtained by the previous operation to the entire plane.

With the above three modifications, a reasonable estimate for the uplink interference is obtained as

$$\hat{I}_{km}^{(UL)} = \frac{\bar{\alpha}_m R^{-2\epsilon}}{P-1} \sum_{n=1,\ n\neq m}^{P} \beta_{kkn}^2 + \frac{(\bar{\alpha}_m+1)}{P} \sum_{l=1,\ l\neq k}^{\infty} b_{kl} \left(\sum_{n=1}^{P} \beta_{kln}^2 \right) R_{kl}^{-2\epsilon}, \tag{7.14}$$

where R_{kkn}'s are i.i.d. random variables with a probability density function (p.d.f.) $f_{R_{kkn}}(r) = \frac{2r}{R^2}$, $0 \leq r \leq R$, R_{kl}'s are from the homogeneous Poisson point process on the plane with density λ_b and β_{kln}'s are i.i.d. random shadow fading factors, and the corresponding uplink SIR is

$$\hat{\mathrm{SIR}}_{km}^{(UL)} = \frac{\beta_{kkm}^2 R_{kkm}^{-\varepsilon}}{\hat{I}_{km}^{(UL)}}. \tag{7.15}$$

Using (7.14) and (7.15), next we derive analytical expressions for the uplink performance metrics.

Theorem 25. *The Laplace transform of* $\hat{I}_{km}^{(UL)}$ *is*

$$\mathcal{L}_{\hat{I}_{km}^{(UL)}}(s) = \left(\mathbb{E}_{\beta}\left[\mathrm{e}^{-\frac{s\bar{\alpha}_m R^{-2\epsilon}\beta^2}{P-1}}\right]\right)^{P-1} \times \exp\left(-\frac{\lambda_b \mathbb{E}\left[\left(\sum_{n=1}^{P}\beta_n^2\right)^{\frac{1}{\epsilon}}\right] s^{\frac{1}{\epsilon}}\left(\bar{\alpha}_m+1\right)^{\frac{1}{\epsilon}}}{P^{\frac{1}{\varepsilon}}\Gamma\left(1+\frac{1}{\varepsilon}\right)\Delta\mathrm{sinc}\left(\frac{\pi}{\epsilon}\right)}\right), \tag{7.16}$$

where β, $\{\beta_n\}_{n=1}^{P}$ *are i.i.d. random variables with the same distribution as* β_{kln}*'s in (7.14),* Δ *and* $\mathrm{sinc}(\cdot)$ *are as in Theorem 23. When* $\{\beta_{klm}\}_{l=1}^{\infty}$ *is a set of i.i.d. unit mean exponential random variables, the c.c.d.f. of uplink SIR using the approximation (7.14) is*

$$\mathbb{P}\left(\left\{\hat{\mathrm{SIR}}_{km}^{(UL)} > \gamma\right\}\right) = \mathbb{E}_{R_{kkm}}\left[\mathcal{L}_{\hat{I}_{km}^{(UL)}}\left(\gamma R_{kkm}^{2\epsilon}\right)\right]. \tag{7.17}$$

Proof. Equation (7.16) can be obtained by following the same steps as for the derivation of (7.12), and (7.17) is obtained by substituting for $\hat{\mathrm{SIR}}_{km}^{(UL)}$ from (7.15) and then evaluating the probability w.r.t. β_{kkm}^2, given all other random variables. □

Next, the per-user achievable rate (in bits/secs/user) in the uplink and downlink are

$$R_{km}^{(UL)} = \frac{B\rho}{\Delta}\log_2\left(1+\mathrm{SIR}_{km}^{(UL)}\right) \text{ and}$$
$$R_{km}^{(DL)} = \frac{B\rho}{\Delta}\log_2\left(1+\mathrm{SIR}_{km}^{(DL)}\right),$$

respectively, where B is the entire allocated bandwidth, ρ is the scaling factor for the rate-loss from training, guard interval, etc. and Δ is the frequency reuse factor. The above are the uplink and downlink Shannon rates obtained by treating interference as noise.

The c.c.d.f. of $R_{km}^{(UL)}$ and $R_{km}^{(DL)}$ for both the orthogonal and non-orthogonal pilots cases can be obtained from Theorems 23-25 by replacing γ in equations (7.9), (7.13) and (7.17) with $\exp\left(\frac{\gamma\Delta}{B\rho}\right)-1$.

Next, we provide some numerical examples that further demonstrate the utility of the analytical study carried out in this section.

7.5 Numerical Results

In order to facilitate a fair comparison between the analytical results obtained in the previous section with the empirical results in [11, Section VI], we restrict our attention to the orthogonal pilots case (Section

7.4.1) and assume the same system parameters as in [11, Section VI]. From Theorem 23, the uplink and downlink performances are identical and the hence the conclusions drawn in this section hold true for both.

7.5.1 Simulation setting

The cellular area of interest is a circle with a radius 50 kilometers with the radius of each cell $R = 1600$ meters and BSs distributed according to a homogeneous Poisson point process with density $\lambda_b = \frac{1}{\pi R^2}$. The total system bandwidth $B = 20$ MHz, and the rate scaling factor $\rho = (3/7) \times (66.7/71.4) \approx 0.4$. Three different values for the frequency reuse factors are considered, $\Delta = 1,\ 3$ and 7, and all the BSs reuse $K = 42$ orthogonal pilot sequences among themselves. For the shadow-fading, two cases are considered: (a) β_{klm}'s follow i.i.d. log-normal distribution with 8.0 dB standard deviation as in [11], and (b) β_{klm}^2's follow i.i.d. unit mean exponential distribution, and finally the path-loss exponent $\epsilon = 3.8$.

7.5.2 Fully loaded case

Fig. 7.2 and Fig. 7.3 show the cumulative distributions for the SIR (7.8) and the average achievable rate per user, respectively, when every cell is fully loaded and serving its maximum capacity of P users. Note that the analytical results obtained from (7.9) with $\eta = 1$ fits the simulation result perfectly. Further, the performance characteristics of the the exponential and the log-normal fading cases are similar. The SIR performance strictly improves as Δ increases because the average interferer distance increases with Δ. The net achievable rate per terminal doesn't necessarily increase as shown in Fig. 7.3 since larger Δ means smaller effective bandwidth per cell. Hence, Δ should be accordingly chosen based on the minimum or average rate and SIR requirements.

Further, comparing Figs. 7.3 - 7.5 with [11, Figs. 2-5], we see that the performances in the hexagonal grid model and the stochastic geometric model are very close to each other. Hence, stochastic geometry based model can provides accurate analytical performance characterizations for these cellular systems.

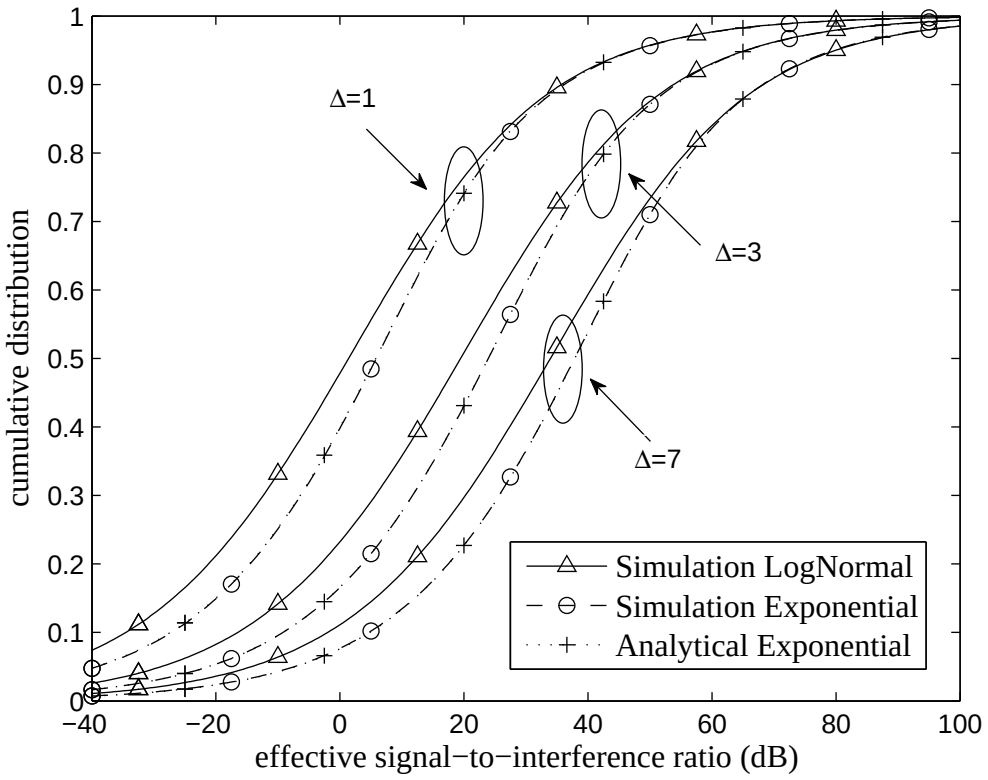

Figure 7.2: Cumulative distribution for the effective signal-to-interference ratio in fully loaded MS case with orthogonal pilots.

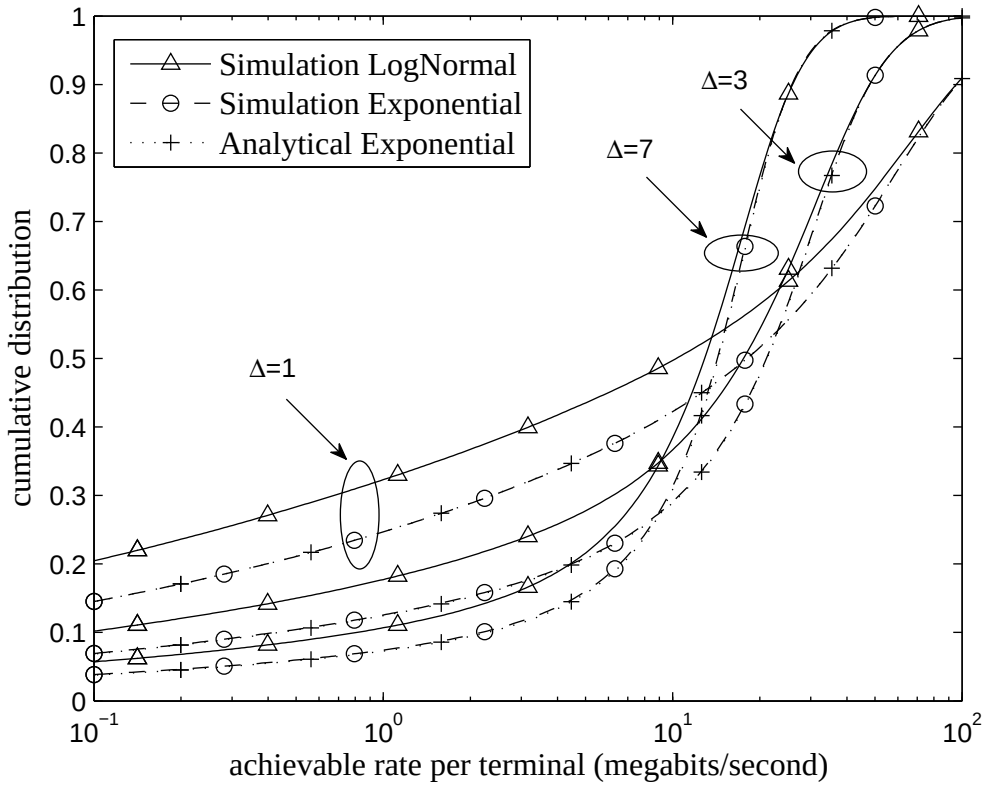

Figure 7.3: Cumulative distribution for the net achievable rate per terminal in fully loaded MS case with orthogonal pilots.

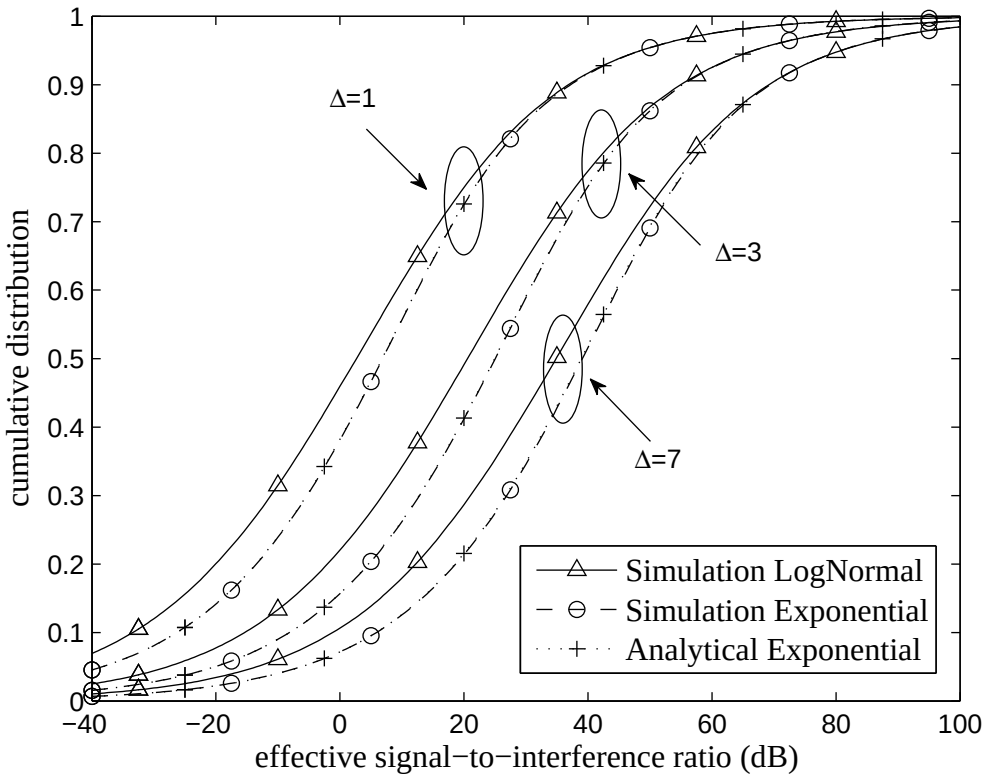

Figure 7.4: Cumulative distribution for the effective signal-to-interference ratio in random MS case with orthogonal pilots.

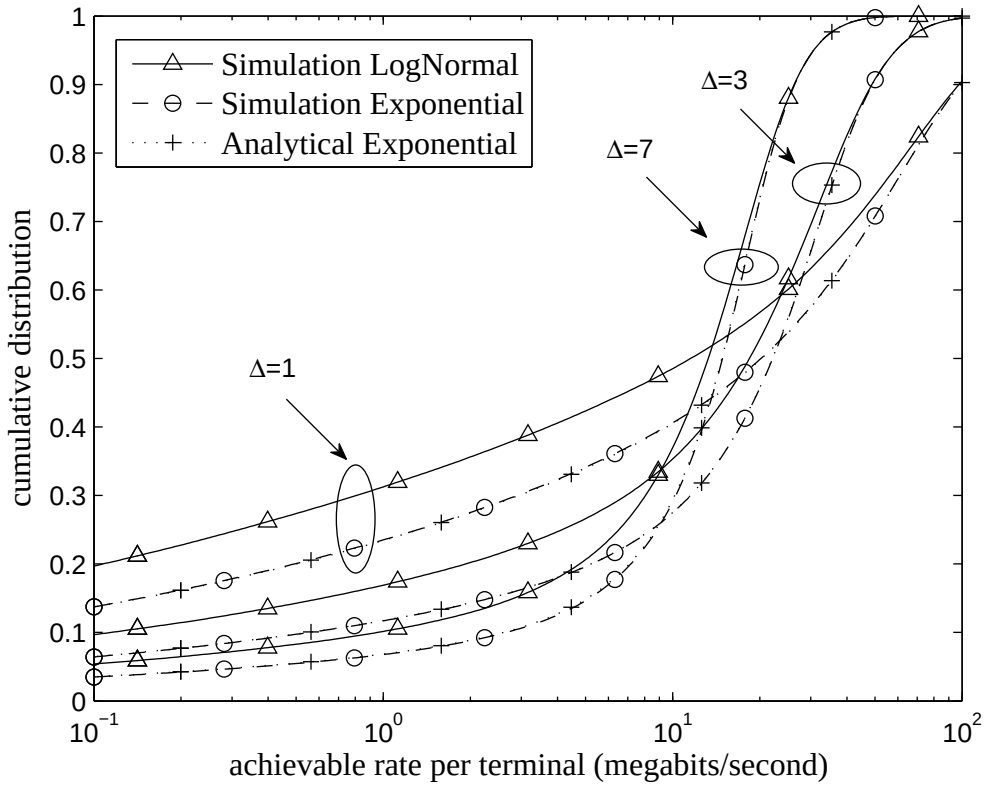

Figure 7.5: Cumulative distribution for the net achievable rate per terminal in random MS case with orthogonal pilots.

7.5.3 Random MS case with orthogonal pilots

Now, consider the case when the number of MSs in each cell is a Poisson random variable with mean P. When there are more than P MSs in the cell, only P of them are served. Thus, the desired BS will only receive interference from the cells that are using the same pilot as the desired MS.

Fig. 7.4 and Fig. 7.5 show the cumulative distributions for the SIR and the average achievable rate per user, respectively. Again, the analytical results using (7.9) fits the simulation perfectly. Also noticed that although the average number of MSs in the cell are same for both cases, the average served MS number is smaller for the random MS case since we can only serve at most P MSs at the same time. Therefore, the overall performance of this case is better than the fully loaded case considered previously.

7.6 Conclusion and Future Works

Massive MIMO system in which base stations are equipped with large numbers of antennas has the potential to deliver enhanced throughput and reliably on both the uplink and downlink in a fast-changing propagation environments [11]. As the number of antennas in the BS tends to infinity, one BS can serve an arbitrary number of MSs at arbitrary high rate as long as accurate channel state information is available. The capacity of the massive MIMO system is highly limited by the accuracy of channel state information and hence the channel estimation method plays a key role. Trade-offs such as total number of pilots vs their correlations between each other need to be thoroughly understood to achieve the best overall performance. Good mathematical tools are necessary to evaluate the system performance with different settings and schemes.

We adopt stochastic geometry to model the BS and MS locations in the cellular system and derive analytical characterizations for the cellular performance in terms of the key system parameters. When using orthogonal pilots, the closed-form expressions for the Laplace transform of interference and the distributions of SIR and achievable rates are obtained and a duality between the distributions of uplink and downlink SIR is revealed. For non-orthogonal pilots case, it is shown that downlink SIR is strictly limited by the inverse of the total pilot correlation and a reasonable estimates for the uplink performance are derived.

Finally, note that the uplink-downlink performance is mainly determined by the interference caused to the link due to pilot contamination. The mathematical tools developed here can be used to study the system performance under other different channel estimation methods and transmission-reception schemes, such as those studied in [96–98].

7.7 Appendix

7.7.1 Proof for Theorem 23

In the orthogonal pilots case, $\alpha_{ij} = \begin{cases} 1, & i = j \\ 0, & i \neq j \end{cases}$. By substituting for α_{ij} in Lemma 10, we get $I_{km}^{(UL)} = \sum_{l=1,\ l\neq k}^{\infty} b_{kl}\beta_{klm}^2 R_{klm}^{-2\epsilon}\mathcal{I}(m,l)$, $I_{km}^{(DL)} = \sum_{l=1,\ l\neq k}^{\infty} b_{kl}\beta_{lkm}^2 R_{lkm}^{-2\epsilon}\mathcal{I}(m,l)$ and by substituting these into (7.6), the uplink and downlink SIR expressions are obtained. Note that $I_{km}^{(DL)}$ is the interference at MS_{km} due to BS_l transmissions ($l \neq k$) to MS_{lm}. Using Slivnyak's theorem [67], the Palm distribution of all the BSs conditioned on the location of BS_k serving MS_{km} is also a Poisson point process and using Campbell's theorem [6, Page 57], the Laplace transform of $I_{km}^{(DL)}$ is equal to (7.7).

On the other hand, $I_{km}^{(UL)}$ is the interference at BS_k (assumed to be at the origin) from MSs using the m^{th} pilot sequence served by other BSs that operate in the same frequency band as BS_k. Using the same argument as before, all the other BSs in the cellular system given BS_k is at the origin is also a homogeneous Poisson point process with BS density λ_b. Hence, the Laplace transform of $I_{km}^{(UL)}$can be expressed as

$$
\begin{aligned}
&\mathcal{L}_{I_{km}^{(UL)}}(s) \\
&\overset{(a)}{=} \mathbb{E}\left[\prod_{l=1,\ l\neq k}^{\infty} \mathrm{e}^{-s b_{kl}\beta_{klm}^2 \|X_l + Y_{lm}\|^{-2\varepsilon}\mathcal{I}(m,l)}\right] \\
&\overset{(b)}{=} \exp\left(-\frac{\lambda_b \eta}{\Delta}\int_{x\in\mathbb{R}^2} \mathbb{E}_{\beta,Y}\left[1-\mathrm{e}^{-s\beta^2\|x+Y\|^{-2\varepsilon}}\right]dx\right) \\
&\overset{(c)}{=} \exp\left(-\frac{\lambda_b \eta}{\Delta}\mathbb{E}_{\beta,Y_1,Y_2}\left[\iint_{x_1=-\infty,\ x_2=-\infty}^{x_1=\infty,\ x_2=\infty}\right.\right. \\
&\left.\left.\left(1-\mathrm{e}^{-s\beta^2\left[(x_1+Y_1)^2+(x_2+Y_2)^2\right]^{-\varepsilon}}\right)dx_1 dx_2\right]\right) \\
&\overset{(d)}{=} \mathrm{e}^{-\frac{\lambda_b\eta}{\Delta}\mathbb{E}_\beta\left[\int_{r=0}^{\infty}\left(1-\mathrm{e}^{-s b_k \beta^2 r^{-2\epsilon}\mathcal{I}(m,l)}\right)2\pi r dr\right]} \\
&\overset{(e)}{=} \exp\left(-\frac{\pi\eta\lambda_b}{\Delta}s^{\frac{1}{\epsilon}}\cdot\mathbb{E}\left[\beta^{\frac{2}{\epsilon}}\right]\cdot\int_0^{\infty}\left(e^{-t^{-\epsilon}}-1\right)\mathrm{d}t\right),
\end{aligned}
\tag{7.18}
$$

where (a) is obtained by rewriting $I_{km}^{(UL)}$ in terms of the locations of BS_l denoted by $X_l \in \mathbb{R}^2$, and the location of MS_{lm} around BS_l denoted by $\{Y_{lm}\}_{l=1}^{\infty} \in \mathbb{R}^2$ which is i.i.d. uniformly distributed in the circle of radius R around the origin, (b) is obtained by first evaluating the expectation w.r.t. b_{kl}'s that are i.i.d. Bernoulli$\left(\frac{1}{\Delta}\right)$ random variables and the indicator functions $\mathcal{I}(m,l)$ such that $\mathbb{E}[\mathcal{I}(m,l)] = \eta = \sum_{n=1}^{P-1} \frac{n}{P} \frac{\left(\lambda_u \pi R^2\right)^n}{n!} e^{-\lambda_u \pi R^2} + \sum_{n=P}^{\infty} \frac{\left(\lambda_u \pi R^2\right)^n}{n!} e^{-\lambda_u \pi R^2}$ is the probability that BS_l is currently using the m^{th} pilot sequence $\forall\ l \neq k$ and then applying Campbell's theorem [6, Page 57] to the Poisson point process of the BS arrangement where the expectation operator is w.r.t. the random variable β which has the same distribution as β_{klm}'s, (c) is obtained by exchanging the order of expectation and integration and expressing the integral over $\mathbb{R}^2$ in the Cartesian coordinate system, (d) is obtained by the following variable changes: $x_1 \leftarrow x_1 + Y_1$ and $x_2 \leftarrow x_2 + Y_2$ and rewriting the integrals in the polar coordinate system, (e) is obtained by a variable change $t \leftarrow \beta^{-\frac{2}{\epsilon}} r^2$ and then evaluating the expectation w.r.t. β, and finally, (7.7) is obtained by rewriting the integral in (e) in terms of $\operatorname{sinc}(\cdot)$.

Now, since $\mathcal{L}_{I_{km}^{(UL)}}(s) = \mathcal{L}_{I_{km}^{(DL)}}(s)$, the $I_{km}^{(UL)}$ and $I_{km}^{(DL)}$ have the same distribution. Further, since the numerator and denominator in the SIR expressions in (7.6) are independent of each other, it is clear that the distribution of SIR in the uplink and downlink are also identical, and hence we have (7.8).

Next, if $\left\{\beta_{klm}^2\right\}_{l=1}^{\infty}$ is a set of i.i.d. unit mean exponential random variables, the c.c.d.f. of $\text{SIR}_{km}^{(DL)}$ is

$$\begin{aligned}
&\mathbb{P}\left(\left\{\text{SIR}_{km}^{(DL)} > \gamma\right\}\right) \\
&\overset{(a)}{=} \mathbb{E}\left[\mathrm{e}^{-\gamma R_{kkm}^{2\epsilon} \sum_{l=1,\ l\neq k}^{\infty} b_{kl} \beta_{klm}^2 R_{klm}^{-2\epsilon} \mathcal{I}(m,l)}\right] \\
&\overset{(b)}{=} \mathbb{E}_{R_{kkm}}\left[\mathrm{e}^{-\frac{\lambda_b \eta}{\Delta} \int_0^{\infty} \left(1 - \mathbb{E}_{\beta^2}\left[e^{-\gamma R_{kkm}^{2\epsilon} \beta^2 r^{-2\epsilon}}\right]\right) 2\pi r \mathrm{d}r}\right] \\
&\overset{(c)}{=} \mathbb{E}_{R_{kkm}}\left[\exp\left(-\frac{\eta \gamma^{\frac{1}{\epsilon}} \lambda_b \pi R_{kkm}^2}{\Delta \operatorname{sinc}\left(\frac{\pi}{\epsilon}\right)}\right)\right],
\end{aligned}$$

where $\gamma \geq 0$, (a) is obtained by evaluating the probability w.r.t. the unit mean exponential random variable β_{kkm}^2 conditioned on all other random variables, (b) is similar to (7.18-(b)), (c) is obtained by evaluating the expectation w.r.t. β^2 which is a unit mean exponential random variable and then evaluating the integral in (b) and finally, (7.9) is obtained by evaluating the expectation w.r.t. $R_{kkm}$with the probability density

function $f_{R_{kkm}}(r) = \begin{cases} \frac{2r}{R^2} & 0 \leq r \leq R \\ 0 & \text{otherwise} \end{cases}$. From (7.8), the above is also the c.c.d.f. of $\text{SIR}_{km}^{(UL)}$.

7.7.2 Proof for Theorem 24

The Laplace transform of the downlink interference $I_{km}^{(DL)}$ is derive below.

$$\mathcal{L}_{I_{km}^{(DL)}}(s) = \mathbb{E}\left[\mathrm{e}^{-s\bar{\alpha}_m\beta_{kkm}^2 R_{kkm}^{-2\epsilon}}\right] \times \mathbb{E}\left[\prod_{l=1,\ l\neq k}^{\infty} \mathrm{e}^{-s(\bar{\alpha}_m+1)b_{kl}\beta_{lkm}^2 R_{lkm}^{-2\epsilon}}\right],$$

is obtained by noting that the two terms in (7.11) are independent of each other. Further, (7.12) is obtained by evaluating the expectation w.r.t. R_{kkm} in the first term of the above product, and then using the Campbell's theorem to evaluate the second theorem. Now, notice that the downlink SIR can be expressed as

$$\text{SIR}_{km}^{(\text{DL})} = \frac{1}{\bar{\alpha}_m + \frac{\bar{\alpha}_m+1}{\text{SIR}_{km}}}, \tag{7.19}$$

where SIR_{km} denotes the SIR for the orthogonal pilots case studied in Section 7.4.1. Hence, the c.c.d.f. of $\text{SIR}_{km}^{(\text{DL})}$ is

$$\begin{aligned} &\mathbb{P}\left(\left\{\text{SIR}_{km}^{(\text{DL})} > \gamma\right\}\right) \\ &= \mathbb{P}\left(\{\text{SIR}_{km} > \bar{\gamma}\} \cap \left\{\gamma < \frac{1}{\bar{\alpha}_m}\right\}\right) \end{aligned} \tag{7.20}$$

where $\bar{\gamma} = \left(\frac{\gamma(1+\bar{\alpha}_m)}{1-\bar{\alpha}_m\gamma}\right)$, and using the c.c.d.f. of SIR_{km} is obtained from (7.9) with $\eta = 1$.

Chapter 8

Conclusions

We analyzed the characteristics of interference and the SINR in different types of large-scale wireless communication systems such as the cellular networks, heterogeneous networks, cognitive radio networks and the massive MIMO networks. The importance of the analysis done in this thesis lies in the fact that all the above mentioned large scale networks have been studied mainly via system simulations. As a result, these systems are poorly understood in terms of the dependence of their performance on the channel conditions, the configuration of the nodes in the network and other system parameters.

The goal of this thesis has been to study the above mentioned networks using a suitable model in order to obtain analytical characterizations of important metrics that quantify the performance of the systems. Note that all the metrics that determine the performance of the system such as the coverage (outage) probability, average rate, spectral efficiency, throughput, network capacity, average load carried by the network, transmission capacity and the transport capacity are basically a function of the interference and the SINR at the receiver in the network, and hence the focus has been to thoroughly understand these metrics in terms of the channel conditions and the other system parameters.

Further, we have identified that these networks are well-modeled as consisting of nodes distributed in a given space randomly according to a suitable stochastic geometric model. This is motivated by results in [2, 10] that the stochastic geometric models are a good approximation for these networks in a scattering and fading rich wireless environment. In this thesis, the stochastic geometric study of the above mentioned wireless system is demonstrated to be beneficial because the performance of complex wireless networks such as the heterogeneous networks have been thoroughly characterized for the most general channel settings.

These results have provided numerous insights that are beneficial for the system designers to understand the dependence of the performance of the various system parameters involved.

The mathematical tools developed in this thesis can also be used to attack several other topics in wireless communications. Firstly, the coverage improvements attainable by the introduction of relay networks can be characterized. The idea of secrecy in the networks can be explored, where the nodes involved in the secure communications as well as the eavesdropper nodes are randomly distributed in a given area. The performance improvements achievable with many of the interference avoidance (mitigation) techniques incorporated in the 4G LTE standard such as multi-cell cooperation and interference cancellation can also be studied. The study of the performance improvements with the introduction of MIMO into the networks using stochastic geometric modeling is also catching wide-spread interest in the research community. The results that have been developed in this work will be useful in the further exploration of these topics.

Bibliography

[1] R. Ganti, F. Baccelli, and J. Andrews, "A new way of computing rate in cellular networks," in IEEE International Conference on Communications (ICC), 2011, pp. 1–5.

[2] T. X. Brown, "Cellular performance bounds via shotgun cellular systems," IEEE J. Sel. Areas Commun, vol. 18, no. 11, pp. 2443–2455, Nov 2000.

[3] H. S. Dhillon, R. K. Ganti, F. Baccelli, and J. G. Andrews, "Coverage and ergodic rate in K-tier downlink heterogeneous cellular networks," in 49th Annual Allerton Conference on Communication, Control, and Computing (Allerton), 2011, sept. 2011, pp. 1627 –1632.

[4] A. Goldsmith, Wireless Communications. New York, NY, USA: Cambridge University Press, 2005.

[5] D. Stoyan, W. S. Kendall, and J. Mecke, Stochastic Geometry and its Applications, 1995.

[6] J. F. C. Kingman, Poisson Processes (Oxford Studies in Probability). Oxford University Press, USA, January 1993.

[7] S. M. Ross, Stochastic Processes. John Wiley & Sons, Inc., 1983.

[8] R. K. Ganti and M. Haenggi, "Regularity in sensor networks," in International Zurich Seminar on Communications (IZS'06), Zurich, Switzerland, FEB 2006. [Online]. Available: http://www.nd.edu/ mhaenggi/pubs/izs06.pdf

[9] D. J. Daley and D. Vere-Jones, An introduction to the theory of point processes, 2nd ed., ser. Probability and its Applications (New York). New York: Springer, 2008, vol. 1, general theory and structure. [Online]. Available: http://www.springerlink.com/content/978-0-387-21337-8

[10] B. Blaszczyszyn, M. K. Karray, and H.-P. Keeler, "Using Poisson processes to model lattice cellular networks," CoRR, 2012. [Online]. Available: http://arxiv.org/abs/1207.7208

[11] T. Marzetta, "Noncooperative cellular wireless with unlimited numbers of base station antennas," IEEE Transactions on Wireless Communications, vol. 9, no. 11, pp. 3590 –3600, november 2010.

[12] T. X. Brown, "Analysis and coloring of a shotgun cellular system," Radio and Wireless Conference, 1998. RAWCON 98. 1998 IEEE, pp. 51–54, Aug 1998.

[13] J. Andrews, F. Baccelli, and R. Ganti, "A tractable approach to coverage and rate in cellular networks," Communications, IEEE Transactions on, vol. 59, no. 11, pp. 3122 –3134, november 2011.

[14] V. Chandrasekhar and J. Andrews, "Uplink capacity and interference avoidance for two-tier femtocell networks," IEEE Transactions on Wireless Communications, vol. 8, no. 7, pp. 3498 –3509, July 2009.

[15] J. G. Andrews, N. Jindal, M. Haenggi, R. Berry, S. Jafar, D. Guo, S. Shakkottai, R. W. H. Jr., M. Neely, S. Weber, and A. Yener, "Rethinking information theory for mobile ad hoc networks," IEEE Communications Magazine, vol. 46, no. 12, pp. 94–101, December 2008.

[16] A. M. Hunter, J. G. Andrews, and S. Weber, "Capacity scaling laws for ad hoc networks with spatial diversity," in Proceedings of the IEEE International Symposium on Information Theory (ISIT), Nice, France, June 2007.

[17] ——, "Capacity scaling of ad hoc networks with spatial diversity," IEEE Transactions on Wireless Communications, vol. 7, no. 12, pp. 5058–5071, December 2008.

[18] N. Jindal, J. G. Andrews, and S. Weber, "Energy-limited vs. interference-limited ad hoc network capacity (invited)," in Proceedings of the 41st Annual Asilomar Conference on Signals, Systems, and Computers, Pacific Grove, CA, November 2007.

[19] K. T. Truong, S. Weber, and R. W. Heath, "Transmission capacity of two-way communication in wireless ad hoc networks," in Proceedings of the International Conference on Communications (ICC), Dresden, Germany, June 2009.

[20] S. Weber, J. G. Andrews, X. Yang, and G. de Veciana, "Transmission capacity of CDMA ad hoc networks employing successive interference cancellation," in Proceedings of the 47th annual IEEE Global Telecommunications Conference (Globecom), Dallas, TX, November 2004.

[21] ——, "Wireless ad hoc networks with successive interference cancellation," in Proceedings of the 43rd annual Allerton conference on communication, control, and computing, Monticello, IL, September 2005.

[22] S. Weber and J. G. Andrews, "A stochastic geometry approach to wideband ad hoc networks with channel variations," in Proceedings of the Second Workshop on Spatial Stochastic Models for Wireless Networks (SPASWIN), Boston, MA, April 2006.

[23] ——, "Transmission capacity of wireless ad hoc networks with channel variations," in Proceedings of the 40th Annual Asilomar Conference on Signals, Systems, and Computers, Pacific Grove, CA, October 2006.

[24] S. Weber, X. Yang, G. de Veciana, and J. Andrews, "Transmission capacity of CDMA ad-hoc networks," in Spread Spectrum Techniques and Applications, 2004 IEEE Eighth International Symposium on, 2004, pp. 245–249.

[25] S. Weber, X. Yang, J. G. Andrews, and G. de Veciana, "Transmission capacity of wireless ad hoc networks with outage constraints," IEEE Transactions on Information Theory, vol. 51, no. 12, pp. 4091–4102, December 2005.

[26] J. Wildman, D. Hamel, R. Measel, D. Oakum, S. Weber, and M. Kam, "Performance and scaling of wireless ad hoc IPv6 stateless address autoconfiguration under mobile gateways," in Proceedings of the Military Communications Conference (MILCOM), Orlando, FL, October 2007.

[27] P. Madhusudhanan, J. G. Restrepo, Y. Liu, T. X. Brown, and K. Baker, "Stochastic ordering based carrier-to-interference ratio analysis for the shotgun cellular systems," Wireless Communications Letters, IEEE, vol. PP, no. 99, pp. 1 –4, 2012.

[28] ——, "Modeling of Interference from Cooperative Cognitive Radios for Low Power Primary Users," in IEEE Globecom 2010 Wireless Communications Symposium, 2010, pp. 1–6.

[29] ——, "Multi-tier network performance analysis using a shotgun cellular system," in IEEE Globecom 2011 Wireless Communications Symposium, Dec. 2011, pp. 1 –6.

[30] P. Madhusudhanan, J. G. Restrepo, Y. Liu, and T. X. Brown, "Downlink coverage analysis in a heterogeneous cellular network," CoRR, 2012. [Online]. Available: http://arxiv.org/abs/1206.4723

[31] S. Weber, J. G. Andrews, and N. Jindal, "Throughput and transmission capacity of ad hoc networks with channel state information," in Proceedings of the 44th Annual Allerton Conference on Communication, Control, and Computing, Monticello, IL, September 2006.

[32] S. Weber, X. Yang, G. de Veciana, and J. G. Andrews, "Transmission capacity of CDMA ad-hoc networks," in Proceedings of the 8th IEEE International Symposium on Spread Spectrum Techniques and Applications (ISSSTA), Sydney, Australia, August 2004.

[33] J. G. Andrews, S. Weber, and M. Haenggi, "Ad hoc networks: to spread or not to spread?" IEEE Communications Magazine, vol. 45, no. 12, pp. 84–91, December 2007.

[34] N. Jindal, S. Weber, and J. G. Andrews, "Fractional power control for decentralized wireless networks," IEEE Transactions on Wireless Communications, vol. 7, no. 12, pp. 5482–5492, December 2008.

[35] N. Jindal, J. G. Andrews, and S. Weber, "Bandwidth partitioning in decentralized wireless networks," IEEE Transactions on Wireless Communications, vol. 7, no. 12, pp. 5408–5419, December 2008.

[36] H. Takagi and L. Kleinrock, "Optimal transmission ranges for randomly distributed packet radio terminals," IEEE Transactions on Communications, vol. 32, no. 3, pp. 246–257, Mar 1984.

[37] M. Zorzi and S. Pupolin, "Outage probability in multiple access packet radio networks in the presence of fading," IEEE Transactions on Vehicular Technology, vol. 43, no. 3, pp. 604–610, Aug 1994.

[38] P. Madhusudhanan, J. G. Restrepo, Y. E. Liu, T. X. Brown, and K. R. Baker, "Stochastic ordering based carrier-to-interference ratio analysis for the shotgun cellular systems," IEEE Wireless Communications Letters, vol. 1, no. 6, pp. 565 –568, december 2012.

[39] M. Shaked and J. G. Shanthikumar, Stochastic Orders, ser. Springer Series in Statistics. Springer, 2007.

[40] ——, Stochastic Orders and Their Applications (Probability and Mathematical Statistics). Academic press, 1994.

[41] A. M. Mathai and H. J. Haubold, Special Functions for Applied Scientists. Springer, March 2008.

[42] R. Menon, R. Buehrer, and J. Reed, "On the Impact of Dynamic Spectrum Sharing Techniques on Legacy Radio Systems," Wireless Communications, IEEE Transactions on, vol. 7, no. 11, pp. 4198 –4207, november 2008.

[43] C.-H. Lee and M. Haenggi, "Interference and Outage in Poisson Cognitive Networks," IEEE Transactions on Wireless Communications, 2012. [Online]. Available: http://www.nd.edu/ mhaenggi/pubs/twc12.pdf

[44] R. Dhillon and T. X. Brown, "Models for analyzing cognitive radio interference to wireless microphones in TV bands," 3rd IEEE Symposium on New Frontiers in Dynamic Spectrum Access Networks, pp. 1–10, October 2008.

[45] X. Hong, C.-X. Wang, and J. Thompson, "Interference modeling of cognitive radio networks," IEEE Vehicular Technology Conference, pp. 1851–1855, May 2008.

[46] P. Madhusudhanan, T. Brown, and Y. Liu, "On the interference due to cooperative cognitive radios in the presence of multiple low-power primary users," in Communication, Control, and Computing (Allerton), 2011 49th Annual Allerton Conference on, Sept. 2011, pp. 1657 –1664.

[47] P. Madhusudhanan, T. X. Brown, and Y. Liu, "Interference characteristics and success probability at the primary user in a cognitive radio network," in Modeling and Optimization in Mobile, Ad Hoc and Wireless Networks (WiOpt), 2012 10th International Symposium on, May 2012, pp. 349 –354.

[48] P. Xia, V. Chandrasekhar, and J. Andrews, "Open vs. closed access femtocells in the uplink," Wireless Communications, IEEE Transactions on, vol. 9, no. 12, pp. 3798 –3809, 2010.

[49] P. Madhusudhanan, J. G. Restrepo, Y. Liu, and T. X. Brown, "Heterogeneous cellular network performance analysis under open and closed access," in Global Telecommunications Conference (GLOBECOM 2012), 2012 IEEE, december 2012, pp. 1 –6.

[50] H. S. Dhillon, R. K. Ganti, F. Baccelli, and J. G. Andrews, "Modeling and analysis of K-tier downlink heterogeneous cellular networks," IEEE Journal on Selected Areas in Communications, vol. 30, no. 3, pp. 550 –560, april 2012.

[51] H. Dhillon, R. Ganti, and J. Andrews, "A tractable framework for coverage and outage in heterogeneous cellular networks," in Information Theory and Applications Workshop (ITA), 2011, feb. 2011, pp. 1 –6.

[52] ——, "Load-aware modeling and analysis of heterogeneous cellular networks," CoRR, vol. abs/1204.1091, 2012. [Online]. Available: http://arxiv.org/abs/1204.1091

[53] H.-S. Jo, Y. J. Sang, P. Xia, and J. G. Andrews, "Heterogeneous cellular networks with flexible cell association: A comprehensive downlink sinr analysis," CoRR, vol. abs/1107.3602, 2011. [Online]. Available: http://arxiv.org/abs/1107.3602

[54] S. Mukherjee, "Distribution of downlink SINR in heterogeneous cellular networks," IEEE Journal on Selected Areas in Communications, vol. 30, no. 3, pp. 575 –585, april 2012.

[55] ——, "Downlink SINR distribution in a heterogeneous cellular wireless network with biased cell association," in IEEE ICC 2012 - 1st International Workshop on Small Cell Wireless Networks, 2012.

[56] C. Tepedelenlioglu, A. Rajan, and Y. Zhang, "Applications of stochastic ordering to wireless communications," IEEE Trans. Wireless Commun., vol. 10, no. 12, pp. 4249–4257, Dec 2011.

[57] B. Błaszczyszyn and D. Yogeshwaran, "Directionally convex ordering of random measures, shot-noise fields and some applications to wireless networks," Adv. Appl. Probab., vol. 41, pp. 623–646, 2009.

[58] P. Madhusudhanan, J. G. Restrepo, Y. Liu, T. X. Brown, and K. R. Baker, "Downlink performance analysis for a generalized shotgun cellular system," CoRR, 2010. [Online]. Available: http://arxiv.org/abs/1002.3943

[59] T. S. Rappaport, Wireless Communications: Principles and Practice. Upper Saddle River, NJ, USA: Prentice-Hall, Inc., 1996.

[60] S.-P. Yeh, S. Talwar, G. Wu, N. Himayat, and K. Johnsson, "Capacity and coverage enhancement in heterogeneous networks," Wireless Communications, IEEE, vol. 18, no. 3, pp. 32 –38, june 2011.

[61] A. Damnjanovic, J. Montojo, Y. Wei, T. Ji, T. Luo, M. Vajapeyam, T. Yoo, O. Song, and D. Malladi, "A survey on 3GPP heterogeneous networks," Wireless Communications, IEEE, vol. 18, no. 3, pp. 10 –21, june 2011.

[62] A. Damnjanovic, J. Montojo, J. Cho, H. Ji, J. Yang, and P. Zong, "UE's role in lte advanced heterogeneous networks," Communications Magazine, IEEE, vol. 50, no. 2, pp. 164 –176, february 2012.

[63] 4G Americas Report. (2011, February) 4G Mobile Broadband Evolution: 3GPP Release 10 and Beyond. [Online]. Available: http://www.4gamericas.org/

[64] Qualcomm. (2010, February) LTE Advanced: Heterogeneous network. [Online]. Available: http://www.qualcomm.com/documents/files/lte-advanced-heterogeneous-networks.pdf

[65] V. Chandrasekhar, J. Andrews, and A. Gatherer, "Femtocell Networks: A Survey," Communications Magazine, IEEE, vol. 46, no. 9, pp. 59–67, September 2008.

[66] X. Lagrange, "Multitier cell design," Communications Magazine, IEEE, vol. 35, no. 8, pp. 60 –64, aug 1997.

[67] M. Haenggi and R. K. Ganti, Interference in Large Wireless Networks, 2008, vol. 3, no. 2. [Online]. Available: http://www.nd.edu/ mhaenggi/pubs/now.pdf

[68] F. Baccelli and B. Błaszczyszyn, Stochastic Geometry and Wireless Networks, Volume I — Theory, ser. Foundations and Trends in Networking. NoW Publishers, 2009, vol. 3, No 3–4.

[69] ——, Stochastic Geometry and Wireless Networks, Volume II — Applications, ser. Foundations and Trends in Networking. NoW Publishers, 2009, vol. 4, No 1–2.

[70] V. M. Nguyen and F. Baccelli, "A stochastic geometry model for the best signal quality in a wireless network," in Modeling and Optimization in Mobile, Ad Hoc and Wireless Networks (WiOpt), 2010 Proceedings of the 8th International Symposium on, 31 2010-june 4 2010, pp. 465 –471.

[71] P. Madhusudhanan, J. G. Restrepo, Y. E. Liu, and T. X. Brown, "Carrier to interference ratio analysis for the shotgun cellular system," in IEEE Globecom 2009 Wireless Communications Symposium, Honolulu, HI, USA, November 2009.

[72] S. Mukherjee, "Downlink SINR distribution in a heterogeneous cellular wireless network with max-SINR connectivity," in Communication, Control, and Computing (Allerton), 2011 49th Annual Allerton Conference on, sept. 2011, pp. 1649 –1656.

[73] G. Boudreau, J. Panicker, N. Guo, R. Chang, N. Wang, and S. Vrzic, "Interference coordination and cancellation for 4G networks," Communications Magazine, IEEE, vol. 47, no. 4, pp. 74 –81, april 2009.

[74] N. Himayat, S. Talwar, A. Rao, and R. Soni, "Interference management for 4G cellular standards [WIMAX/LTE UPDATE]," Communications Magazine, IEEE, vol. 48, no. 8, pp. 86 –92, august 2010.

[75] T. D. Novlan, R. K. Ganti, A. Ghosh, and J. G. Andrews, "Analytical evaluation of fractional frequency reuse for OFDMA cellular networks," IEEE Transactions on Wireless Communications, vol. 10, no. 12, pp. 4294 –4305, december 2011.

[76] ——, "Analytical evaluation of fractional frequency reuse for heterogeneous cellular networks," IEEE Transactions on Communications, vol. 60, no. 7, pp. 2029 –2039, july 2012.

[77] "Unlicensed Operation in the TV Broadcast Bands," Federal Communications Commission, no. ET Docket No. 10-174, 2010.

[78] K. Shin, H. Kim, A. Min, and A. Kumar, "Cognitive radios for dynamic spectrum access: from concept to reality," IEEE Wireless Communications, vol. 17, no. 6, pp. 64 –74, december 2010.

[79] "Unlicensed Operation in the TV Broadcast Bands," Federal Communications Commission, no. ET Docket No. 04-186, 2004.

[80] K.-M. Kang, J. C. Park, S.-I. Cho, B. J. Jeong, Y.-J. Kim, H.-J. Lim, and G.-H. Im, "Deployment and coverage of cognitive radio networks in tv white space," IEEE Communications Magazine, vol. 50, no. 12, pp. 88–94, December 2012.

[81] H.-J. Lim, D.-Y. Seol, and G.-H. Im, "Joint sensing adaptation and resource allocation for cognitive radio with imperfect sensing," IEEE Transactions on Communications, vol. 60, no. 4, pp. 1091 –1100, april 2012.

[82] T. X. Brown, "An analysis of unlicensed device operation in licensed broadcast service bands," in 2005 First IEEE International Symposium on New Frontiers in Dynamic Spectrum Access Networks, 2005. DySPAN 2005., nov. 2005, pp. 11 –29.

[83] W. Yu-Chun, W. Haiguang, and P. Zhang, "Protection of Wireless Microphones in IEEE 802.22 Cognitive Radio Network," IEEE International Conference on Communications Workshops, pp. 1 –5, June 2009.

[84] Z. Lei and F. Chin, "A Reliable and Power Efficient Beacon Structure for Cognitive Radio Systems," IEEE International Conference on Communications, pp. 2038 –2042, May 2008.

[85] S. M. Weiss, R. D. Weller, and S. D. Driscoll, "New measurements and predictions of UHF television receiver local oscillator radiation interference," in Proceedings of the 2003 IEEE Broadcast Technology Society Symposium, 2003.

[86] R. Menon, R. Buehrer, and J. Reed, "Outage probability based comparison of underlay and overlay spectrum sharing techniques," First IEEE International Symposium on New Frontiers in Dynamic Spectrum Access Networks, pp. 101–109, November 2005.

[87] R. Dahama, K. Sowerby, and G. Rowe, "Outage probability estimation for licensed systems in the presence of cognitive radio interference," IEEE 69th Vehicular Technology Conference, pp. 1–5, April 2009.

[88] J. Lee, J. Andrews, and D. Hong, "Spectrum-Sharing Transmission Capacity," Wireless Communications, IEEE Transactions on, vol. 10, no. 9, pp. 3053 –3063, september 2011.

[89] S. Zaidi, M. Ghogho, and D. McLernon, "Transmission Capacity Analysis of Cognitive Radio Networks under Co-existence Constraints," in Signal Processing Advances in Wireless Communications (SPAWC), 2010 IEEE Eleventh International Workshop on, june 2010, pp. 1 –5.

[90] C. Yin, L. Gao, T. Liu, and S. Cui, "Transmission Capacities for Overlaid Wireless Ad Hoc Networks with Outage Constraints," in Communications, 2009. ICC '09. IEEE International Conference on, june 2009, pp. 1 –5.

[91] P. Hall, Introduction to the theory of coverage processes. John Wiley & Sons, Inc., 1988.

[92] M. Haenggi, "Mean interference in hard-core wireless networks," IEEE Communications Letters, vol. 15, no. 8, pp. 792 –794, august 2011.

[93] D. J. Daley and D. Vere-Jones, An introduction to the theory of point processes, 2nd ed., ser. Probability and its Applications (New York). New York: Springer, 2008, vol. 2, general theory and structure. [Online]. Available: http://www.springerlink.com/content/978-0-387-21337-8

[94] T. Marzetta, "How much training is required for multiuser MIMO?" in 40th Asilomar Conference on Signals, Systems and Computers, Nov 2006, pp. 359 –363.

[95] F. Rusek, D. Persson, B. K. Lau, E. Larsson, T. Marzetta, O. Edfors, and F. Tufvesson, "Scaling up MIMO: Opportunities and challenges with very large arrays," IEEE Signal Processing Magazine, vol. 30, no. 1, pp. 40 –60, Jan 2013.

[96] J. Hoydis, S. ten Brink, and M. Debbah, "Massive MIMO in the UL/DL of cellular networks: How many antennas do we need?" IEEE Journal on Selected Areas in Communications, vol. 31, no. 2, pp. 160–171, Feb 2013.

[97] A. Ashikhmin and T. Marzetta, "Pilot contamination precoding in multi-cell large scale antenna systems," in IEEE International Symposiumon Information Theory Proceedings (ISIT), July 2012, pp. 1137–1141.

[98] J. Jose, A. Ashikhmin, T. Marzetta, and S. Vishwanath, "Pilot contamination and precoding in multi-cell tdd systems," IEEE Transactions on Wireless Communications, vol. 10, no. 8, pp. 2640–2651, Aug 2011.